

DNA-TEMPLATED SYNTHESIS OF CATIONIC STYRYL DYES



A Dissertation Submitted in Partial Fulfillment of the Requirements
for the Degree of Doctor of Philosophy in Chemistry

Department of Chemistry

FACULTY OF SCIENCE

Chulalongkorn University

Academic Year 2022

Copyright of Chulalongkorn University

การสังเคราะห์สีย้อมสไตริลที่มีประจุบวกด้วยดีเอ็นเอแม่แบบ



วิทยานิพนธ์นี้เป็นส่วนหนึ่งของการศึกษาตามหลักสูตรปริญญาวิทยาศาสตรดุษฎีบัณฑิต
สาขาวิชาเคมี ภาควิชาเคมี
คณะวิทยาศาสตร์ จุฬาลงกรณ์มหาวิทยาลัย
ปีการศึกษา 2565
ลิขสิทธิ์ของจุฬาลงกรณ์มหาวิทยาลัย

เกรียงศักดิ์ ฝ้ายเครือ : การสังเคราะห์สีย้อมสไตริลที่มีประจุบวกด้วยดีเอ็นเอแม่แบบ. (DNA-TEMPLATED SYNTHESIS OF CATIONIC STYRYL DYES) อ.ที่ปรึกษาหลัก : ศ. ดร.ธีรยุทธ วิไลวัลย์

สีย้อมสไตริลเป็นโมเลกุลที่ประกอบด้วยระบบคอนจูเกตของพันธะไพซึ่งสามารถแสดงสมบัติเชิงแสงที่น่าสนใจ เช่น มีความเสถียรเชิงแสงและมีสมบัติเชิงแสงที่เปลี่ยนไปตามชนิดของตัวทำละลาย อีกทั้งยังมีค่า quantum yield ที่สูงและมีการตอบสนองเชิงแสงที่ดีเมื่อจับกับสารชีวโมเลกุลเป้าหมาย เช่น กรดนิวคลีอิก ทำให้สีย้อมในกลุ่มสไตริลบางชนิดถูกนิยมนำมาประยุกต์ใช้อย่างแพร่หลายสำหรับตรวจวัดสารชีวโมเลกุลและใช้เป็นสีย้อมระดับเซลล์ โดยทั่วไปการสังเคราะห์สีย้อมในกลุ่มสไตริลสามารถเกิดผ่านปฏิกิริยา Aldol-type reaction ระหว่างสารตั้งต้นสองชนิด ได้แก่ สารประกอบเฮเทอโรไซคลิกที่มีหมู่เมทิลกับสารประกอบแอลดีไฮด์ภายใต้สภาวะที่มีตัวเร่งปฏิกิริยาจำพวกกรดหรือเบสควบคู่กันกับการให้ความร้อน อย่างไรก็ตามการสังเคราะห์ด้วยวิธีดังกล่าวมีประสิทธิภาพต่ำ สิ้นเปลืองเวลาและสารเคมี อีกทั้งยังต้องการทำให้บริสุทธิ์ก่อนที่จะนำมาศึกษาสมบัติเชิงแสงต่อไป การสังเคราะห์ด้วยดีเอ็นเอแม่แบบเป็นหนึ่งในวิธีการที่น่าสนใจและมีประสิทธิภาพในการสังเคราะห์สารอินทรีย์ได้หลากหลายชนิด นอกจากนี้การสังเคราะห์ด้วยวิธีการดังกล่าวยังสะดวก รวดเร็ว สามารถทำได้ในสเกลขนาดเล็กซึ่งมีความสำคัญมากสำหรับการค้นพบและบ่งชี้โมเลกุลเป้าหมาย ในงานวิจัยนี้มีวัตถุประสงค์เพื่อพัฒนาวิธีการสังเคราะห์สีย้อมสไตริลที่มีประจุบวกโดยใช้ดีเอ็นเอเป็นแม่แบบ หลักการสำคัญคือเมื่อสารตั้งต้นที่ถูกตัดแปรรูปโครงสร้างให้มีประจุบวกทั้งสองชนิดได้แก่ สารประกอบเฮเทอโรไซคลิกที่มีหมู่เมทิลกับสารประกอบแอลดีไฮด์ เกิดแรงกระทำทางไฟฟ้าสถิตกับประจุลบบนโครงสร้างของดีเอ็นเอแม่แบบ แรงกระทำดังกล่าวจะเหนี่ยวนำให้สารตั้งต้นทั้งสองชนิดเข้าใกล้กันมากยิ่งขึ้นจนสามารถถูกเร่งให้เกิดปฏิกิริยาบนโครงสร้างของดีเอ็นเอแม่แบบ ในงานวิจัยนี้ได้การพิสูจน์และยืนยันแนวคิดดังกล่าวอีกทั้งยังสามารถสังเคราะห์สีย้อมสไตริลที่มีโครงสร้างที่หลากหลายผ่านการสังเคราะห์แบบ combinatorial synthesis โดยสามารถยืนยันสีย้อมสไตริลที่เกิดขึ้นด้วยการวัดการดูดกลืนแสง UV-Visible, การวัดสัญญาณ fluorescence, NMR spectroscopy และ mass spectrometry และที่สำคัญยังสามารถตรวจสอบการเกิดของสีย้อมสไตริลและการตอบสนองเชิงแสงต่อดีเอ็นเอเป้าหมายซึ่งก็คือดีเอ็นเอแม่แบบได้ทันที ทำให้วิธีนี้สามารถระบุสีย้อมสไตริลที่ตอบสนองอย่างจำเพาะกับดีเอ็นเอแม่แบบได้ นอกจากนี้การสังเคราะห์ด้วยกรดนิวคลีอิกแม่แบบยังสามารถประยุกต์ใช้สำหรับสังเคราะห์สีย้อมในเซลล์ของสิ่งมีชีวิตได้อีกด้วย อย่างไรก็ตาม จากการทดลองย่อยด้วยเอนไซม์นิวคลีโอเอสสามารถยืนยันได้ว่าอาร์เอ็นเอในเซลล์ของสิ่งมีชีวิตทำหน้าที่เป็นแม่แบบสำหรับการสังเคราะห์สีย้อมสไตริลแทนที่จะเป็นดีเอ็นเอเนื่องจากดีเอ็นเอเข้าถึงได้ยากกว่า งานวิจัยนี้จึงประสบความสำเร็จในการพัฒนาการสังเคราะห์และคัดเลือกสีย้อมสไตริลที่มีความจำเพาะกับกรดนิวคลีอิกเป้าหมายหรือ organelle ในเซลล์สิ่งมีชีวิต

สาขาวิชา เคมี

ลายมือชื่อนิสิต

ปีการศึกษา 2565

ลายมือชื่อ อ.ที่ปรึกษาหลัก

6271056823 : MAJOR CHEMISTRY

KEYWORD: DNA, RNA, Templated reaction, Combinatorial synthesis, Styryl dyes

Kriangsak Faikhrua : DNA-TEMPLATED SYNTHESIS OF CATIONIC STYRYL DYES. Advisor: Prof. TIRAYUT VILAVAN, Ph.D.

Styryl dye is a class of pi-conjugated dye that shows several desirable optical properties, such as high photostability, solvatochromic characteristics, and high fluorescence quantum yields. Due to the responsiveness to the binding with the target biomolecules such as nucleic acids, some of these dyes have been widely employed for biomolecular detection and cellular imaging. These dyes are typically synthesized via an aldol-type reaction between a methyl heterocycle and an aromatic aldehyde in the presence of acid or base as a catalyst. However, the conventional method of synthesizing these dyes is inefficient, time-consuming, and involves the use of excessive chemicals, as each dye must be prepared and isolated before evaluating its optical properties. DNA-templated synthesis has recently emerged as a powerful approach for synthesizing different types of organic molecules. This method allows for the rapid and convenient synthesis of diverse targets at microscopic scales, which is crucial during the discovery phase. The objective of this study is to develop a novel DNA-templated reaction for synthesizing cationic styryl cyanine dyes. The key to the success of the proposed method relies on the electrostatic binding of two cationic coupling partners (the heterocycles and aromatic aldehydes) to the DNA template. This brings the two coupling partners in close proximity and proper orientation for the reaction, resulting in an accelerated formation of the dye. The concept of the DNA-templated synthesis strategy was proven, and it successfully produced the desired styryl dyes from a wide range of substrates in a combinatorial fashion. The success of the dye formation was confirmed by UV-Vis and fluorescence spectroscopy, and in some cases, NMR spectroscopy and mass spectrometry. Importantly, the formation and responsiveness of these dyes to the DNA template, which also acted as the nucleic acid target, could be easily observed in situ. By utilizing different DNA templates and substrates, it was possible to identify new dyes that are responsive to a specific type of DNA template. Lastly, the templated styryl dye synthesis was successfully performed within live HeLa cells. However, nuclease digestion experiments confirm that the cellular RNA acted as the template instead of DNA probably due to the inaccessibility of the latter. Overall, this approach holds potential as a valuable tool for synthesizing and screening dyes that specifically target various types of nucleic acids or organelles within cells.

Field of Study: Chemistry

Student's Signature

Academic Year: 2022

Advisor's Signature

ACKNOWLEDGEMENTS

I would like to take this opportunity to express my deepest appreciation and gratitude to the individuals and institutions who have supported and contributed to the completion of this PhD thesis.

First and foremost, I am immensely grateful to my supervisor, Professor Dr. Tirayut Vilaivan, for the invaluable guidance, support, and expertise throughout my doctoral journey. His continuous encouragement, insightful feedback, and unwavering belief in my abilities have been instrumental in shaping the direction of this research. Furthermore, I would like to acknowledge Professor Dr. Wanchai Assavalapsakul and Dr. Chanat Aonbangkhen for their invaluable help, mentorship and guidance for fundamental biological techniques. Their assistances have been helpful in my growth and success. Their belief in my abilities and their constant encouragement motivated me to overcome obstacles and strive for excellence in the field.

I would like to extend my heartfelt appreciation to the current members of the TV lab, Chotima Vilaivan, Dr. Kotchakorn Supabowornsathit, Phanomsak Yukhet, Nattasiri Phaisarn, Mongkonkorn Thanakorncharoenwit, and Wachiraya Pinthongnoi for providing a stimulating academic environment and access to resources that have been essential for conducting this research. The support and encouragement I received from my colleagues have been truly inspiring. I am also truly grateful for former TV lab's members, Thitipong Khamkhenshornphanuch, Dr. Duangrat Nim-anussornkul, Dr. Jaru Taechalertpaisarn, Dr. Chayan Charoenpakdee, Dr. Boonsong Ditmangklo, Dr. Penthip Muangkaew, and Dr. Pattarakiat Seankongsuk. Their knowledge and experience have been involved in molding my own skills and capabilities, and I am truly grateful for the lessons I learned from them.

Unforgettably, I would like to express my gratitude to my family, especially my dad and my mom, for their unwavering love, encouragement, and patience throughout this demanding journey. Their constant support, understanding, and belief in my abilities have been a source of strength and motivation. Thank you to Kaiki for being cute all the time.

For my Master's sun, I do not think that I could handle difficult situations on my own without you. I am grateful for your constant support in everything you undertake and everything else you bring as my trusted companion.

Finally, I would like to acknowledge the financial support provided by The Second Century Fund Chulalongkorn University (C2F) and The 90th Anniversary of Chulalongkorn University Scholarship. These grants not only facilitated the completion of this research but has also opened doors to numerous opportunities for professional development.

To all those mentioned above and to anyone else who has contributed to this research attempt in any way, large or small, I offer my sincere gratitude. Your support, encouragement, and contributions have been involved in the completion of this PhD thesis. Thank you for being part of this significant milestone in my academic journey.

Kriangsak Faikhruea



TABLE OF CONTENTS

| | Page |
|--|-------------|
| ABSTRACT (THAI)..... | iii |
| ABSTRACT (ENGLISH)..... | iv |
| ACKNOWLEDGEMENTS..... | v |
| TABLE OF CONTENTS..... | vii |
| LIST OF TABLES..... | 1 |
| LIST OF FIGURES..... | 2 |
| LIST OF ABBREVIATIONS..... | 14 |
| CHAPTER I INTRODUCTION..... | 15 |
| 1.1 Background of nucleic acid staining dyes..... | 15 |
| 1.2 Styryl dyes..... | 19 |
| 1.2.1 Optical properties and mechanism of modulation..... | 20 |
| 1.2.2 Styryl dyes for nucleic acid detection..... | 22 |
| 1.2.3 Combinatorial synthesis of styryl dyes for targeted nucleic acid staining..... | 31 |
| 1.3 DNA templated reaction..... | 35 |
| 1.3.1 Conventional DNA-templated synthesis..... | 35 |
| 1.3.2 DNA-templated synthesis not involving base-pairing..... | 37 |
| 1.4 Templated synthesis of cyanine dyes..... | 43 |
| 1.5 Rationale and objective of this study..... | 46 |
| CHAPTER II EXPERIMENTAL SECTION..... | 47 |
| 2.1 Chemicals and reagents..... | 47 |
| 2.2 Synthesis of cationic methylated heterocycles as coupling partners..... | 49 |

| | |
|---|----|
| 2.2.1 Monocationic heteroaromatic substrates (<i>N</i> -methylation)..... | 49 |
| 2.2.2 Synthesis of polycationic 2-methylbenzothiazolium salt | 51 |
| 2.2.3 Modification of cationic side chain aromatic aldehyde | 53 |
| 2.3 Conventional synthesis of cationic styryl dyes | 56 |
| 2.4 DNA-templated synthesis of cationic styryl dyes | 61 |
| 2.5 Spectroscopic studies..... | 61 |
| 2.5.1 Fluorescence quantum yield of synthesized dyes | 61 |
| 2.5.2 Dye-DNA binding interaction study | 62 |
| 2.5.2 Evaluation of optical properties of the dyes from DNA-templated synthesis..... | 63 |
| 2.6 Kinetic study of DNA-templated synthesis..... | 64 |
| 2.7 Quantitation of styryl dye product from DNA-templated synthesis | 64 |
| 2.7.1 Quantitative NMR analysis..... | 64 |
| 2.7.2 UV-Visible spectroscopic analysis..... | 65 |
| 2.7.3 HPLC analysis..... | 65 |
| 2.8 Biological study..... | 66 |
| 2.8.1 Cell culture | 66 |
| 2.8.2 Cell imaging experiment..... | 66 |
| 2.8.3 Cell viability using MTT assay..... | 66 |
| 2.8.4 Templated synthesis of styryl dyes in cells | 67 |
| 2.8.5 Double-stranded RNA (dsRNA) production | 68 |
| CHAPTER III RESULTS AND DISCUSSION | 69 |
| 3.1 Concept validation of DNA-templated styryl dye synthesis | 69 |
| 3.1.1 Study of salt or buffer for templated reaction..... | 76 |

| | |
|---|-----|
| 3.1.2 Approachability of the templated styryl dye formation with various templates..... | 77 |
| 3.2 Kinetic study of the styryl dye formation from DNA-templated synthesis..... | 79 |
| 3.3 Isolation and quantitation of the styryl dye product..... | 80 |
| 3.4 Design and synthesis of more diversified cationic coupling partners..... | 85 |
| 3.5 Combinatorial DNA-templated styryl dye synthesis..... | 86 |
| 3.5.1 The effect of substituent on the benzothiazolium substrates..... | 86 |
| 3.5.2 Substituent effect on aromatic aldehyde substrates..... | 90 |
| 3.5.3 Effect of heterocycles bearing with an acidic methyl group..... | 95 |
| 3.6 DNA-templated styryl dye synthesis as a screening tool for dyes that are responsive to specific DNA structures..... | 97 |
| 3.7 Application of DNA-templated styryl dye synthesis in cells..... | 103 |
| 3.7.1 Fluorescence staining behavior in living cells of BT ⁺ -Ald ⁺ dye..... | 104 |
| 3.7.2 Toxicity of coupling partners..... | 108 |
| 3.7.3 Nucleic acid-templated reaction in live cells..... | 109 |
| 3.7.4 Concept validation of nucleic acid-templated reaction in live cells..... | 112 |
| 3.7.5 Applications of nucleic acid-templated dye synthesis in cells..... | 116 |
| CHAPTER IV CONCLUSION..... | 118 |
| REFERENCES..... | 120 |
| APPENDIX..... | 131 |
| VITA..... | 180 |

LIST OF TABLES

| | |
|---|-----|
| Table 2.1 Sequences of oligonucleotides employed in this study..... | 48 |
| Table 3.1 Retention time of the components in the DNA-templated reaction..... | 83 |
| Table 3.2 Evaluation of substituent effect on the BT substrates carrying electron-withdrawing and electron-donating substituents for the DNA-templated styryl dye synthesis..... | 89 |
| Table 3.3 Optical properties of the individually synthesized dyes (5-OMe-BT ⁺ -Ald ⁺ and 6-OMe-BT ⁺ -Ald ⁺). Condition: [Dye] = 1 μ M, [DNA] = 2 μ M in 10 mM PB (pH 7.0) (dsDNA = 5'-CCAGGGCATGGTAGATCACTGTACGCCGCG-3' + 5'-CGCGGCGTACAGTGATCTACCATGCCCTGG-3'). | 90 |
| Table 3.4 DNA-templated reaction for combinatorial synthesis of styryl dyes from various cationic benzothiazolium salts and aromatic aldehydes with positively-charged side chains. Condition: [Coupling partners] = 1 mM, [DNA] = 1 mg/mL incubating at room temperature for 2 days..... | 94 |
| Table 3.5 Optical properties (absorption (I_{Abs}) and relative fluorescence emission (I_{Em}/I_{Abs}) from combinatorial screening using heteroaromatic and cationic diethyl amino aromatic aldehyde substrate. | 97 |
| Table 3.6 Selectivity and binding constant of 2-QL ⁺ -MorpAld ⁺ dye towards various DNAs. Condition: [Dye] = 2 μ M, [DNA] = 0–1 μ M, [KCl] = 50 mM in 10 mM Tris-HCl buffer (pH 7.4). | 102 |
| Table A.1 Optical properties of the individually synthesized dyes from various heteroaromatic and <i>N,N</i> -diethylamino aromatic aldehyde. Conditions: [Dye] = 2 μ M, [DNA] = 1 μ M; [DNA (in bp)] : [Dye] = 15 : 1; all measurements were performed in 10 mM sodium phosphate buffer (pH 7.0). dsDNA = 5'-CGCGGCGTACAGTGATCTACCATGCCCTGG-3' + 3'-GCGCCGCATGTCAGTAGATGGTACGGGACC-5'. | 135 |

LIST OF FIGURES

| | |
|--|-----------|
| Figure 1.1 Nucleic acid structures..... | 15 |
| Figure 1.2 Commercial dyes for nucleic acid detection..... | 18 |
| Figure 1.3 General structure of polymethine dyes, examples of symmetrical and unsymmetrical cyanine dyes and generic designs of styryl dyes..... | 19 |
| Figure 1.4 Dynamics of Twisted Intramolecular Charge Transfer (TICT)..... | 21 |
| Figure 1.5 Visualization of nucleolus and chromosomes using co-staining with SYTO-RNA and Hoechst 33342, respectively. Digest experiments performed using RNase and DNase enzymes, emission analysis of probe 1 in viscous solution and in the presence of nucleic acid, and models illustrating the interaction of probe 1 with DNA and RNA fragments in Wang's work..... | 23 |
| Figure 1.6 (A) Structural comparison of FM1-43 and the newly developed styryl probes, SP-468 (Styrylpyridinium) and SQ-535 (Styryl Quinolinium), along with their respective orientation within the plasma membrane. (B) Laser scanning confocal imaging of plant cells (<i>Nicotiana benthamiana</i>) and live cells from Hela cell lines stained with FM1-43 and SP-468 in Collot's work. | 24 |
| Figure 1.7 Compound 12e exhibits binding to rRNA in cells in Saady's work. | 25 |
| Figure 1.8 Intracellular localization of O-PY, BZ-Se and BZ-IND in Ćipor's work. | 26 |
| Figure 1.9 Applications of dicationic styryl dye (BT2+NEt ₂) for cellular nucleic acid detection in Supabowornsathit's work. | 27 |
| Figure 1.10 Cationic styryl dyes for DNA labelling and selectivity toward cancer cells in Wangngae's work..... | 28 |
| Figure 1.11 Formation of helical aggregations by ctDNA in the presence of Bis(styryl)pyridinium dyes with OMe or/and NMe ₂ substituents..... | 29 |
| Figure 1.12 Styryl dyes with <i>N</i> -methylpiperazine and <i>N</i> -phenylpiperazine substituents for targeting AT-rich and G-quadruplex DNA and cell staining. | 31 |

| | |
|--|-----------|
| Figure 1.13 Combinatorial synthesis of organelle-targeted fluorescent dye by Rosania et al. | 33 |
| Figure 1.14 Combinatorial synthesis of RNA-selective styryl dyes and cell-based screening. | 34 |
| Figure 1.15 (A) Molecular architecture of reactants for DTS, (B) Distance-independent DTS, and (C) Multistep DTS. | 37 |
| Figure 1.16 DNA-templated asymmetric Diels-Alder reaction. | 38 |
| Figure 1.17 The concept of target-guided synthesis (TGS) involves bringing together specific reactive molecules in close proximity through the target molecule itself, allowing them to undergo irreversible reactions and ultimately form the desired ligand. | 40 |
| Figure 1.18 In situ synthesis of triazoles via click chemistry catalyzed by G-quadruplex DNA (H-Telo). | 41 |
| Figure 1.19 Schematic representation of templated cycloaddition between selective azide and alkyne partners using $G_4 \cdot Au@Fe_3O_4$ nanoparticles. | 42 |
| Figure 1.20 Schematic representation of the target-guided synthesis of G4-selective ligands by DNA-functionalized magnetic gold nanoparticles. | 43 |
| Figure 1.21 Reversible synthesis of fluorescent imine from non-fluorescent amine and weakly fluorescent aldehyde in aqueous media using either surfactants (below and above their CMC) or double-stranded DNA (acting as a reaction host). ... | 44 |
| Figure 1.22 Symmetrical trimethine cyanine dye synthesis from two non-fluorescent labeled-PNA precursors via DNA-templated reaction guided by (A) distance of precursors and (B) DNA structure. | 45 |
| Figure 2.1 <i>N</i> -methylation of nitrogen-contained heterocycles. | 49 |
| Figure 2.2 Modification of cationic side chain heterocycles. | 51 |
| Figure 2.3 Modification of cationic side chain aromatic aldehydes. | 53 |

- Figure 3.1** (A) A model reaction for DNA-templated synthesis and (B) Work-flow for the combinatorial screening of DNA-templated styryl dye synthesis.70
- Figure 3.2** (A) Combinatorial screening of the DNA-templated styryl dye synthesis from benzothiazoles and diethylamino-substituted aldehydes. Condition: [Coupling partners] = 1 mM, [stDNA] = 1 mg/mL incubating at room temperature (30 °C) (B) UV-visible spectra and (C) Fluorescence spectra ($\lambda_{\text{ex}} = 565 \text{ nm}$) of crude reaction products from the DNA templated reaction.....71
- Figure 3.3** (A) Control experiment with only one of two coupling partners in presence of DNA and (B) UV-Visible spectrum. Condition: [Coupling partners] = 1 mM, [DNA] = 1 mg/mL incubating at room temperature (30 °C) for 2 days.....73
- Figure 3.4** (A) Model reaction of dGMP-Ald⁺ (B) ¹H NMR and (C) HMBC spectrum of the crude. Condition: [dGMP] = 1 mM, [Ald⁺] = 1 mM incubating at room temperature (30 °C) for 2 days.....75
- Figure 3.5** Effect of buffers and salt. Condition: [coupling partners] = 1 mM, [DNA] = 1 mg/mL, [salt]/[buffer] = 10 mM incubating at room temperature (30 °C).77
- Figure 3.6** Effect of templates on DNA-templated synthesis. Condition: [coupling partners] = 1 mM, [DNA] = 1 mg/mL, [salt]/[buffer] = 10 mM incubating at room temperature for 2 days.....78
- Figure 3.7** Kinetic study of the DNA-templated synthesis of BT⁺-Ald⁺ in the presence of (A) 1 mg/mL stDNA, and (B) 2 mg/mL of stDNA. (C) Plots between ln (A₅₇₀) and time. Condition: [Ald⁺] = 10 mM, [DNA] = 1 mg/mL, incubating at room temperature (25 °C).....80
- Figure 3.8** (A) Extraction of styryl dye from Dye-DNA complex using [BMIM]PF₆ ionic liquid. Condition: [Ald⁺] = 1 mM, [DNA] = 1 mg/mL, incubating at room temperature for 14 days. (B) ¹H NMR spectra (128 scans) of the extracted styryl dye comparing with reference BT²⁺ dye and the corresponding coupling partners, BT⁺ and Ald⁺.....82
- Figure 3.9** HPLC chromatograms of templated reaction for BT⁺-Ald⁺ synthesis after incubating for 2 days. Condition: [Ald⁺] = 1 mM, [DNA] = 1 mg/mL incubating at room

temperature, reversed-phase HPLC was performed using C18 column eluting with acetonitrile:water with 0.1% TFA gradients.84

Figure 3.10 Schematic illustration of the concept of the nucleic acid-templated synthesis of cationic styryl dyes. (A) Diverse sets of cationic heteroaromatic and aldehyde substrates can (B) bind to the anionic (from phosphate backbone) nucleic acid template and then react to form styryl dyes in the DNA-bound form. (C) The spectroscopic profiles (UV-vis absorption and fluorescence emission) of the DNA-dye-bound form are simultaneously evaluated.85

Figure 3.11 Synthesis of the cationic coupling partners used in this study.....86

Figure 3.12 Structures and yields of cationic coupling partners successfully prepared in this work.87

Figure 3.13 Study of substituent effect on BT heteroaromatic substrate using diverse sets of electron-withdrawing and electron-donating substituents. Condition: $[Ald^+] = 1$ mM, $[DNA] = 1$ mg/mL incubating at room temperature for 2 days.89

Figure 3.14 DNA-templated reaction for combinatorial synthesis of styryl dyes from various cationic benzothiazolium salts and aromatic aldehydes with positively-charged side chains. Condition: $[coupling\ partners] = 1$ mM, $[DNA] = 1$ mg/mL, incubating at room temperature for 2 days.....93

Figure 3.15 Observation of DNA-templated synthesis (under white light and UV 312 nm) from a combinatorial screening of various methyl heteroaromatic substrates and Ald^+ after incubation for 2 and 14 days. Condition: $[Coupling\ partners] = 2$ mM, $[DNA] = 1$ mg/mL incubating at room temperature.....96

Figure 3.16 (A) Hydrogen bonding pattern in a G-quadruplex. Three topologies adopted by G4 nucleic acids and their respective circular dichroism signatures of (B) parallel (C) antiparallel and (D) hybrid form.....99

Figure 3.17 CD spectra of GQ-DNAs (A) c-MYC (B) 22AG in low concentration of buffer. Condition: $[DNA] = 1$ μ M in 1 mM Tris-HCl (pH 7.4)..... 100

Figure 3.18 Application of DNA-templated synthesis for the discovery of styryl dyes that are responsive to some specific DNA structures using quinolinium substrates and various alkyl amino aromatic aldehydes in the presence of different DNA templates (ssDNA, dsDNA, and GQs). Condition: [coupling partners] = 2 mM, [DNA] = 0.5 $\mu\text{g/mL}$, [KCl] = 5 mM in 1 mM Tris-HCl (pH 7.4) incubating at room temperature for 14 days.

..... 101

Figure 3.19 Photographs of 2-QL⁺-MorpAld⁺ prepared by the conventional method in the absence and presence of various DNAs (*under white light and 312 nm UV light*). Condition: [Dye] = 2 μM , [DNA] = 4 μM , [KCl] = 50 mM in 10 mM Tris-HCl buffer (pH 7.4).

..... 102

Figure 3.20 Applicability of nucleic acid-templated synthesis of styryl dye in cells. 103

Figure 3.21 Co-localization between BT⁺-Ald⁺ dye and RNA staining dyes in HeLa cells. Condition: HeLa cell (5×10^4 cells/well) in DMEM, [Dye] = 20 μM incubated for 45 minutes at 37 °C under 5% CO₂ atmosphere, SYTO RNA select® Green 500 μM for 20 minutes, DAPI (200 ng/mL) for 15 minutes.

..... 105

Figure 3.22 Fluorescence images of nucleic acid staining confirmed by enzymatic digestion (DNase I and RNase A). Condition: HeLa cell (5×10^4 cells/well) in DMEM, [Dye] = 20 μM incubated for 45 minutes at 37 °C under 5% CO₂ atmosphere, SYTO RNA select® Green 500 μM for 20 minutes, DAPI (200 ng/mL) for 15 minutes.

..... 106

Figure 3.23 Fluorescence responsiveness of BT⁺-Ald⁺ dye toward several nucleic acid. Condition: [Dye] = 1 μM , [Nucleic acid] = 2 μM in bp in 10 mM PB (pH 7.0).

..... 107

Figure 3.24 Structure of DNA-Histone complexes.

..... 108

Figure 3.25 Toxicity of the cationic coupling partners for a model templated styryl dye formation in HeLa cells. Condition: HeLa cell (1×10^4 cells/well) in DMEM, [Dye] = 10-100 μM incubated for 24 hours at 37 °C under 5% CO₂ atmosphere.

..... 109

Figure 3.26 (A) UV-Visible and (B) Fluorescence spectra of nucleic acid-templated styryl dye formation in cell culture media. Condition: [coupling partners] = 0.2 mM,

[stDNA] = 1 mg/mL in DMEM incubated for 3 days at 37 °C under 5% CO₂ atmosphere. 110

Figure 3.27 Live cells imaging from nucleic acid-templated synthesis of styryl dye in HeLa cells. The fluorescence images were observed from BT⁺+Ald⁺ and BT⁺+AldPy⁺ coupling partners after incubation for 3 days. Condition: HeLa cell (5x10⁴ cells/well) in DMEM, [coupling partner] = 0.2 mM incubated for 3 days at 37 °C under 5% CO₂ atmosphere, Hoechst22345 (1 ng/mL) for 15 minutes. 112

Figure 3.28 Applicability of nucleic acid-templated synthesis of styryl dye in HeLa cells. The fluorescence images were observed from (A) BT⁺+Ald⁺ and (B) BT⁺+AldPy⁺ coupling partners (0.2 mM of each) after incubation for 3 days (Red channel; $\lambda_{\text{Ex}} = 305 \text{ nm}$, $\lambda_{\text{Em}} = 617 \text{ nm}$, Blue channel; $\lambda_{\text{Ex}} = 353 \text{ nm}$, $\lambda_{\text{Em}} = 465 \text{ nm}$). Condition: HeLa cell (5x10⁴ cells/well) in DMEM, [coupling partner] = 0.2 mM incubated for 3 days at 37 °C under 5% CO₂ atmosphere, RNase A (25 $\mu\text{g/mL}$) or DNase I (30 $\mu\text{g/mL}$) at 37 °C for 4 hours, DAPI (1 $\mu\text{g/mL}$) for 20 minutes at room temperature. 114

Figure 3.29 Control experiment of nucleic acid-templated synthesis of styryl dye in HeLa cells. Condition: HeLa cell (5x10⁴ cells/well) in DMEM, [coupling partner] = 0.2 mM incubated for 3 days at 37 °C under 5% CO₂ atmosphere, DAPI (1 $\mu\text{g/mL}$) for 20 minutes at room temperature. 115

Figure 3.30 Applicability of nucleic acid-templated synthesis of styryl dye in fixed HeLa cells. Condition: HeLa cell (5x10⁴ cells/well) in DMEM, [coupling partner] = 0.2 mM incubated for 7 days at 37 °C under 5% CO₂ atmosphere. 116

Figure A.1 Study of substituent effect on BT heteroaromatic substrate using diverse sets of (A) electron-withdrawing and (B) electron-donating substituents. Spectroscopic profiles; (C) Absorption spectra and (D) Emission spectra ($\lambda_{\text{Ex}} = 565 \text{ nm}$) of dye-DNA bound form from combinatorial screening. 132

Figure A.2 Study of heteroaromatic effect on DNA-templated synthesis using various heterocycle substrates (A) templated reaction (B) UV-visible and fluorescence spectra. 134

- Figure A.3** HPLC chromatogram of (A) BT⁺ (B) Ald⁺ and (C) [BMIM]PF₆ observed at 220 nm. 136
- Figure A.4** HPLC chromatogram of BT⁺-Ald⁺ dye observed at (A) 220 nm and (B) 550 nm. 137
- Figure A.5** HPLC chromatogram of crude from DNA-templated synthesis for BT⁺-Ald⁺ after incubating for 14 days observed at (A) 220 nm and (B) 550 nm. 138
- Figure A.6** HPLC chromatogram of crude from DNA-templated synthesis for 4-F-BT⁺-Ald⁺ after incubating for 2 days observed at (A) 220 nm and (B) 550 nm. 139
- Figure A.7** HPLC chromatogram of crude from DNA-templated synthesis for 5-Br-BT⁺-Ald⁺ after incubating for 2 days observed at (A) 220 nm and (B) 550 nm. 140
- Figure A.8** HPLC chromatogram of crude from DNA-templated synthesis for 5-Cl-BT⁺-Ald⁺ after incubating for 2 days observed at (A) 220 nm and (B) 550 nm. 141
- Figure A.9** HPLC chromatogram of crude from DNA-templated synthesis for 5-F-BT⁺-Ald⁺ after incubating for 2 days observed at (A) 220 nm and (B) 550 nm. 142
- Figure A.10** HPLC chromatogram of crude from DNA-templated synthesis for 5-NO₂-BT⁺-Ald⁺ after incubating for 2 days observed at (A) 220 nm and (B) 550 nm. 143
- Figure A.11** HPLC chromatogram of crude from DNA-templated synthesis for 6-F-BT⁺-Ald⁺ after incubating for 2 days observed at (A) 220 nm and (B) 550 nm. 144
- Figure A.12** HPLC chromatogram of crude from DNA-templated synthesis for 5,6-F-BT⁺-Ald⁺ after incubating for 2 days observed at (A) 220 nm and (B) 550 nm. 145
- Figure A.13** HPLC chromatogram of crude from DNA-templated synthesis for 6-CF₃-BT⁺-Ald⁺ after incubating for 2 days observed at (A) 220 nm and (B) 550 nm. 146
- Figure A.14** HPLC chromatogram of crude from DNA-templated synthesis for 6-OCF₃-BT⁺-Ald⁺ after incubating for 2 days observed at (A) 220 nm and (B) 550 nm. 147
- Figure A.15** HPLC chromatogram of crude from DNA-templated synthesis for 7-F-BT⁺-Ald⁺ after incubating for 2 days observed at (A) 220 nm and (B) 550 nm. 148

| | |
|--|------------|
| Figure A.16 HPLC chromatogram of crude from DNA-templated synthesis for 5-OMe-BT ⁺ -Ald ⁺ after incubating for 2 days observed at (A) 220 nm and (B) 550 nm. | 149 |
| Figure A.17 HPLC chromatogram of crude from DNA-templated synthesis for 5-Me-BT ⁺ -Ald ⁺ after incubating for 2 days observed at (A) 220 nm and (B) 550 nm. | 150 |
| Figure A.18 HPLC chromatogram of crude from DNA-templated synthesis for 5,6-Me-BT ⁺ -Ald ⁺ after incubating for 2 days observed at (A) 220 nm and (B) 550 nm. | 151 |
| Figure A.19 HPLC chromatogram of crude from DNA-templated synthesis for 6-OMe-BT ⁺ -Ald ⁺ after incubating for 2 days observed at (A) 220 nm and (B) 550 nm. | 152 |
| Figure A.20 HPLC chromatogram of crude from DNA-templated synthesis for 6-NPr ₃ -BT ⁺ -Ald ⁺ after incubating for 2 days observed at (A) 220 nm and (B) 550 nm. | 153 |
| Figure A.21 Mass spectrum (MALDI-TOF) of crude from DNA-templated synthesis for BT ⁺ -Ald ⁺ | 154 |
| Figure A.22 Mass spectrum (MALDI-TOF) of crude from DNA-templated synthesis for 4-F-BT ⁺ -Ald ⁺ | 154 |
| Figure A.23 Mass spectrum (MALDI-TOF) of crude from DNA-templated synthesis for 5-Br-BT ⁺ -Ald ⁺ | 155 |
| Figure A.24 Mass spectrum (MALDI-TOF) of crude from DNA-templated synthesis for 5-Cl-BT ⁺ -Ald ⁺ | 155 |
| Figure A.25 Mass spectrum (MALDI-TOF) of crude from DNA-templated synthesis for 5-F-BT ⁺ -Ald ⁺ | 156 |
| Figure A.26 Mass spectrum (MALDI-TOF) of crude from DNA-templated synthesis for 5-NO ₂ -BT ⁺ -Ald ⁺ | 156 |
| Figure A.27 Mass spectrum (MALDI-TOF) of crude from DNA-templated synthesis for 6-F-BT ⁺ -Ald ⁺ | 157 |
| Figure A.28 Mass spectrum (MALDI-TOF) of crude from DNA-templated synthesis for 5,6-F-BT ⁺ -Ald ⁺ | 157 |

| | |
|--|------------|
| Figure A.29 Mass spectrum (MALDI-TOF) of crude from DNA-templated synthesis for 6-CF ₃ -BT ⁺ -Ald ⁺ | 158 |
| Figure A.30 Mass spectrum (MALDI-TOF) of crude from DNA-templated synthesis for 6-OCF ₃ -BT ⁺ -Ald ⁺ | 158 |
| Figure A.31 Mass spectrum (MALDI-TOF) of crude from DNA-templated synthesis for 7-F-BT ⁺ -Ald ⁺ | 159 |
| Figure A.32 Mass spectrum (MALDI-TOF) of crude from DNA-templated synthesis for 5-OMe-BT ⁺ -Ald ⁺ | 159 |
| Figure A.33 Mass spectrum (MALDI-TOF) of crude from DNA-templated synthesis for 5-Me-BT ⁺ -Ald ⁺ | 160 |
| Figure A.34 Mass spectrum (MALDI-TOF) of crude from DNA-templated synthesis for 5,6-Me-BT ⁺ -Ald ⁺ | 160 |
| Figure A.35 Mass spectrum (MALDI-TOF) of crude from DNA-templated synthesis for 6-OMe-BT ⁺ -Ald ⁺ | 161 |
| Figure A.36 Mass spectrum (MALDI-TOF) of crude from DNA-templated synthesis for 6-NPr ₂ -BT ⁺ -Ald ⁺ | 161 |
| Figure A.37 Mass spectrum (MALDI-TOF) of crude from DNA-templated synthesis for BX ⁺ -Ald ⁺ | 162 |
| Figure A.38 Mass spectrum (MALDI-TOF) of crude from DNA-templated synthesis for TMIN ⁺ -Ald ⁺ | 162 |
| Figure A.39 Mass spectrum (MALDI-TOF) of crude from DNA-templated synthesis for 2-QL ⁺ -Ald ⁺ | 163 |
| Figure A. 40 Mass spectrum (MALDI-TOF) of crude from DNA-templated synthesis for 4-QL ⁺ -Ald ⁺ | 163 |
| Figure A.41 Mass spectrum (MALDI-TOF) of crude from DNA-templated synthesis for 4-PY ⁺ -Ald ⁺ | 164 |

| | |
|--|------------|
| Figure A.42 Mass spectrum (MALDI-TOF) of crude from DNA-templated synthesis for BT-NH ₂ ⁺ -Ald ⁺ | 164 |
| Figure A.43 Mass spectrum (MALDI-TOF) of crude from DNA-templated synthesis for 2-QL ⁺ -MorpAld ⁺ catalysed by c-MYC. | 165 |
| Figure A.44 Mass spectrum (MALDI-TOF) of crude from DNA-templated synthesis for 2-QL ⁺ -MorpAld ⁺ catalysed by c-MYC. | 165 |
| Figure A.45 Mass spectrum (MALDI-TOF) of crude from dGMP-Ald ⁺ | 166 |
| Figure A. 46 ¹ H NMR spectrum of 2,3-dimethylbenzo[d]thiazol-3-ium iodide (BT ⁺). 167 | |
| Figure A. 47 ¹ H NMR spectrum of 2-amino-3-methylbenzo[d]thiazol-3-ium iodide (BT-NH ₂ ⁺). | 167 |
| Figure A.48 ¹ H NMR spectrum of 2-methyl-3-(3-(pyridin-1-ium-1-yl)propyl)benzo[d]thiazol-3-ium bromide (BTC3Py ²⁺)..... | 168 |
| Figure A.49 ¹ H NMR spectrum of 2-methyl-3-(4-(pyridin-1-ium-1-yl)butyl)benzo[d]thiazol-3-ium bromide (BTC4Py ²⁺). | 168 |
| Figure A.50 ¹ H NMR spectrum of 2-methyl-3-(5-(pyridin-1-ium-1-yl)pentyl)benzo[d]thiazol-3-ium bromide (BTC5Py ²⁺)..... | 169 |
| Figure A.51 ¹ H NMR spectrum of 3,3'-(propane-1,3-diyl)bis(2-methylbenzo[d]thiazol-3-ium) bromide (BisBT) ²⁺). | 169 |
| Figure A.52 ¹ H NMR spectrum of 1,4-dimethylpyridin-1-ium iodide (4-Py ⁺)..... | 170 |
| Figure A.53 ¹ H NMR spectrum of 1,2,3,3-tetramethyl-3H-indol-1-ium iodide (TMIN ⁺). | 170 |
| Figure A.54 ¹ H NMR spectrum of 2,3-dimethylbenzo[d]oxazol-3-ium iodide (BX ⁺). . | 171 |
| Figure A.55 ¹ H NMR spectrum of 1,2-dimethylquinolin-1-ium iodide (2-QL ⁺). | 171 |
| Figure A.56 ¹ H NMR spectrum of 1,4-dimethylquinolin-1-ium iodide (4-QL ⁺). | 172 |
| Figure A.57 ¹ H NMR spectrum of 4-(5-(diethylamino)-2-formylphenoxy)-N,N,N-trimethylbutan-1-aminium bromide (Ald(NEt ₂) ⁺). | 172 |

- Figure A.58** ^1H NMR spectrum of 4-(2-formyl-5-(4-methylpiperazin-1-yl)phenoxy)-*N,N,N*-trimethylbutan-1-aminium bromide (Ald(Piz) $^+$)..... 173
- Figure A.59** ^1H NMR spectrum of 4-(2-formyl-5-morpholinophenoxy)-*N,N,N*-trimethylbutan-1-aminium bromide (Ald(Morp) $^+$)..... 173
- Figure A.60** ^1H NMR spectrum of 4-((9-formyl-2,3,6,7-tetrahydro-1*H*,5*H*-pyrido[3,2,1-*ij*]quinolin-8-yl)oxy)-*N,N,N*-trimethylbutan-1-aminium bromide (Ald(Ju) $^+$)..... 174
- Figure A.61** ^1H NMR spectrum of 4-((1-formylnaphthalen-2-yl)oxy)-*N,N,N*-trimethylbutan-1-aminium bromide (NaphAld $^+$)..... 174
- Figure A.62** ^1H NMR spectrum of 4-(5-(azetidin-1-yl)-2-formylphenoxy)-*N,N,N*-trimethylbutan-1-aminium bromide (Ald(Aze) $^+$). 175
- Figure A.63** ^1H NMR spectrum of (*E*)-2-(4-(diethylamino)-2-(4-(trimethylammonio)butoxy)styryl)-5-methoxy-3-methylbenzo[d]thiazol-3-ium bromide iodide (5-OMe-BT $^+$ -Ald(NEt $_2$) $^+$). 175
- Figure A.64** ^1H NMR spectrum of (*E*)-2-(4-(diethylamino)-2-(4-(trimethylammonio)butoxy)styryl)-6-methoxy-3-methylbenzo[d]thiazol-3-ium bromide iodide ((6-OMe-BT $^+$ -Ald(NEt $_2$) $^+$). 176
- Figure A.65** ^1H NMR spectrum (*E*)-1-methyl-2-(4-morpholino-2-(4-(trimethylammonio)butoxy)styryl)quinolin-1-ium bromide iodide (2-QL $^+$ -MorpAld $^+$). 176
- Figure A.66** ^1H NMR spectrum (*E*)-2-(4-(Diethylamino)-2-(4-(trimethylammonio)butoxy)styryl)-1,3,3-trimethyl-3*H*-indol-1-ium hexafluorophosphate (TMIN $^+$ -Ald $^+$)..... 177
- Figure A.67** ^1H NMR spectrum (*E*)-2-(4-(diethylamino)-2-(4-(trimethylammonio)butoxy)styryl)-3-methylbenzo[d]oxazol-3-ium hexafluorophosphate (BX $^+$ -Ald $^+$)..... 177
- Figure A.68** ^1H NMR spectrum (*E*)-2-(4-(diethylamino)-2-(4-(trimethylammonio)butoxy)styryl)-1-methylquinolin-1-ium hexafluorophosphate (2-QL $^+$ -Ald $^+$). 178


Figure A.69 ^1H NMR spectrum (*E*)-4-(4-(diethylamino)-2-(4-(trimethylammonio)butoxy)styryl)-1-methylquinolin-1-ium hexafluorophosphate (4-QL⁺-Ald⁺) 178

Figure A.70 ^1H NMR spectrum (*E*)-4-(4-(diethylamino)-2-(4-(trimethylammonio)butoxy)styryl)-1-methylpyridin-1-ium hexafluorophosphate (2-PY⁺-Ald(NEt₂)⁺). 179



LIST OF ABBREVIATIONS

| | | |
|---------|---|-----------------------|
| DNA | = | Deoxyribonucleic acid |
| RNA | = | Ribonucleic acid |
| ssDNA | = | Single-stranded DNA |
| dsDNA | = | Double-stranded DNA |
| dsRNA | = | Double-stranded RNA |
| tRNA | = | Transfer RNA |
| rRNA | = | Ribosomal RNA |
| siRNA | = | Small interfering RNA |
| GQ | = | G-quadruplex |
| IL | = | Ionic liquid |
| mM | = | Milli molar |
| μ M | = | Micro molar |
| μ L | = | Micro liter |
| Em | = | Emission |
| Ex | = | Excitation |
| Abs | = | Absorption |

The image contains a large, faint watermark of the Chulalongkorn University logo. The logo features a central emblem with a crown and a sunburst, surrounded by a circular border with Thai script. Below the emblem, the text 'จุฬาลงกรณ์มหาวิทยาลัย' and 'CHULALONGKORN UNIVERSITY' is visible.

CHAPTER I

INTRODUCTION

1.1 Background of nucleic acid staining dyes

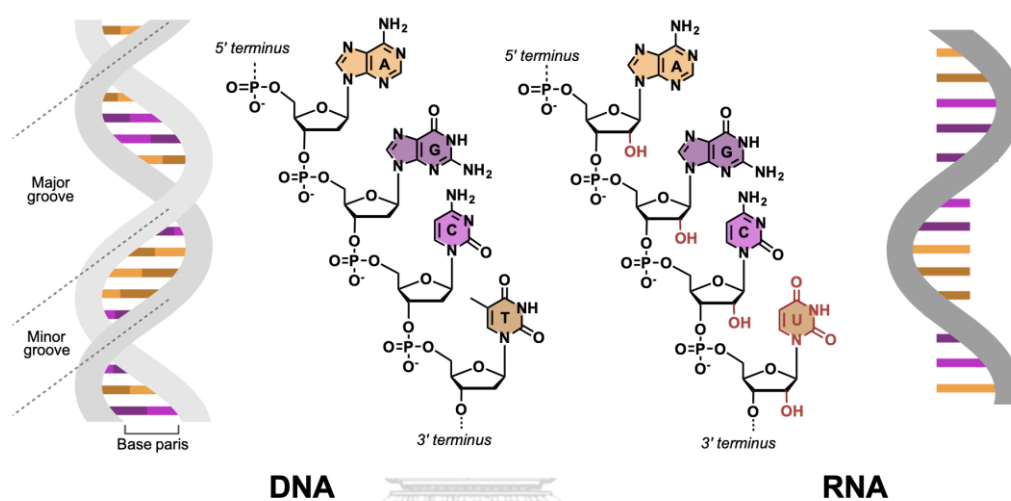


Figure 1.1 Nucleic acid structures.

Nucleic acids (**Figure 1.1**) are complex biomolecules that play a fundamental role in the storage and expression of genetic information. They are present in all living organisms, including plants, animals, and microorganisms. There are two primary types of nucleic acids: deoxyribonucleic acid (DNA) and ribonucleic acid (RNA). Both DNA and RNA are crucial for the transfer and expression of genetic information. However, there are fundamental differences in the structures and functions between the two. DNA acts as a genetic material, carrying the necessary instructions for protein production (via mRNA) and the overall development and functioning of an organism. On the other hand, RNA plays a critical role in converting the genetic information stored in DNA into functional proteins not only by acting as a

template (mRNA) but also involving in the machinery necessary for the protein synthesis (tRNA, rRNA).¹ In addition, RNA also plays important regulatory roles in the protein production.²

Nucleic acid detection is essential for various applications, enabling the identification, diagnosis, monitoring, and understanding of genetic information, diseases, and biological processes. It provides valuable insights that help improve human health, advance scientific knowledge, and support decision-making in various fields, such as medical diagnostics,³ research,⁴ forensics,⁵ and infectious disease monitoring.⁶

In general, commonly used techniques for nucleic acid detection can be categorized into the Polymerase Chain Reaction (PCR)⁷ and related isothermal amplification techniques, such as loop-mediated isothermal amplification (LAMP) and recombinase polymerase amplification (RPA) whereby the sequence of the template is read by the polymerase enzymes.⁸ Another important technique is the Nucleic Acid Hybridization,⁹ including Nucleic Acid Chips/Beads Arrays,¹⁰ whereby the sequence is read by specific hybridization with a specific nucleic acid probe. Finally, in Nucleic Acid Sequencing,¹¹ the sequence of the nucleic acid can be read by the use of polymerase and chain-terminating ddNTP or by measuring the electrical signal change upon passing the nucleic acid strand through a nanopore channel.¹² Each strategy still have limitation in terms of practicality, sensitivity, specificity not only among different related nucleic acid targets but also the ability to withstand interference when applied to biological substances such as serum, saliva, urine, and cell extracts.¹³

Nucleic acid stains are dyes that can bind to nucleic acids and show detectable optical responses, mostly in the form of fluorescence. Due to their

simplicity, speed, visual detection capabilities, versatility, cost-effectiveness, compatibility with other techniques, non-destructive nature, and high sensitivity, several dyes have long been used as an important tool for the detection and visualization of nucleic acids. These staining dyes allow for rapid qualitative analysis, direct visual readout, and broad applicability across different sample types, both isolated nucleic acids and cells/tissues. While they may not provide the same level of specificity or quantification as some advanced methods, nucleic acid staining techniques are valuable tools in research, diagnostics, and education settings, providing accessible and efficient detection of nucleic acids. In addition, they can be used as a purely visualizing agent in combination with a more specific technique such as PCR/LAMP or probe-based hybridization.¹⁴

Different types of organic dyes have the capability to bind to nucleic acids, leading to unique optical responses that can be utilized for the identification of specific sequences, abnormalities, and structural changes in nucleic acids both in vitro and within the biological systems. These optical responses may serve both qualitative and quantitative purposes. Examples of commercially available staining dyes that exhibit strong fluorescence signals (such as DAPI,¹⁵ ethidium bromide,^{16, 17} and SYBR® Green I^{18, 19}) or color changes (like methylene blue²⁰ and crystal violet²¹) in the presence of nucleic acids are shown in **Figure 1.2**.

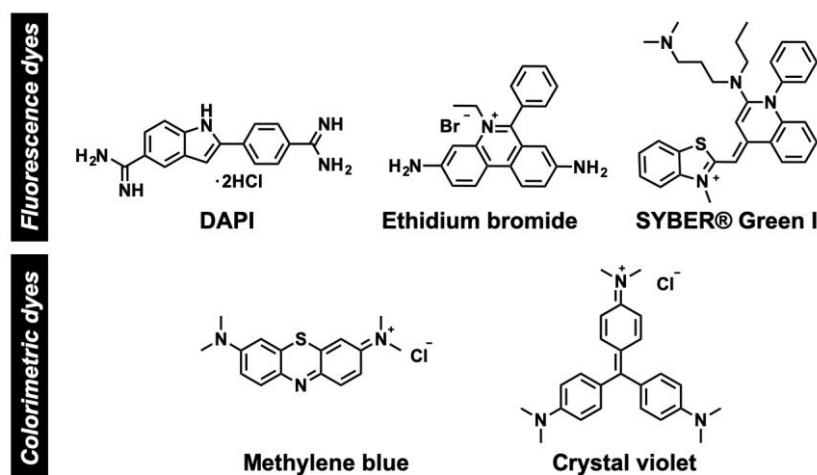


Figure 1.2 Commercial dyes for nucleic acid detection.

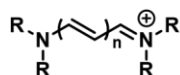
However, many of these commercially available staining dyes have concerning issues with mutagenicity and toxicity, thus posing risks to researchers and the environment. Moreover, these dyes are often expensive and may lack certain desirable properties, such as specific excitation/emission wavelengths and selectivity for different nucleic acid structures or sequences.²² Consequently, there is a persistent challenge to find new nucleic acid staining agents that possess lower toxicity, adjustable optical properties, and other desirable characteristics.

Among the various nucleic acid stains, cationic planar and conjugated organic molecules are particularly promising candidates. These molecules exhibit inherent binding affinity towards nucleic acids and offer optical properties that can be easily adjusted by modifying their molecular structure. This tunability allows researchers to fine-tune the photonic and electronic properties of these molecules, making them attractive alternatives in the search for novel nucleic acid staining agents.²³

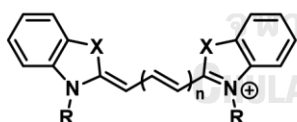
1.2 Styryl dyes

Styryl dyes are a generic class of conjugated organic dyes relating to the well-known cyanine dyes. Cyanine dyes belong to a subgroup called polymethines, which have an odd number of methine groups connecting between two nitrogen atoms as end groups that can be part of heteroaromatic rings.²⁴ On the other hand, styryl dyes consist of two aromatic parts with complementary electronic properties linking together through one or more conjugated double bonds with even number of methine groups.²⁵ The majority of styryl dyes have an electron-rich aromatic ring system connected to an electron-deficient heteroaromatic ring system via a C=C connector (Ar-CH=CH-) (a styryl group), hence the origin of the name “styryl dye” (Figure 1.3).

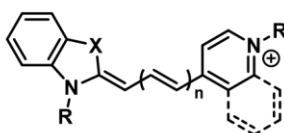
Polymethine dyes:



Cyanine dyes:

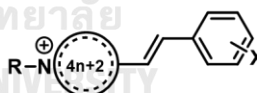


Symmetrical cyanine dyes

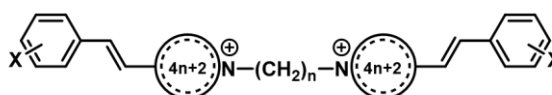


Unsymmetrical cyanine dyes

Styryl dyes:



Monocationic styryl dyes



Dimeric styryl dyes

Figure 1.3 General structure of polymethine dyes, examples of symmetrical and unsymmetrical cyanine dyes and generic designs of styryl dyes.

Optical properties of styryl dyes are generally highly sensitive to changes in their environment, such as solvent polarity,²⁶ pH or aggregation states. They typically exhibit visible color and/or fluorescence changes even with slight alterations in the surrounding environment. Moreover, styryl dyes demonstrate remarkable photostability and exhibit a high fluorescence quantum yield (Φ_F) under the right environment. These dyes have found extensive use in the photographic industry as sensitizers and additives.^{27, 28} Additionally, they have great potential in various other applications such as molecular photovoltaic cells,²⁹ optical molecular systems,³⁰ and artificial photosynthesis.³¹ In recent years, styryl dyes have been employed as fluorescent probes in numerous analytes, particularly for detecting peroxidase activities,³² specific ions,³³ or biomolecules.³⁴ They have also been utilized as fluorescent probes for nucleic acids sensing in various applications.³⁵⁻⁴⁶

1.2.1 Optical properties and mechanism of modulation

Styryl dyes have an asymmetrical donor- π -acceptor structure, often referred to as a push-pull system, which contributes to their remarkable optical characteristics. These dyes exhibit significant changes in their optical properties depending on the surrounding environment due to their dipolar nature. For example, the absorption and emission wavelengths and intensities of the same dye are different in different solvents. Such solvatochromic behavior can be understood by considering dipole moments of the dye. If the excited state possesses a higher dipole moment than the ground state, it is preferentially stabilized by more polar solvents. As a result, the energy gap between the two states became narrower, leading to a shift in the absorption and emission spectra towards the red region.⁴⁷

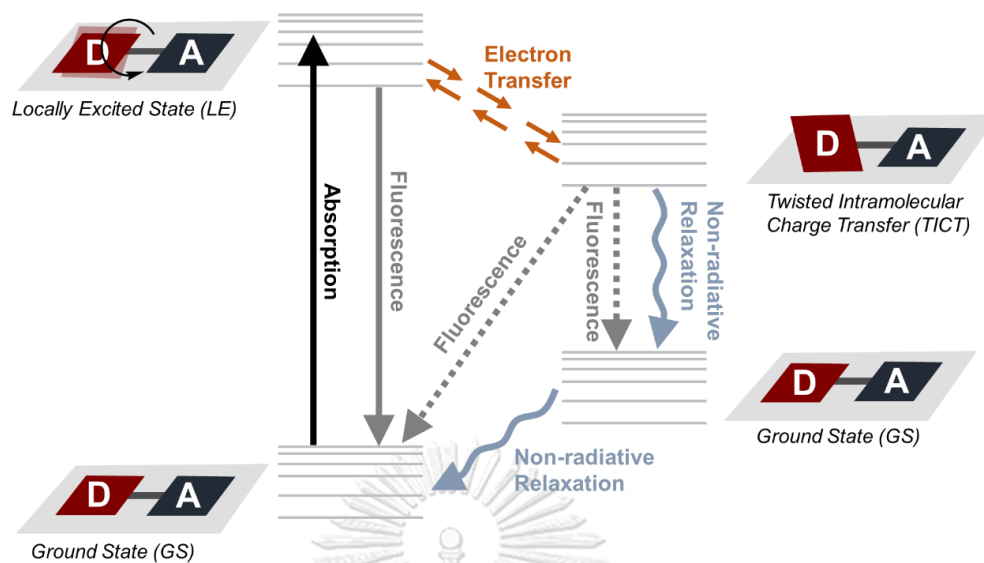


Figure 1.4 Dynamics of Twisted Intramolecular Charge Transfer (TICT)

Styryl dyes also possess a unique characteristic known as molecular rotor, whereby they can adopt twisted states by rotating one segment of the molecule relative to the rest of the molecule in the excited state. This property is particularly observed in a class of fluorophores called twisted intramolecular charge transfer (TICT) complexes. TICT refers to a phenomenon known as electron transfer, which takes place when molecules are excited by light. Typically, these molecules comprise a donor part connected to an acceptor part.⁴⁸ When a photon is absorbed, a molecular rotor can return to the ground state either from the locally energized (LE) state or from the twisted state. The energy gaps between the LE and twisted states and the ground state are significantly different. De-excitation from the twisted state leads to either a red-shifted emission wavelength or no emission at all. However, if the molecular motion is restricted, such as through binding to a host molecule, the non-radiative relaxation pathway is hindered, resulting in higher fluorescent quantum yields (**Figure 1.4**).⁴⁹

The mechanism behind the fluorescence enhancement of styryl dyes in the presence of nucleic acids can be attributed to the restriction in conformational freedom of the dye molecules. When the styryl dye molecules intercalate or insert into the grooves of DNA with matching dimension, their conformational flexibility becomes limited. This restricted mobility prevents the non-radiative relaxation pathway for the excited dye molecules, leading to an increase in fluorescence emission.⁵⁰

1.2.2 Styryl dyes for nucleic acid detection

As previously mentioned, styryl dyes have found extensive use as staining agents for nucleic acid detection.³⁵⁻⁴⁶ Here, a selection of recent literature published within the past five years that utilizes styryl dyes for the purpose of nucleic acid staining is presented. In 2018, Wang et al.³⁹ published a study in which they introduced two styryl dyes based on the benzothiazolium system to visualize nucleoli and chromosomes in real-time during the cell cycle. Through molecular simulation studies, they proposed that the dye molecules bind to dsDNA at hydrophobic minor grooves, with additional stabilization occurring through hydrogen bonding between the dye and nucleobases. The simulation also suggested that the dye could potentially bind to dsRNA at hydrophobic major grooves through π -cation interactions and hydrogen bonding (**Figure 1.5**).

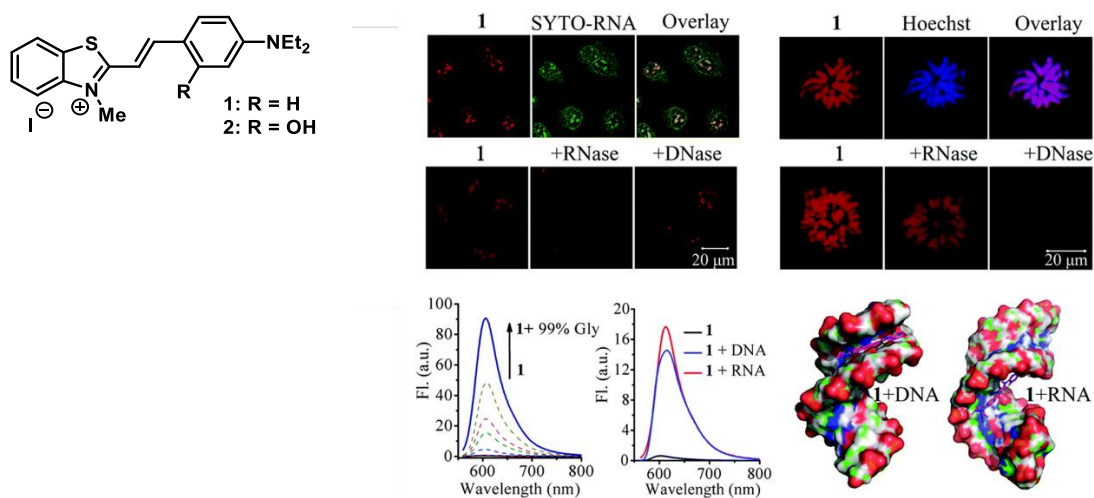


Figure 1.5 Visualization of nucleolus and chromosomes using co-staining with SYTO-RNA and Hoechst 33342, respectively. Digest experiments performed using RNase and DNase enzymes, emission analysis of probe 1 in viscous solution and in the presence of nucleic acid, and models illustrating the interaction of probe 1 with DNA and RNA fragments in Wang's work.³⁹

(Used with permission of Royal Society of Chemistry, from Red fluorescent probes for real-time imaging of the cell cycle by dynamic monitoring of the nucleolus and chromosome, Wang, K.-N. Chao, X.-J. Liu, B. Zhou, D.-J. He, L. Zheng, X.-H. Cao, Q. Tan, C.-P. Zhang, C. Mao, Z.-W. *Chem. Commun.* **2018**, *54*, 2635-2638.; permission conveyed through Copyright Clearance Center, Inc.)

In 2020, Collot and co-workers⁵¹ demonstrated improvement of the eukaryotic cells plasma membrane (PM) staining properties of FM1-43, a known probe, by modifying its structure (**Figure 1.6**). By making rational chemical adjustments while preserving the core fluorophore and using suitable targeting moieties, styryl dyes were transformed into efficient PM probes for bioimaging. Since FM1-43 had limitations in its affinity and cationic accumulation, modifications were made to eliminate the cationic nature, enhance hydrophobicity, and introduce amphiphilic moieties for efficient plasma membrane targeting. Additionally, the fluorophore was modified to extend its π -conjugation and shift the absorbance and emission spectra. These modifications resulted in SP-468, a neutral zwitterionic dye

with improved imaging properties, and SQ-535, which could be used in the red channel with reduced bleedthrough in the green channel. Unlike FM1-43 which showed weak PM signal and intracellular staining, the new dyes efficiently stained the PM in various mammalian cell lines, including primary neurons. Notably, the new probes also showed excellent PM staining in fixed cells and brain slices. A newly developed dye called SP-468, with its enhanced photostability and large Stokes shift, enabled live neuronal super-resolution imaging using STED microscopy. Some of these new dyes maintained their ability to stain the PM of plant cells, making them versatile for both mammalian and plant experiments. This study emphasizes the importance of designing molecular fluorescent probes that meet bioimaging requirements.

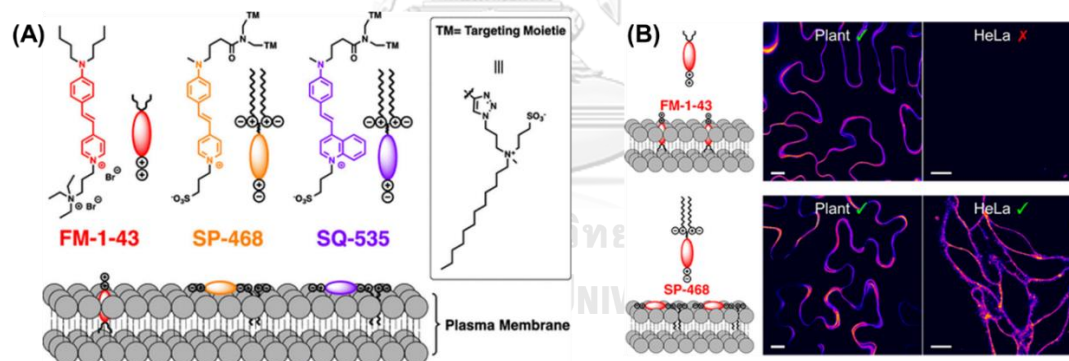


Figure 1.6 (A) Structural comparison of FM1-43 and the newly developed styryl probes, SP-468 (Styrylpyridinium) and SQ-535 (Styryl Quinolinium), along with their respective orientation within the plasma membrane. (B) Laser scanning confocal imaging of plant cells (*Nicotiana benthamiana*) and live cells from HeLa cell lines stained with FM1-43 and SP-468 in Collot's work.⁵¹

(Reprinted (adapted) with permission from Collot, M.; Boutant, E.; Fam, K. T.; Danglot, L.; Klymchenko, A. S. Molecular Tuning of Styryl Dyes Leads to Versatile and Efficient Plasma Membrane Probes for Cell and Tissue Imaging. *Bioconjugate Chem.* 2020, 31 (3), 875-883. Copyright 2020 American Chemical Society.)

In the same year, Saady et al.⁴³ also developed a quinolinium-based styryl dyes that exhibited specific staining of nucleoli and cytoplasm without showing toxicity. The dyes displayed higher affinity for rRNA compared to nuclear dsDNA. It was hypothesized that the dyes bound to secondary/tertiary structures of rRNA, which are partially double-stranded. However, in the case of nuclear dsDNA, the presence of histones forming nucleosomes on the cellular DNA hindered the dye binding, resulting in a lower fluorescent response. This observation highlights the differential binding behavior of the dyes towards different nucleic acid targets and provides insights into its selective staining properties that may not always reflect the behavior in the isolated targets (**Figure 1.7**).

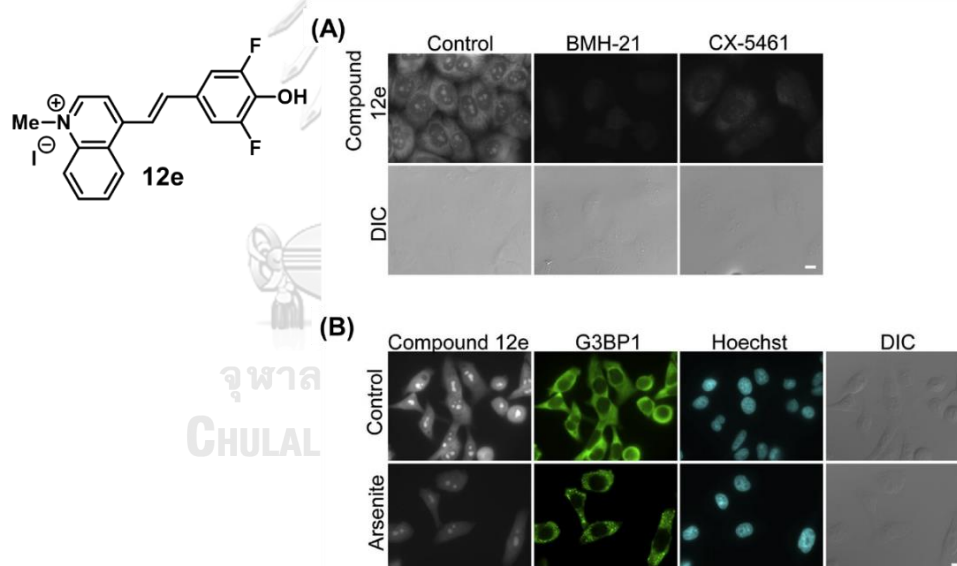


Figure 1.7 Compound 12e exhibits binding to rRNA in cells in Saady's work.⁴³ **(A)** Fluorescence signal of compound 12e is reduced in cells upon transcriptional inhibition of RNA polymerase I using CX-5461 and BMH-21. **(B)** Stress granules formed by arsenite treatment and labeled with anti-G3BP1 (green) do not exhibit co-localization with compound 12e (white). DNA staining with Hoechst is shown in cyan. (Reprinted from Saady, A. Varon, E. Jacob, A. Shav-Tal, Y. Fischer, B. Applying styryl quinolinium fluorescent probes for imaging of ribosomal RNA in living cells. *Dyes Pigm.* **2020**, *174*, 107986. Copyright 2020, with permission from Elsevier.)

In yet another example, a series of monocationic styryl dyes were developed by Čipor and co-workers in 2020.⁵² All dyes in this study exhibited moderate shifts in UV/Vis spectra, increased fluorescence, slight changes in CD spectra, and minor stabilization of DNA/RNA duplexes. The binding constants indicated a higher affinity for dyes with larger condensed aromatic surfaces. Most dyes showed low cytotoxicity, except for BZ-IND, which exhibited moderate cytotoxicity at micromolar concentrations due to potential DNA/RNA intercalation. Most dyes localized with mitochondria, but BZ-Se localized to lysosomes, and BZ-IND showed equal distribution between mitochondria and lysosomes. This suggested different mechanisms of action, but further experiments are still required to understand the basis of such selectivity (Figure 1.8).

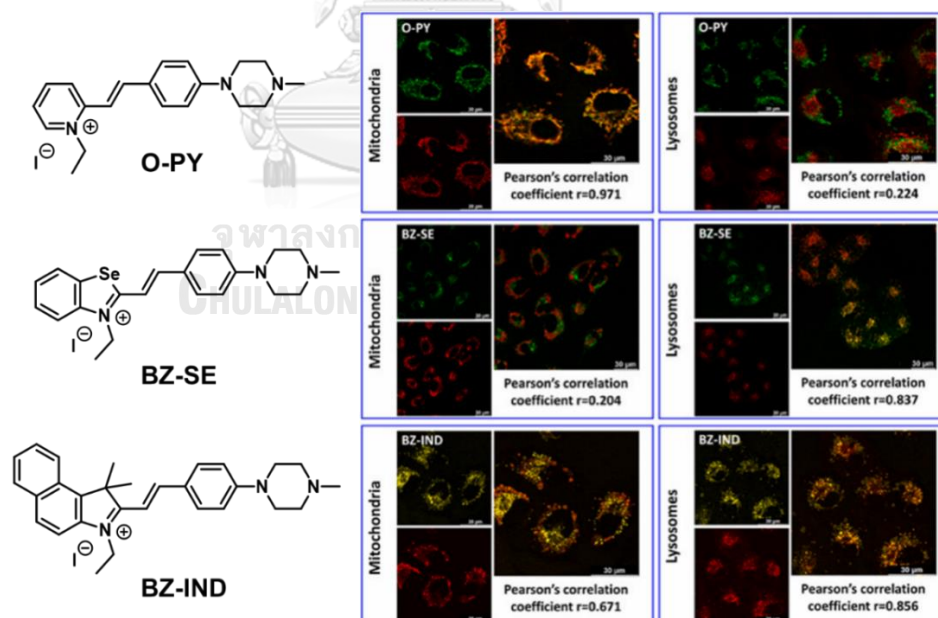


Figure 1.8 Intracellular localization of O-PY, BZ-Se and BZ-IND in Čipor's work.⁵²

(Reprinted from Čipor, I. Kurutos, A. Dobrikov, G. M. Kamounah, F. S. Majhen, D. Nestić, D. Piantanida, I., Structure-dependent mitochondria or lysosome-targeting styryl fluorophores bearing remarkable Stokes shift. *Dyes Pigm.* 2022, 206, 110626. Copyright 2022, with permission from Elsevier.)

In 2022, Supabowornsathit et al.⁵³ introduced new dicationic styryl dyes with heteroaromatic cores (pyridinium, benzothiazolium, and quinolinium) to enhance their binding interaction with nucleic acids. The dyes were modified with an additional positive charge via a quaternary ammonium group attached to an electron-rich aromatic ring. The optical properties and DNA binding of the dicationic dyes were compared to their monocationic counterparts. The dicationic dyes exhibited a bathochromic shift in absorption spectra and significant fluorescence enhancement in the presence of dsDNA. They also show stronger affinity towards dsDNA when compared to the corresponding monocationic dyes. Importantly, they demonstrated improved sensitivity in DNA detection, with detection limits comparable to commercial dyes. The potential applications of these dicationic styryl dyes in foodborne pathogen detection and cellular nucleic acid imaging had been demonstrated. In agreement with previous works, cellular RNA was found to be the primary target for cellular nucleic acid imaging (**Figure 1.9**).

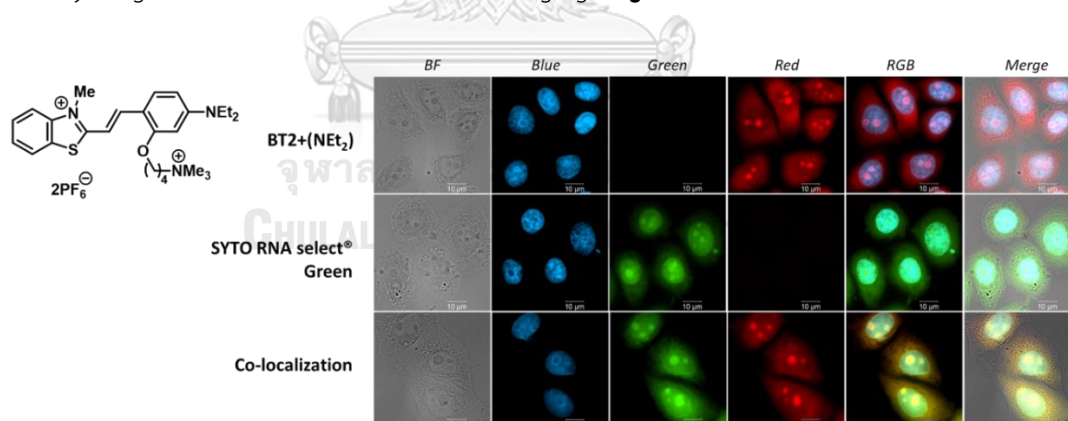


Figure 1.9 Applications of dicationic styryl dye (BT2+NEt₂) for cellular nucleic acid detection in Supabowornsathit's work.⁵³

(Reprinted from Supabowornsathit, K.; Faikhrua, K.; Ditmangklo, B.; Jaroenchuensiri, T.; Wongsuwan, S.; Junpra-ob, S.; Choopara, I.; Palaga, T.; Aonbangkhen, C.; Somboonna, N.; Taechalertpaisarn, J.; Vilaivan, T. Dicationic styryl dyes for colorimetric and fluorescent detection of nucleic acids. *Sci. Rep.* **2022**, *12* (1), 14250. Copyright © 2022 with permission from Nature Portfolio)

In 2023, two cationic cyanine-styryl derivatives, Styryl-QL and Styryl-BT, were developed by Wangngae⁵⁴ and were found to possess favorable optical properties for bio-imaging. They exhibited acceptable fluorescence quantum yields and large Stokes shifts. Styryl-QL displayed stronger intramolecular charge transfer (ICT) compared to Styryl-BT, resulting in more red-shifted absorption spectra. The dyes showed fluorescence enhancement only when bound to DNA, comparing with other possible interferents highlighting their specificity towards DNA. Molecular docking confirmed the importance of electrostatic interactions between the positively charged dyes and the DNA phosphate backbone. These styryl dyes demonstrated selective uptake by cancer cells and displayed antibacterial and anticancer properties (Figure 1.10).

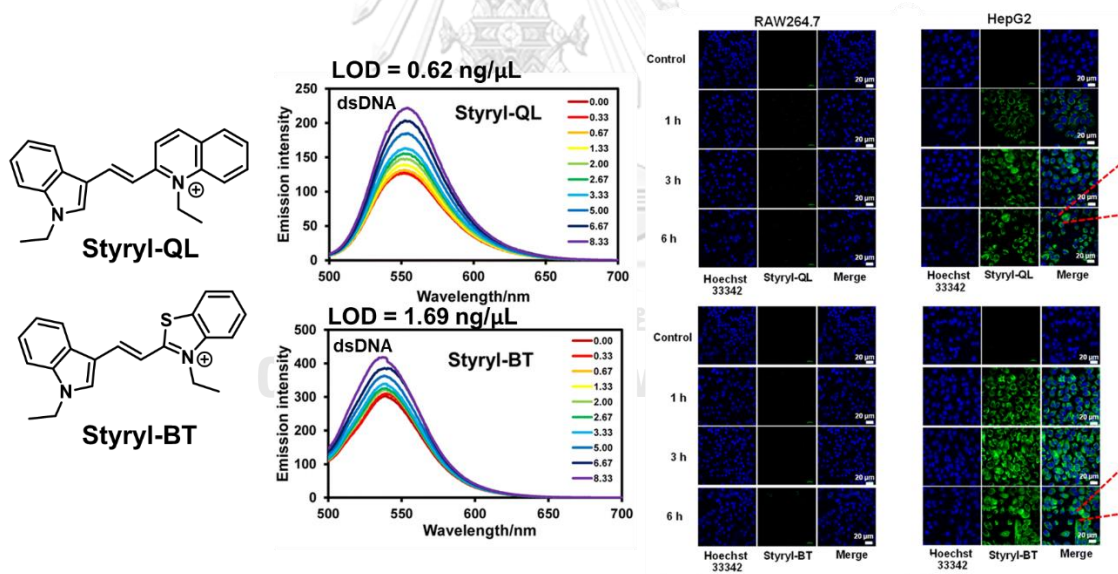


Figure 1.10 Cationic styryl dyes for DNA labelling and selectivity toward cancer cells in Wangngae's work.⁵⁴

(Used with permission of Royal Society of Chemistry, from A. Cationic styryl dyes for DNA labelling and selectivity toward cancer cells and Gram-negative bacteria, Wangngae, S. Ngivprom, U. Khrootkaew, T. Worakaensai, S. Lai, R.-Y. Kamkaew, *RSC Adv.* **2023**, *13* (3), 2115-2122.; permission conveyed through Copyright Clearance Center, Inc.)

The optical properties change of styryl dyes in the presence of nucleic acid might involve different aggregation states. In 2021, Ustimova et al. demonstrated the formation of helical aggregates of bis(styryl) dyes in the presence of a DNA template.⁵⁵ Three dimeric styryl pyridinium dyes with different substituents on the phenyl moiety were synthesized and their interactions with calf thymus DNA (ct-DNA) were investigated. The dyes containing the NMe₂ group exhibited a higher fluorescence enhancement upon binding to DNA. At high concentrations (ligand–DNA ratio = 0.6), these molecules formed aggregates within the minor groove of ct-DNA, indicating by CD signal. Based on CD spectroscopic studies, it was proposed that the bis(styryl) dye with an OMe substituent formed right-handed chiral helical dye aggregates, while the dye with an NMe₂ group formed left-handed chiral aggregates. These findings highlight the structural influence of substituents on the aggregation behavior of styryl dyes and their interaction with DNA (Figure 1.11).

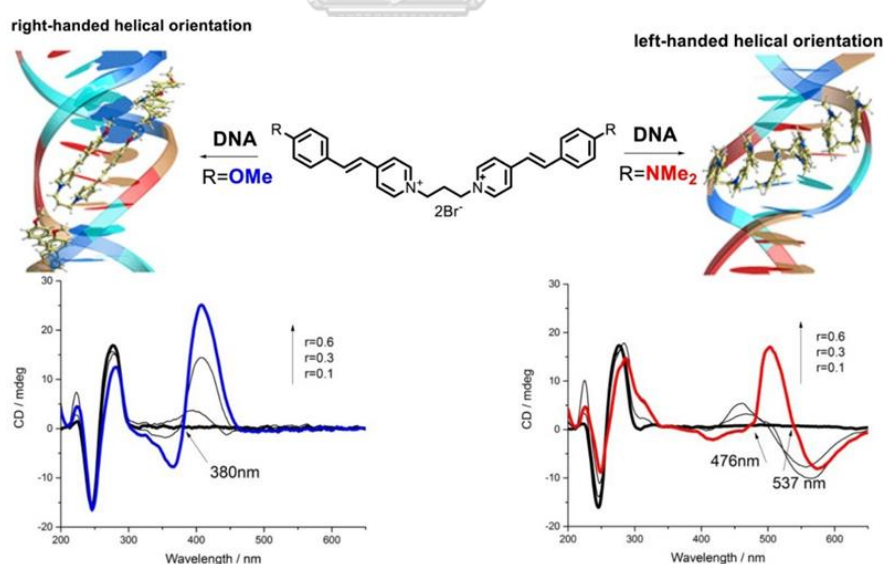


Figure 1.11 Formation of helical aggregations by ctDNA in the presence of Bis(styryl)pyridinium dyes with OMe or/and NMe₂ substituents.⁵⁵

(Reprinted from Ustimova, M. A. Fedorov, Y. V. Tsvetkov, V. B. Tokarev, S. D. Shepel, N. A. Fedorova, O. A., Helical aggregates of bis(styryl) dyes formed by DNA templating. *J. Photochem. Photobiol., A* **2021**, *418*, 113378. Copyright 2021, with permission from Elsevier.)

In another study by Zonjić in 2022, the binding and optical properties change of styryl dyes with benzothiazole connecting to *N*-methylpiperazinylphenyl or *N*-phenylpiperazinylphenyl scaffolds for various nucleic acid structures were investigated.⁵⁶ The introduction of methyl or phenyl groups to the piperazine unit had a profound impact on the binding properties, affinities, spectroscopic responses, and antiproliferative effects of the dyes, which *N*-phenylpiperazinylphenyl dyes showed more prominent antiproliferative activity among various tumour cell lines compared with *N*-methylpiperazinylphenyl dyes. Styryl dyes with *N*-methylpiperazine substituents exhibited a preferential binding to the minor groove of AT-rich DNA sequences, leading to increased fluorescence, significant stabilization of the double helix, and positive induced circular dichroism spectra. These compounds also formed complexes with G-quadruplex through π - π stacking interactions with the top or bottom G-tetrad. On the other hand, styryl dyes with *N*-phenylpiperazine substituents bound to ds-polynucleotides through partial intercalation and exhibited stronger stabilization of G-quadruplex compared to the methyl-substituted dyes. However, the fluorescence responsiveness from *N*-methylpiperazinylphenyl styryl dyes was very low. Furthermore, the dyes effectively penetrated cells and accumulated in the mitochondria, showing co-localization with standard mitochondrial markers. The findings also suggested the possibility to develop styryl dyes that show selectivity towards different nucleic acid templates (**Figure 1.12**).

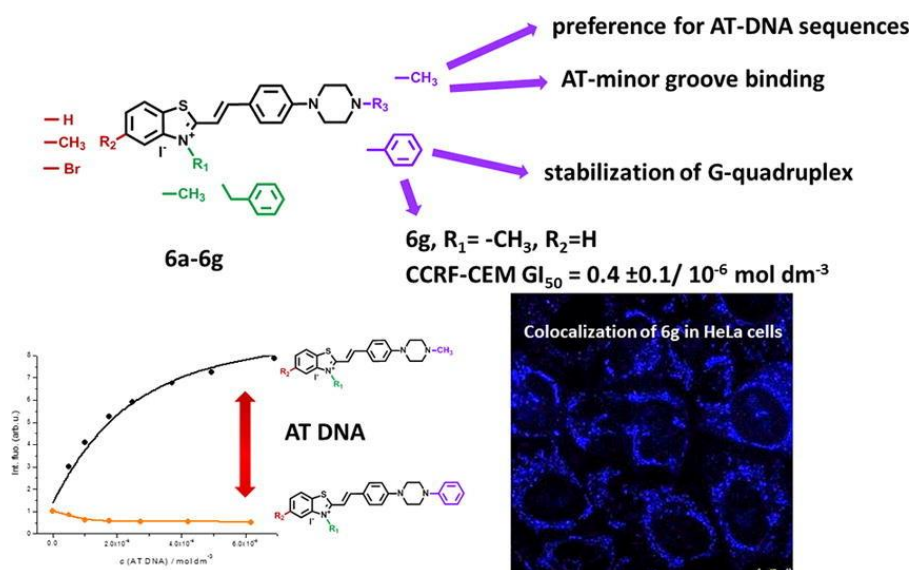


Figure 1.12 Styryl dyes with *N*-methylpiperazine and *N*-phenylpiperazine substituents for targeting AT-rich and G-quadruplex DNA and cell staining. ⁵⁶

(Reprinted from Zonjić, I. Radić Stojković, M. Crnolatac, I.; Tomašić Paić, A. Pšeničnik, S. Vasilev, A. Kandinska, M. Mondeshki, M. Balushev, S. Landfester, K., Styryl dyes with *N*-Methylpiperazine and *N*-Phenylpiperazine Functionality: AT-DNA and G-quadruplex binding ligands and theranostic agents. *Bioorg. Chem.* **2022**, *127*, 105999. Copyright 2022, with permission from Elsevier.)

1.2.3 Combinatorial synthesis of styryl dyes for targeted nucleic acid staining

The traditional approach for designing fluorescent sensors involves combining fluorescence dye molecules with specially designed receptors for specific analytes. The goal is to achieve the desired change in the fluorescence properties of the dye when a recognition event occurs between the receptor and the analyte. Although many fluorescent sensors have been successfully developed using this approach, it requires great efforts in both sensor design, synthesis, evaluation and optimization. Furthermore, these sensors are limited in their application to the specific analytes that they were designed for, known as “Analyte Directed Sensors”.^{57, 58} Since such sensors are designed for specific analytes, they may not be easily adaptable or reconfigurable for detecting different substances. Modifying or expanding their

capabilities to detect new analytes often requires significant redesign and re-engineering. To overcome these limitations, the combinatorial approach offers a promising alternative known as “Diversity Directed Sensors”.⁵⁹ This approach relies on the development of an efficient synthetic route for generating a diverse range of dyes. While combinatorial chemistry has been widely used in chemical biology and medicinal/pharmaceutical fields to discover biologically active molecules or drug candidates, its application to fluorescent dyes is still limited.

In 2003, Rosania et al.⁶⁰ employed the combinatorial approach for discovering fluorescent dyes that targeted specific organelles. By combining various aldehydes and methyl pyridinium salts, they were able to create a diverse library of styryl dyes that emitted a wide range of colors. Through screening with specific biological targets such as DNA, RNA, proteins, or organelles without purification, it was found that 119 out of 276 fluorescent compounds localize to specific subcellular compartments (i.e., mitochondria, endoplasmic reticulum, vesicles, nucleoli, chromatin, cytoplasm, or granules). Considering that the library compounds which were positively charged, it was not unexpected that 64 out of 119 selected compounds localize specifically to mitochondria. Hence, this study disclosed that combinatorial chemistry is a powerful technique for the discovery of new organelle-targeted fluorescent dyes (**Figure 1.13**).

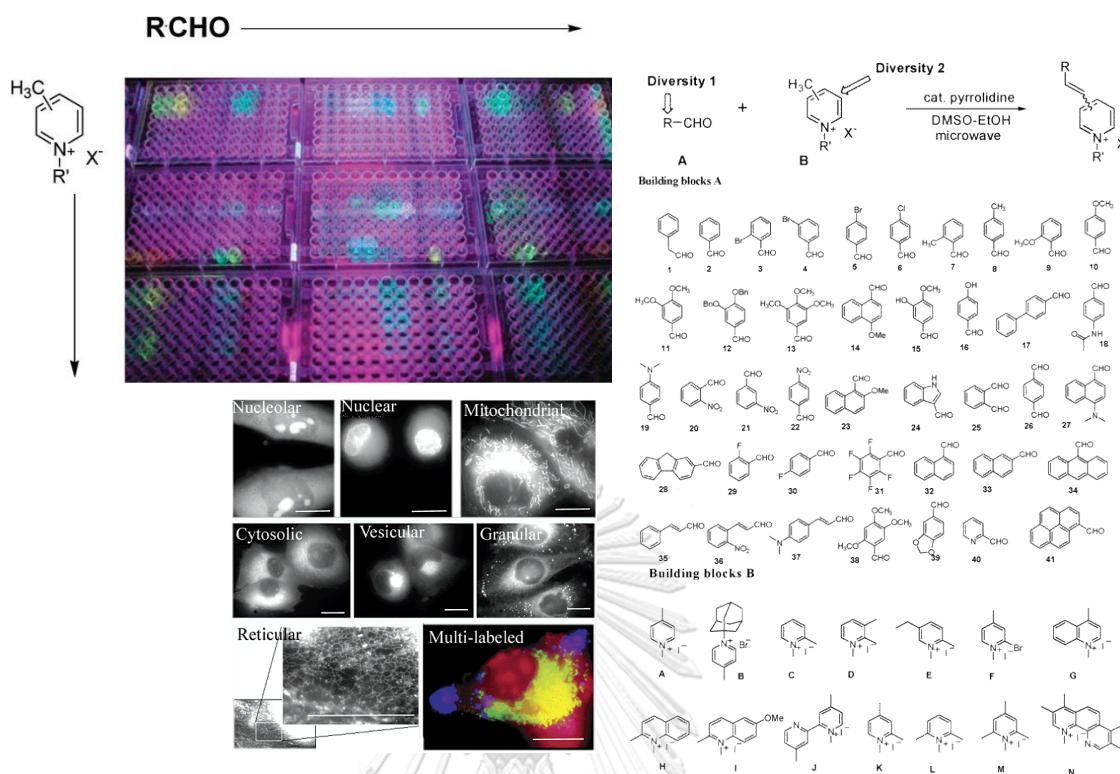


Figure 1.13 Combinatorial synthesis of organelle-targeted fluorescent dye by Rosania et al.⁶⁰

(Reprinted (adapted) with permission from Rosania, G. R.; Lee, J. W.; Ding, L.; Yoon, H.-S.; Chang, Y.-T. Combinatorial Approach to Organelle-Targeted Fluorescent Library Based on the Styryl Scaffold *J. Am. Chem. Soc.* **2003**, *125* (5), 1130-1131. Copyright 2003 American Chemical Society.)

In the same year, Lee et al.³⁵ utilized a combinatorial synthesis and cell-based screening techniques to identify styryl dyes with new structural motifs for a DNA sensor. They constructed a library of 855 different styryl dyes and identified 8 promising molecules for further investigation. One of these was ultimately identified as a nuclear staining dye capable of penetrating cells, exhibiting a 13-fold increase in fluorescence in the presence of DNA. The researchers demonstrated its application in live-cell imaging. Subsequently, in 2006, the same research group developed styryl dyes that were selective for RNA, enabling visualization of nuclear structure and function within living cells.³⁶ From a collection of 88 styryl dyes synthesized using the

combinatorial approach, the dyes demonstrating the highest nucleolar targeting ability, intense fluorescence, minimal photobleaching, and minimal impact on cell viability were selected. The investigation unveiled three novel styryl dyes suitable for RNA imaging within living cells, showing fluorescence increase by 5.5-55 times in the presence of RNA (Figure 1.14).

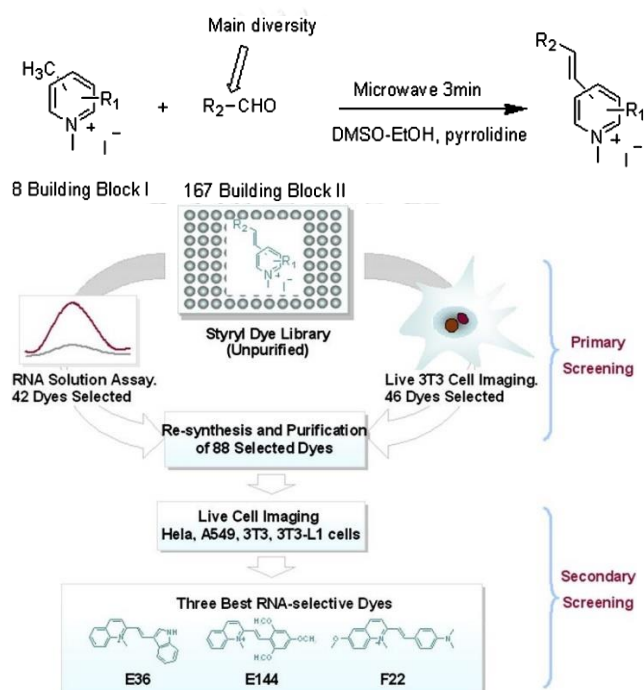


Figure 1.14 Combinatorial synthesis of RNA-selective styryl dyes and cell-based screening.³⁶

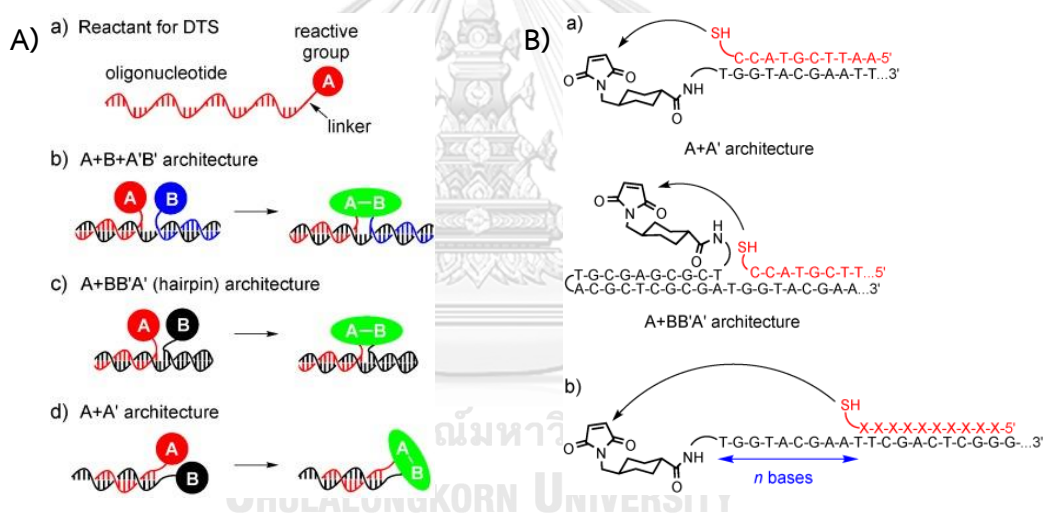
(Reprinted from Li, Q. Kim, Y. Namm, J. Kulkarni, A. Rosania, G. R. Ahn, Y.-H. Chang, Y.-T., RNA-Selective, Live Cell Imaging Probes for Studying Nuclear Structure and Function. *Chem. Biol.* **2006**, *13* (6), 615-623. Copyright 2006, with permission from Elsevier.)

1.3 DNA templated reaction

1.3.1 Conventional DNA-templated synthesis

DNA-templated synthesis (DTS) refers to a process where DNA molecules are used as templates or scaffolds to guide the assembly of other molecules, such as small organic compounds. It takes advantage of the specific base pairing properties of DNA to direct the synthesis of desired structures or functional materials. The power of DNA templated ligation reaction has long been extensively exploited in biological fields.⁶¹⁻⁶³ Only recently that the concept of DNA-templated synthesis (DTS) has attracted attention in the area of organic synthesis for some time due to its advantageous features, including specificity, simplicity, rapidity, and cost-effectiveness. Most importantly, the ability to amplify DNA offer a unique advantage in the identification of the target molecule that may be present in too small amounts to be directly detected. The pioneering work by Gartner and Liu in 2001⁶⁴ popularized this approach. The fundamental principle involves attaching reactants with reactive groups to two complementary oligonucleotide strands through covalent bonds. When the two oligonucleotide strands were complementary they hybridized to form a duplex. The hybridization brought the two reactive groups into close proximity, thus enhancing local concentrations and facilitating the formation of the desired products. This research had demonstrated the applicability of sequence-specific DNA-templated reactions, encompassing various reaction types such as S_N2 substitutions, additions to α,β -unsaturated carbonyl systems, and additions to vinyl sulfones. Nucleophiles such as thiols and amines could participate in these reactions, and acceptable yields with notable sequence specificity have been achieved. In 2004, the same research group⁶⁵ designed DNA-templated synthetic libraries with high complexity and structural diversity, primarily focusing on macrocycles. This

involved the utilization of multistep DNA-templated organic synthesis to convert libraries of DNA sequences (comprising three "codons") into sequence-programmed synthetic small-molecule macrocycles. In vitro selections for protein affinity were performed on the resulting DNA-macrocycle conjugates. The structure of the selected macrocycle was then identified from the sequence of the DNA template following amplification. Thus, following the translation, selection, and amplification of libraries of nucleic acids that encode synthetic small molecules, a single macrocycle with a known target protein affinity was identified (**Figure 1.15**).



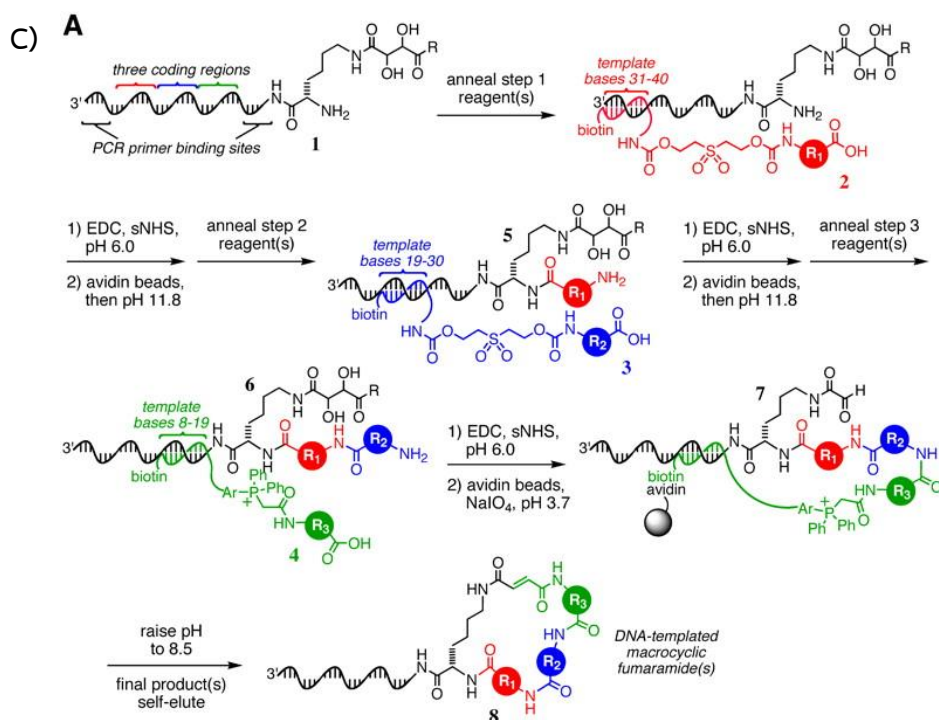


Figure 1.15 (A) Molecular architecture of reactants for DTS, (B) Distance-independent DTS, and (C) Multistep DTS.⁶⁵ (Reprinted from Li X.; Liu, D. R. DNA-Templated Organic Synthesis: Nature's Strategy for Controlling Chemical Reactivity Applied to Synthetic Molecules. *Angew. Chem. Int. Ed.* **2004**, 43 (37), 4848-4870. Copyright © 2004 with permission from John Wiley and Sons)

1.3.2 DNA-templated synthesis not involving base-pairing

In contrast to the previous examples where the complementarity of two DNA strands was crucial for the DNA-templated reactions, there exists a different but related principle in DNA-templated synthesis (DTS) where global features of DNA, such as base stacks, grooves, hydrophobic surfaces, and chirality, play a significant role in determining the success of the reaction rather than nucleic acid sequence complementarity. One notable example is the DNA-based Cu-catalyzed asymmetric synthesis proposed by Roelfes et al. in 2005.^{66, 67} When a copper complex of an intercalating ligand was bound to DNA, a chiral environment was created around the copper catalyst. Indeed, the Diels-Alder products could be obtained in high enantioselectivities. Despite the inherent right-handed chirality of the DNA used,

appropriate selection of ligands enabled access to both enantiomers of the Diels-Alder product. The modular nature of this system, coupled with noncovalent binding of the catalytic moiety to the chiral environment (DNA) through achiral ligands, facilitates rapid structural variations and the customization of catalysts for novel processes. Additionally, this method offers the advantage of separating the product from the catalyst. The Cu-ligand complex forms a tight intercalation complex with DNA and remains in the aqueous phase, allowing for easy separation from the product through simple extraction (Figure 1.16A).

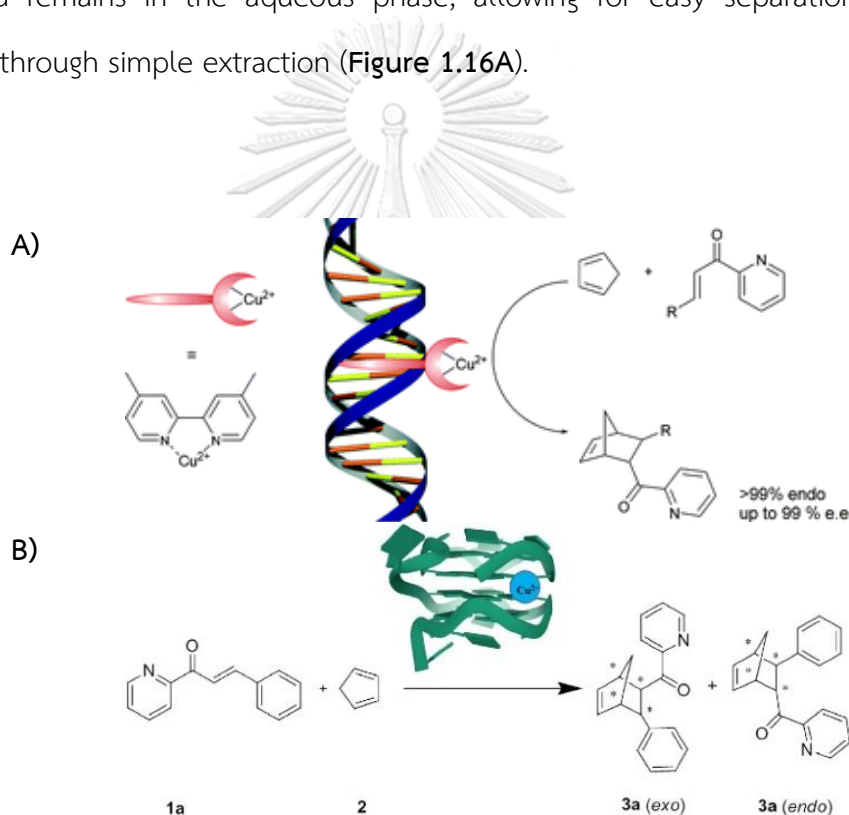


Figure 1.16 DNA-templated asymmetric Diels-Alder reaction.⁶⁶⁻⁶⁸

((A) Used with permission of Royal Society of Chemistry, from Highly enantioselective DNA-based catalysis, Roelfes, G. Boersma, A. J. Feringa, B. L., 6, 2006; permission conveyed through Copyright Clearance Center, Inc. (B) Reprinted from Chen, K., He, Z., Xiong, W. Wang, C.-J. Zhou, X., Enantioselective Diels-Alder reactions with left-handed G-quadruplex DNA-based catalysts. *Chin. Chem. Lett.* **2021**, 32 (5), 1701-1704. Copyright 2021, with permission from Elsevier.)

Apart from generic DNA duplexes, enantioselective Diels-Alder reactions with left-handed G-quadruplex DNA-based catalyst were developed by Chen *et al.* in 2021.⁶⁸ A G-quadruplex DNA is a secondary structure that can form in DNA sequences containing guanine-rich regions. It is a non-canonical structure that is distinctive from the conventional double helix structure of DNA. The G-quadruplex structure is further stabilized by the presence of cations, such as potassium or sodium ions, which bind to the central channel formed by the G-quartets. Without the addition of ligands, left-handed G-quadruplex (L-G4) was shown to have strong enantioselectivity (-52% *ee*) catalysis. The negative value of enantiomeric excess (*ee*) indicated the formation of products with opposite enantioselectivity to the normal right-handed dsDNA. When combined with copper(II) ions, G4 was further stabilized when G4 ligands were added, resulting in greater enantioselectivity (up to -80% *ee*) (**Figure 1.16B**).

The naturally occurring supramolecular structures of biomolecules such as DNA, RNA, and proteins inspired the use supramolecular self-assembly as a means to design and create artificial molecular systems. In “target-guided synthesis (TGS)”,⁶⁹⁻⁷³ biological targets such as proteins and nucleic acids assemble their most effective binders from a specific set of molecular fragments. The formation of chemical bonds requires close proximity and precise orientation of reactants. Therefore, the supramolecular assembling of reactant units on the template fulfills this requirement by bringing the dispersed molecular units together and facilitating predefined interactions between them to provide the desired product (**Figure 1.17**).

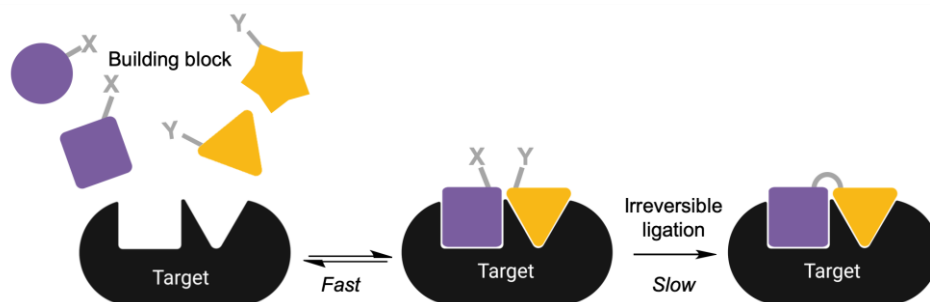


Figure 1.17 The concept of target-guided synthesis (TGS) involves bringing together specific reactive molecules in close proximity through the target molecule itself, allowing them to undergo irreversible reactions and ultimately form the desired ligand.

During the past decades, several research groups utilized secondary structures of nucleic acids for templated ligand assembly. In 2012, Antonio et al. discovered a potent telomere-targeting small molecule by using in situ “Click chemistry” of a series of alkyne and azide building blocks that were facilitated by a G-quadruplex DNA template.⁷⁴ A human telomeric DNA (H-Telo) was chosen as a target due to its significance in cancer biology and possess the capability to initiate a DNA damage response at telomeres, leading to senescence and apoptosis. Interestingly, the formations of the single 1,4-adduct, which results from the cycloaddition in the presence of H-Telo were observed and identified by LC-MS. They demonstrated the effectiveness of unbiased approaches, such as in situ click chemistry, in enhancing the interaction of small molecules with specific nucleic acid structures (**Figure 1.18**).

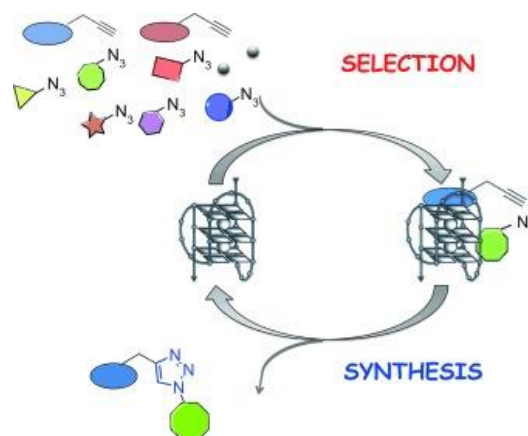


Figure 1.18 In situ synthesis of triazoles via click chemistry catalyzed by G-quadruplex DNA (H-Telo).⁷⁴

(Reprinted from Antonio, D. M.; Biffi, G.; Mariani, A.; Raiber, E.-A. Selective RNA Versus DNA G-Quadruplex Targeting by In Situ Click Chemistry. *Angew. Chem. Int. Ed.* **2012**, *51* (44), 11073-11078. Copyright © 2012 with permission from John Wiley and Sons)

In 2017, Panda et al.⁷⁵ successfully demonstrated another example of TGS using DNA nano-templates that promote the click reaction from an array of azide and alkyne fragments for discovering a selective G-quadruplex binding c-MYC inhibitor. The G-quadruplex nano-template played a crucial role in producing a primary triazole product that demonstrated inhibitory properties on c-MYC expression. The G-quadruplex DNA nano-templates were designed to assemble on gold-coated magnetic nanoparticles. The immobilization of the G4 DNA on the magnetic beads allows washing to remove the excess reactants and weakly-bound products. After thermal denaturation of the G4 DNA, and the strongly bound clicked products were obtained and identified by LC-MS. The nano-templates facilitate the regioselective formation of 1,4-substituted triazole products, which are easily isolated by magnetic decantation. The triazole product specifically targeted the c-MYC promoter G-quadruplex, which is a particular DNA structure responsible for controlling the expression of the c-MYC gene. The binding property of a potent lead compound

from the templated reaction was compared with individually synthesized compound. It was concluded that the lead binds and stabilizes the G-quadruplex structure in c-MYC P1 promoter and specifically reduces c-MYC expression. These findings indicated that the TGS method has the potential to be employed in the development of ligands that selectively target specific molecules for drug discovery purposes (Figure 1.19).

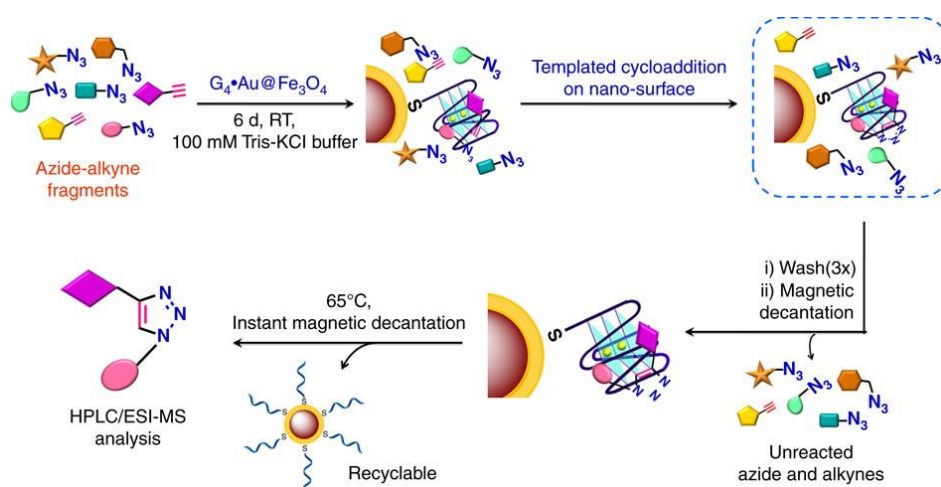


Figure 1.19 Schematic representation of templated cycloaddition between selective azide and alkyne partners using $G_4 \cdot Au@Fe_3O_4$ nanoparticles. ⁷⁵

(Reprinted from Panda, D.; Saha, P.; Das, T.; Dash, J. Target guided synthesis using DNA nano-templates for selectively assembling a G-quadruplex binding c-MYC inhibitor. *Nat. Commun.* **2017**, *8* (1), 16103. Copyright © 2017 with permission from Nature Portfolio)

Relating to the aforementioned work, in 2023 Chaudhuri et al.⁷⁶ reported that G-quadruplex DNA could act as a template for guiding an even more challenging bio-orthogonal macrocyclization reaction to synthesize gene modulators from bifunctional azide and alkyne fragments. In the non-templated reaction, the efficiency is generally limited due to oligo- and polymerization. G4s immobilized on gold-coated magnetic nanoparticles were employed to facilitate the isolation and detection of G4-targeting peptidomimetic macrocycles. In addition, comparable

macrocycles were synthesized with the aim to understand their functional significance in regulating gene function. The G4-templated reaction revealed a lead compound showing high specificity towards DNA target (*c-MYC* and *h-Telo*). Importantly, they were able to observe the formation of the macrocycle both *in vitro* and *in cells* from corresponding alkyne and azide fragments. The achievement of *in vitro* and intracellular macrocyclization would introduce a novel opportunity for target-oriented therapeutic applications (Figure 1.20).

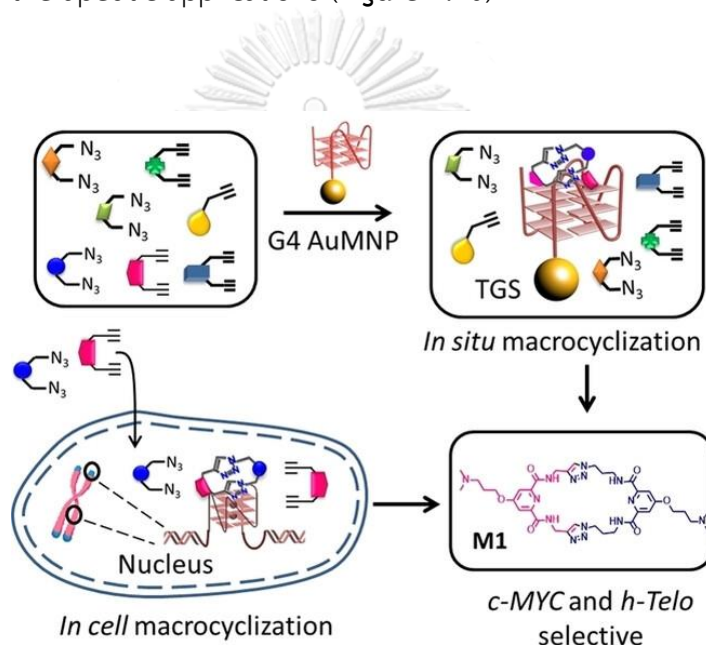


Figure 1.20 Schematic representation of the target-guided synthesis of G4-selective ligands by DNA-functionalized magnetic gold nanoparticles.⁷⁶

(Reprinted from Chaudhuri, R.; Prasanth, T.; Dash, Expanding the Toolbox of Target Directed Bio-Orthogonal Synthesis: *In Situ* Direct Macrocyclization by DNA Templates. *J. Angew. Chem. Int. Ed.* **2023**, *62* (7), e202215245, Copyright © 2023 with permission from John Wiley and Sons)

1.4 Templated synthesis of cyanine dyes

In general, the formation of larger molecules from smaller components, where one product molecule is created from two reactant molecules, is not

thermodynamically favored due to the inherent decrease in entropy. To address this challenge, compartmentalization techniques are often employed, such as by using micelles or receptors. In 2013, Maguelliati et al.⁷⁷ reported a surfactant-mediated fluorogenic imine formation in water (**Figure 1.21**). The imine formation could be readily observed from the fluorescence of the product. Without the surfactant no reaction occurred. The inclusion of double-stranded DNA in the system also enhanced the reaction efficiency, likely because the resulting fluorescent imine product was stabilized within the minor groove of DNA. This environment-responsive fluorogenic system could also function as a DNA hybridization probe, where the hybridization between two complementary DNA strands could be detected by the production of a fluorescent dye within the DNA host. Notably, no fluorescence was observed in the presence of a single-stranded DNA “template”.

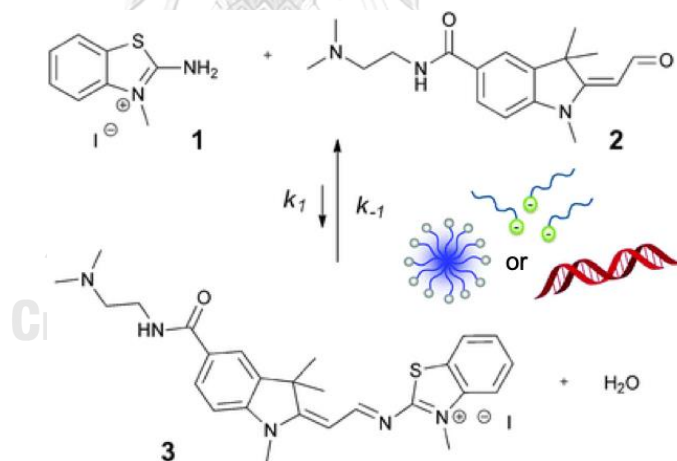


Figure 1.21 Reversible synthesis of fluorescent imine from non-fluorescent amine and weakly fluorescent aldehyde in aqueous media using either surfactants (below and above their CMC) or double-stranded DNA (acting as a reaction host).

(Used with permission of Royal Society of Chemistry, from Enhanced imine synthesis in water: from surfactant-mediated catalysis to host-guest mechanisms, K. Maguelliati, A. Fallah-Araghi, J. Baret, A. El Harrak, T. Mangeat, C. M. Marques, A. D. Griffiths, S. Ladame, *Chem. Commun.* **2013**, 49, 11332-11334. permission conveyed through Copyright Clearance Center, Inc.)

The same research group also reported on a DNA-templated ligation of peptide nucleic acid (PNA) through the formation of a cyanine dye.⁷⁸ The two PNA strands were modified at their N- or C-terminus with non-fluorescent cyanine dye precursors. The positioning of these modifiers was designed to allow optimal orientation for simultaneous binding of both fluorogenic PNA probes to their complementary DNA template. This arrangement led to the irreversible formation of a highly fluorescent symmetrical trimethine cyanine dye. Moreover, the similar idea was also further extended to producing a trimethine cyanine dye, which is guided by the formation of a parallel-stranded G-quadruplex DNA. The process involves attaching the aldehyde and indoline building blocks to the ends of two PNA strands that are complementary to the single-stranded regions flanking the DNA quadruplex-forming sequence. The fluorogenic reaction occurs exclusively when the quadruplex structure is formed, ensuring the specificity of the synthesis process (Figure 1.22).⁷⁹

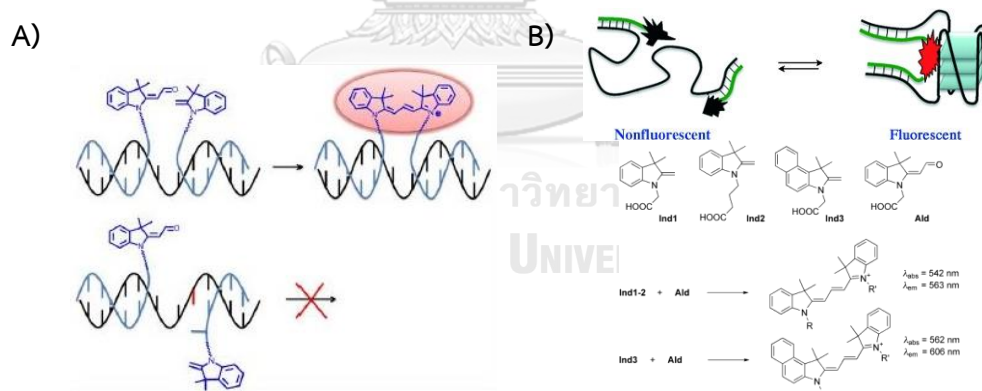


Figure 1.22 Symmetrical trimethine cyanine dye synthesis from two non-fluorescent labeled-PNA precursors via DNA-templated reaction guided by (A) distance of precursors and (B) DNA structure.

((A) Reprinted from Single Nucleotide Polymorphism Detection Using a Biocompatible, Fluorogenic and DNA-Templated Reaction of Cyanine Dye Formation. Meguellati, K.; Ladame, S. *J. Analyt. Molecul. Tech.* **2013**, 1 (1), 5. Copyright © 2013 with permission from Avens Publishing Group, (B) Reprinted from DNA-Templated Synthesis of Trimethine Cyanine Dyes: A Versatile Fluorogenic Reaction for Sensing G-Quadruplex Formation. Meguellati, K.; Koripelly, G.; Ladame, *Angew. Chem. Int. Ed.* **2010**, 49, 2738. Copyright © 2010 with permission from John Wiley and Sons)

Although previous research has demonstrated the DNA-templated synthesis of fluorescence-conjugated imines, the literature lacks information on the DNA-templated synthesis of styryl dyes directly from their precursors. It remains unknown whether the formation of styryl dyes, which involves deprotonation and C-C bond formation, is feasible in the presence of a DNA template without first attaching them to the DNA or PNA strand under sufficiently mild conditions. Hence, this present study aims to investigate the potential of such challenging and previously unknown DNA-templated C-C bond formation.

1.5 Rationale and objective of this study

In this study, our primary objective is to create an innovative method for synthesizing styryl dyes through a DNA-templated approach. We initiate the synthesis by utilizing two coupling partners, namely a methylated heteroaromatic system and an aromatic aldehyde, along with a DNA template. The proposed concept suggests that these precursors will bind to the DNA template and undergo a reaction, ultimately producing the styryl dye while remaining bound to the DNA.

This approach offers significant advantages. Firstly, the synthesis of the dye can be accomplished rapidly due to the facilitated reaction within the DNA template. Additionally, the optical properties of the dye can be directly measured, enabling efficient characterization of the dyes properties in situ. Moreover, we envision that by utilizing different DNA templates, it may be possible to selectively accelerate the formation of new dyes that specifically bind to a particular DNA template. This, in turn, would allow for rapid generation and identification of dyes with the ability to selectively attach to specific DNA structures.

CHAPTER II

EXPERIMENTAL SECTION

2.1 Chemicals and reagents

All chemicals used in this study were purchased from standard suppliers (Sigma-Aldrich, TCI, Alfa Aesa, Fluka, Acros, and Merck), and were analytical grade and used as received without further purification. Deoxyribonucleic acid sodium salt from salmon testes (stDNA) was purchased from Sigma-Aldrich. Synthetic deoxyribonucleic acids were purchased from Integrated DNA Technologies and the sequences are summarized in **Table 2.1**. The dsRNA was kindly prepared by Mr. Kitipong Angsujinda and Prof. Dr. Wanchai Assavalapsakul (Department of Microbiology, Faculty of Science, Chulalongkorn university) (Section 2.8.5). The tRNA sample was provided by Dr. Pornchai Kaewsapsak (Faculty of Medicine, Chulalongkorn University). Substituted BT derivatives were kindly provided by Ms. Thitiya Lasing and Assist. Prof. Dr. Tanatorn Khotavivattana (Department of Chemistry, Faculty of Science, Chulalongkorn University). Ionic liquid ([BMIM]PF₆) was synthesized according to the literature.⁸⁰ MilliQ water was obtained from a Milli-Q[®] Reference water purification system (type 1) equipped with a Millipak[®] 40 filter unit 0.22 μm, Millipore (USA). The nuclease-free water was purchased from Invitrogen. In terms of instrumentation, the electronic absorption spectra and fluorescence spectra were recorded on a Varian Cary 100 UV-Visible spectrometer, Varian Eclipse fluorescence spectrophotometer, or a PerkinElmer EnSight multimode plate reader. CD spectra were measured on a JASCO J815 spectrophotometer and nuclear magnetic resonance spectra were recorded on a JEOL JNM-ECZR500R/S1 500 MHz FT-NMR spectrometer. Mass spectra were obtained from MALDI-TOF mass spectrometer (SpiralTOF JEOL JMS-S3000). High-

performance liquid chromatography (HPLC) experiments were performed on a Nexera LC-40 series HPLC system (Shimadzu, Japan).

Table 2.1 Sequences of oligonucleotides employed in this study.

| Name | Sequence (5'→3') |
|-------|--|
| ssDNA | CCAGGGCATGGTAGATCACTGTACGCCGCG |
| dsDNA | CCAGGGCATGGTAGATCACTGTACGCCGCG + CGCGGCGTACAGTGATCTACCATGCCCTGG |
| c-MYC | TGAGGGTGGGTAGGGTGGGTAA |
| 22AG | AGGGTTAGGGTTAGGGTTAGGG |
| dT30 | TT |

2.2 Synthesis of cationic methylated heterocycles as coupling partners

2.2.1 Monocationic heteroaromatic substrates (*N*-methylation)

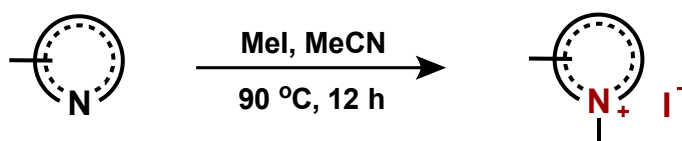


Figure 2.1 *N*-methylation of nitrogen-containing heterocycles

The solution of methyl-substituted nitrogen-containing heterocycle (1.0 equiv.) and iodomethane (2.0 equiv.) in acetonitrile was heated at 90 °C for 12 hours. The precipitate was collected by vacuum filtration. The obtained solid was washed with diethyl ether and dried over a vacuum.

2,3-Dimethylbenzo[d]thiazol-3-ium iodide (BT⁺)

Yield 99%; ¹H NMR (500 MHz, DMSO-*d*₆) δ (ppm) 8.39 (d, *J* = 8.2 Hz, 1H), 8.24 (d, *J* = 8.5 Hz, 1H), 7.87 – 7.83 (m, 1H), 7.76 (dd, *J* = 8.0, 7.4 Hz, 1H), 4.15 (s, 3H), 3.13 (s, 3H).

2-Amino-3-methylbenzo[d]thiazol-3-ium iodide (BT-NH₂⁺)

Yield 95%; ¹H NMR (500 MHz, DMSO-*d*₆) δ (ppm) 7.97 (d, *J* = 7.8 Hz, 1H), 7.64 (d, *J* = 8.2 Hz, 1H), 7.54 (t, *J* = 7.8 Hz, 1H), 7.39 (t, *J* = 7.6 Hz, 1H), 3.69 (s, 3H).

1,4-Dimethylpyridin-1-ium iodide (4-Py⁺)

Yield 71%; ¹H NMR (500 MHz, DMSO-*d*₆) δ (ppm) 8.70 (d, *J* = 6.6 Hz, 2H), 7.83 (d, *J* = 6.4 Hz, 2H), 4.15 (s, 3H), 3.23 (s, 3H).

1,2,3,3-Tetramethyl-3H-indol-1-ium iodide (TMIN⁺)

Yield 95%; ¹H NMR (500 MHz, DMSO-*d*₆) δ (ppm) 7.89 – 7.86 (m, 1H), 7.79 (dt, *J* = 6.7, 3.3 Hz, 1H), 7.60 – 7.55 (m, 2H), 3.94 (s, 3H), 2.74 (s, 3H), 1.49 (s, 6H).

2,3-Dimethylbenzo[d]oxazol-3-ium iodide (BX⁺)

Yield 87%; ¹H NMR (500 MHz, DMSO-*d*₆) δ (ppm) 7.13 (ddd, *J* = 7.8, 6.3, 1.7 Hz, 2H), 6.92 – 6.89 (m, 1H), 6.80 (td, *J* = 7.5, 1.2 Hz, 1H), 2.97 (s, 3H), 1.63 (s, 3H).

1,2-Dimethylquinolin-1-ium iodide (2-QL⁺)

Yield 85%; ¹H NMR (500 MHz, DMSO-*d*₆) δ (ppm) 9.06 (d, *J* = 8.5 Hz, 1H), 8.55 (d, *J* = 9.0 Hz, 1H), 8.36 (dd, *J* = 8.1, 1.3 Hz, 1H), 8.19 (ddd, *J* = 8.8, 7.0, 1.5 Hz, 1H), 8.08 (d, *J* = 8.5 Hz, 1H), 7.95 (t, *J* = 7.6 Hz, 1H), 4.41 (s, 3H), 3.04 (s, 3H).

1,4-Dimethylquinolin-1-ium iodide (4-QL⁺)

Yield 92%; ¹H NMR (500 MHz, DMSO-*d*₆) δ (ppm) 9.38 – 9.25 (m, 1H), 8.52 – 8.41 (m, 2H), 8.31 – 8.20 (m, 1H), 8.05 – 7.97 (m, 2H), 4.54 (s, 3H), 2.96 (s, 3H).

2.2.2 Synthesis of polycationic 2-methylbenzothiazolium salt

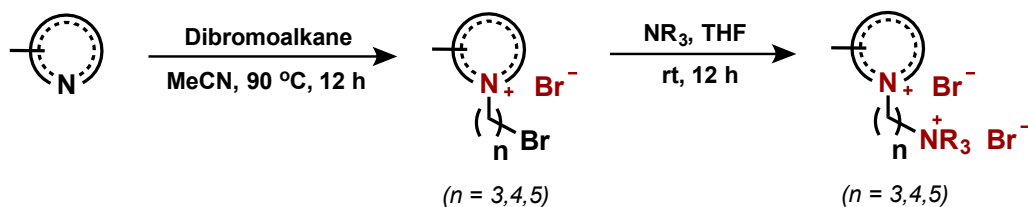


Figure 2.2 Modification of cationic side chain heterocycles

The solution of 2-methylbenzothiazole (1.0 equiv.) and dibromoalkane (5.0 equiv.) in acetonitrile was refluxed for 6-12 hours. The precipitate was washed with diethyl ether and dried under a vacuum. Next, the introduction of the positive charge on the side chain was performed by stirring the mixture between bromoalkoxyl heterocycle and trimethylamine (30% v/v in THF) at room temperature overnight. The precipitate obtained was collected by filtration, washed with diethyl ether, and dried under a vacuum.

2-Methyl-3-(3-(pyridin-1-ium-1-yl)propyl)benzo[d]thiazol-3-ium bromide

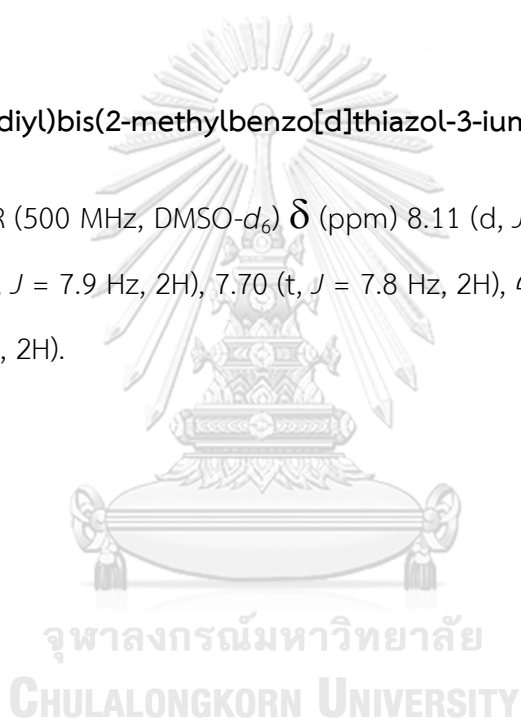
(BTC3Py²⁺) Yield 56%; ¹H NMR (500 MHz, DMSO-*d*₆) δ (ppm) 9.17 (d, *J* = 5.9 Hz, 2H), 8.59 (dd, *J* = 11.3, 4.3 Hz, 1H), 8.45 (dd, *J* = 10.4, 8.7 Hz, 2H), 8.18 – 8.14 (m, 2H), 7.87 (dd, *J* = 8.3, 7.4 Hz, 1H), 7.78 (t, *J* = 7.7 Hz, 1H), 4.88 (dd, *J* = 16.2, 9.9 Hz, 4H), 3.18 (s, 3H), 2.53 (dq, *J* = 15.5, 7.8 Hz, 2H).

2-Methyl-3-(5-(pyridin-1-ium-1-yl)pentyl)benzo[d]thiazol-3-ium bromide (BTC5Py²⁺)

Yield 72%; ¹H NMR (500 MHz, DMSO-*d*₆) δ (ppm) 9.08 (t, *J* = 5.9 Hz, 2H), 8.58 (dd, *J* = 12.2, 4.4 Hz, 1H), 8.42 (d, *J* = 8.0 Hz, 1H), 8.30 (d, *J* = 8.5 Hz, 1H), 8.14 (t, *J* = 7.0 Hz, 2H), 7.87 – 7.83 (m, 1H), 7.77 (t, *J* = 7.7 Hz, 1H), 4.72 – 4.63 (m, 2H), 4.59 (t, *J* = 7.3 Hz, 2H), 3.18 (s, 3H), 1.96 (dd, *J* = 13.1, 5.7 Hz, 2H), 1.90 – 1.82 (m, 2H), 1.48 – 1.38 (m, 2H).

3,3'-(Propane-1,3-diyl)bis(2-methylbenzo[d]thiazol-3-ium) bromide (BisBT(C3)²⁺)

Yield 80%; ¹H NMR (500 MHz, DMSO-*d*₆) δ (ppm) 8.11 (d, *J* = 8.3 Hz, 2H), 8.00 (d, *J* = 8.6 Hz, 2H), 7.78 (t, *J* = 7.9 Hz, 2H), 7.70 (t, *J* = 7.8 Hz, 2H), 4.96 – 4.88 (m, 4H), 3.10 (s, 6H), 2.61 – 2.50 (m, 2H).



2.2.3 Modification of cationic side chain aromatic aldehyde

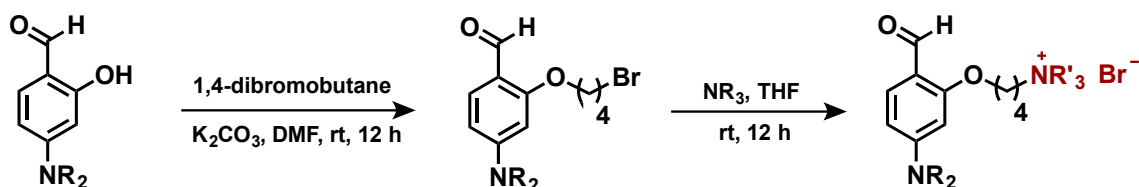


Figure 2.3 Modification of cationic side chain aromatic aldehydes

The synthesis of the positively charged aldehyde consisted of two steps – bromoalkylation and positive charge introduction. First, the solution of 2-salicylaldehyde derivative (1.0 equiv.), 1,4-dibromobutane (5.0 equiv.), and dried K_2CO_3 (1.5 equiv.) in anhydrous DMF was stirred at room temperature for 12 hours. Then, the crude reaction mixture was diluted in DCM and extracted with water (3 x 20 mL). After that, the organic layer was dried over $MgSO_4$ and then the solvent residue was removed under vacuum. The crude product was purified by column chromatography (Hexane:EtOAc (4:1)) to afford the bromoalkoxy aldehyde intermediate as a yellow-brown oil. Next, the positive charge installation on the side chain of the aldehyde was performed by stirring the mixture between the bromoalkoxy aldehyde and trimethylamine (30%v/v in THF, 5.0 equiv.) at room temperature overnight. The precipitated product was collected by filtration, washed with diethyl ether, and dried under vacuum.

4-(5-(Diethylamino)-2-formylphenoxy)-*N,N,N*-trimethylbutan-1-aminium bromide (Ald⁺)

Yield 65%; ¹H NMR (500 MHz, DMSO-*d*₆) δ (ppm) 9.98 (s, 1H), 7.47 (d, *J* = 8.9 Hz, 1H), 6.31 (dt, *J* = 5.5, 2.7 Hz, 1H), 6.09 (d, *J* = 2.2 Hz, 1H), 4.11 – 4.06 (m, 2H), 3.02 (s, 9H), 1.89 – 1.81 (m, 2H), 1.79 – 1.71 (m, 2H), 1.08 (t, *J* = 7.0 Hz, 6H). ¹³C NMR (126 MHz, DMSO-*d*₆) δ (ppm) 186.1, 163.5, 154.1, 130.4, 113.7, 104.8, 93.8, 67.3, 65.5, 52.7, 44.6, 26.1, 24.6, 19.8, 18.0, 13.0.

4-(5-(Azetidin-1-yl)-2-formylphenoxy)-*N,N,N*-trimethylbutan-1-aminium bromide (AzeAld⁺)

Yield 74%; ¹H NMR (500 MHz, DMSO-*d*₆) δ (ppm) 9.97 (d, *J* = 38.6 Hz, 1H), 7.44 (t, *J* = 22.4 Hz, 1H), 5.97 (d, *J* = 8.3 Hz, 1H), 5.82 (d, *J* = 33.5 Hz, 1H), 4.06 (s, 2H), 3.94 (t, *J* = 6.8 Hz, 4H), 3.03 (s, 9H), 2.46 (m, 2H), 2.36 – 2.27 (m, 2H), 1.84 (m, 2H), 1.74 (m, 2H). ¹³C NMR (126 MHz, DMSO-*d*₆) δ (ppm) 186.5, 163.2, 157.0, 130.2, 114.5, 103.7, 93.0, 67.5, 65.5, 52.7, 51.7, 26.0, 19.8, 16.3.

4-(2-Formyl-5-(4-methylpiperazin-1-yl)phenoxy)-*N,N,N*-trimethylbutan-1-aminium bromide (PizAld⁺)

Yield 46%; ¹H NMR (500 MHz, DMSO-*d*₆) δ (ppm) 10.01 (s, 1H), 7.48 (d, *J* = 8.9 Hz, 1H), 6.34 (dd, *J* = 8.9, 1.8 Hz, 1H), 6.14 (d, *J* = 2.0 Hz, 1H), 4.11 (t, *J* = 5.9 Hz, 2H), 3.03 (s, 9H), 1.89 – 1.80 (m, 2H), 1.79 – 1.71 (m, 2H). ¹³C NMR (126 MHz, DMSO-*d*₆) δ (ppm) 186.4, 163.2, 156.4, 130.1, 114.1, 105.2, 94.6, 67.4, 65.5, 64.9, 52.8, 52.7, 46.7, 26.1, 19.8. HRMS (MALDI-TOF): *m/z* calcd for C₁₉H₃₂N₃O₂⁺: 334.2489 [M-H]⁺ found: 334.2477.

4-(2-Formyl-5-morpholinophenoxy)-*N,N,N*-trimethylbutan-1-aminium bromide (MorpAld⁺)

Yield 53%; ¹H NMR (500 MHz, DMSO-*d*₆) δ (ppm) 10.02 (s, 1H), 7.48 (dd, *J* = 7.2, 3.7 Hz, 1H), 6.34 (dt, *J* = 7.4, 1.9 Hz, 1H), 6.14 (t, *J* = 5.7 Hz, 1H), 4.11 (dd, *J* = 10.5, 4.7 Hz, 2H), 3.01 (t, *J* = 6.4 Hz), 1.89 – 1.82 (m, 2H), 1.78 – 1.72 (m, 2H), 1.70 – 1.64 (m, 8H). ¹³C NMR (126 MHz, DMSO-*d*₆) δ (ppm) 187.0, 163.1, 157.2, 130.0, 116.0, 106.8, 97.1, 67.6, 66.3, 65.5, 52.7, 47.2, 26.0, 19.8.

4-((1-Formylnaphthalen-2-yl)oxy)-*N,N,N*-trimethylbutan-1-aminium bromide (NaphAld⁺)

Yield 83%; ¹H NMR (500 MHz, DMSO-*d*₆) δ (ppm) 10.80 (s, 1H), 9.08 (d, *J* = 8.6 Hz, 1H), 8.26 (d, *J* = 9.2 Hz, 1H), 7.92 (d, *J* = 7.9 Hz, 1H), 7.61 (ddd, *J* = 8.5, 6.9, 1.3 Hz, 1H), 7.57 (d, *J* = 9.2 Hz, 1H), 7.45 – 7.41 (m, 1H), 4.33 (t, *J* = 5.8 Hz, 2H), 3.40 – 3.33 (m, 2H), 3.04 (s, 9H), 1.93 – 1.78 (m, 4H). ¹³C NMR (126 MHz, DMSO-*d*₆) δ (ppm) 192.0, 163.9, 138.6, 131.2, 130.4, 129.2, 128.7, 125.2, 124.4, 116.1, 115.1, 69.0, 65.4, 52.7, 26.2, 19.8. HRMS (MALDI-TOF): *m/z* calcd for C₁₅H₁₈NO₂⁺: 286.1802 [M-H]⁺ found: 286.1829

4-((9-Formyl-2,3,6,7-tetrahydro-1*H*,5*H*-pyrido[3,2-*ij*]quinolin-8-yl)oxy)-*N,N,N*-trimethylbutan-1-aminium bromide (JuAld⁺)

Yield 80%; ¹H NMR (500 MHz, DMSO-*d*₆) δ (ppm) 9.85 – 9.76 (m, 1H), 7.11 (s, 1H), 3.81 (d, *J* = 6.1 Hz, 2H), 3.22 (s, 4H), 3.03 (d, *J* = 1.1 Hz, 9H), 2.61 (d, *J* = 5.4 Hz, 4H), 1.76 (dd, *J* = 49.7, 15.4 Hz, 8H). ¹³C NMR (126 MHz, DMSO-*d*₆) δ (ppm) 186.8, 159.2, 149.2, 126.9, 117.4, 116.5, 112.5, 74.6, 66.8, 65.6, 55.0, 52.7, 50.9, 49.8, 49.6, 49.5, 27.3, 27.0, 21.3, 21.0, 20.7, 19.6. HRMS (MALDI-TOF): *m/z* calcd for C₂₀H₃₁N₂O₂⁺: 331.2380 [M-H]⁺ found: 331.2378.

2.3 Conventional synthesis of cationic styryl dyes

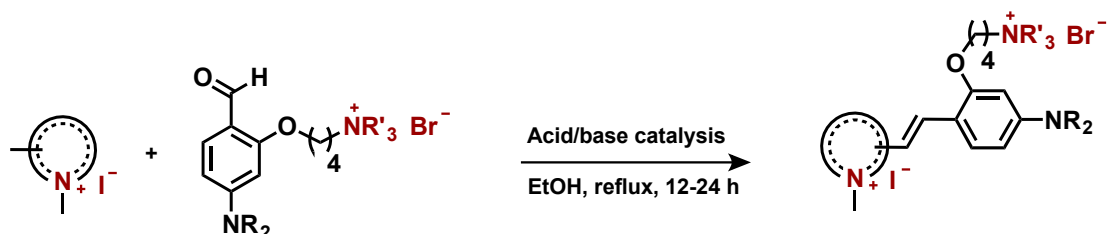


Figure 2.4 Synthesis of cationic styryl dyes

The aldol-type condensation between the quaternized heterocyclic compound bearing an acidic methyl group and the aromatic aldehyde was performed as described in the literature.⁵³ In brief, the solution of the cationic heterocycle (1 equiv.) and aromatic aldehyde (1 equiv.) was carried out in ethanol (1 mL/mmol) was heated at 90 °C overnight without any added catalyst. For the less reactive QL^+ as the heterocyclic coupling partner, the reaction was performed in acetic anhydride (1 mL/mmol) to allow acid catalyzed pathway. The products were obtained as dark red to dark purple solids. To facilitate the isolation of the products, the counterions in all cationic dyes were exchanged to hexafluorophosphate (PF_6^-) by treatment of the crude product with excess NH_4PF_6 in ethanol. The precipitated salts were isolated by filtration and then recrystallized in EtOH.

(E)-2-(4-(Diethylamino)-2-(4-(trimethylammonio)butoxy)styryl)-5-methoxy-3-methylbenzo[d]thiazol-3-ium bromide iodide (5-OMe-BT⁺-Ald⁺)

Yield 43%; ¹H NMR (500 MHz, DMSO-*d*₆) δ (ppm) 8.12 (d, *J* = 8.9 Hz, 1H), 8.05 (d, *J* = 15.2 Hz, 1H), 7.88 (d, *J* = 9.2 Hz, 1H), 7.54 (d, *J* = 2.3 Hz, 1H), 7.45 (d, *J* = 15.2 Hz, 1H), 7.23 (dd, *J* = 8.9, 2.3 Hz, 1H), 6.48 (dd, *J* = 9.2, 2.1 Hz, 1H), 6.17 (d, *J* = 2.1 Hz, 1H), 4.18 (t, *J* = 5.8 Hz, 2H), 4.10 (s, 3H), 3.89 (s, 3H), 3.48 (dt, *J* = 22.7, 8.0 Hz, 6H), 3.09 (s, 9H), 1.95 – 1.82 (m, 4H), 1.13 (t, *J* = 7.0 Hz, 6H). ¹³C NMR (126 MHz, DMSO-*d*₆) δ (ppm) 172.2, 161.5, 160.9, 154.1, 154.0, 144.0, 143.6, 124.9, 118.2, 116.3, 111.4, 106.7, 105.2, 100.3, 94.4, 67.8, 65.4, 56.9, 52.7, 44.5, 35.8, 26.1, 19.8, 13.2. HRMS (MALDI-TOF): *m/z* calcd for C₂₈H₄₁N₃O₂S⁺: 482.2836 [M-H]⁺ found: 482.2834.

(E)-2-(4-(Diethylamino)-2-(4-(trimethylammonio)butoxy)styryl)-6-methoxy-3-methylbenzo[d]thiazol-3-ium bromide iodide (6-OMe-BT⁺-Ald(NEt₂)⁺)

Yield 43%; ¹H NMR (500 MHz, DMSO-*d*₆) δ (ppm) 8.00 (d, *J* = 15.3 Hz, 1H), 7.94 (d, *J* = 9.2 Hz, 1H), 7.85 (t, *J* = 6.2 Hz, 2H), 7.44 (d, *J* = 15.2 Hz, 1H), 7.32 (dd, *J* = 9.2, 2.6 Hz, 1H), 6.47 (dd, *J* = 9.1, 2.1 Hz, 1H), 6.18 (d, *J* = 2.1 Hz, 1H), 4.18 (t, *J* = 5.8 Hz, 2H), 4.08 (s, 3H), 3.85 (s, 3H), 3.44 (ddt, *J* = 29.2, 14.0, 7.0 Hz, 7H), 3.08 (s, 9H), 1.95 – 1.82 (m, 4H), 1.13 (t, *J* = 7.0 Hz, 6H). ¹³C NMR (126 MHz, DMSO-*d*₆) δ (ppm) 169.7, 161.4, 159.1, 153.8, 143.5, 136.7, 128.5, 117.6, 117.1, 111.3, 107.5, 106.5, 105.4, 94.4, 67.8, 65.5, 56.7, 56.6, 52.8, 44.9, 35.2, 26.1, 19.7, 13.2. HRMS (MALDI-TOF): *m/z* calcd for C₂₈H₄₁N₃O₂S⁺: 482.2836 [M-H]⁺ found: 482.2805.

(E)-1-Methyl-2-(4-morpholino-2-(4-(trimethylammonio)butoxy)styryl)quinolin-1-ium bromide iodide (2-QL⁺-Ald(Morp)⁺)

Yield 26%; ¹H NMR (500 MHz, DMSO-*d*₆) δ (ppm) 8.77 (d, *J* = 9.1 Hz, 1H), 8.40 (dd, *J* = 9.1, 3.1 Hz, 1H), 8.27 – 8.17 (m, 2H), 8.07 (s, 1H), 7.84 (dd, *J* = 8.1, 6.4 Hz, 1H), 7.65 (d, *J* = 15.6 Hz, 2H), 6.71 – 6.66 (m, 1H), 6.53 (d, *J* = 2.1 Hz, 1H), 4.38 (s, 3H), 4.18 (s, 2H), 3.80 – 3.62 (m, 4H), 3.10 – 3.04 (m, 18H), 1.99 – 1.79 (m, 4H). ¹³C NMR (126 MHz, DMSO-*d*₆) δ (ppm) 160.7, 157.2, 155.7, 143.7, 142.8, 139.8, 134.9, 132.9, 130.4, 128.7, 127.4, 120.7, 119.4, 114.4, 114.0, 107.6, 97.6, 68.0, 66.4, 65.5, 52.8, 47.3, 26.2, 19.9. HRMS (MALDI-TOF): *m/z* calcd for C₂₉H₃₉N₃O₂⁺: 460.2958 [M-H]⁺ found: 460.2951.

(E)-2-(4-(Diethylamino)-2-(4-(trimethylammonio)butoxy)styryl)-3-ethylbenzo[d]thiazol-3-ium hexafluorophosphate (BT⁺-Ald⁺)

Yield 63 %; ¹H NMR (500 MHz, DMSO-*d*₆) δ (ppm) 8.18 (d, *J* = 7.9 Hz, 1H), 8.12 (d, *J* = 15.1 Hz, 1H), 8.03 (d, *J* = 8.3 Hz, 1H), 7.90 (d, *J* = 9.1 Hz, 1H), 7.75 (t, *J* = 7.7 Hz, 1H), 7.64 (t, *J* = 7.6 Hz, 1H), 7.50 (d, *J* = 15.2 Hz, 1H), 6.54 (d, *J* = 8.9 Hz, 1H), 6.21 (s, 1H), 4.21 (t, 2H), 4.12 (s, 3H), 3.64 – 3.47 (m, 6H), 3.09 (s, 9H), 1.92 (q, 4H), 1.18 (t, *J* = 6.9 Hz, 6H); ¹³C NMR (126 MHz, DMSO-*d*₆) δ (ppm) 171.1, 161.3, 153.8, 146.3, 144.2, 142.0, 128.8, 127.2, 126.2, 123.6, 115.6, 111.0, 106.3, 104.4, 93.9, 67.3, 65.1, 52.3, 44.5, 35.1, 25.6, 19.2, 12.7.; HRMS (MALDI-TOF): *m/z* calcd for C₂₇H₃₈N₃OS⁺: 452.2735 [M-H]⁺ found: 452.2774.

(E)-2-(4-(Diethylamino)-2-(4-(trimethylammonio)butoxy)styryl)-1,3,3-trimethyl-3H-indol-1-ium hexafluorophosphate (TMIN⁺-Ald⁺)

Yield 91 %; ¹H NMR (500 MHz, DMSO-*d*₆) δ (ppm) 8.41 (d, *J* = 15.4 Hz, 1H), 8.06 (d, *J* = 8.9 Hz, 1H), 7.70 (d, *J* = 7.3 Hz, 1H), 7.63 (d, *J* = 8.0 Hz, 1H), 7.53 (t, *J* = 8.2 Hz, 1H), 7.44 (t, *J* = 7.7 Hz, 1H), 7.19 (d, *J* = 15.5 Hz, 1H), 6.60 (d, *J* = 7.4 Hz, 1H), 6.23 (s, 1H),

4.23 (s, 2H), 3.86 (s, 3H), 3.58 (q, $J = 7.0$ Hz, 6H), 3.09 (s, 9H), 1.91 (s, 4H), 1.70 (s, 6H), 1.19 (t, $J = 7.1$ Hz, 6H). ^{13}C NMR (126 MHz, DMSO- d_6) δ (ppm) 179.0, 162.7, 155.5, 142.8, 142.3, 129.3, 127.4, 123.0, 113.5, 112.6, 107.5, 94.2, 67.9, 65.5, 52.7, 50.6, 45.3, 33.0, 27.7, 26.2, 19.8, 13.2.; HRMS (MALDI-TOF): m/z calcd for $\text{C}_{30}\text{H}_{45}\text{N}_3\text{O}^+$: 462.3479 [M-H] $^+$ found: 462.3410.

(E)-2-(4-(Diethylamino)-2-(4-(trimethylammonio)butoxy)styryl)-3-methylbenzo[d]oxazol-3-ium hexafluorophosphate (BX $^+$ -Ald $^+$)

Yield 38%; ^1H NMR (500 MHz, DMSO- d_6) δ (ppm) 8.31 (t, $J = 11.9$ Hz, 1H), 7.89 (ddd, $J = 7.3, 6.2, 5.0$ Hz, 3H), 7.59 (m, 1.4 Hz, 2H), 7.14 (d, $J = 15.3$ Hz, 1H), 6.51 (dt, $J = 9.9, 4.9$ Hz, 1H), 6.19 (d, $J = 2.2$ Hz, 1H), 4.21 (t, $J = 5.7$ Hz, 2H), 3.97 (s, 3H), 3.50 (q, $J = 7.0$ Hz, 5H), 3.46 – 3.40 (m, 2H), 3.06 (s, 9H), 1.87 (q, $J = 3.7$ Hz, 4H), 1.13 (d, $J = 7.1$ Hz, 6H). ^{13}C NMR (126 MHz, DMSO- d_6) δ (ppm) 163.7, 161.9, 154.5, 147.3, 132.1, 127.7, 127.4, 113.6, 112.2, 111.2, 106.8, 94.5, 94.3, 67.9, 66.3, 65.5, 54.4, 52.7, 49.4, 45.0, 44.3, 40.5, 40.4, 40.2, 40.0, 39.9, 39.7, 39.5, 33.8, 32.0, 30.0, 26.0, 25.7, 19.8, 19.2, 13.2, 12.3.; HRMS (MALDI-TOF): m/z calcd for $\text{C}_{27}\text{H}_{39}\text{N}_3\text{O}_2^+$: 436.2958 [M-H] $^+$ found: 436.2889.

(E)-2-(4-(Diethylamino)-2-(4-(trimethylammonio)butoxy)styryl)-1-methylquinolin-1-ium hexafluorophosphate (2-QL $^+$ -Ald $^+$)

Yield 54 %; ^1H NMR (500 MHz, DMSO- d_6) δ (ppm) 8.67 (d, $J = 9.1$ Hz, 1H), 8.37 (dd, $J = 16.8, 9.1$ Hz, 2H), 8.27 (d, $J = 15.3$ Hz, 1H), 8.20 (d, $J = 7.9$ Hz, 1H), 8.05 (t, $J = 8.0$ Hz, 1H), 7.81 (t, $J = 8.6$ Hz, 2H), 7.54 (d, $J = 15.4$ Hz, 1H), 6.49 (d, $J = 9.0$ Hz, 1H), 6.24 (s, 1H), 4.34 (s, 3H), 4.22 (t, $J = 5.3$ Hz, 2H), 3.51 (q, $J = 6.9$ Hz, 6H), 3.09 (s, 9H), 1.93 (s, 4H), 1.17 (t, $J = 7.0$ Hz, 6H). ^{13}C NMR (126 MHz, DMSO- d_6) δ (ppm) 161.4, 157.0, 153.2, 144.5, 141.7, 139.8, 134.5, 133.9, 130.3, 128.2, 127.0, 120.3, 119.0, 112.2, 111.3, 106.0, 94.6, 67.8, 65.6, 52.7, 44.8, 39.0, 26.2, 19.9, 13.1.

(E)-4-(4-(Diethylamino)-2-(4-(trimethylammonio)butoxy)styryl)-1-methylquinolin-1-ium hexafluorophosphate (4-QL⁺-Ald⁺)

Yield 26 %; ¹H NMR (500 MHz, DMSO-*d*₆) δ 8.93 (d, *J* = 6.5 Hz, 1H), 8.84 (d, *J* = 8.5 Hz, 1H), 8.28 (m, 2H), 8.17 (m, 2H), 8.01 – 7.91 (m, 3H), 6.47 (d, *J* = 9.0 Hz, 1H), 6.24 (s, 1H), 4.40 (s, 3H), 4.21 (t, 2H), 3.54 – 3.47 (m, 6H), 3.07 (s, 9H), 1.93 (q, 4H), 1.17 (t, *J* = 6.7 Hz, 3H); ¹³C NMR (126 MHz, DMSO-*d*₆) δ (ppm) 160.2, 153.4, 152.0, 146.3, 139.3, 138.9, 134.5, 131.7, 128.5, 125.9, 125.6, 119.1, 113.1, 112.1, 112.0, 105.4, 94.3, 67.2, 65.2, 52.3, 44.2, 43.9, 25.8, 19.4, 12.7.; HRMS (MALDI-TOF): *m/z* calcd for C₂₉H₄₀N₃O⁺: 446.3171 [M-H]⁺ found: 446.3202.

(E)-4-(4-(Diethylamino)-2-(4-(trimethylammonio)butoxy)styryl)-1-methylpyridin-1-ium hexafluorophosphate (4-PY⁺-Ald⁺)

Yield 100 %; ¹H NMR (500 MHz, DMSO-*d*₆) δ (ppm) 8.60 (d, *J* = 5.9 Hz, 2H), 7.97 (m, 3H), 7.57 (d, *J* = 8.0 Hz, 1H), 7.16 (d, *J* = 16.0 Hz, 1H), 6.40 (d, *J* = 8.9 Hz, 1H), 6.21 (s, 1H), 4.16 (m, 5H), 3.54 – 3.43 (m, 6H), 3.09 (s, 9H), 1.89 (d, *J* = 6.9 Hz, 4H), 1.13 (t, *J* = 6.6 Hz, 3H); ¹³C NMR (126 MHz, DMSO-*d*₆) δ (ppm) 159.7, 153.8, 151.2, 144.1, 137.1, 131.2, 121.7, 116.5, 111.2, 105.0, 94.5, 67.1, 65.1, 52.2, 46.2, 44.1, 25.6, 19.5, 12.6.; HRMS (MALDI-TOF): *m/z* calcd for C₂₅H₃₈N₃O⁺: 396.3015 [M-H]⁺ found: 396.3040.

2.4 DNA-templated synthesis of cationic styryl dyes

The quaternized heterocycles and aldehydes were mixed at 1:1 molar ratio (1-2 mM of final concentration from the 5 mM stock solution in MilliQ) in the presence of the nucleic acid template (1 mg/mL, 1.5 μ M in bp) at 200 μ L final volume (in MilliQ) in a 96-well plate. The mixture was shaken continuously and incubated at room temperature (30–40 $^{\circ}$ C) in the absence of light for 2–14 days. The color change was observed under ambient light and UV light (312 and 365 nm) under a transilluminator. The spectroscopic data including UV-Vis absorption and fluorescence emission were collected using multimode plate reader.

For screening of G-quadruplex binding dye, the dye precursors (heteroaromatic and aldehyde) were mixed at the final concentration of 2 mM (molar ratio = 1:1) in 5 mM KCl, 10 mM Tris-HCl (pH 7.4) in the presence of 1 mg/mL DNA (0.75 μ M in base quadruplets) in 100 μ L final volume in a 96-well plate. The mixture was incubated at room temperature for 14 days.



2.5 Spectroscopic studies

2.5.1 Fluorescence quantum yield of synthesized dyes

The optical properties of the cationic styryl dyes in the presence and absence of nucleic acids were studied by measuring the absorption and fluorescence change of the dyes in the presence and absence of nucleic acids in a quartz cuvette with a path length of 1.0 cm at ambient temperature. The fluorescence quantum yield (Φ_f) of the free dyes and bound dyes with DNA were calculated using rhodamine 6G

($\Phi_F = 0.95$, $\lambda_{ex} = 470\text{--}510\text{nm}$) or cresyl violet ($\Phi_F = 0.54$, $\lambda_{ex} = 540\text{--}590\text{nm}$) as the reference dyes. The integrated fluorescence intensities and the absorbance values at λ_{ex} of the standard and the samples were plot and the obtained slopes were assigned as $\text{grad}_{\text{standard}}$ and $\text{grad}_{\text{sample}}$, respectively.

The quantum yield can then be calculated according to equation (2.1):

$$F_{\text{sample}} = F_{\text{standard}} \left(\frac{\text{grad}_{\text{sample}}}{\text{grad}_{\text{standard}}} \right) \left(\frac{h_{\text{sample}}^2}{h_{\text{standard}}^2} \right) \quad (2.1)$$

Where grad is the slope from the plot of integrated fluorescence intensity as a function of absorbance and η is the refractive index of the solvent used for the fluorescence measurement.

2.5.2 Dye-DNA binding interaction study

The binding constant (K_b) and binding site (n) values were determined by fluorescence titration to compare the relative binding affinity between the dye molecules and DNA strands of interest (ssDNA, dsDNA, and GQ (c-MYC) as shown in **Table 2.1**). Firstly, the dye-DNA mixtures at various dye-DNA (in bp) ratios were prepared in 10 mM Tris-HCl buffer (pH 7.4) and 100 mM KCl at a fixed concentration of dyes (2 μM) and designated amounts of DNA in a 96-well microplate with a final volume of 200 μL . Then, the fluorescence at the desired wavelengths were recorded on the microplate reader. The fluorescence intensities were recorded until they reached constant values which represented excess amounts of DNA in the system. Only the data at the optimal ratios for dye-DNA (in bp) which showed a linear relationship were used to calculate the binding parameters: K_b and n . Following the

method of Akbay and co-workers,⁸¹ the McGhee and von Hippel equation was modified based on an assumption that only one type of interaction between dye and DNA leads to the non-cooperative binding. Therefore, K_b and n values can be calculated from fluorescent titration curves using equation (2.2):

$$Y = F_{\max} - \frac{X}{C_{\text{dye}}K_b} \frac{\left(1 - \left[(n-1)\frac{X}{F_{\max}}\right]\right)^{n-1}}{\left(1 - n\frac{X}{F_{\max}}\right)^n} \quad (2.2)$$

where Y =fluorescence intensity at maximum emission wavelength (F) and $X = F \times C_{\text{dye}} / C_{\text{DNA}}$ (bp). Therefore, K_b , n and F_{\max} values can be calculated as approximation parameters of fitting the experimentally obtained data plotted as the dependence of Y on X according to Eq. (2.2).

2.5.2 Evaluation of optical properties of the dyes from DNA-templated synthesis

From the DNA-templated reaction, the yield of the dye product was evaluated by UV-vis absorption at individual absorption maxima. The fluorescence responsiveness of the dye product in a presence of DNA was quantitated by the relative fluorescence that the fluorescence signal from the dye-DNA bound form was divided by the absorbance to decouple the extent of dye formation from the DNA responsiveness as shown in equation (2.3):

$$F = \frac{I_{\text{Fluorescence emission}}}{I_{\text{Absorption}}} \quad (2.3)$$

2.6 Kinetic study of DNA-templated synthesis

The kinetic study was performed by measuring the absorption and fluorescence change as a function of time. Under pseudo-first-order condition of BT^+ , the $\text{Ald}(\text{NEt}_2)^+$ was validated in a range concentration 1-10 mM with salmon testes DNA (1 mg/mL) in 200 μL final volume in a 96-well plate. The dye formation was observed by UV-Vis absorption at 570 nm of absorption maxima and fluorescence emission at 590 nm ($\lambda_{\text{ex}}=565$ nm). At 10 mM $\text{Ald}(\text{NEt}_2)^+$, the reaction reached its steady state after 30 hours at 25 °C.

2.7 Quantitation of styryl dye product from DNA-templated synthesis

2.7.1 Quantitative NMR analysis

The BT^+ - Ald^+ dye was extracted from the crude reaction mixture (200 μL) by using the ionic liquid $[\text{BMIM}]\text{PF}_6$ (IL) (5 μL). The IL layer was washed with water (3 x 20 μL) and then dried under vacuum. The extracted product was dissolved in 500 μL $\text{DMSO-}d_6$ and then 50 μL of methyl-3,5-dinitrobenzoate solution (10 mM in $\text{DMSO-}d_6$) was added as an internal standard (final concentration of IS = 0.91 mM). The yield of the desired product was calculated from the integration of the ^1H NMR signal (number of scans = 128) according to equation (2.4):

$$\frac{I_{\text{sample}}}{I_{\text{std}}} = \frac{H_{\text{sample}}C_{\text{sample}}}{H_{\text{std}}C_{\text{std}}} \quad (2.4)$$

Where H is number of hydrogen atoms and C is concentration

2.7.2 UV-Visible spectroscopic analysis

For the quantitation of dye formation after a specified period of time, the volume of the crude product was adjusted from 0.2 mL to 1.0 mL in 1.0 mL of a quartz cuvette. The BT⁺-Ald⁺ dye concentration was converted and calculated from the absorption at 570 nm ($\epsilon_{570} = 7.9 \times 10^4 \text{ M}^{-1}\text{cm}^{-1}$ for BT⁺-Ald⁺ dye) according to Beer's law according to equation (5):

$$A = \epsilon bc \quad (5)$$

Where c is pathlength (1 cm) and ϵ is epsilon (ϵ)

2.7.3 HPLC analysis

The analysis was performed by reverse-phase HPLC using a Vertical[®] UPS C18 column (4.6 mm × 50 mm, 3 μm). The mobile phase consisted of solvent A (0.1% TFA in MilliQ water) and solvent B (0.1% TFA in acetonitrile). The column was equilibrated at 1%B for 5 min, raised to 60% B over 5 min, held at 60% B for 4 min, and then lowered to 1% B in 3 min at a constant flow rate of 1.0 mL/min.

To analyse the dye formation, the crude dye was extracted with ionic liquid [BMIM]PF₆ (5 μL) and washed. Then, the IL layer was collected and re-dissolved in methanol (1 mL) for HPLC analysis. The injection volume was 10 μL .

2.8 Biological study

2.8.1 Cell culture

HeLa cells were cultured in Dulbecco's Modified Eagle's Medium (DMEM, HyClone™ Thermo Scientific, USA) containing 4.5 g/L D-glucose, 4 mM L-glutamine and supplemented with 10% of heat-inactivated fetal bovine serum (FBS; Gibco™ Invitrogen) at 37 °C at 5% CO₂.

2.8.2 Cell imaging experiment

The HeLa cells were seeded on a 24-well chamber cell culture plate at 5×10^4 cells per well. The cells were grown in cultured media in a humidification incubator at 37 °C and 5% CO₂. The live cells were stained with 20 μM BT⁺-Ald⁺, 500 nM PhenoVue512 at 37 °C. After 18 h of treatment, the cells were stained with DAPI (0.2 μg/mL) and incubated for 15 minutes. The fluorescence images of the live cells were recorded using an inverted fluorescence microscope (ZEISS Axio Observer).

2.8.3 Cell viability using MTT assay

HeLa cells were seeded in 96-well plates at 1×10^4 cells per well. The cells were incubated at 37 °C in a humidification incubator with 5% CO₂. After 24 hours of incubation, the cells were treated with different concentrations of 10, 50, 100, 200 μM coupling partners (BT⁺, Ald⁺, AldPy⁺). They were incubated under the same conditions for 3 days. MTT solution (5 mg/mL of 3-(4,5-dimethylthiazol-2-yl)-2,5-diphenyltetrazolium bromide in DMEM) was added to the wells and again incubated at 37 °C for 3 hours. The media was then removed and mixed with DMSO. The absorbance at 570 nm was measured with a PerkinElmer, EnSight Multimode Microplate Reader and the cytotoxicity was calculated.

2.8.4 Templated synthesis of styryl dyes in cells

The HeLa cells were seeded on a 24-well plate at 5×10^4 cells per well. The cells were grown in an incubator at 37 °C and 5% CO₂ for 18 hours. In a screening experiment, the cell lines were treated with the coupling partners at 37 °C and 5% CO₂. After 3 days of treatment, the cells were fixed with 4% paraformaldehyde (in PBS) for 10 minutes and then permeabilized with 1% Triton X-100 (in PBS) for 2 minutes at room temperature. Then, the fixed cells were stained with DAPI (1 µg/mL) for 20 minutes at room temperature. For RNase and DNase treatment, after cellular fixation and permeabilization, the fixed cells were incubated with RNase A (25 µg/mL) or DNase I (30 µg/mL) at 37 °C for 4 hours. After that the cells were used for studying DNA-templated reactions with the same normal protocol.

The fluorescence images of the live cells after treatment were recorded using a fluorescence microscope (ZEISS Axio Observer with optical sectioning and deconvolution algorithm).

2.8.5 Double-stranded RNA (dsRNA) production

This experiment was performed by Dr. Kitipong Angsujinda from Aquatic Resources Research Institute, Chulalongkorn University. To express dsRNA, a single colony of *E. coli* strain HT115(DE3) harboring a plasmid encoding dsRNA specific to a ribonucleotide reductase small subunit gene of White spot syndrome virus (pET-17b-dsWSV-rr2) was grown on in the LB medium containing 12 µg/ml tetracycline and 50 µg/ml ampicillin at 30 °C with shaking until OD_{600 nm} reach 0.4. The dsRNA expression was induced with the addition of isopropyl-β-d-thiogalactopyranoside (IPTG) at 0.4 mM final concentration. Following incubation at 30 °C for 3 h, the cells were collected by centrifugation at 15,557 × g for 15 min at 4 °C. To extract the dsRNA, the induced recombinant bacteria were resuspended in 0.1% SDS in 1× PBS. After boiling for 2 min and immediately keeping on ice for 30 sec, the cell lysate was added with a total of 0.05 µg of RNase A in 1× RNase buffer (300 mM sodium acetate, 10 mM Tris-HCl, pH 7.5, and 5 mM EDTA) and incubated at 37 °C for 30 min. At last, the dsRNA was isolated from the mixture by using a TRI reagent (Molecular Research Center, Cincinnati, OH) following the manufacturer's instruction. The dsRNA obtained was solubilized in DEPC-treated water, verified by polyacrylamide gel electrophoresis, and kept on ice prior to use for further analysis.

CHAPTER III

RESULTS AND DISCUSSION

3.1 Concept validation of DNA-templated styryl dye synthesis

Generally, the aldol-type condensation between an acidic methyl group connected to a heteroaromatic ring and an aromatic aldehyde to form styryl dyes requires heating in the presence of an acid or a base as a catalyst, typically in a polar organic solvent such as ethanol.²⁵ No reaction is expected under biological or ambient conditions without a catalyst. To demonstrate the concept of the newly proposed DNA-templated synthesis of cationic styryl dyes, salmon testes DNA (stDNA) was employed as a generic dsDNA template. Based on the excellent optical properties of the benzothiazolium-based styryl dyes, the benzothiazole scaffold was chosen as the electron-deficient heteroaromatic substrate.

To study the effect of the positive charge on the benzothiazole substrate for the DNA-templated styryl dye synthesis, 2-methylbenzothiazole (BT) was utilized as a model for neutral substrate, while the corresponding *N*-methylated derivative (BT⁺) was employed as a model for cationic substrate. For the aromatic aldehyde part, 4-(diethylamino)salicylaldehyde (Ald) and its trimethylammonium cationic modification derivative (Ald⁺) were selected as the models for neutral and cationic aldehyde substrates, respectively. The templated styryl dye synthesis experiments were conducted in a 96-well plate by pairwise mixing of the benzothiazoles and aldehyde substrates in the absence (−) and presence (+) of the DNA template in water. The reaction mixture was then incubated at ambient temperature (30 °C) on a shaker and the formation of the dye was observed visually and spectroscopically (**Figure 3.1**).

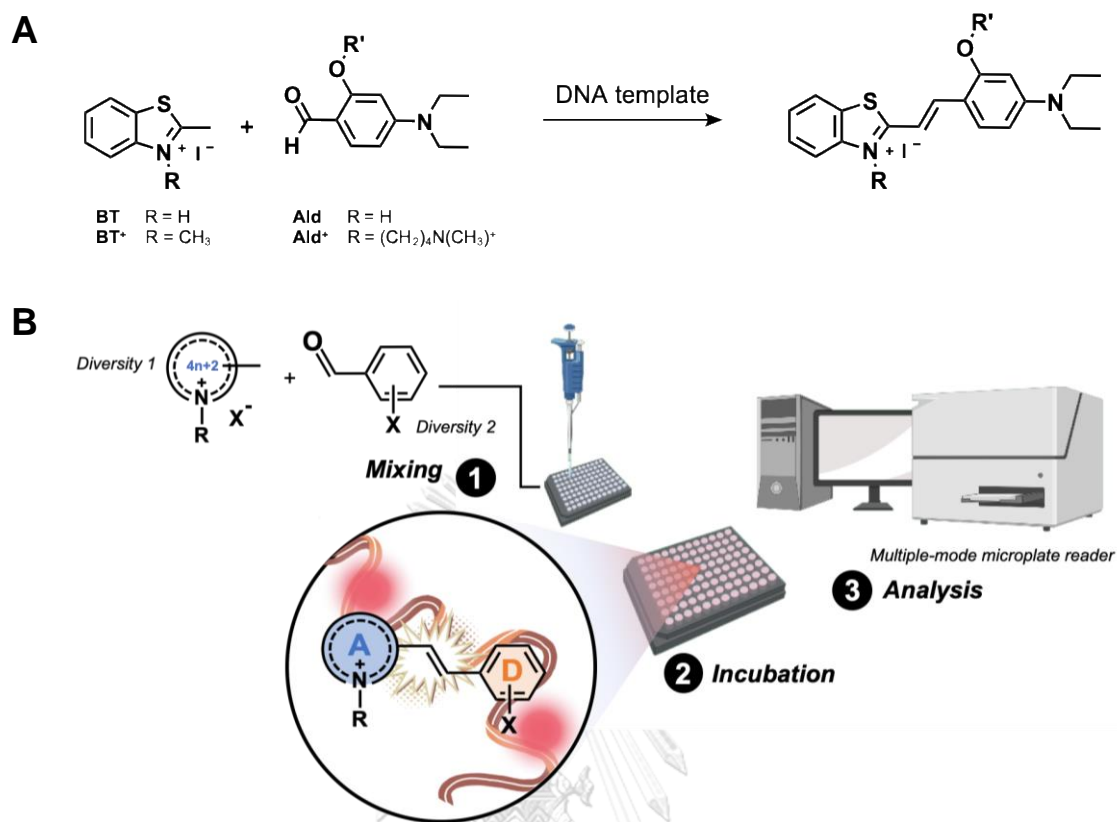


Figure 3.1 (A) A model reaction for DNA-templated synthesis and (B) Work-flow for the combinatorial screening of DNA-templated styryl dye synthesis.

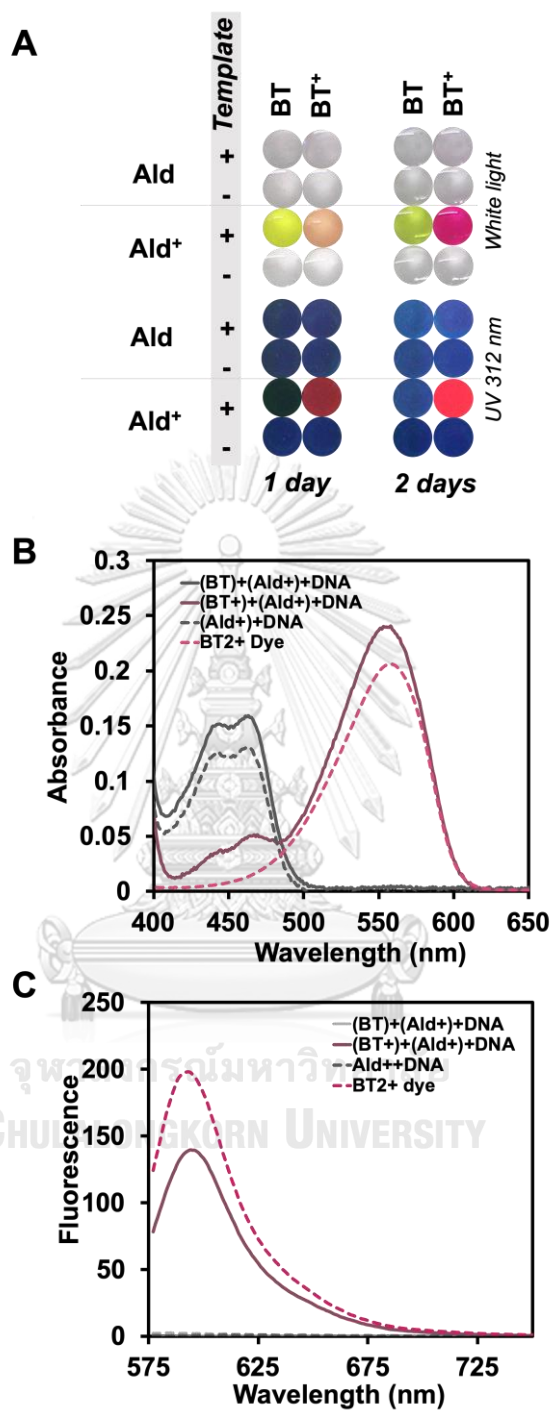


Figure 3.2 (A) Combinatorial screening of the DNA-templated styryl dye synthesis from benzothiazoles and diethylamino-substituted aldehydes. Condition: [Coupling partners] = 1 mM, [stDNA] = 1 mg/mL incubating at room temperature (30 °C) (B) UV-visible spectra and (C) Fluorescence spectra ($\lambda_{\text{ex}} = 565 \text{ nm}$) of crude reaction products from the DNA templated reaction.

In agreement with the expectation, an obvious color change was observed only in the wells that contain both the positively charged aldehyde (Ald^+) and the DNA template after one day of incubation. As shown in the **Figure 3.2A**, yellow-colored solutions were obtained when BT was used as the coupling partner with Ald^+ , while a light pink coloration was observed only from the BT^+ - Ald^+ combination in the presence of the DNA template. When the incubation time was extended to 2 days, the combination of BT^+ - Ald^+ in the presence of the DNA template exhibited a bright pink solution under daylight and a strong red fluorescence under UV light (312 nm). Spectroscopic profiles (absorbance and fluorescence) of the reaction product from the BT^+ - Ald^+ reaction in the presence of the DNA template were compared with the same styryl dye that was independently synthesized by the conventional method from the same coupling partners (BT^+ - Ald^+). The results revealed successful formation of the expected styryl dye product as shown by the absorption maxima at 560 nm and emission maxima at 600 nm (**Figures 3.2B, C**), which was identical to the reference styryl dye independently synthesized by the conventional method.²⁵ Importantly, no color change was observed for any substrate combinations in the absence of the DNA template, indicating the importance of the template. Likewise, no color change was observed when Ald was used instead of Ald^+ thus suggesting the importance of positive charge on the aldehyde substrate.

In another set of control experiments, with only one of the two coupling partners being present, no dye formation was observed despite the presence of the DNA template (**Figure 3.3A**). However, it appears that Ald^+ might also be able to interact with DNA as evidenced by the yellow-colored non-fluorescent solution with an absorption maximum at 470 nm (**Figure 3.3B**). The same yellow solution was also observed in all combinations that contain both Ald^+ and DNA, with the exception of the reaction that also contain BT^+ whereby the styryl dye was successfully formed.

Based on these results, we propose that in the absence of the BT^+ coupling partner, the unreacted Ald^+ may form an adduct with DNA.

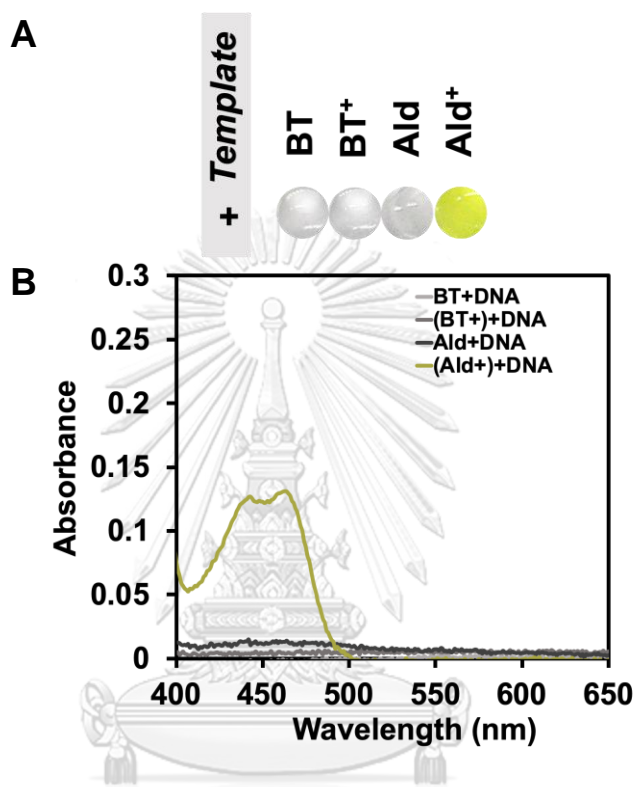
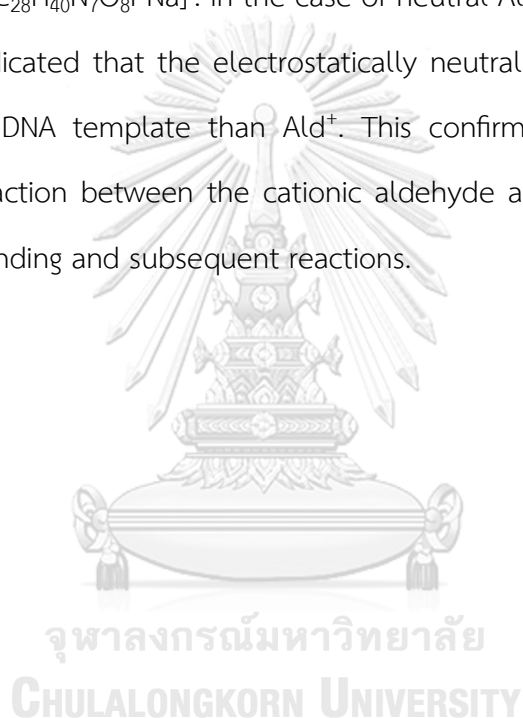


Figure 3.3 (A) Control experiment with only one of two coupling partners in presence of DNA and (B) UV-Visible spectrum. Condition: [Coupling partners] = 1 mM, [DNA] = 1 mg/mL incubating at room temperature (30 °C) for 2 days.

As a hypothesis, it is possible that the Ald^+ substrate could react with one or more nucleobases bearing the exocyclic amino group in the DNA template to form an imine adduct.⁸²⁻⁸⁴ To confirm the hypothesis, an NMR experiment was performed on a mixture of deoxyguanosine monophosphate (dGMP) and Ald^+ at a stoichiometric ratio in water. The mixture was incubated at room temperature for 2 days. To investigate the structure of the Ald^+ -dGMP adduct was analyzed by 2D NMR to

determine the correlations between ^1H - ^1H and ^1H - ^{13}C signals of the adduct molecule. As shown in **Figure 3.4**, the color of the mixture changed from yellow to dark brown. Based on the key HMBC correlation between the ^1H signal of imine at 9.3 ppm and ^{13}C signal of C2 on guanine at 131 ppm, a possible structure of the adduct in which the aldehyde formed an imine with the exocyclic amino group of dG was proposed. Furthermore, the imine product showed the (-ve) m/z at 657.4669 which corresponded to $[\text{C}_{28}\text{H}_{40}\text{N}_7\text{O}_8\text{PNa}]^-$. In the case of neutral Ald, no colored product was observed. This indicated that the electrostatically neutral Ald may bind with lower efficiency to the DNA template than Ald^+ . This confirms the critical role of the electrostatic interaction between the cationic aldehyde and anionic DNA backbone to promote the binding and subsequent reactions.



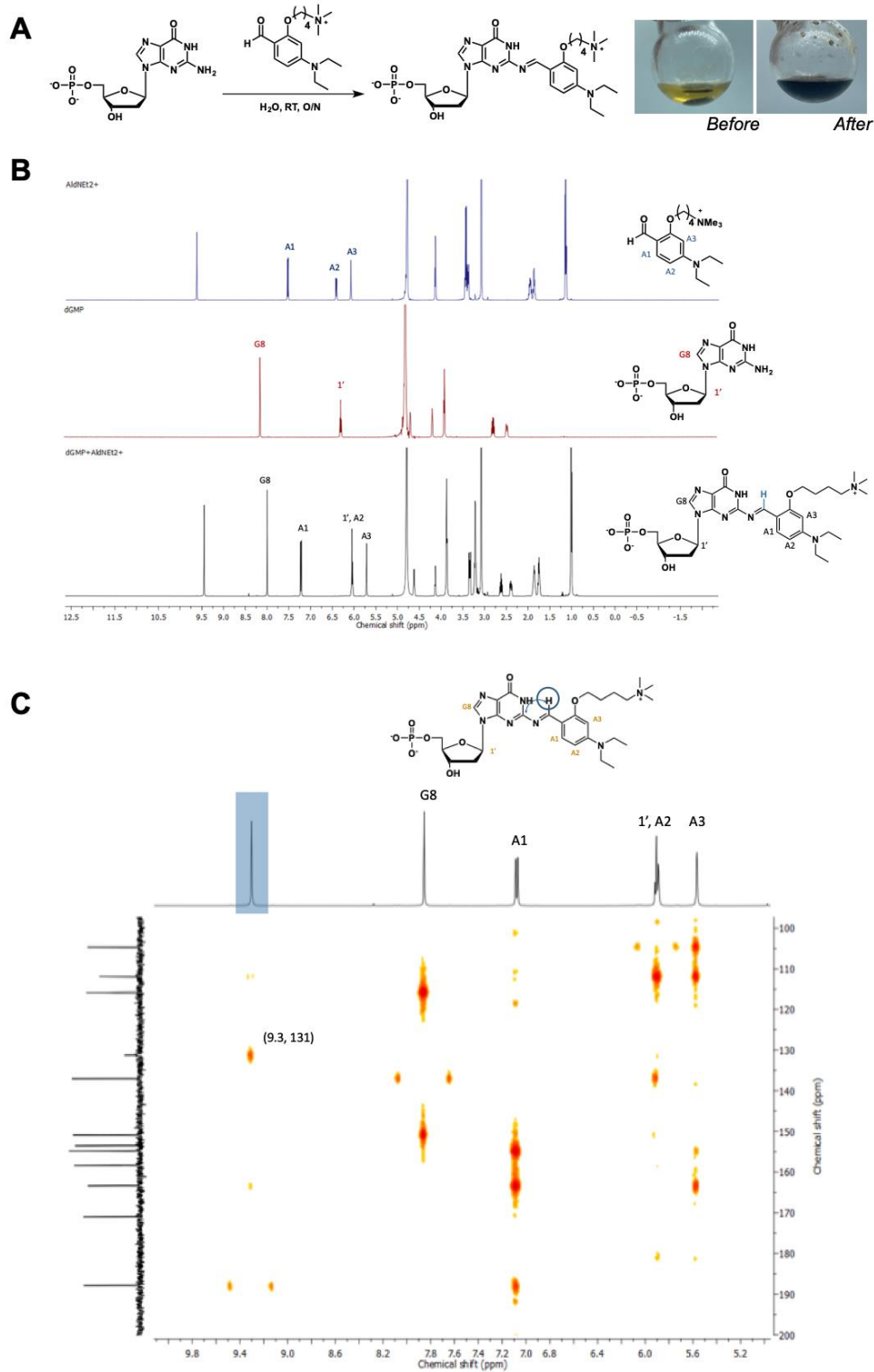


Figure 3.4 (A) Model reaction of dGMP-Ald⁺ (B) ¹H NMR and (C) HMBC spectrum of the crude. Condition: [dGMP] = 1 mM, [Ald⁺] = 1 mM incubating at room temperature (30 °C) for 2 days.

3.1.1 Study of salt or buffer for templated reaction

According to our proposal, the electrostatic interactions between the cationic substrates and the anionic phosphate backbone of the DNA template is responsible for bringing the coupling partners together on the DNA template. To confirm the important role of electrostatic interaction in the DNA-templated dye synthesis, the effects of salt and buffer which contribute to the ionic strength of the reaction medium were studied. As shown in **Figure 3.5**, the addition of NaCl, Tris-HCl, or phosphate buffer attenuated the reaction between BT^+ - Ald^+ as shown by the less pronounced color change when compared to the reaction without these additives. The results confirmed that the increased ionic strength resulting from the addition of salt or buffer to the system suppressed the electrostatic interaction. Rather unexpectedly, the coupling between Ald^+ and the neutral benzothiazole substrate (BT) was more effective in the presence of NaCl as an additive as shown by the formation of pink-colored and fluorescent product, presumably the corresponding monocationic styryl dye. This might be explained by the enhancement of the hydrophobic interaction upon increasing ionic strength thus enabling the coupling between the neutral BT and Ald^+ .

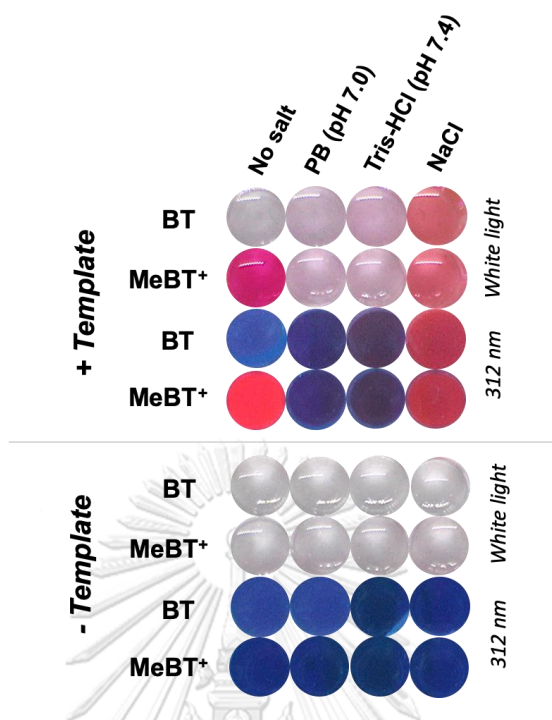


Figure 3.5 Effect of buffers and salt. Condition: [coupling partners] = 1 mM, [DNA] = 1 mg/mL, [salt]/[buffer] = 10 mM incubating at room temperature (30 °C).

3.1.2 Approachability of the templated styryl dye formation with various templates

The reaction between BT⁺ and Ald⁺ was also investigated with other macromolecular templates including polystyrene sulfonate (PSS) (an anionic polymer containing aromatic groups similar to DNA) and polyethylene imine (PEI) (a cationic polymer without aromatic groups). As shown in **Figure 3.6**, in all cases no styryl dye was formed indicating that the templated reaction is specific to the DNA template. In addition, dsDNA was far more effective in templating the dye formation than ssDNA possibly due to the more rigid structure of the dsDNA that provides a more well-defined cavities for the coupling partners to bind (via groove binding or intercalation) and react to form the dye. In addition to DNA, RNAs may also serve as a template for the styryl dye formation as they also possess negatively charged phosphate

backbone and can provide binding cavities that can promote the dye formation via the same mechanism as DNA. When dsRNA was used as the template at the same concentration, the dye formation was less pronounced when compared to dsDNA template. In case of tRNA, the folding structure was only not suitable for dye formation. This could be due to the non-optimal cavity for the coupling partners to bind and the yield of the dye product might also be limited by the degradation of the RNAs during the long incubation time.



Figure 3.6 Effect of templates on DNA-templated synthesis. Condition: [coupling partners] = 1 mM, [DNA] = 1 mg/mL, [salt]/[buffer] = 10 mM incubating at room temperature for 2 days.

3.2 Kinetic study of the styryl dye formation from DNA-templated synthesis

Kinetic studies were performed to evaluate the acceleration of the dye formation by the DNA template. The combination between BT⁺ and Ald⁺ in the presence of salmon testes DNA template was also used as a model reaction. To examine the rate constant of the DNA-templated dye synthesis, the concentration of BT⁺ was fixed at 500 mM to ensure a pseudo-first-order kinetic model. The concentration of Ald⁺ was validated in a range of 1, 2, 5, and 10 mM with stDNA 1 mg/mL (0.8 μM in bp). The absorption of the styryl dye at 570 nm was measured at hourly intervals at 25 °C and plotted as a function of time. From the results, it was found that the absorbance of the dye product increased by a different extent depending on the concentration of the Ald⁺. In the presence of 1 mg/mL stDNA, the kinetic of the dye formation reached the steady state after incubating for 30 and 50 hours in the presence of 10 and 5 mM of Ald⁺, respectively (**Figure 3.7A**). At a higher stDNA concentration (2 mg/mL), the dye formation was significantly faster and the kinetics of the dye formation reached the steady state at 15 and 25 hours in the presence of 10 and 5 mM of Ald⁺, respectively. However, the absorptions dropped after 40 hours of incubation due to aggregation or precipitation of the dye at high concentrations (**Figure 3.7B**). To evaluate the kinetic constants, the condition at 10 mM Ald⁺ 500 mM BT⁺ with 1 mg/mL stDNA which showed reasonably fast kinetics was chosen for the study. As shown in **Figure 3.7C**, the plot between logarithm of A₅₇₀ and time provided a linear relationship indicating that the first-order reaction. Following the pseudofirst-order kinetics model, the rate constant (*k*) of the DNA-templated reaction was estimated at 1.51x10⁻¹ M⁻¹h⁻¹ (or 2.6x10⁻³ M⁻¹s⁻¹) at 25 °C. Due to the slow kinetics of the non-templated reaction, the rate constant could not be calculated.

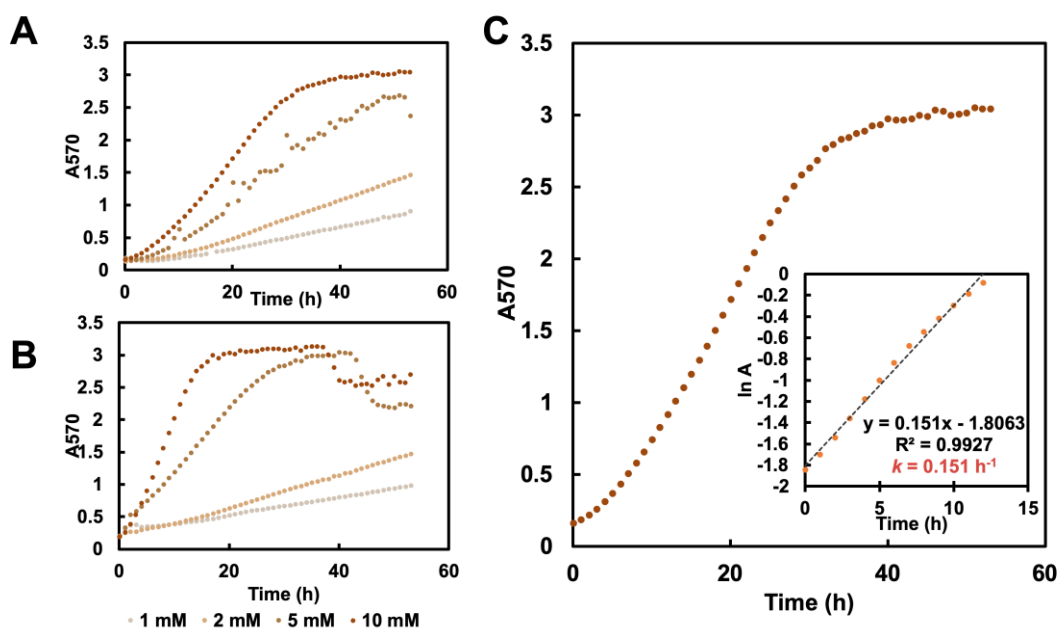


Figure 3.7 Kinetic study of the DNA-templated synthesis of BT⁺-Ald⁺ in the presence of (A) 1 mg/mL stDNA, and (B) 2 mg/mL of stDNA. (C) Plots between ln (A₅₇₀) and time. Condition: [Ald⁺] = 10 mM, [DNA] = 1 mg/mL, incubating at room temperature (25 °C).

3.3 Isolation and quantitation of the styryl dye product

The developed DNA-templated styryl dye synthesis already provided a powerful way for convenient synthesis, rapid screening and identification of dyes with favourable optical properties without the need to isolate the dyes from the reaction mixture. However, it might be desirable in some instances to isolate the dyes from the system. From the literature report, it was found that the ionic liquid [BMIM]PF₆ has been suggested as a solvent to extract dyes from nucleic acid-dye complexes.⁸⁵ This concept was successfully applied to the styryl dye extraction from the DNA template. The dye product was successfully extracted from the reaction mixture to the [BMIM]PF₆ ionic liquid (IL) layer (**Figure 3.8A**). The ionic liquid layer containing the

extracted dye was analyzed by ^1H NMR to calculate the percentage yield of the dye formation. To quantitate the dye formation, a known amount of IS was quantitatively introduced into the solution of the crude IL extract. The concentration and amount of the dye product was determined from the integration of ^1H signals of the product relative to the IS. After 14 days of incubation, a total of 27% of the dye $\text{BT}^+\text{-Ald}^+$ was obtained based on NMR studies. The figure is in good agreement with the calculated percentage yield from UV-Visible spectrophotometry at 23% yield of the dye $\text{BT}^+\text{-Ald}^+$ ($\lambda_{\text{max}} = 570 \text{ nm}$, $\epsilon_{570} = 7.9 \times 10^4 \text{ M}^{-1}\text{cm}^{-1}$). Furthermore, the identity of the dye was further confirmed by MALDI-TOF mass spectrometry which revealed the molecular ion at (+ve) m/z 452.2859 which is consistent with the expected mass of the dye at m/z 452.2735 for $[\text{C}_{27}\text{H}_{38}\text{N}_3\text{OS}]^+$ (M-H^+).

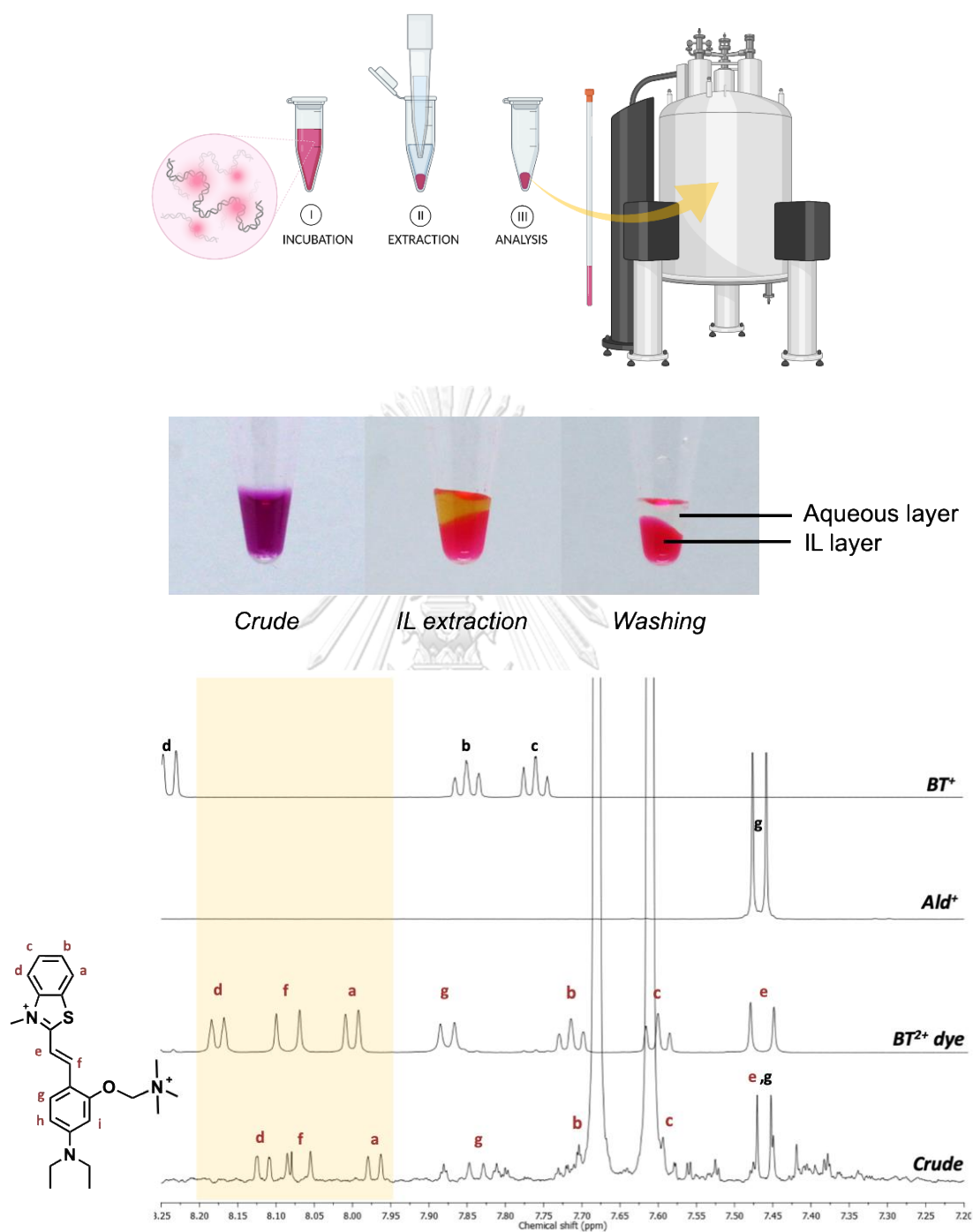


Figure 3.8 (A) Extraction of styryl dye from Dye-DNA complex using $[\text{BMIM}]\text{PF}_6$ ionic liquid. Condition: $[\text{Ald}^+] = 1 \text{ mM}$, $[\text{DNA}] = 1 \text{ mg/mL}$, incubating at room temperature for 14 days. (B) ^1H NMR spectra (128 scans) of the extracted styryl dye comparing with reference BT^{2+} dye and the corresponding coupling partners, BT^+ and Ald^+ .

In addition to the spectroscopic studies, the efficiency of the dye formation was also evaluated by high-performance liquid chromatography (HPLC). After the DNA-templated reaction was completed, the dye was isolated by [BMIM]PF₆ extraction as described above and the extract was diluted with methanol. The analysis was performed on a reversed phase column (C18) eluting with the gradients of acetonitrile–water mixtures containing 0.1% TFA (v/v) as the mobile phase. The retention time of the reference starting materials (BT⁺ and Ald⁺), the isolated dye (BT⁺-Ald⁺ dye), and IL ([BMIM]PF₆) was investigated under 190 nm absorption was determined as shown in **Table 3.1**. Moreover, the formation of the BT⁺-Ald⁺ dye was also monitored at 550 nm which was the specific absorption wavelength of the dye (**Figure 3.9**). The *R_t* at 9.7 min of the extracted product perfectly matched the *R_t* of the reference BT⁺-Ald⁺ dye. The yield of the dye was estimated from the peak area at *R_t* = 9.7 min at 550 nm using the external calibration method. A good linear correlation between peak area and reference BT⁺-Ald⁺ dye concentration over the range of 5–100 μM was obtained. According to HPLC analyses, the yield of the dye BT⁺-Ald⁺ was 1.5% after 2 days of incubation, and 19% of was obtained after 14 days incubation. The obtained results are also consistent with the calculated yield from the previous spectroscopic analysis. These promising results could be used to confirm the performance of the dye formation. The isolation technique method is thus demonstrated to be useful for isolating the styryl dye from the DNA template.

Table 3.1 Retention time of the components in the DNA-templated reaction

| | <i>R_t</i> (min) |
|---------------------------------------|----------------------------|
| BT ⁺ | 6.93 ^a |
| Ald ⁺ | 9.26 ^a |
| BT ⁺ -Ald ⁺ dye | 9.74 ^a |
| [BMIM]PF ₆ | 4.06 ^b |

^a Absorption at 220 nm, ^b Absorption at 190 nm

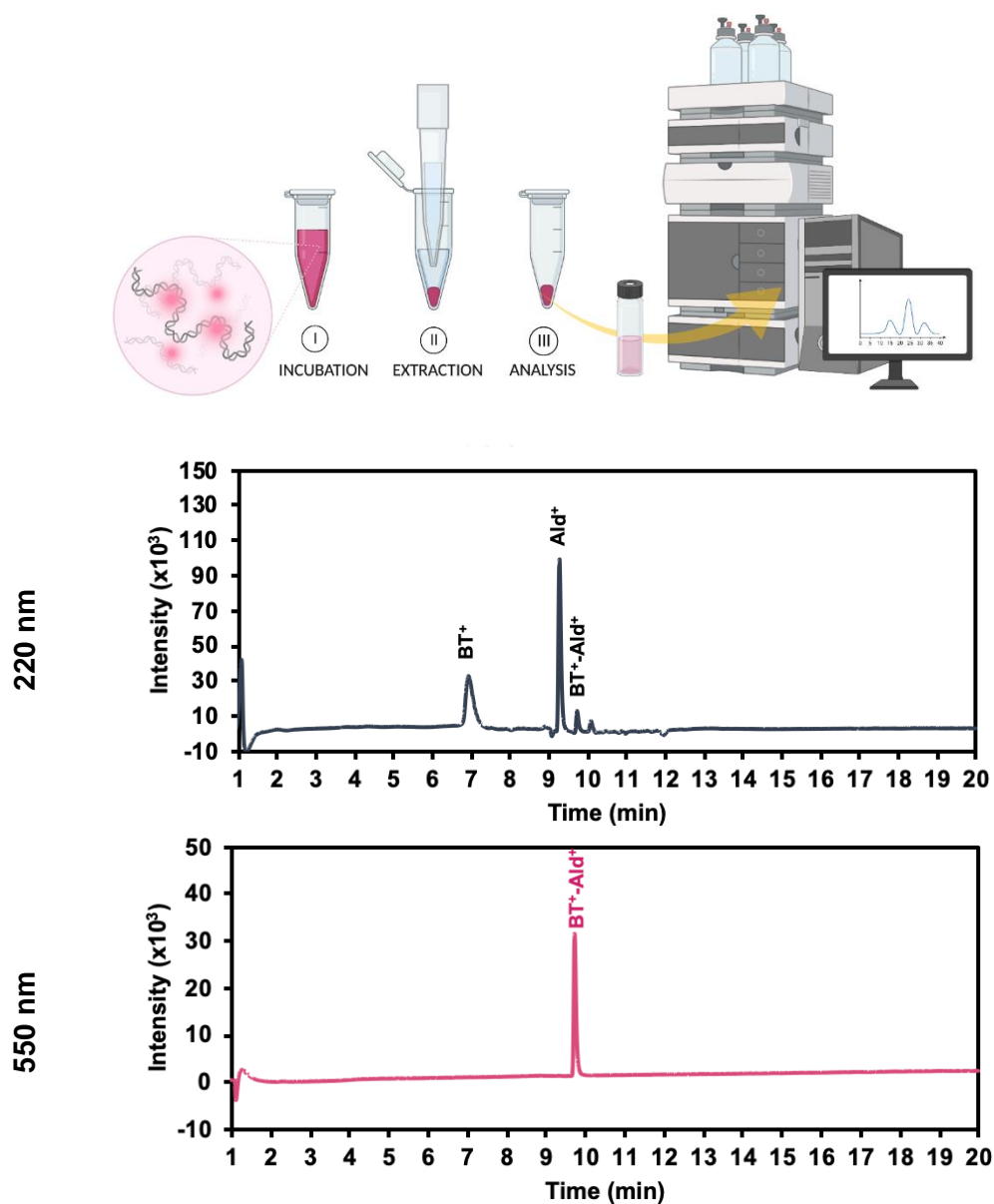


Figure 3.9 HPLC chromatograms of templated reaction for BT⁺-Ald⁺ synthesis after incubating for 2 days. Condition: [Ald⁺] = 1 mM, [DNA] = 1 mg/mL incubating at room temperature, reversed-phase HPLC was performed using C18 column eluting with acetonitrile:water with 0.1% TFA gradients.

3.4 Design and synthesis of more diversified cationic coupling partners

The results from the concept validation experiments discussed above clearly demonstrated the possibility of the DNA-templated styryl dye synthesis. In addition, it also revealed the criteria of substrates that could participate in the DNA-templated dye formation that they must be cationic, indicating the critical role of electrostatic interaction in promoting the binding of the coupling partners the DNA template that would eventually determine the efficiency of the styryl dye formation. To explore the substrate scope further, we tested the DNA-templated dye synthesis with additional substrates. First, various cationic heterocycles and aromatic aldehydes with a cationic side chain were synthesized.

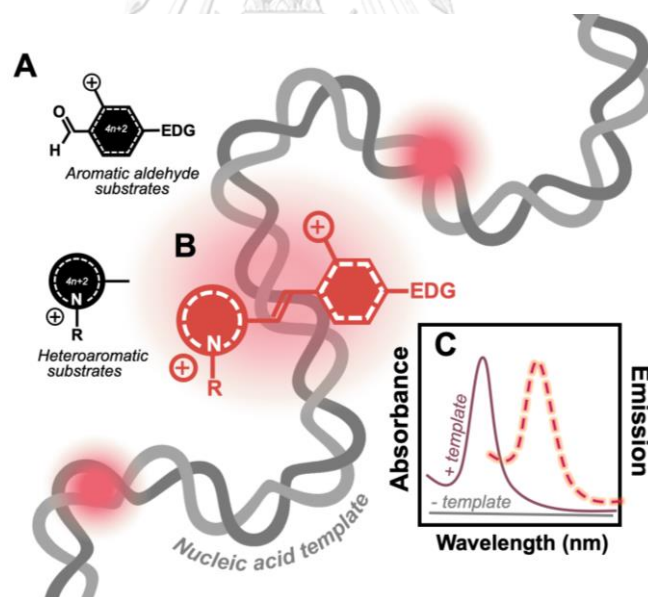


Figure 3.10 Schematic illustration of the concept of the nucleic acid-templated synthesis of cationic styryl dyes. (A) Diverse sets of cationic heteroaromatic and aldehyde substrates can (B) bind to the anionic (from phosphate backbone) nucleic acid template and then react to form styryl dyes in the DNA-bound form. (C) The spectroscopic profiles (UV-vis absorption and fluorescence emission) of the DNA-dye-bound form are simultaneously evaluated.

To introduce the additional positive charge to the methylated heterocycles a trimethylammonium or pyridinium group was attached by nucleophilic displacement of the corresponding *N*-bromoalkylated heteroaromatic compounds. For the positively charged aromatic aldehydes, the hydroxy substituent on the aromatic aldehyde was bromoalkylated and subsequently reacted with trimethylamine or pyridine. The structures of all synthesized compounds were confirmed by ^1H and ^{13}C NMR spectroscopy. New compounds were also further characterized by HRMS.

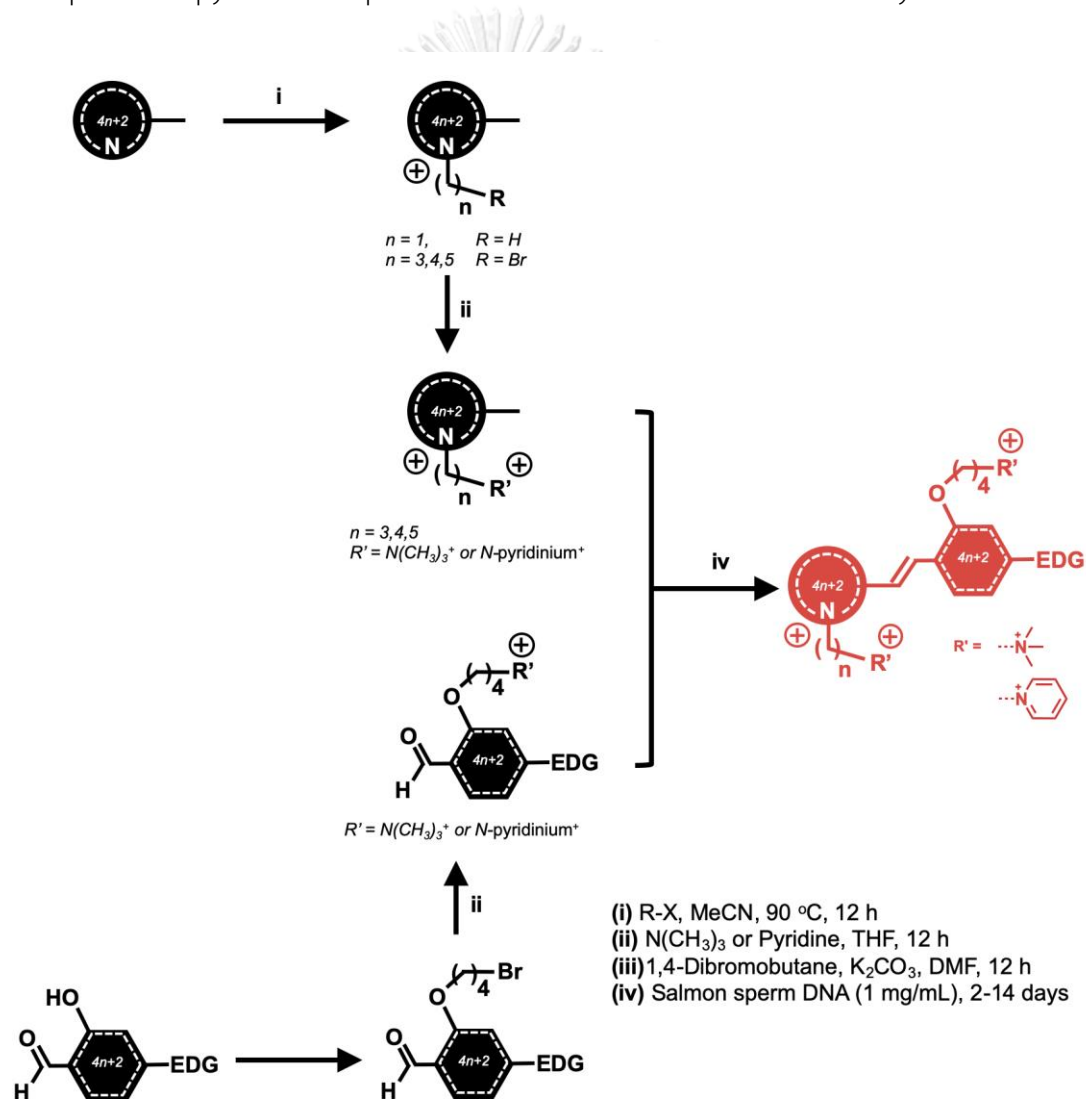


Figure 3.11 Synthesis of the cationic coupling partners used in this study.

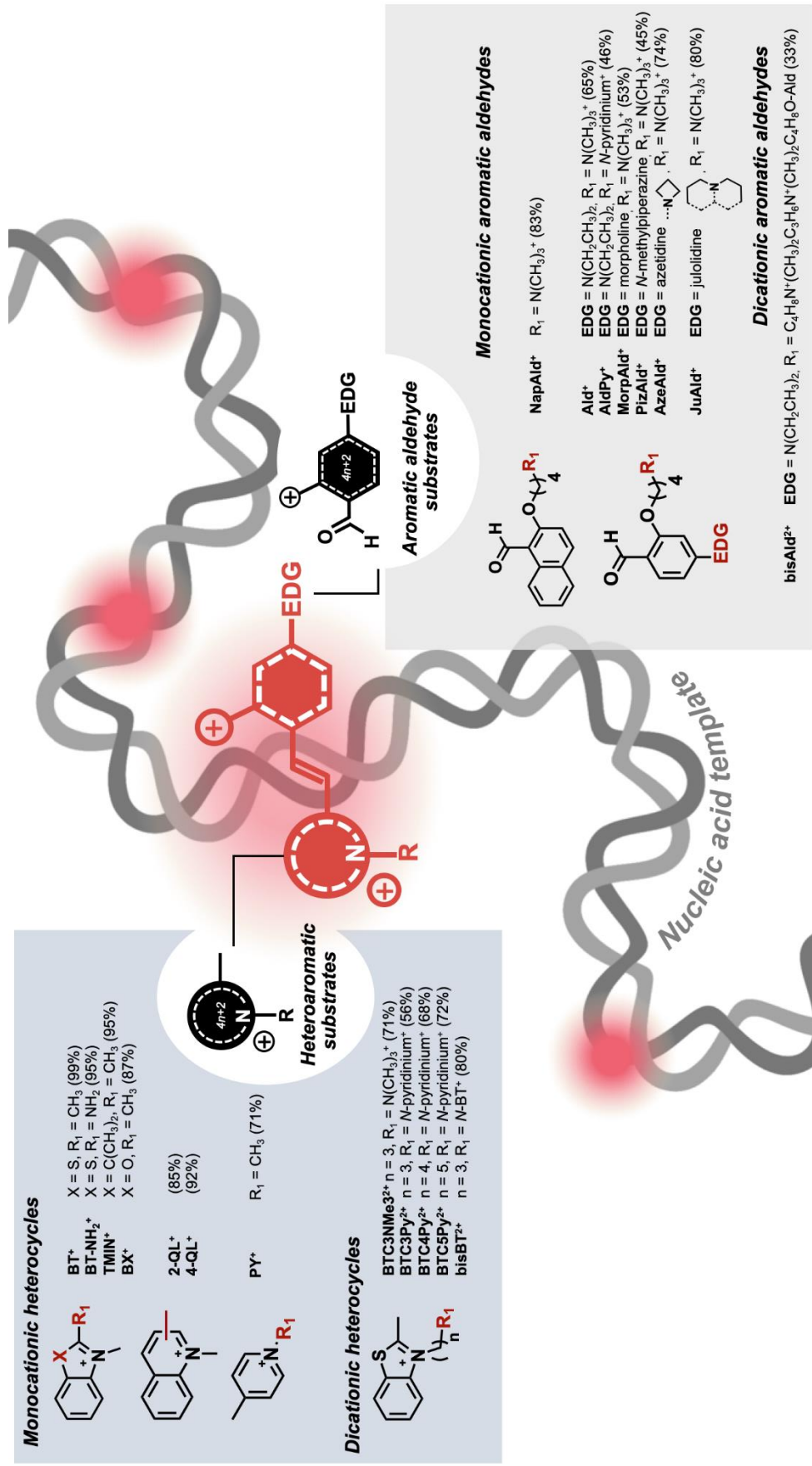


Figure 3.12 Structures and yields of cationic coupling partners successfully prepared in this work.

3.5 Combinatorial DNA-templated styryl dye synthesis

Having identified BT⁺-Ald⁺ as the most productive coupling partners and the conditions for promoting the DNA-templated reaction, we further explored the applicability of the method for other cationic coupling partners.

3.5.1 The effect of substituent on the benzothiazolium substrates

In the first set of experiments, the DNA-templated reaction between Ald⁺ with a diverse set of benzothiazolium-core substrates was studied. The *N*-methylbenzothiazolium salts with various substituents including electron withdrawing (-F, -CF₃, -OCF₃, -NO₂, -Cl, -Br) (the benzothiazole precursors were a gift from Asst. Prof. Dr. Tanatorn Khotavivattana's lab, Department of Chemistry, Faculty of Science, Chulalongkorn university) and electron-donating (-OMe, -NPr₂, -Ph, -Me) (the precursors were synthesized from commercial chemicals) were prepared as the heteroaromatic coupling partner. The stoichiometric mixture of the Ald⁺ and benzothiazolium salts at 1:1 ratio and final concentration of 1 mM each and stDNA template (1 mg/mL) under the same conditions previously developed for the BT⁺-Ald⁺ pair. After 2 days, a range of colored products was formed in most wells (**Figure 3.13**). The solutions appeared yellow to purple in color with absorption maxima in the range of 530 to 570 nm with the emission wavelength in the range of 595 to 615 nm (**Table 3.2**). The dye products were isolated by IL extraction and characterized by MALDI-TOF spectrometry. From the results, all of the desired molecular mass from combinatorial templated reaction were consistently found as the calculation. The promising analysis results confirm the successful of the styryl dye synthesis using DNA-templated approach.

In an attempt to quantitate the extent of the dye formation, the absorbance of the reaction mixture in each well was measured spectrophotometrically. Assuming a similar molar extinction coefficient, the absorbance at λ_{\max} (I_{Abs}) was taken as the indication of the extent of the dye formation. The styryl dye products obtained from BT⁺ substrates bearing electron-withdrawing substituents showed much more intense color comparing to the BT⁺ substrates with electron-donating substituents. For example, up to 17 times of the intensity at the maximum absorption wavelength of 5-NO₂ was observed when compared to the unsubstituted benzothiazole H-BT⁺. The results suggested that the BT⁺ substrates with electron-withdrawing groups reacted faster with the Ald⁺ than the substrates with electron-donating substituents. This is consistent with the ease of deprotonation of the 2-methyl group and better stabilization of the carbanion intermediate and thus facilitating the aldol condensation with the aromatic aldehyde. The more exact comparison could be made by quantitative HPLC analysis of the styryl dyes formed from Ald⁺ and three BT⁺ derivatives including H-BT⁺, 5-NO₂-BT⁺, and 5-OMe-BT⁺ as representatives of neutral, electron-deficient and electron-rich substrates, respectively. From the external standard calibration curves prepared from independently synthesized reference compounds, the percentage yields of BT⁺-Ald⁺, 5-NO₂-BT⁺-Ald⁺ and 5-OMe-BT⁺-Ald⁺ after 2 days were calculated at 1.5%, 26% (17 times of BT⁺-Ald⁺) and 0.9% (0.6 times vs BT⁺-Ald⁺), respectively. Although a strongly-colored dye was obtained in the case of the 5-NO₂-BT-Ald⁺, no fluorescence was observed which could be attributed to the quenching effect of the -NO₂ group by energy transfer.⁸⁶ Moreover, the steric effect may also play a crucial role in determining the efficiency of the reaction as shown in the case of 6-Ph-BT-Ald⁺ combination whereby no dye was formed as shown by the almost colorless solution without fluorescence.

To quantitate the responsiveness of the dye in the presence of DNA, it was necessary to decouple the fluorescence intensity from the extent of the dye formation. This was achieved by dividing the fluorescence intensity (I_{Em}) with the absorbance (I_{Abs}) at the respective λ_{max} and the larger value of I_{Em}/I_{Abs} would indicate the dye that is more responsive. Based on these assumptions, the best yields were obtained with the 5-NO₂-BT⁺-Ald⁺ and the most responsive dyes in terms of fluorescence enhancement in the presence of salmon testes DNA were 5-OMe-BT⁺-Ald⁺ and 6-OMe-BT⁺-Ald⁺. Inspired by the combinatorial screening results, the two dyes were individually synthesized in 40-43 % yields by conventional methods.

The optical properties of these dyes were compared with the BT⁺-Ald⁺ dye as shown in **Table 3.3**. Indeed, the 5-OMe-BT⁺-Ald⁺ and 6-OMe-BT⁺-Ald⁺ dyes showed the similar molar extinction coefficient (ϵ) in dye-DNA form and fluorescence brightness than the parent BT⁺-Ald⁺ dye. The two dyes exhibited very low fluorescence quantum yields in the free state and became highly fluorescence in the presence of DNA. Although the two new dyes exhibited similar fluorescence responsiveness to the BT⁺-Ald⁺ dye, their brightness was considerably stronger due to the larger molar absorptivity. The results suggested that the combinatorial screening can identify dyes with desirable characteristics including the absorption and emission wavelengths as well as the responsiveness with DNA quickly. Thus, the power of the developed DNA-templated dye synthesis method was clearly demonstrated. Nevertheless, it was not clear yet whether the affinity of the dyes to the DNA has any correlation with the extent of the dye's formation and/or their responsiveness.

Table 3.2 Evaluation of substituent effect on the BT substrates carrying electron-withdrawing and -electron-donating substituents for the DNA-templated styryl dye synthesis.

| X-BT ⁺ | Mass (m/z) | | Yield (%) ^a | λ_{Abs} (nm) | λ_{Em} (nm) ^b | I_{Em} | I_{Em}/I_{Abs} | |
|--------------------|------------|---------|------------------------|----------------------|----------------------------------|----------|------------------|-------------|
| | Calc | Found | | | | | | |
| H | 452.273 | 452.286 | 1.5 | 565 | 0.0271 | 595 | 63.19 | 2332 |
| 4-F | 470.264 | 470.248 | 0.4 | 560 | 0.0347 | 597 | 49.36 | 1422 |
| 5-Br | 530.184 | 530.205 | 8.7 | 550 | 0.2558 | 605 | 26.85 | 105 |
| 5-Cl | 486.234 | 486.251 | 13.0 | 550 | 0.2872 | 605 | 33.25 | 116 |
| 5-F | 470.264 | 470.279 | 2.2 | 565 | 0.0740 | 600 | 84.23 | 1138 |
| 5-NO ₂ | 497.258 | 497.285 | 27.1 | 560 | 0.3682 | - | - | - |
| 6-F | 470.264 | 470.282 | 1.7 | 550 | 0.0313 | 595 | 54.98 | 1757 |
| 5,6-F | 488.2542 | 488.276 | 5.5 | 560 | 0.0549 | 600 | 55.91 | 1018 |
| 6-CF ₃ | 520.260 | 520.269 | 23.5 | 555 | 0.3046 | 603 | 44.89 | 147 |
| 6-OCF ₃ | 536.255 | 536.278 | 6.0 | 550 | 0.0771 | 595 | 64.87 | 841 |
| 7-F | 470.264 | 470.284 | 1.0 | 575 | 0.1642 | 603 | 99.63 | 607 |
| 5-OMe | 482.284 | 482.313 | 0.7 | 560 | 0.0216 | 600 | 56.86 | 2632 |
| 5-Me | 466.289 | 466.308 | 1.1 | 550 | 0.0870 | 600 | 115.88 | 1332 |
| 5,6-diMe | 480.304 | 480.328 | 1.1 | 550 | 0.0542 | 600 | 70.86 | 1307 |
| 6-OMe | 482.284 | 482.314 | 0.7 | 540 | 0.0237 | 600 | 59.17 | 2497 |
| 6-NP ₂ | 551.378 | 551.353 | 0.2 | 570 | 0.0128 | 615 | 21.05 | 1645 |
| 6-Ph | 528.304 | - | - | - | - | - | - | - |

^a HPLC analysis. ^b Excitation wavelength (λ_{Em}), 565 nm

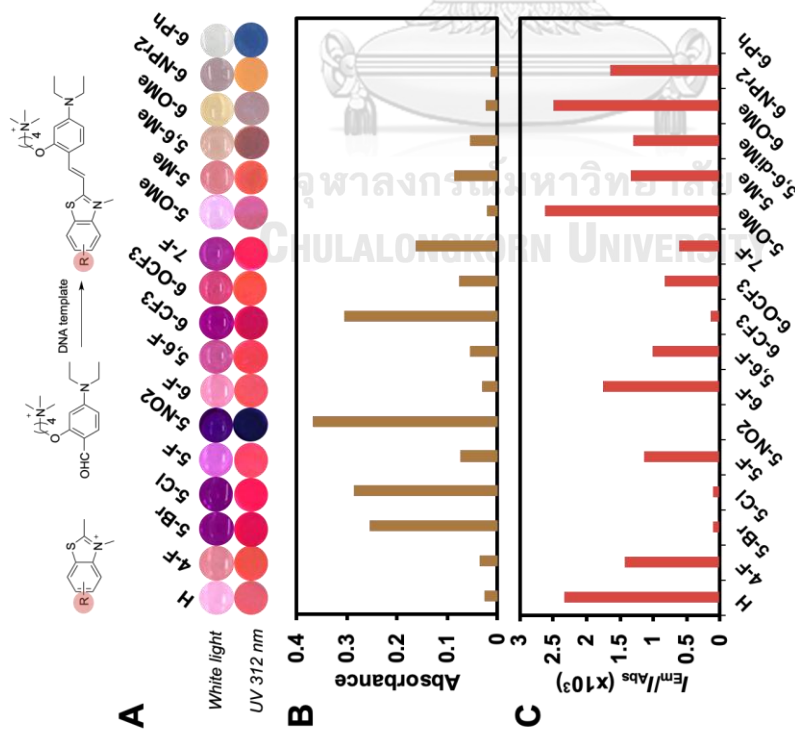


Figure 3.13 Study of substituent effect on BT heteroaromatic substrate using diverse sets of electron-withdrawing and electron-donating substituents. Condition: [Ald⁺] = 1 mM, [DNA] = 1 mg/mL incubating at room temperature for 2 days.

Table 3.3 Optical properties of the individually synthesized dyes (5-OMe-BT⁺-Ald⁺ and 6-OMe-BT⁺-Ald⁺). Condition: [Dye] = 1 μM, [DNA] = 2 μM in 10 mM PB (pH 7.0) (dsDNA = 5'-CCAGGGCATGGTAGATCACTGTACGCCGCG-3' + 5'-CGCGGCGTACAGTGATCTACCATGCCCTGG-3').

| Dye | ϵ ($\times 10^4 M^{-1} cm^{-1}$) | F/F_0 | | Brightness ($\times 10^3$) | | Φ_F | | $\frac{\Phi_{F(DNA)}}{\Phi_{F(dye)}}$ |
|---|--|---------|----------------|---------------------------------|------|----------|-------|---------------------------------------|
| | | Value | λ (nm) | Dye | +DNA | Dye | +DNA | |
| BT ⁺ -Ald ⁺ | 2.8 7.9 (+DNA) | 126 | 600 | 0.1 | 1.0 | 0.004 | 0.371 | 88 ^a |
| 5-OMe-BT ⁺ - Ald ⁺ | 8.9 6.7 (+DNA) | 31 | 600 | 0.2 | 15.2 | 0.002 | 0.170 | 71 |
| 6-OMe-BT ⁺ - Ald ⁺ | 7.7 5.2 (+DNA) | 38 | 600 | 0.2 | 16.2 | 0.003 | 0.211 | 73 |

^a Data taken from *Sci. Rep.* **2022**, *12*, 14250.

3.5.2 Substituent effect on aromatic aldehyde substrates

In the next experiments, we expanded the substrate scopes for both the aromatic aldehyde and heteroaromatic coupling partners. Several aromatic aldehydes with positively-charged modification (see the structures in **Figure 3.14**) are effective coupling partners in the DNA-templated synthesis of styryl dye as shown by the characteristic color change and fluorescence of the dye formed in the presence of BT⁺ as the heteroaromatic part. The styryl dyes deriving from the reactions between BT⁺ and aromatic aldehydes with various -NR₂ substituents, e.g. diethylamino (NEt₂), morpholino (Morp), and *N*-methylpiperazino (Piz), showed similar optical properties, exhibiting the same range of absorption maxima (565–570 nm). This may be explained by comparable PET effects of these electron donating substituents. In terms of fluorescence, BT⁺-MorpAld⁺ and BT⁺-PizAld⁺ showed low responsiveness to the DNA template comparing to the BT⁺-Ald⁺ pair. This might be because the substituents are more sterically hindered than diethylamino group leading to the deterioration of DNA binding. Some aldehydes such as those deriving

from julolidine and naphthaldehyde were not effective coupling partners as shown by the absence of the expected reddish color in **Figure 3.14**. These aldehydes may be too sterically hindered or may intercalate into the DNA duplex that make the dye formation difficult. In addition, the doubly-positively-charged bisAld²⁺ was not suitable as coupling partners because these highly charged molecules caused immediate precipitation upon mixing with stDNA.

For the heteroaromatic part variation, BT derivatives with two positive charges were synthesized by the introduction of positively charged sidechain bearing quaternized nitrogen substituents including trimethylammonium (BTC3NMe₃²⁺) and pyridinium (BTC3Py²⁺, BTC4Py²⁺, and BTC5Py²⁺) to the BT scaffold. Furthermore, bisBT²⁺ substrates (bisBT(C3)²⁺ and bisBT(N-linker)⁴⁺) were also included as the di- and tetra-cationic coupling partners, respectively. The results from the DNA-templated coupling of these BT⁺ derivatives (see the structures in **Figure 3.14**) with Ald⁺ revealed that the introduction of more positive charges to the BT substrates as in bisBT(C3)²⁺ and BTC3NMe₃²⁺ did not increase the rate of dye formation when compared to BT⁺ as they gave similar absorption intensities in the same timeframe. Nevertheless, for bisBTC3⁺, the product colors changed to dark purple or dark red (red-shifted from 565 nm to 580 nm). The explanation for is that the bis-styryl dyes may fold to form internal aggregate that result in the change of optical properties. In an aqueous solution, the two styryl molecules may stack on top of each other to form an intramolecular face-to-face sandwich H-dimer.⁵⁵ In addition, it has been previously reported that bis-cationic styryl dyes demonstrated some red shift on absorption (20-30 nm) and large Stoke's shift on the fluorescence because of the effective resonance energy transfer. The fluorescence from the BTC3NMe₃²⁺-Ald⁺ pair was 1.6 times higher than the BT⁺-Ald⁺ pair, which suggested that the presence of the additional positive charge improves the responsiveness. For BTC3Py²⁺, the styryl dye

product formation was enhanced as shown by the high intensity of the absorbance (6 times of the BT⁺-Ald⁺ pair) but the dye showing a smaller fluorescence response (1.5 times lower of I_{Em}/I_{Abs} value). These results demonstrated the power of the DNA-templated synthesis in revealing subtle effects of the structural characteristic of the coupling partners to the optical properties of the dyes. The fact that different positively charged sidechains (-NMe₃⁺ and -Py⁺) showed similar spectroscopic properties (**Table 3.4**) indicates that the quaternized species on the side chain of the coupling partners did not much affect the HOMO-LUMO energy levels which is not unexpected as they were not directly conjugated to the fluorophore. The steric hindrance also plays minor effects since they are not directly linked to the fluorophore, and thus similar binding affinities with DNA are obtained in the case of dyes from substrates with -NMe₃⁺ and -Py⁺ sidechains. In case of BTC4Py⁺ and BTC5Py⁺, only a small variation in the solution color was obtained and the length of the sidechain showed only minor effects. These results revealed the consistency with the previous literature that the shorter linker length appeared to enhance the fluorescence responsiveness. Nonetheless, the length of modified linker was less pronounced than introduction of positive charged for DNA binding.⁵³ In agreement with the previous experiments with aldehydes bearing multiple positive charges, the bisBT(N-linker)⁴⁺ was also not suitable as coupling partners due to the precipitation upon mixing with the DNA template (**Table 3.4**).

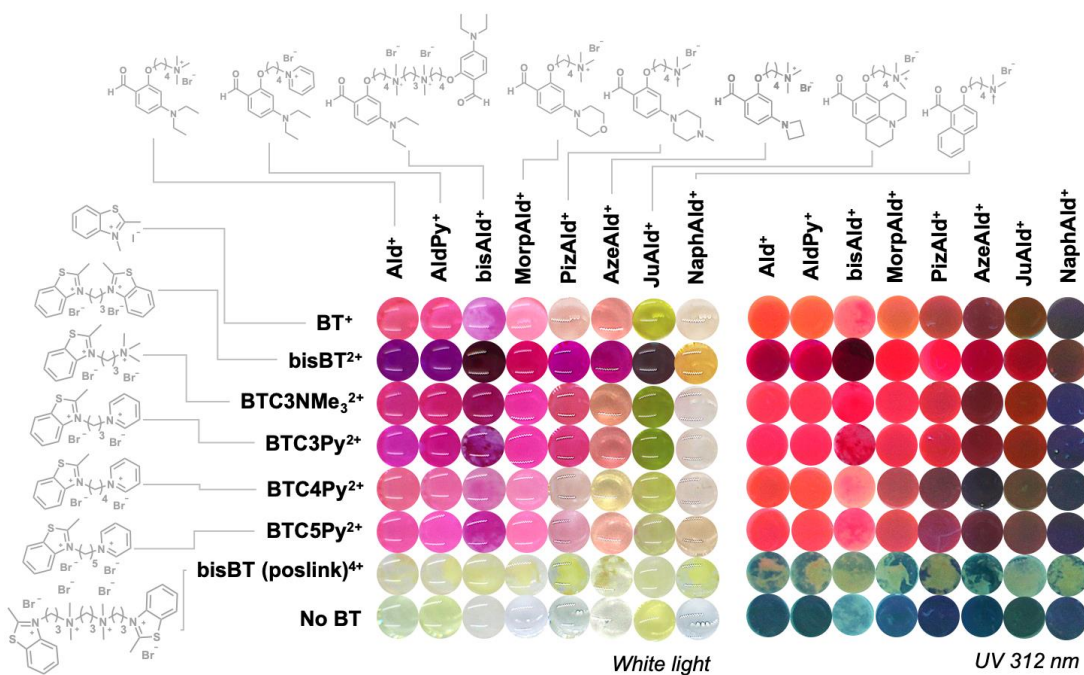
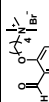
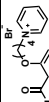
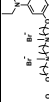
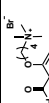




Figure 3.14 DNA-templated reaction for combinatorial synthesis of styryl dyes from various cationic benzothiazolium salts and aromatic aldehydes with positively-charged side chains. Condition: [coupling partners] = 1 mM, [DNA] = 1 mg/mL, incubating at room temperature for 2 days.

Table 3.4 DNA-templated reaction for combinatorial synthesis of styryl dyes from various cationic benzothiazolium salts and aromatic aldehydes with positively-charged side chains. Condition: [Coupling partners] = 1 mM, [DNA] = 1 mg/mL incubating at room temperature for 2 days.

| | Ald ⁺ | | AldPy ⁺ | | bisAld ⁺ | | MorpAld ⁺ | |
|---|------------------|----------------|--------------------|----------------|---------------------|----------------|----------------------|----------------|
| | λ_{Abs} | λ_{Em} | λ_{Abs} | λ_{Em} | λ_{Abs} | λ_{Em} | λ_{Abs} | λ_{Em} |
| | I_{Em}/I_{Abs} | | I_{Em}/I_{Abs} | | I_{Em}/I_{Abs} | | I_{Em}/I_{Abs} | |
|  | 565, 595, | 144 | 565, 600, | 116 | 570, 600, | 2 | 560, 595, | 33 |
| | 0.365 | 52.47 | 0.349 | 40.55 | 0.774 | 1.52 | 0.135 | 4.57 |
|  | 580, 605, | 75 | 580, 605, | 19 | 580, 605, | 3 | 570, 600, | 23 |
| | 0.366 | 27.51 | 0.811 | 15.34 | 1.773 | 4.57 | 0.859 | 19.93 |
|  | 570, 595, | 179 | 570, 695, | 48 | 580, 600, | 12 | 565, 600, | 7 |
| | 0.41 | 93.30 | 1.123 | 54.06 | 0.77 | 9.19 | 1.579 | 10.31 |
|  | 565, 605, | 32 | 565, 605, | 29 | 580, 600, | 0.02 | 570, 600, | 3 |
| | 2.257 | 72.38 | 2.272 | 65.29 | 3.062 | 0.068 | 2.958 | 8.11 |
|  | 565, 603, | 29 | 565, 600, | 14 | 570, 600, | 2.00 | 560, 600, | 2 |
| | 1.215 | 34.75 | 1.71 | 24.52 | 0.516 | 1.03 | 2.016 | 3.79 |
|  | 570, 603, | 48 | 570, 600, | 23 | 575, 600, | 0.51 | 565, 600, | 3 |
| | 1.044 | 49.8 | 1.799 | 41.04 | 1.188 | 0.61 | 2.523 | 6.26 |

3.5.3 Effect of heterocycles bearing with an acidic methyl group

In addition to the benzothiazolium core structure, other heteroaromatic ring systems carrying an acidic methyl group were also explored as potential substrates. As demonstrated in **Figure 3.15** and **Table 3.5**, *N*-methylated 2-quinolinium (2-QL⁺), 4-quinolinium (4-QL⁺), trimethylindoleninium (TMIN⁺), 4-pyridinium (4-PY⁺), benzoxazolium (BX⁺), and 2-aminobenzothiazolium (BT-NH₂⁺) were examined as coupling partners with Ald⁺. A preliminary study revealed that a 1 mM substrate concentration that had been optimized from previous experiments with the more reactive BT⁺ substrate required too long incubation time owing to the less acidic methyl groups on these heteroaromatic rings comparing with BT⁺. Consequently, the concentrations of the substrates and DNA template were increased to ensure a reasonable reaction rate under the same timeframe.

Except for TMIN⁺, other heterocyclic derivatives were found to be less effective coupling partners than BT⁺ as shown by the weak color change after 2 days of incubation. As shown in **Figure 3.15**, strongly colored solutions indicative of the dye formation were observed only with the BT⁺-Ald⁺ and TMIN⁺-Ald⁺ combinations. The obtained dyes showed similar absorption and emission profiles with the isolated dyes that were conventionally synthesized (**Table 3.5**). When the incubation period was extended to 14 days, the color change was ultimately observed in all combinations. For 2-QL⁺-Ald⁺ and 4-QL⁺-Ald⁺, deep violet or blue solutions were obtained, while the combinations of 4-PY⁺, BX⁺ or BT-NH₂⁺ with Ald⁺ gave pink to red solutions. Under the conditions with increased concentrations of the DNA and the coupling components, some non-templated reactions also occurred. The color change can confirm that the DNA-templated synthesis served a convenience to synthesize the styryl dye under mild condition even for 2-QL⁺, 4-QL⁺, 4-PY⁺, and BX⁺ which required Ac₂O as a catalyst. Nevertheless, spectroscopic measurement in

comparison with reference dyes confirmed that the dyes were formed more effectively in the presence of the DNA template (Table 3.6). Interestingly, the developed DNA-templated styryl dye synthesis also enabled imine-based styryl dye synthesis strategy in aqueous media.⁷⁷ Compared to literature, the fluorogenic imine was successfully synthesized by catalysing by dsDNA. The dsDNA can act as a host to drive the equilibration of the reaction toward the formation of fluorescent imino dye which is stabilized upon binding to dsDNA.

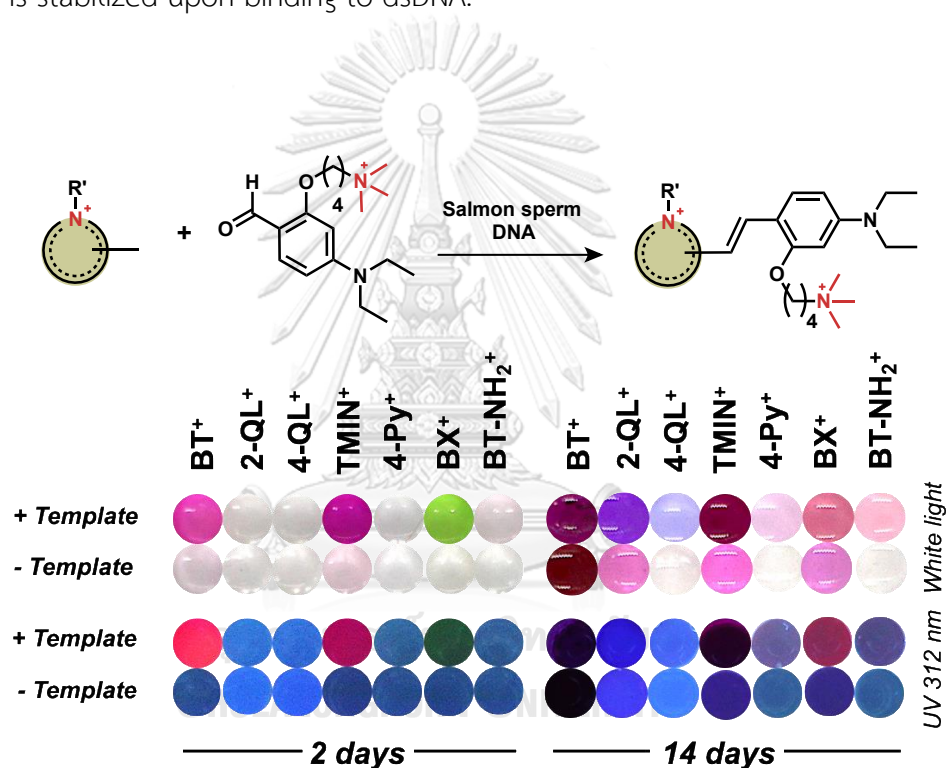


Figure 3.15 Observation of DNA-templated synthesis (under white light and UV 312 nm) from a combinatorial screening of various methyl heteroaromatic substrates and Ald⁺ after incubation for 2 and 14 days. Condition: [Coupling partners] = 2 mM, [DNA] = 1 mg/mL incubating at room temperature.

Table 3.5 Optical properties (absorption (I_{Abs}) and relative fluorescence emission (I_{Em}/I_{Abs}) from combinatorial screening using heteroaromatic and cationic diethyl amino aromatic aldehyde substrate.

| Heterocycle | Mass (m/z) | | λ_{Abs} (nm) | I_{Abs} | λ_{Em} (nm) | I_{Em} | I_{Em}/I_{Abs} | Φ_F^c |
|---------------------------------|------------|---------|-------------------------|-------------------|------------------------|---------------------|------------------|------------|
| | Calc | Found | | | | | | |
| BT ⁺ | 452.273 | 452.286 | 565 | 0.75 ^a | 600 | 248.70 ^a | 1660 | 0.371 |
| TMIN ⁺ | 462.348 | 462.341 | 565 | 1.84 ^a | 620 | 39.30 ^a | 108 | 0.124 |
| BX ⁺ | 436.296 | 436.289 | 570 | 0.30 | 595 | 334.19 ^b | 1114 | 0.426 |
| 2-QL ⁺ | 446.317 | 446.281 | 570 | 0.64 | 630 | 149.73 | 234 | 0.025 |
| 4-QL ⁺ | 446.317 | 446.238 | 570 | 0.10 | 590 | 433.28 | 4333 | 0.057 |
| 4-PY ⁺ | 396.301 | 396.308 | 565 | 0.079 | 590 | 86.49 | 1094 | 0.127 |
| BT-NH ₂ ⁺ | 453.268 | 453.286 | 570 | 0.024 | 590 | 204.89 | 8537 | N/A |

^a Diluted 5x. ^b Medium PMT voltage. ^c Optical properties of the individually synthesized dyes. Conditions: [Dye] = 2 μ M, [DNA] = 1 μ M; [DNA (in bp)] : [Dye] = 15 : 1; all measurements were performed in 10 mM sodium phosphate buffer pH 7.0. dsDNA = 5'-CGCGGCGTACAGTGATCTACCATGCCCTGG-3' + 3'-GCGCCGATGTCACTAGATGGTACGGGACC-5'.

3.6 DNA-templated styryl dye synthesis as a screening tool for dyes that are responsive to specific DNA structures

The ability of DNA to act as a template for dye synthesis offers an opportunity for the development of dyes that can bind and show responsiveness for a specific type of DNA template. Thus, we aimed to test if the use of different DNA templates can accelerate the formation of styryl dyes that show specific responsiveness towards different DNA structures. The G-quadruplex DNAs (GQs) which possess distinctive secondary structures were utilized as templates for combinatorial dyes synthesis in comparison with dsDNA and ssDNA. GQ DNAs are ubiquitous and are biologically relevant because excess amount of GQ DNA in human can cause abnormal gene expressions and genetic disorders. Therefore, development of dyes

that can specifically stain GQs is significant for medical diagnosis.⁸⁷⁻⁸⁹ Typically, GQs are formed from G-rich DNA sequences whereby four guanine bases hydrogen bonded together to form a tetrad which was further stabilized by cations (e.g. K^+ , NH_4^+) and base stacking.^{90,91} In the last decades, many studies have been developed specific dyes which selectively bind with GQs structures. Most of developed dyes were intercalator, and quinolinium-based dyes have been reported as an excellent candidate for selective GQs staining dyes.⁹²⁻⁹⁶

To demonstrate that the DNA-templated dye synthesis can be used for the identification of dyes that are selective to GQs, various DNAs with different structures including dsDNA, ssDNA, and GQs (c-MYC and 22AG) were employed as the template for the styryl dye synthesis. It has been demonstrated that the c-MYC G-quadruplex possesses significant stability and adopts a parallel topology. Furthermore, its elongated surface is particularly well-suited for strong interaction with organic small molecules.^{97,98} For the 22AG sequence, is known to fold into quadruplex structures of different topology in the presence of cations.⁹⁹ Typically, while Na^+ induces antiparallel quadruplex folding, its structure in the presence of K^+ is still debated. However, the current consensus considers that 22AG is a mixture of hybrid-type structures in K^+ .¹⁰⁰ Typically, GQs are stabilized under a high salt concentration environment. However, one limitation of the DNA-templated dye synthesis is the slow reaction rate under a high ionic strength environment. Consequently, only low salt and buffer concentrations were employed in this work (from 50 –100 mM KCl, 10 mM to 5 mM in 1 mM Tris-HCl). Circular dichroism (CD) spectroscopy was used to confirm that the G4 structures were formed under the chosen conditions. CD spectra of G-quadruplexes typically exhibit characteristic peaks and troughs that correspond to specific structural features (**Figure 3.16**). The CD spectra have to be compared with reference spectra of known G-quadruplex structures. This can help identify

similarities and differences, aiding in the characterization of the DNA structure (Figure 3.17).

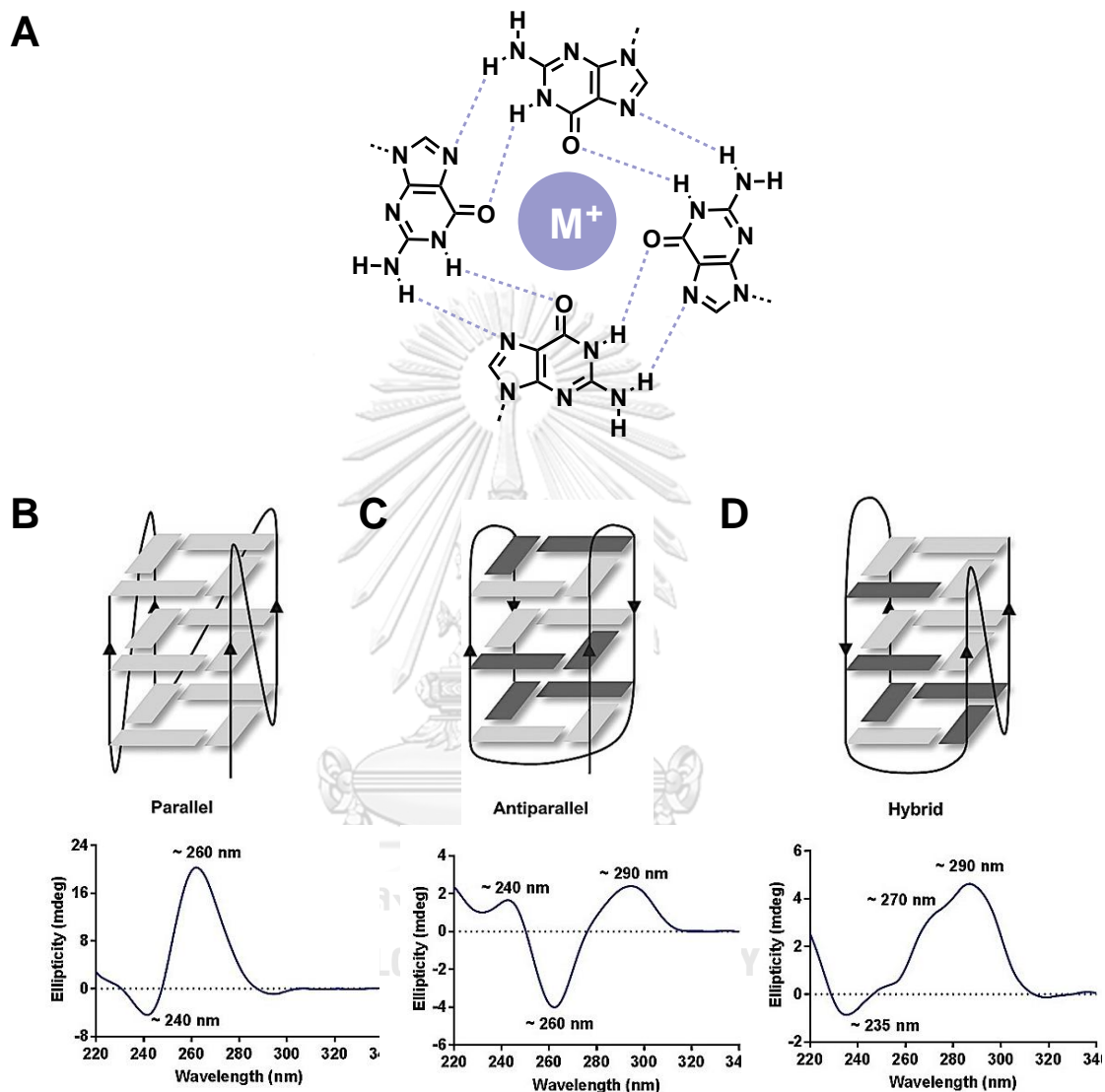


Figure 3.16 (A) Hydrogen bonding pattern in a G-quadruplex. Three topologies adopted by G4 nucleic acids and their respective circular dichroism signatures of (B) parallel (C) antiparallel and (D) hybrid form. ¹⁰¹

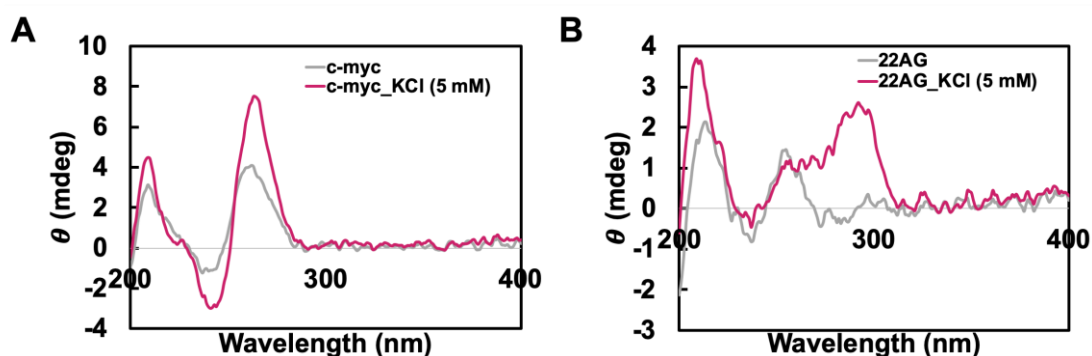


Figure 3.17 CD spectra of GQ-DNAs (A) c-MYC (B) 22AG in low concentration of buffer. Condition: [DNA] = 1 μ M in 1 mM Tris-HCl (pH 7.4).

For the heterocyclic substrates, 1,2-dimethylquinolinium (2-QL⁺) and 1,4-dimethylquinolinium (4-QL⁺) iodide were chosen to couple with various positively-charged aromatic aldehydes in the presence of various DNA templates as shown in **Figure 3.18**. After 14 days of incubation, some combinations revealed distinctive color changes indicating the dye formation. The 2-QL⁺ substrate showed a faster coupling rate compared to the 4-QL⁺ substrate. Importantly, the 2-QL⁺ and MorpAld⁺ combination appeared to give a specific color change in the presence of c-MYC and 22AG DNA over other types of DNAs. The dye formation could be identified by MALDI-TOF spectrometry and the observed mass from the GQ-DNA templated-synthesis (460.2841 and 460.2848 for c-MYC and 22AG, respectively) was in good agreement with the calculated mass 460.2959 for [C₂₉H₃₈N₃O₂]⁺ (M-H⁺). Then, the 2-QL⁺-MorpAld⁺ dye was synthesized by the conventional method to investigate the optical properties in comparison with the dye obtained from the DNA-templated synthesis and to study its selectivity towards different DNA targets. By visual observation, the synthesized dye exhibited red fluorescence in the presence of GQ-DNA including c-MYC and 22AG (**Figure 3.18**). As shown in **Figure 3.19**, the isolated

dye also gave a larger response to GQ-DNA than ssDNA or dsDNA. The binding constants of the 2-QL⁺-MorpAld⁺ dye with different DNA structures were determined by fluorescence spectrophotometry. The results (Table 3.6) showed a larger binding constant with c-MYC than ssDNA and dsDNA, although the level of difference is only marginal. Hence, screening for the dyes that are responsive to different DNA structures was possible using the developed DNA-templated reaction.

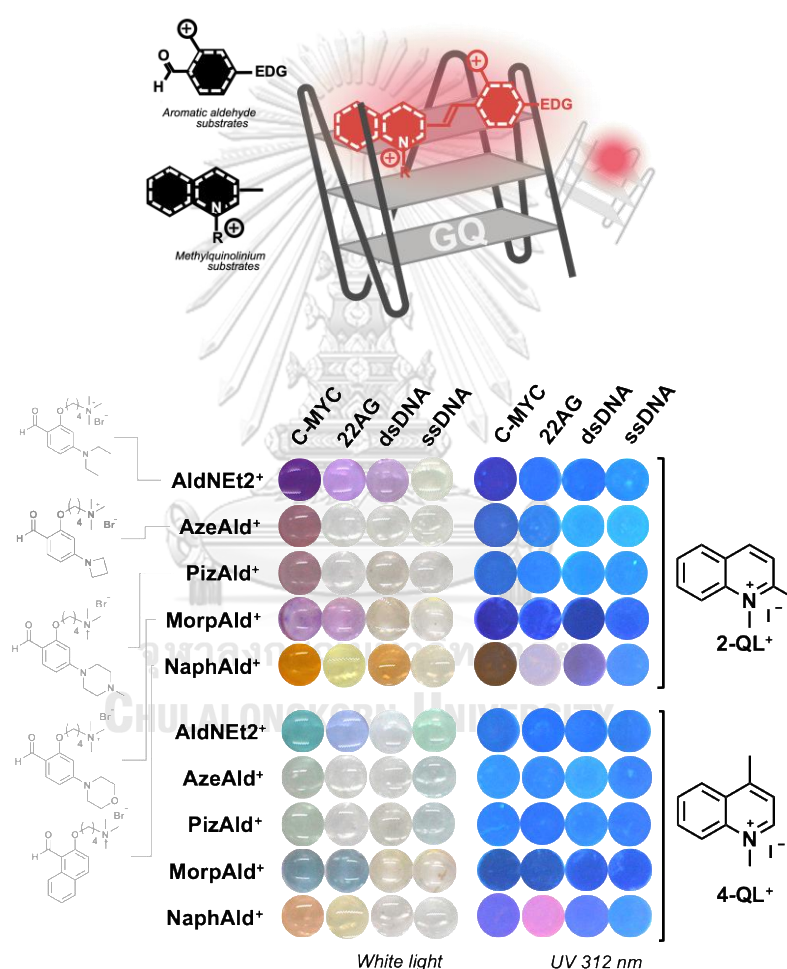


Figure 3.18 Application of DNA-templated synthesis for the discovery of styryl dyes that are responsive to some specific DNA structures using quinolinium substrates and various alkyl amino aromatic aldehydes in the presence of different DNA templates (ssDNA, dsDNA, and GQs). Condition: [coupling partners] = 2 mM, [DNA] = 0.5 μ g/mL, [KCl] = 5 mM in 1 mM Tris-HCl (pH 7.4) incubating at room temperature for 14 days.

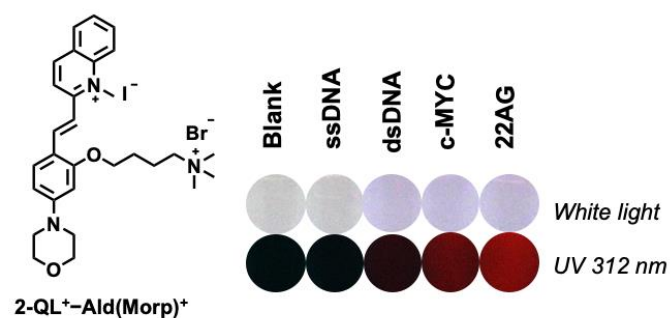


Figure 3.19 Photographs of 2-QL⁺-MorpAld⁺ prepared by the conventional method in the absence and presence of various DNAs (*under white light and 312 nm UV light*). Condition: [Dye] = 2 μM, [DNA] = 4 μM, [KCl] = 50 mM in 10 mM Tris-HCl buffer (pH 7.4).

Table 3.6 Selectivity and binding constant of 2-QL⁺-MorpAld⁺ dye towards various DNAs. Condition: [Dye] = 2 μM, [DNA] = 0–1 μM, [KCl] = 50 mM in 10 mM Tris-HCl buffer (pH 7.4).

| DNA | F/F_0 | K_b ($\times 10^6$ M) | n |
|-------|---------|--------------------------|------|
| c-MYC | 54.9 | 1.6 | 3.03 |
| 22AG | 100.3 | 1.3 | 4.10 |
| ssDNA | 6.3 | 0.9 | 2.11 |
| dsDNA | 18.9 | 0.3 | 1.79 |

3.7 Application of DNA-templated styryl dye synthesis in cells

The previous results demonstrated the successful DNA-templated (and RNA-templated) dye synthesis using natural (stDNA) or synthetic nucleic acids as a template. As nucleic acids are abundant in the cells, it was envisioned that cellular nucleic acids could act as the template for the dye synthesis in the cells providing that the coupling partners were able to enter the target cells and exhibited low toxicity. This could open up new opportunities to synthesize the dyes directly in the cells and study their staining behaviors.

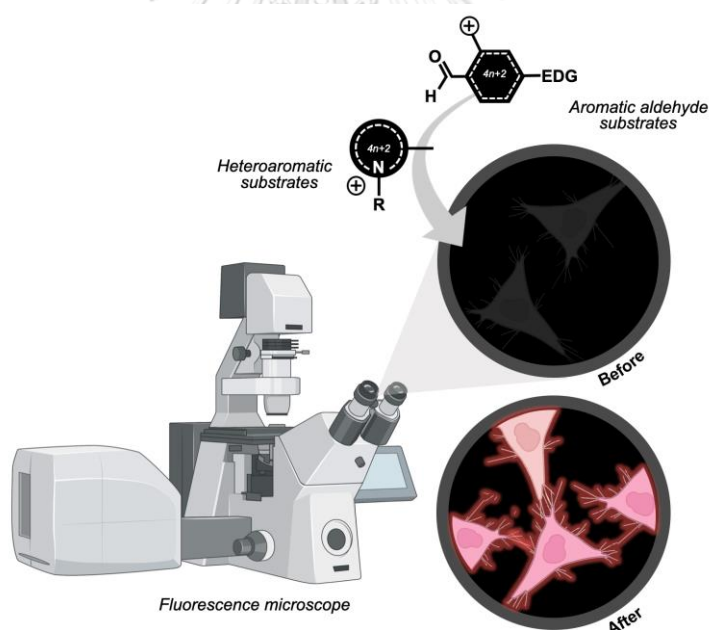


Figure 3.20 Applicability of nucleic acid-templated synthesis of styryl dye in cells.

3.7.1 Fluorescence staining behavior in living cells of BT⁺-Ald⁺ dye

Before studying the templated reaction in the cells, the conventionally synthesized BT⁺-Ald⁺ dye, was utilized as a model to evaluate the behavior of the dye for cellular fluorescence staining. The HeLa cell line which is an immortal human cell was employed for cytological studies. The BT⁺-Ald⁺ dye was previously shown to selectively stain cellular RNA rather than DNA.⁵³ In addition, this dicationic dye is also less cytotoxic when compared with monocationic dye.

In 2002, Supabowornsathit *et al.* reported the staining behaviour of the BT⁺-Ald⁺ dye in live HeLa cells.⁵³ Live HeLa cells were treated with 20 μ M of BT⁺-Ald⁺ dye in cell culture media for 18 hours. From the fluorescence images, the red fluorescence from BT⁺-Ald⁺ dye was observed in several of the whole cells. Moreover, the brightest area appeared in the nuclei region that are not overlapping with in the DAPI stain indicating that the dye did not bind to DNA. To further confirm that RNA was the target, the HeLa cells were co-stained with the SYTO RNA select[®] Green. In the co-localization experiments, the fluorescence image showed collocative overlapping between red fluorescence from BT⁺-Ald⁺ dye and green fluorescence from RNA select dye (Pearson coefficient = 0.684), confirming the similar staining pattern and thus RNA selectivity of BT⁺-Ald⁺ and SYTO RNA select[®] Green (Figure 3.21).

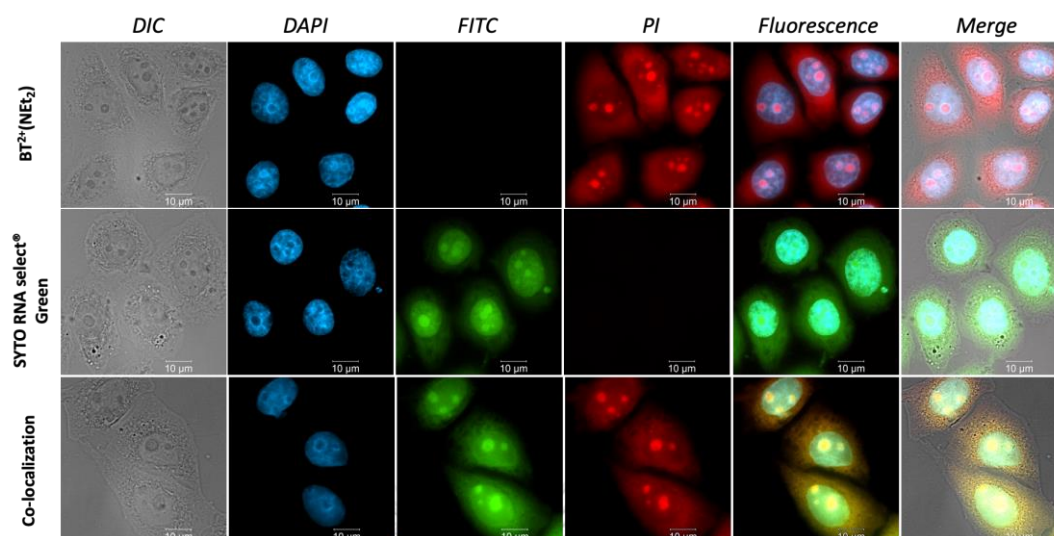


Figure 3.21 Co-localization between BT^+ -Ald $^+$ dye and RNA staining dyes in HeLa cells. Condition: HeLa cell (5×10^4 cells/well) in DMEM, [Dye] = 20 μ M incubated for 45 minutes at 37 $^{\circ}$ C under 5% CO_2 atmosphere, SYTO RNA select $^{\circ}$ Green 500 μ M for 20 minutes, DAPI (200 ng/mL) for 15 minutes. ⁵³

In addition to the co-staining experiments, nuclease digestion experiments were used to confirm the nucleic acid target in cells. As shown in the **Figure 3.22**, the image in the blue channel showed nuclear DNA staining from DAPI, the red and green channels showed RNA staining from BT^+ -Ald $^+$ and SYTO RNA Select $^{\circ}$ Green dye in HeLa cells. When the cells were treated with DNase I which degraded all cellular DNAs, only the blue signal was disappeared while the red and green in the cells nucleoli and cytoplasm still remained. The absence of the DAPI signal confirmed that the nuclear DNA was completely digested. However, the fluorescence of BT^+ -Ald $^+$ and SYTO RNA select $^{\circ}$ Green confirmed that the observed fluorescence was not due to cellular DNA binding. In the contrast, when the HeLa cells were treated with RNase A, the blue fluorescence remained but the red and green fluorescence

disappeared. Thus, the nuclease digestion experiments further confirmed that cellular RNA is indeed the target for the BT⁺-Ald⁺ dye.

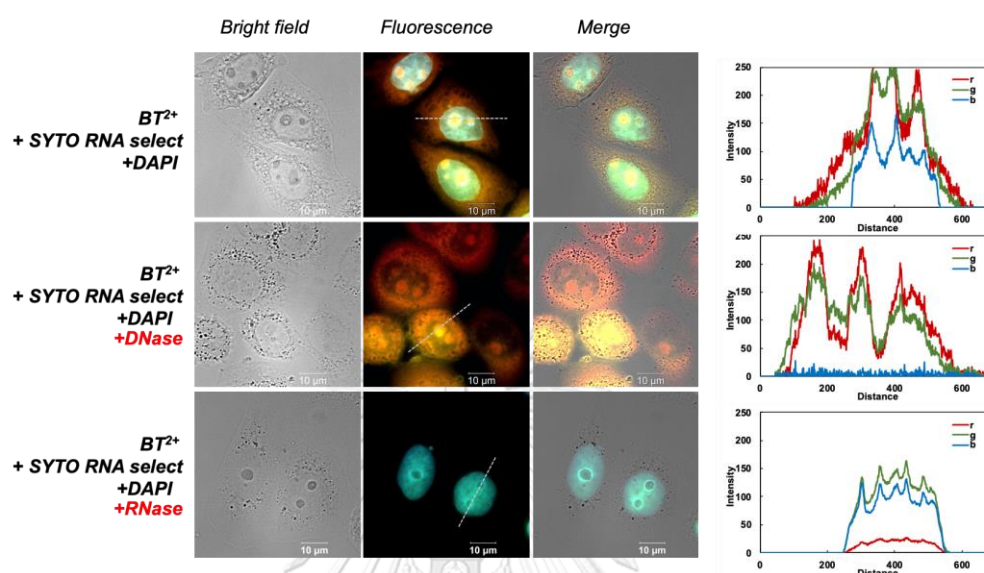


Figure 3.22 Fluorescence images of nucleic acid staining confirmed by enzymatic digestion (DNase I and RNase A). Condition: HeLa cell (5×10^4 cells/well) in DMEM, [Dye] = 20 μ M incubated for 45 minutes at 37 °C under 5% CO₂ atmosphere, SYTO RNA select® Green 500 μ M for 20 minutes, DAPI (200 ng/mL) for 15 minutes.

The RNA binding of the dye was also confirmed by observing the fluorescence responsiveness of BT⁺-Ald⁺ towards different nucleic acid targets in vitro. As shown in **Figure 3.23**, the fluorescence of the dye was observed in the presence of both dsDNA and dsRNA when visualized under UV (312 nm) indicating that the dye could also bind to dsRNA and gave fluorescence enhancement.

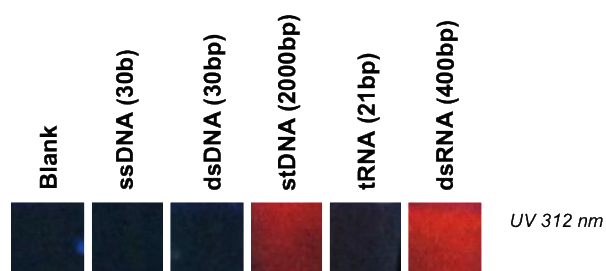


Figure 3.23 Fluorescence responsiveness of $\text{BT}^+\text{-Ald}^+$ dye toward several nucleic acid. Condition: [Dye] = 1 μM , [Nucleic acid] = 2 μM in bp in 10 mM PB (pH 7.0).

For the staining experiments in the cells, it appeared that $\text{BT}^+\text{-Ald}^+$ dye selectively bind to only RNA in cells and no nuclear DNA staining was observed. This can be explained that the cellular DNA are naturally bound to histone to form nucleoprotein complexes (NPC) called a nucleosome that are generally found in chromosomes. It has been reported that some styryl dyes that could bind to DNAs in vitro did not bind to the NPCs in the cells and thus the histone could be the key factor that prevented the dye from binding to cellular DNAs (**Figure 3.24**). In contrast, RNAs are found in several parts of cells such as the cytoplasm or nucleoli in the nucleus which consists of condensed rRNA. Notably, RNAs are frequently found in free form (mRNA) or protein-bound form (rRNA) but perhaps the RNA in ribonucleoprotein complexes are more accessible to the small molecules.¹⁰²⁻¹⁰⁵ It has been reported that some styryl dyes could penetrate in to the nucleus and thus bound to rRNA in nucleoli.^{43, 106} This explanation may account for the binding behaviour of $\text{BT}^+\text{-Ald}^+$ in the cells in the present study.

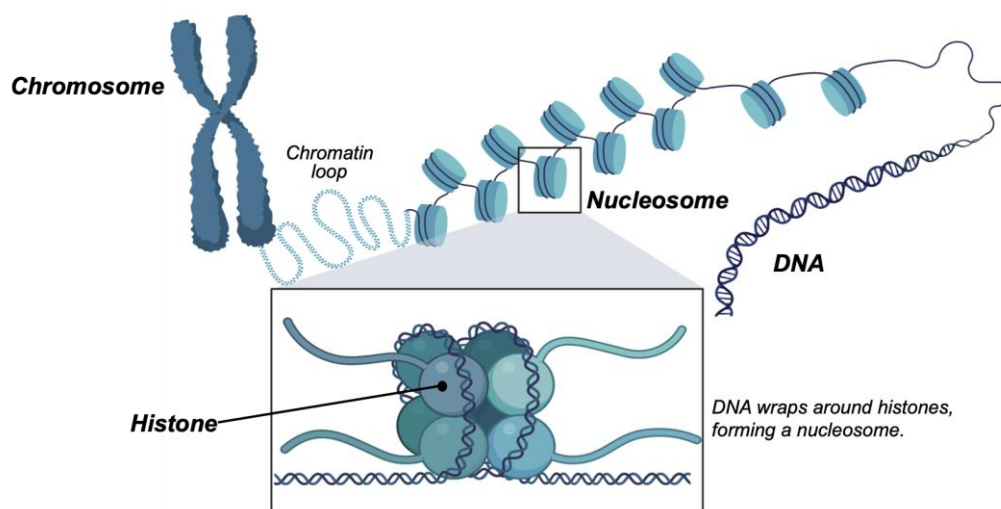


Figure 3.24 Structure of DNA-Histone complexes.

3.7.2 Toxicity of coupling partners

Before studying the templated reaction in cells, the toxicity of the cationic substrates (BT⁺ and diethylamino salicylaldehyde carrying with cationic modification including -NMe₃⁺ and -Py⁺) towards HeLa cell lines was evaluated by MTT assays. The cells were grown in the cell culture media for 24 hours and then treated with each coupling partners at 10, 20, 50 and 100 μM. The incubation time was set at 3 days which should cover the time required for the templated dye formation. As shown in **Figure 3.25**, the cell viabilities were over 80% after incubating the cells with each coupling partner over 3 days. The results indicated the low cytotoxicity of the cationic substrates for the dye synthesis, which is one of the requirements for achieving the templated reaction in cells.

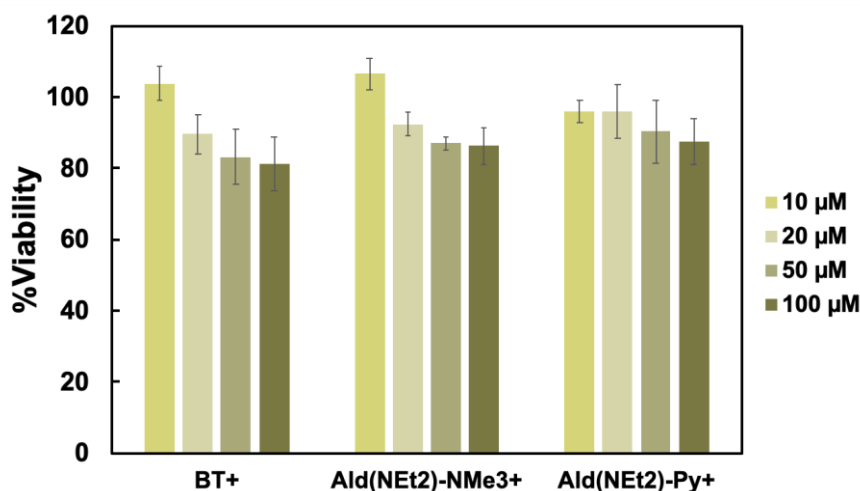


Figure 3.25 Toxicity of the cationic coupling partners for a model templated styryl dye formation in HeLa cells. Condition: HeLa cell (1×10^4 cells/well) in DMEM, [Dye] = 10-100 μM incubated for 24 hours at 37 °C under 5% CO_2 atmosphere.

3.7.3 Nucleic acid-templated reaction in live cells

Before studying the nucleic acid-templated dye synthesis in the cells, the effect of interferences in cell culture media was investigated to ensure that the dye formation is not an artifact. In the study, the coupling partners (0.2 mM) were incubated in cell culture media included DMEM with 10% FBS, and 1% penicillin, in the absence of the cells at 37 °C for 3 days. Next, the dye formation was evaluated by using spectroscopic techniques. From the UV-Visible spectrum, there were no difference in the absorption spectra of the media and the media in the presence of coupling partners in the absence of stDNA indicating that the dye did not spontaneously form in the cell culture media (**Figure 3.26**). However, in the presence of stDNA template, no signal could be observed. This might be due to the formation of the dye in too small amounts to be detectable by UV-Vis spectrophotometry. Fluorescence spectrophotometry was therefore used to further confirm the dye formation. No fluorescence signal was observed when the coupling partners were

mixed in the culture media in the absence of stDNA template. In contrast, the fluorescence signal corresponding to the BT⁺-Ald⁺ dye ($\lambda_{Em}=595$ nm) was clearly visible when the salmon testes DNA was introduced to the media. This clearly indicated that the dye formation was successful in the cell culture media only when the DNA template is present (Figure 3.26B).

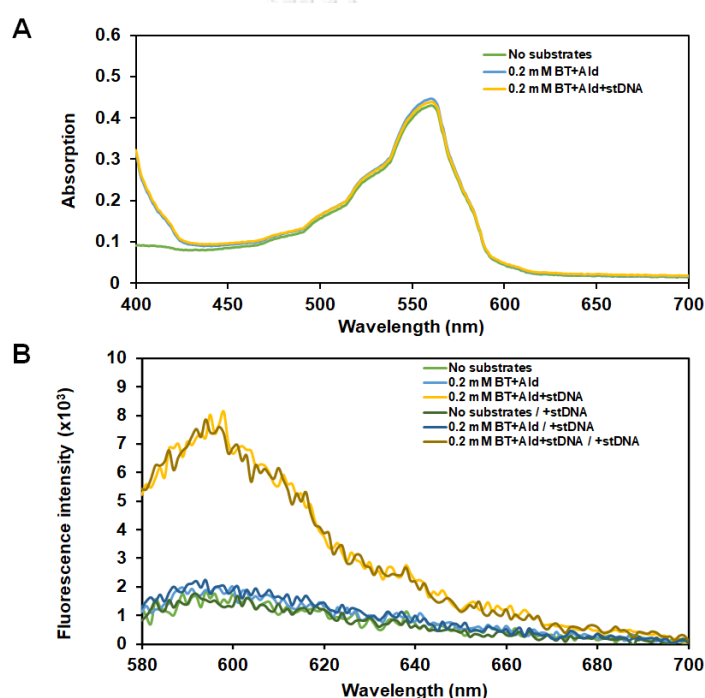


Figure 3.26 (A) UV-Visible and (B) Fluorescence spectra of nucleic acid-templated styryl dye formation in cell culture media. Condition: [coupling partners] = 0.2 mM, [stDNA] = 1 mg/mL in DMEM incubated for 3 days at 37 °C under 5% CO₂ atmosphere.

Next, the nucleic acid-templated styryl dye synthesis was attempted in living cells. In a preliminary experiment, the BT^+ and Ald^+ coupling partners (0.2 mM each) were introduced to HeLa cells in 12-well plate and incubated for 3 days. After the incubation time, the live cells were treated with Hoechst22345 for 15 minutes to stain the nuclear DNA before observing with fluorescence microscopy. The fluorescence images of the cells after incubation with the coupling partners (BT^+ and Ald^+) were consistent with those obtained from cell staining with the previously synthesized BT^+ - Ald^+ dye. In both cases, red fluorescent signals were observed in both cytoplasm and nucleus in exactly the same pattern. Similarly, the intense red fluorescence with similar staining pattern was also observed in the cells incubated with BT^+ and cationic pyridinium-modified aldehyde ($AldPy^+$) (**Figure 3.27**). These results were in line with a previous report that the pyridinium sidechain can improve the dye's binding with nucleic acids. Moreover, there are some literatures reported that amphiphilicity of pyridinium-modified moiety could increase cell penetrating property on small molecules.¹⁰⁷⁻¹¹⁰ Notably, the bright fluorescence from BT^+ - $AldPy^+$ from templated reaction might imply the formation of the dye product in high yield. Accordingly, these promising results can confirm the possibility of nucleic acid-templated reaction in live cells for screening of staining behavior of the dye under biological conditions.

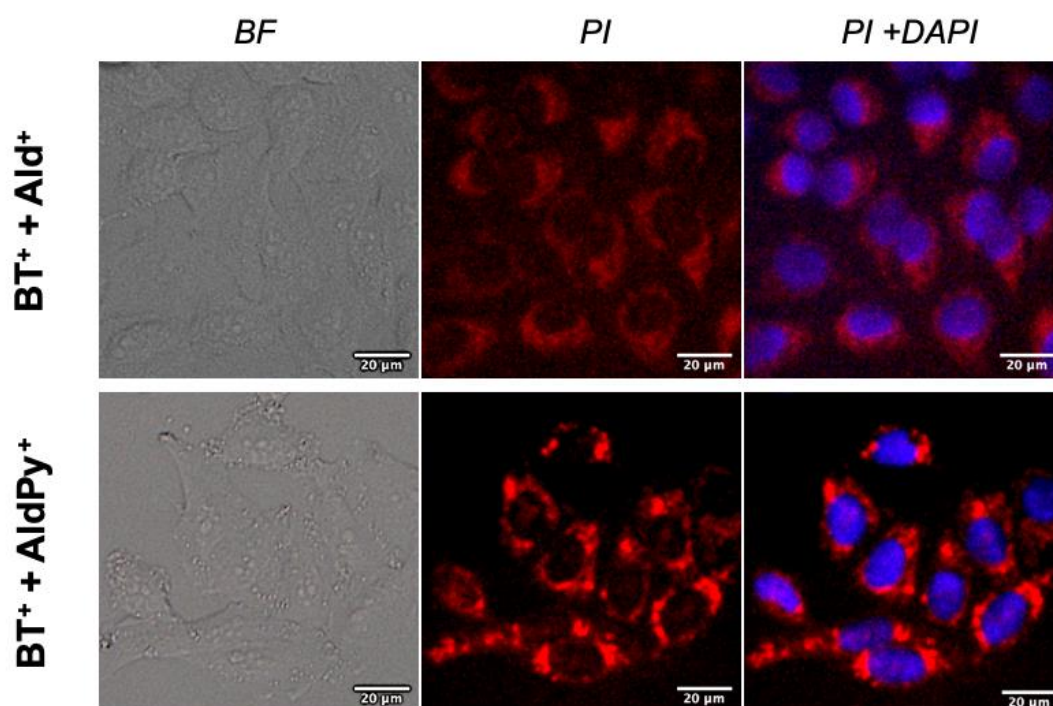


Figure 3.27 Live cells imaging from nucleic acid-templated synthesis of styryl dye in HeLa cells. The fluorescence images were observed from $BT^+ + Ald^+$ and $BT^+ + AldPy^+$ coupling partners after incubation for 3 days. Condition: HeLa cell (5×10^4 cells/well) in DMEM, [coupling partner] = 0.2 mM incubated for 3 days at 37 °C under 5% CO_2 atmosphere, Hoechst22345 (1 ng/mL) for 15 minutes.

CHULALONGKORN UNIVERSITY

3.7.4 Concept validation of nucleic acid-templated reaction in live cells

To additionally confirm the roles of cellular nucleic acids as the template for the dye formation, the HeLa cells were fixed and separately treated with DNase I and RNase A to selectively digest the DNA or RNA before performing the templated reaction using BT^+ and $Ald^+/AldPy^+$ as the coupling partners under the same conditions. Deoxyribonuclease I (DNase I) is a common enzyme that cleaves DNA, resulting in the formation of two smaller fragments called oligonucleotides. These fragments have one end with a phosphate group attached at the 5' position and the

other end with a hydroxyl group at the 3' position. On the other hand, RNase A efficiently catalyzes the cleavage of the P–O5' bond of RNA specifically after pyrimidine residues. As expected, no red fluorescence signals were observed in the cells that were treated with RNase A. The absence of templated reactions confirmed that RNA was indeed act as a template for the dye formation. In contrast, the red fluorescence signals of the dye products remained in the cells that treated with DNase I. The lack of nuclear DNA staining by DAPI confirmed that the DNA was indeed completely digested. However, the dye formation was still observed in the cells indicating that DNA was not the template for the styryl dye formation in the cells (**Figure 3.28**).



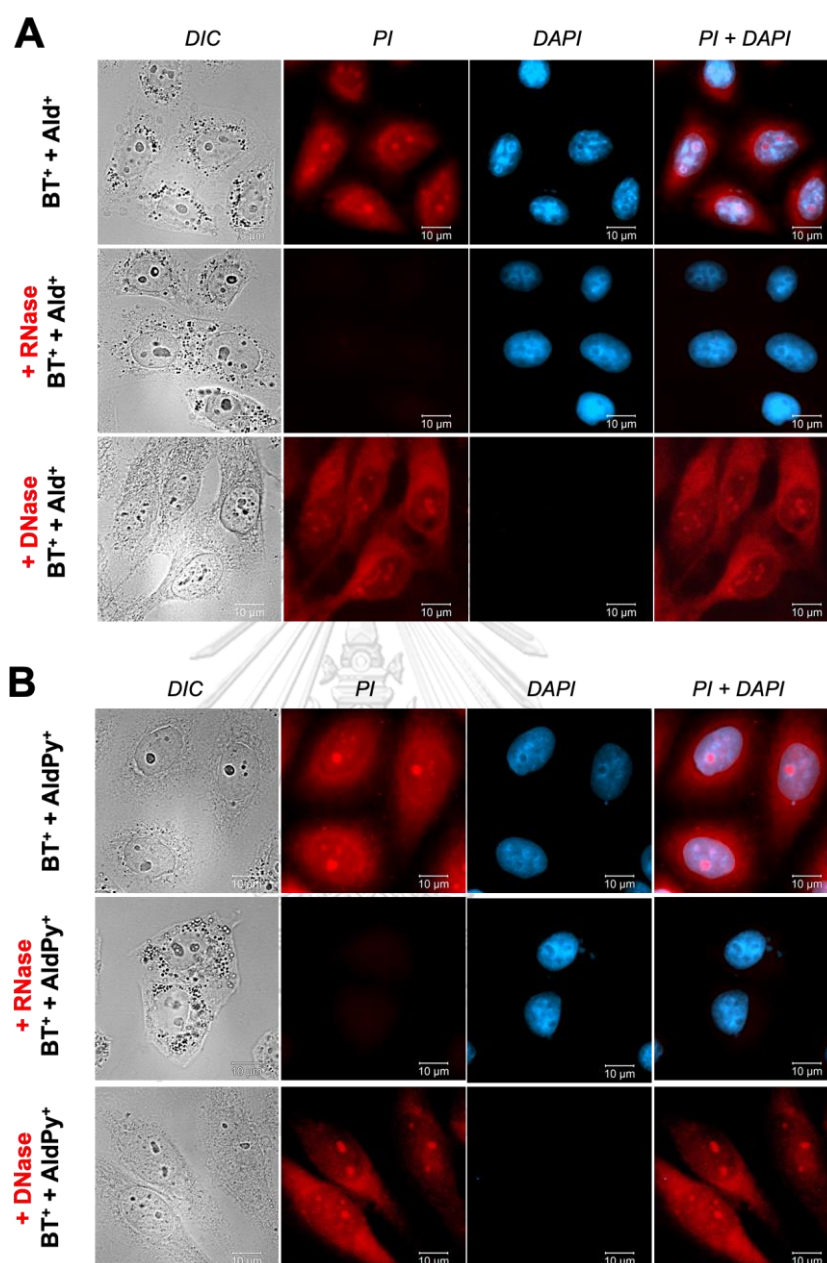


Figure 3.28 Applicability of nucleic acid-templated synthesis of styryl dye in HeLa cells. The fluorescence images were observed from (A) BT⁺+Ald⁺ and (B) BT⁺+AldPy⁺ coupling partners (0.2 mM of each) after incubation for 3 days (Red channel; $\lambda_{\text{Ex}} = 305 \text{ nm}$, $\lambda_{\text{Em}} = 617 \text{ nm}$, Blue channel; $\lambda_{\text{Ex}} = 353 \text{ nm}$, $\lambda_{\text{Em}} = 465 \text{ nm}$). Condition: HeLa cell (5×10^4 cells/well) in DMEM, [coupling partner] = 0.2 mM incubated for 3 days at 37 °C under 5% CO₂ atmosphere, RNase A (25 $\mu\text{g}/\text{mL}$) or DNase I (30 $\mu\text{g}/\text{mL}$) at 37 °C for 4 hours, DAPI (1 $\mu\text{g}/\text{mL}$) for 20 minutes at room temperature.

For the control experiments, when the cells were treated with only BT⁺ or Ald⁺ substrate, no red fluorescence could be observed (**Figure 3.29**). These findings support the conclusion that the dye formation was possible in the cells and the process was facilitated by intracellular nucleic acids.

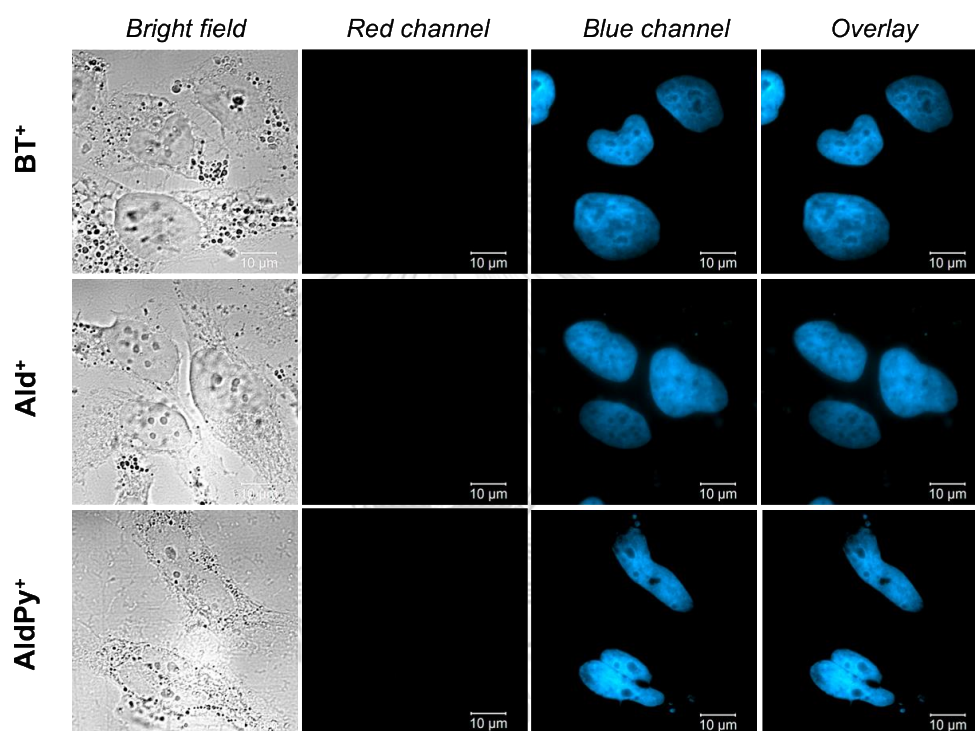


Figure 3.29 Control experiment of nucleic acid-templated synthesis of styryl dye in HeLa cells. Condition: HeLa cell (5×10^4 cells/well) in DMEM, [coupling partner] = 0.2 mM incubated for 3 days at 37 °C under 5% CO₂ atmosphere, DAPI (1 µg/mL) for 20 minutes at room temperature.

3.7.5 Applications of nucleic acid-templated dye synthesis in cells

The nucleic acid-templated reaction in the cells was extended to various cationic heterocycles. However, it was observed that the formation of dyes involving less acidic methyl on quinolinium and pyridinium salts exhibited slow kinetics thus were not suitable for live cells experiments. To overcome this limitation, the combinatorial screening of a diverse set of cationic heterocycles and aromatic aldehydes was conducted in fixed HeLa cells instead. After a 7-day incubation period, the fluorescence imaging experiments revealed the presence of red fluorescence, except for the PY^+ substrate. As mentioned earlier, $TMIN^+$ displayed the fastest rate of dye formation under the same conditions regardless of the Ald^+ coupling partners. All new dyes exhibited a similar staining pattern to that of the BT^+ - Ald^+ dye, whereby they selectively stained RNA in the nucleoli (**Figure 3.30**).

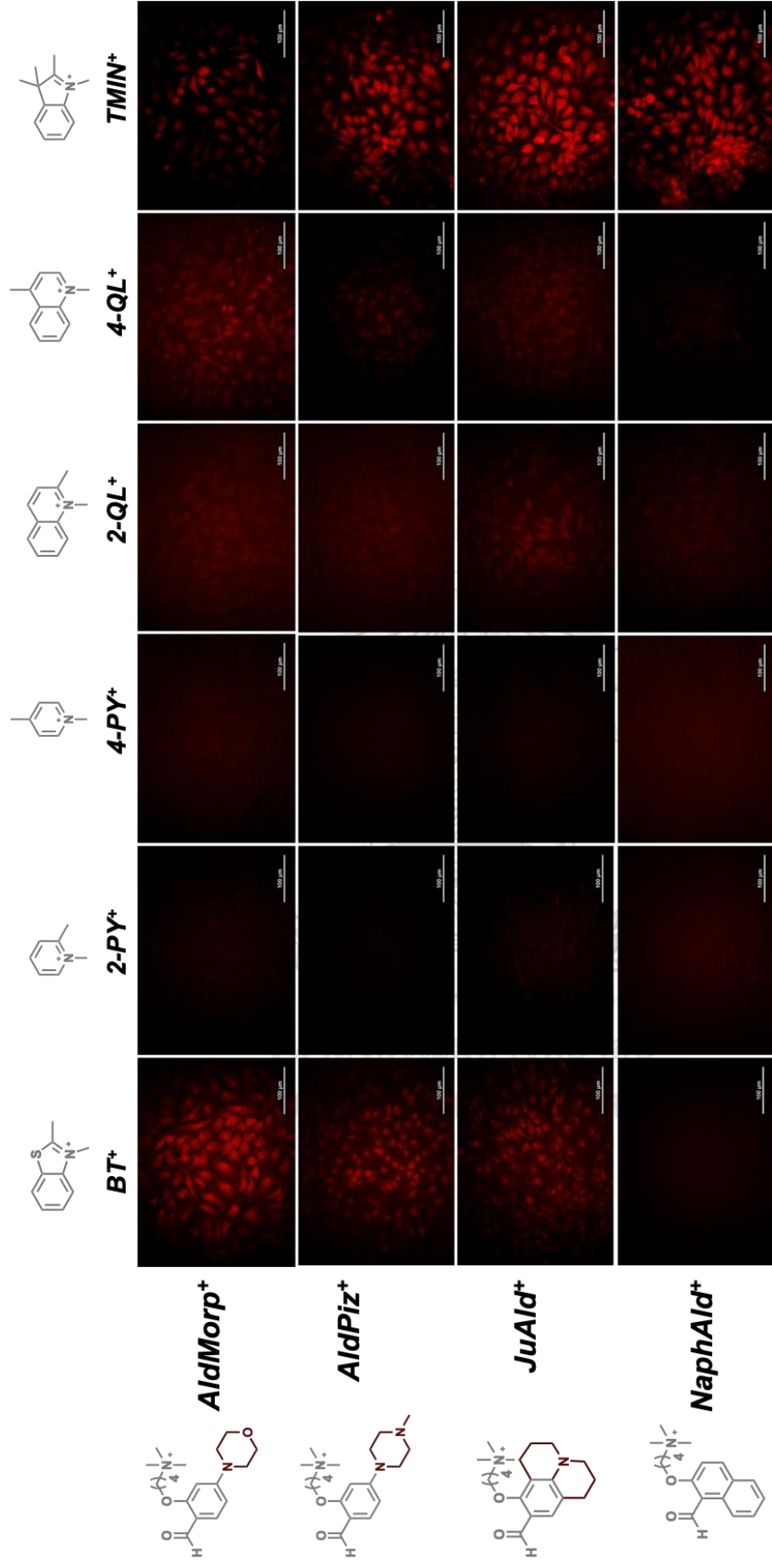


Figure 3.30 Applicability of nucleic acid-templated synthesis of styryl dye in fixed HeLa cells. Condition: HeLa cell (5×10^4 cells/well) in DMEM, [coupling partner] = 0.2 mM incubated for 7 days at 37 °C under 5% CO₂ atmosphere.

All the results described above indicated the successful formation of styryl dyes through DNA-templated synthesis (in vitro) and RNA-templated synthesis in cells. Previous literature reports have described various monocationic styryl dyes that selectively stain cellular RNA especially at the nucleoli.^{36, 43, 56, 111, 112} The consistency observed in the staining patterns between nucleic acid-templated synthetic screening and this general observation suggests that nucleic acid-templated synthesis can be employed to evaluate the localization and binding behavior of cationic styryl dyes.

To further investigate these findings, validating the results by comparing the behavior of the DNA-templated synthesized dyes with dyes synthesized through traditional methods (isolated dyes) will help establish the reliability and significance of the nucleic acid-templated synthesis approach. This comparative analysis can provide insights into the advantages, limitations, and potential applications of DNA-templated synthesis for styryl dye formation and their subsequent binding behavior.

CHAPTER IV

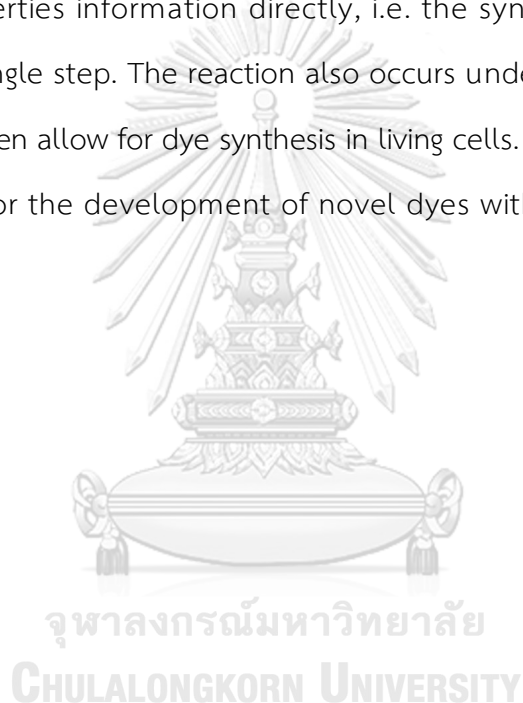
CONCLUSION

This study presents a novel approach for the formation of styryl dyes from cationic heterocycles and aldehydes through the nucleic acid-templated synthesis under mild conditions that are biologically compatible. The presence of a cationic moiety on both coupling precursors plays a crucial role in the reaction process which can be attributed to the electrostatic interaction between the cationic precursors and the polyanionic phosphate backbone of the DNA. This method offers a powerful strategy for the synthesis and screening of diverse sets of styryl dyes with various optical properties and allows for the facile generation of a library of styryl dyes with diverse structures. Different types of DNA templates can accelerate the selective formation of styryl dyes, depending on the template used. This template-dependent effect allows for the identification of new dyes that exhibit selectivity towards different types of DNAs. By leveraging the structural diversity of DNA, it becomes possible to create a wide range of dye structures with different optical properties and specificity towards DNA structures.

Another important aspect of this study is that the templated dye synthesis can also occur inside living cells. When the coupling partners were incubated with HeLa cells, the dye formation took place inside the cells as shown by the same staining pattern when compared to the cells that were stained with the independently synthesized dye. Due to the blockage of cellular DNA by binding to histones, cytoplasmic and nucleoli RNA were the primary targets for the staining by the styryl dyes. Nuclease digestion experiments confirmed that cellular RNAs rather than DNA acted as the template for styryl dye synthesis. It was envisioned that this

newly developed DNA-templated styryl dye synthesis approach will greatly facilitate the rapid discovery of new styryl dyes with desirable characteristics. These dyes hold great potential for a wide range of biological applications, appreciation to their tunable properties and the ability to selectively target specific DNA templates.

Overall, DNA-templated synthesis offers a powerful and versatile approach to the combinatorial synthesis of styryl dyes. The synthesis is convenient and provides the optical properties information directly, i.e. the synthesis and screening are performed in a single step. The reaction also occurs under biologically compatible conditions that even allow for dye synthesis in living cells. These advantages make it a valuable tool for the development of novel dyes with tailored properties and applications.



REFERENCES

1. Flügel, R.; Godefroy-Colburn, T.; Inoue, Y.; Iwanami, Y.; Miura, K.; Nishimura, S.; Ohtsuka, E.; Tsuboi, M.; Uchida, T. 1 - Nucleic Acids. In *Nucleic Acids, Proteins and Carbohydrates*, Korte, F., Goto, M. Eds.; Academic Press, 1976; pp 1-102.
2. Brown, W. A. C.; Clancy, S. Translation: DNA to mRNA to Protein. 2008.
3. Yu, A. C.-H.; Vatcher, G.; Yue, X.; Dong, Y.; Li, M. H.; Tam, P. H. K.; Tsang, P. Y. L.; Wong, A. K. Y.; Hui, M. H. K.; Yang, B.; et al. Nucleic acid-based diagnostics for infectious diseases in public health affairs. *Frontiers of Medicine* **2012**, *6* (2), 173-186.
4. Yuan, X.; Sui, G.; Zhang, D.; Chen, M.; Zhao, W. Recent developments and trends of automatic nucleic acid detection systems. *J. Biosaf. Biosecurity* **2022**, *4* (1), 54-58.
5. Ballard, D.; Winkler-Galicki, J.; Wesoly, J. Massive parallel sequencing in forensics: advantages, issues, technicalities, and prospects. *Int. J. Leg. Med.* **2020**, *134* (4), 1291-1303.
6. Chen, H.; Liu, K.; Li, Z.; Wang, P. Point of care testing for infectious diseases. *Clin. Chim. Acta* **2019**, *493*, 138-147.
7. Garibyan, L.; Avashia, N. Polymerase Chain Reaction. *J. Invest. Dermatol.* **2013**, *133* (3), 1-4.
8. Oliveira, B. B.; Veigas, B.; Baptista, P. V. Isothermal Amplification of Nucleic Acids: The Race for the Next “Gold Standard”. *Frontiers in Sensors* **2021**, *2*,
9. Kim, J. H.; Kalitsis, P.; Pertile, M. D.; Magliano, D.; Wong, L.; Choo, A.; Hudson, D. F. Nucleic Acids: Hybridisation. In *Encyclopedia of Life Sciences*.
10. Bumgarner, R. Overview of DNA Microarrays: Types, Applications, and Their Future. *Curr. Protoc. Mol. Biol.* **2013**, *101* (1), 22.21.21-22.21.11.
11. Dorado, G.; Gálvez, S.; Rosales, T. E.; Vásquez, V. F.; Hernández, P. Analyzing Modern Biomolecules: The Revolution of Nucleic-Acid Sequencing – Review. *Biomolecules* **2021**, *11* (8), 1111.
12. Wang, Y.; Zhao, Y.; Bollas, A.; Wang, Y.; Au, K. F. Nanopore sequencing technology, bioinformatics and applications. *Nat. Biotechnol.* **2021**, *39* (11), 1348-1365.
13. Zhou, H.; Liu, J.; Xu, J.-J.; Zhang, S.; Chen, H.-Y. Chapter Two - Advances in DNA/RNA

detection using nanotechnology. In *Adv. Clin. Chem.*, Makowski, G. S. Ed.; Vol. 91; Elsevier, 2019; pp 31-98.

14. Srimongkol, G.; Ditmangklo, B.; Choopara, I.; Thaniyavarn, J.; Dean, D.; Kokpol, S.; Vilaivan, T.; Somboonna, N. Rapid Colorimetric Loop-Mediated Isothermal Amplification for Hypersensitive Point-of-Care Staphylococcus aureus Enterotoxin a Gene Detection in Milk and Pork Products. *Sci. Rep.* **2020**, *10* (1), 7768.

15. Wilson, W. D.; Tanious, F. A.; Barton, H. J.; Jones, R. L.; Fox, K.; Wydra, R. L.; Strekowski, L. DNA sequence dependent binding modes of 4',6-diamidino-2-phenylindole (DAPI). *Biochemistry* **1990**, *29* (36), 8452-8461.

16. Ma, Y.; Zhang, G.; Pan, J. Spectroscopic Studies of DNA Interactions with Food Colorant Indigo Carmine with the Use of Ethidium Bromide as a Fluorescence Probe. *J. Agric. Food Chem.* **2012**, *60* (43), 10867-10875.

17. Sánchez, M. I.; Martínez-Costas, J.; Gonzalez, F.; Bermudez, M. A.; Vázquez, M. E.; Mascareñas, J. L. In Vivo Light-Driven DNA Binding and Cellular Uptake of Nucleic Acid Stains. *ACS Chem. Biol.* **2012**, *7* (7), 1276-1280.

18. Bourzac, K. M.; LaVine, L. J.; Rice, M. S. Analysis of DAPI and SYBR Green I as Alternatives to Ethidium Bromide for Nucleic Acid Staining in Agarose Gel Electrophoresis. *J. Chem. Educ.* **2003**, *80* (11), 1292.

19. D'Andrea, M.; Coisson, J. D.; Travaglia, F.; Garino, C.; Arlorio, M. Development and Validation of a SYBR-Green I Real-Time PCR Protocol To Detect Hazelnut (*Corylus avellana* L.) in Foods through Calibration via Plasmid Reference Standard. *J. Agric. Food Chem.* **2009**, *57* (23), 11201-11208.

20. Johnson, K.; Hanekamp, T.; Stayton, M. Methylene blue: an alternative, multi-purpose stain for detection, analysis and isolation of nucleic acids. *Biopolym. Cell.* **1997**, *13* (3), 250-253.

21. Yang, Y.-I.; Jung, D.-W.; Bai, D.-G.; Yoo, G.-S.; Choi, J.-K. Counterion-dye staining method for DNA in agarose gels using crystal violet and methyl orange. *Electrophor.* **2001**, *22* (5), 855-859.

22. Haines, A. M.; Tobe, S. S.; Kobus, H. J.; Linacre, A. Properties of nucleic acid staining dyes used in gel electrophoresis. *Electrophor.* **2015**, *36* (6), 941-944.

23. Rye, H. S.; Yue, S.; Wemmer, D. E.; Quesada, M. A.; Haugland, R. P.; Mathies, R. A.;

- Glazer, A. N. Stable fluorescent complexes of double-stranded DNA with bis-intercalating asymmetric cyanine dyes: properties and applications. *Nucleic Acids Res.* **1992**, *20* (11), 2803-2812.
24. Yarmoluk, S. M.; Kovalska, V. B.; Volkova, K. D. Optimized Dyes for Protein and Nucleic Acid Detection. In *Advanced Fluorescence Reporters in Chemistry and Biology III: Applications in Sensing and Imaging*, Demchenko, A. P. Ed.; Springer Berlin Heidelberg, 2011; pp 161-199.
25. Deligeorgiev, T.; Vasilev, A.; Kaloyanova, S.; Vaquero, J. J. Styryl Dyes – Synthesis and Applications During the Last 15 Years. *Color. Technol.* **2010**, *126* (2), 55-80.
26. Kabatc, J.; Jędrzejewska, B.; Orliński, P.; Pańczowski, J. The Synthesis and the Solvent and Substituent Effect on the Spectroscopic Characteristic of 3-Ethyl-2-(p-Substitued Styryl)Benzothiazolium Iodides. *Spectrochim. Acta - A: Mol. Biomol. Spectrosc.* **2005**, *62* (1), 115-125.
27. Heilbron, I. M.; Walker, G. H.; Buck, J. S. XCVIII.—Styrylbenzopyrylium Salts. Part V. Distyryl Derivatives of 7-Hydroxy-2 : 4-Dimethylbenzopyrylium Chloride. *J. Chem. Soc., Trans.* **1925**, *127* (0), 690-696.
28. Vasilev, A.; Deligeorgiev, T.; Gadjev, N.; Kaloyanova, S.; Vaquero, J. J.; Alvarez-Builla, J.; Baeza, A. G. Novel Environmentally Benign Procedures for the Synthesis of Styryl Dyes. *Dyes Pigm.* **2008**, *77* (3), 550-555.
29. O'Regan, B.; Grätzel, M. A Low-Cost, High-Efficiency Solar Cell Based On Dye-Sensitized Colloidal TiO₂ Films. *Nature* **1991**, *353* (6346), 737-740.
30. Fedorova, O. A.; Andryukhina, E. N.; Fedorov, Y. V.; Panfilov, M. A.; Alfimov, M. V.; Jonusauskas, G.; Grelard, A.; Dufourc, E. Supramolecular Assemblies of Crown-Containing 2-Styrylbenzothiazole with Amino Acids. *Org. Biomol. Chem.* **2006**, *4* (6), 1007-1013.
31. Gust, D.; Moore, T. A. Mimicking Photosynthesis. *Science* **1989**, *244* (4900), 35.
32. Krieg, R.; Eitner, A.; Günther, W.; Halbhuber, K. J. Optimization of Heterocyclic 4-Hydroxystyryl Derivatives for Histological Localization of Endogenous and Immunobound Peroxidase Activity. *Biotech. Histochem.* **2007**, *82* (4-5), 235-262.
33. Gwon, S.-Y.; Rao, B. A.; Kim, H.-S.; Son, Y.-A.; Kim, S.-H. Novel Styrylbenzothiazolium Dye-Based Sensor for Mercury, Cyanide and Hydroxide Ions. *Spectrochim. Acta - A: Mol. Biomol. Spectrosc.* **2015**, *144*, 226-234.

34. Krieg, R.; Eitner, A.; Halbhuber, K.-J. Tailoring and Histochemical Application of Fluorescent Homo-Dimeric Styryl Dyes Using Frozen Sections: From Peroxidase Substrates to New Cytochemical Probes for Mast Cells, Keratin, Cartilage and Nucleic Acids. *Acta Histochem.* **2011**, *113* (7), 682-702.
35. Lee, J. W.; Jung, M.; Rosania, G. R.; Chang, Y.-T. Development of Novel Cell-Permeable DNA Sensitive Dyes Using Combinatorial Synthesis and Cell-Based Screening. *Chem. Commun.* **2003**, (15), 1852-1853.
36. Li, Q.; Kim, Y.; Namm, J.; Kulkarni, A.; Rosania, G. R.; Ahn, Y.-H.; Chang, Y.-T. RNA-Selective, Live Cell Imaging Probes for Studying Nuclear Structure and Function. *Chem. Biol.* **2006**, *13* (6), 615-623.
37. Zhu, C.-Q.; Zhuo, S.-J.; Zheng, H.; Chen, J.-L.; Li, D.-H.; Li, S.-H.; Xu, J.-G. Fluorescence enhancement method for the determination of nucleic acids using cationic cyanine as a fluorescence probe. *Analyst* **2004**, *129* (3), 254-258.
38. Bohländer, P. R.; Wagenknecht, H.-A. Synthesis and Evaluation of Cyanine–Styryl Dyes With Enhanced Photostability for Fluorescent DNA Staining. *Org. Biomol. Chem.* **2013**, *11*, 7458-7462.
39. Wang, K.-N.; Chao, X.-J.; Liu, B.; Zhou, D.-J.; He, L.; Zheng, X.-H.; Cao, Q.; Tan, C.-P.; Zhang, C.; Mao, Z.-W. Red fluorescent probes for real-time imaging of the cell cycle by dynamic monitoring of the nucleolus and chromosome. *Chem. Commun.* **2018**, *54* (21), 2635-2638.
40. Schwartz, J. W.; Blakely, R. D.; DeFelice, L. J. Binding and Transport in Norepinephrine Transporters: REAL-TIME, SPATIALLY RESOLVED ANALYSIS IN SINGLE CELLS USING A FLUORESCENT SUBSTRATE*. *J. Biol. Chem.* **2003**, *278* (11), 9768-9777.
41. Feng, G.; Luo, X.; Lu, X.; Xie, S.; Deng, L.; Kang, W.; He, F.; Zhang, J.; Lei, C.; Lin, B.; et al. Engineering of Nucleic Acids and Synthetic Cofactors as Holo Sensors for Probing Signaling Molecules in the Cellular Membrane Microenvironment. *Angew. Chem. Int. Ed.* **2019**, *58* (20), 6590-6594.
42. Ditmangklo, B.; Taechalertpaisarn, J.; Siriwong, K.; Vilaivan, T. Clickable styryl dyes for fluorescence labeling of pyrrolidiny PNA probes for the detection of base mutations in DNA. *Org. Biomol. Chem.* **2019**, *17* (45), 9712-9725.
43. Saady, A.; Varon, E.; Jacob, A.; Shav-Tal, Y.; Fischer, B. Applying Styryl Quinolinium

- Fluorescent Probes for Imaging of Ribosomal RNA in Living Cells. *Dyes Pigm.* **2020**, *174*, 107986.
44. Abeywickrama, C. S.; Wijesinghe, K. J.; Stahelin, R. V.; Pang, Y. Lysosome imaging in cancer cells by pyrene-benzothiazolium dyes: An alternative imaging approach for LAMP-1 expression based visualization methods to avoid background interference. *Bioorg. Chem.* **2019**, *91*, 103144.
45. Dahal, D.; Pokhrel, S.; McDonald, L.; Bertman, K.; Paruchuri, S.; Konopka, M.; Pang, Y. NIR-Emitting Hemicyanines with Large Stokes' Shifts for Live Cell Imaging: from Lysosome to Mitochondria Selectivity by Substituent Effect. *ACS Appl. Bio Mater.* **2019**, *2* (9), 4037-4043.
46. Kovalska, V. B.; Kryvorotenko, D. V.; Balanda, A. O.; Losytskyy, M. Y.; Tokar, V. P.; Yarmoluk, S. M. Fluorescent homodimer styrylcyanines: synthesis and spectral-luminescent studies in nucleic acids and protein complexes. *Dyes Pigm.* **2005**, *67* (1), 47-54.
47. Przhonska, O. V.; Webster, S.; Padilha, L. A.; Hu, H.; Kachkovski, A. D.; Hagan, D. J.; Van Stryland, E. W. Two-Photon Absorption in Near-IR Conjugated Molecules: Design Strategy and Structure–Property Relations. In *Advanced Fluorescence Reporters in Chemistry and Biology I: Fundamentals and Molecular Design*, Demchenko, A. P. Ed.; Springer Berlin Heidelberg, 2010; pp 105-147.
48. Sasaki, S.; Drummen, G. P. C.; Konishi, G.-i. Recent advances in twisted intramolecular charge transfer (TICT) fluorescence and related phenomena in materials chemistry. *J. Mater. Chem. C* **2016**, *4* (14), 2731-2743.
49. Haidekker, M. A.; Nipper, M.; Mustafic, A.; Lichlyter, D.; Dakanali, M.; Theodorakis, E. A. Dyes with Segmental Mobility: Molecular Rotors. In *Advanced Fluorescence Reporters in Chemistry and Biology I: Fundamentals and Molecular Design*, Demchenko, A. P. Ed.; Springer Berlin Heidelberg, 2010; pp 267-308.
50. Mahmood, T.; Paul, A.; Ladame, S. Synthesis and Spectroscopic and DNA-Binding Properties of Fluorogenic Acridine-Containing Cyanine Dyes. *J. Org. Chem.* **2010**, *75* (1), 204-207.
51. Collot, M.; Boutant, E.; Fam, K. T.; Danglot, L.; Klymchenko, A. S. Molecular Tuning of Styryl Dyes Leads to Versatile and Efficient Plasma Membrane Probes for Cell and

- Tissue Imaging. *Bioconjugate Chem.* **2020**, *31* (3), 875-883.
52. Čipor, I.; Kurutos, A.; Dobrikov, G. M.; Kamounah, F. S.; Majhen, D.; Nestić, D.; Piantanida, I. Structure-dependent mitochondria or lysosome-targeting styryl fluorophores bearing remarkable Stokes shift. *Dyes Pigm.* **2022**, *206*, 110626.
53. Supabowornsathit, K.; Faikhruea, K.; Ditmangklo, B.; Jaroenchuensiri, T.; Wongsuwan, S.; Junpra-ob, S.; Choopara, I.; Palaga, T.; Aonbangkhen, C.; Somboonna, N.; et al. Dicationic styryl dyes for colorimetric and fluorescent detection of nucleic acids. *Sci. Rep.* **2022**, *12* (1), 14250.
54. Wangngae, S.; Ngivprom, U.; Khrootkaew, T.; Worakaensai, S.; Lai, R.-Y.; Kamkaew, A. Cationic styryl dyes for DNA labelling and selectivity toward cancer cells and Gram-negative bacteria. *RSC Advances* **2023**, *13* (3), 2115-2122.
55. Ustimova, M. A.; Fedorov, Y. V.; Tsvetkov, V. B.; Tokarev, S. D.; Shepel, N. A.; Fedorova, O. A. Helical aggregates of bis(styryl) dyes formed by DNA templating. *J. Photochem. Photobiol., A* **2021**, *418*, 113378.
56. Zonjić, I.; Radić Stojković, M.; Crnolatac, I.; Tomašić Paić, A.; Pšeničnik, S.; Vasilev, A.; Kandinska, M.; Mondeshki, M.; Balushev, S.; Landfester, K.; et al. Styryl dyes with N-Methylpiperazine and N-Phenylpiperazine Functionality: AT-DNA and G-quadruplex binding ligands and theranostic agents. *Bioorg. Chem.* **2022**, *127*, 105999.
57. Srinivasan, N.; Kilburn, J. D. Combinatorial approaches to synthetic receptors. *Curr. Opin. Chem. Biol.* **2004**, *8* (3), 305-310.
58. Martínez-Mañez, R.; Sancenón, F. Fluorogenic and Chromogenic Chemosensors and Reagents for Anions. *Chem. Rev.* **2003**, *103* (11), 4419-4476.
59. Wang, S.; Chang, Y.-T. Combinatorial Synthesis of Benzimidazolium Dyes and Its Diversity Directed Application toward GTP-Selective Fluorescent Chemosensors. *J. Am. Chem. Soc.* **2006**, *128* (32), 10380-10381.
60. Rosania, G. R.; Lee, J. W.; Ding, L.; Yoon, H.-S.; Chang, Y.-T. Combinatorial Approach to Organelle-Targeted Fluorescent Library Based on the Styryl Scaffold. *J. Am. Chem. Soc.* **2003**, *125* (5), 1130-1131.
61. Li, Y.; Zhao, P.; Zhang, M.; Zhao, X.; Li, X. Multistep DNA-Templated Synthesis Using a Universal Template. *J. Am. Chem. Soc.* **2013**, *135* (47), 17727-17730.
62. Li, D.; Wang, X.; Shi, F.; Sha, R.; Seeman, N. C.; Canary, J. W. Templated DNA ligation

with thiol chemistry. *Org. Biomol. Chem.* **2014**, *12* (44), 8823-8827.

63. Murayama, K.; Okita, H.; Kuriki, T.; Asanuma, H. Nonenzymatic polymerase-like template-directed synthesis of acyclic l-threoninol nucleic acid. *Nat. Commun.* **2021**, *12* (1), 804.

64. Gartner, Z. J.; Liu, D. R. The Generality of DNA-Templated Synthesis as a Basis for Evolving Non-Natural Small Molecules. *J. Am. Chem. Soc.* **2001**, *123* (28), 6961-6963.

65. Gartner, Z. J.; Tse, B. N.; Grubina, R.; Doyon, J. B.; Snyder, T. M.; Liu, D. R. DNA-Templated Organic Synthesis and Selection of a Library of Macrocycles. *Science* **2004**, *305* (5690), 1601-1605.

66. Roelfes, G.; Feringa, B. L. DNA-Based Asymmetric Catalysis. *Angew. Chem. Int. Ed.* **2005**, *44* (21), 3230-3232.

67. Roelfes, G.; Boersma, A. J.; Feringa, B. L. Highly enantioselective DNA-based catalysis. *Chem. Commun.* **2006**, (6), 635-637.

68. Chen, K.; He, Z.; Xiong, W.; Wang, C.-J.; Zhou, X. Enantioselective Diels–Alder reactions with left-handed G-quadruplex DNA-based catalysts. *Chin. Chem. Lett.* **2021**, *32* (5), 1701-1704.

69. Whitney, A. M.; Ladame, S.; Balasubramanian, S. Templated Ligand Assembly by Using G-Quadruplex DNA and Dynamic Covalent Chemistry. *Angew. Chem. Int. Ed.* **2004**, *43* (9), 1143-1146.

70. Ladame, S.; Whitney, A. M.; Balasubramanian, S. Targeting Nucleic Acid Secondary Structures with Polyamides Using an Optimized Dynamic Combinatorial Approach. *Angew. Chem. Int. Ed.* **2005**, *44* (35), 5736-5739.

71. Suzuki, T.; Ota, Y.; Kasuya, Y.; Mutsuga, M.; Kawamura, Y.; Tsumoto, H.; Nakagawa, H.; Finn, M. G.; Miyata, N. An Unexpected Example of Protein-Templated Click Chemistry. *Angew. Chem. Int. Ed.* **2010**, *49* (38), 6817-6820.

72. Rzuczek, S. G.; Park, H.; Disney, M. D. A Toxic RNA Catalyzes the In Cellulo Synthesis of Its Own Inhibitor. *Angew. Chem. Int. Ed.* **2014**, *53* (41), 10956-10959.

73. Antti, H.; Sellstedt, M. Cell-Based Kinetic Target-Guided Synthesis of an Enzyme Inhibitor. *ACS Med. Chem. Lett.* **2018**, *9* (4), 351-353.

74. Di Antonio, M.; Biffi, G.; Mariani, A.; Raiber, E.-A.; Rodriguez, R.; Balasubramanian, S. Selective RNA Versus DNA G-Quadruplex Targeting by In Situ Click Chemistry. *Angew.*

Chem. Int. Ed. **2012**, *51* (44), 11073-11078.

75. Panda, D.; Saha, P.; Das, T.; Dash, J. Target guided synthesis using DNA nano-templates for selectively assembling a G-quadruplex binding c-MYC inhibitor. *Nat. Commun.* **2017**, *8* (1), 16103.

76. Chaudhuri, R.; Prasanth, T.; Dash, J. Expanding the Toolbox of Target Directed Bio-Orthogonal Synthesis: In Situ Direct Macrocyclization by DNA Templates. *Angew. Chem. Int. Ed.* **2023**, *62* (7), e202215245.

77. Meguellati, K.; Fallah-Araghi, A.; Baret, J.-C.; El Harrak, A.; Mangeat, T.; Marques, C. M.; Griffiths, A. D.; Ladame, S. Enhanced imine synthesis in water: from surfactant-mediated catalysis to host-guest mechanisms. *Chem. Commun.* **2013**, *49* (96), 11332-11334.

78. Meguellati, K.; Koripelly, G.; Ladame, S. Single nucleotide polymorphism detection using a biocompatible, fluorogenic and DNA-templated reaction of cyanine dye formation. *J. Analyt. Molecul. Tech* **2013**, *1* (1), 5.

79. Meguellati, K.; Koripelly, G.; Ladame, S. DNA-Templated Synthesis of Trimethine Cyanine Dyes: A Versatile Fluorogenic Reaction for Sensing G-Quadruplex Formation. *Angew. Chem. Int. Ed.* **2010**, *49* (15), 2738-2742.

80. Dupont, J.; Consorti, C. S.; Suarez, P.; Souza, R. F.; Fulmer, S. L.; Richardson, D. P.; Smith, T. E.; Wolff, S. Preparation of 1-butyl-3-methyl imidazolium-based room temperature ionic liquids. *Org. Synth.* **2002**, *79*, 236-243.

81. Akbay, N.; Losytskyy, M. Y.; Kovalska, V. B.; Balanda, A. O.; Yarmoluk, S. M. The Mechanism of Benzothiazole Styrylcyanine Dyes Binding with dsDNA: Studies by Spectral-Luminescent Methods. *J. Fluoresc.* **2008**, *18* (1), 139-147.

82. Heymann, H. M.; Gardner, A. M.; Gross, E. R. Aldehyde-Induced DNA and Protein Adducts as Biomarker Tools for Alcohol Use Disorder. *Trends Mol. Med.* **2018**, *24* (2), 144-155.

83. Meguellati, K.; Spichy, M.; Ladame, S. Synthesis, spectroscopic and DNA alkylating properties of malondialdehyde (MDA) bis-imine fluorescent adducts. *Mol. Biosyst.* **2010**, *6* (9), 1694-1699.

84. Bhoge, B. A.; Mala, P.; Kurian, J. S.; Srinivasan, V.; Saraogi, I. Selective functionalization at N2-position of guanine in oligonucleotides via reductive amination. *Chem. Commun.* **2020**, *56* (89), 13832-13835.

85. Khimji, I.; Doan, K.; Bruggeman, K.; Huang, P.-J. J.; Vajha, P.; Liu, J. Extraction of DNA staining dyes from DNA using hydrophobic ionic liquids. *Chem. Commun.* **2013**, *49* (40), 4537-4539.
86. Wright, N. D.; Huff, J. S.; Barclay, M. S.; Wilson, C. K.; Barcenas, G.; Duncan, K. M.; Ketteridge, M.; Obukhova, O. M.; Krivoshey, A. I.; Tatarets, A. L.; et al. Intramolecular Charge Transfer and Ultrafast Nonradiative Decay in DNA-Tethered Asymmetric Nitro- and Dimethylamino-Substituted Squaraines. *J. Phys. Chem.* **2023**, *127* (5), 1141-1157.
87. Gonzalez, V.; Guo, K.; Hurley, L.; Sun, D. Identification and characterization of nucleolin as a c-myc G-quadruplex-binding protein. *J. Biol. Chem.* **2009**, *284* (35), 23622-23635.
88. Rankin, S.; Reszka, A. P.; Huppert, J.; Zloh, M.; Parkinson, G. N.; Todd, A. K.; Ladame, S.; Balasubramanian, S.; Neidle, S. Putative DNA quadruplex formation within the human c-kit oncogene. *J. Am. Chem. Soc.* **2005**, *127* (30), 10584-10589.
89. Cogo, S.; Paramasivam, M.; Filichev, V.; Geci, I.; Pedersen, E. B.; Xodo, L. E. Identification of a new G-quadruplex motif in the KRAS promoter and design of pyrene-modified G4-decoys with antiproliferative activity in pancreatic cancer cells. *J. Med. Chem.* **2009**, *52* (2), 564-568.
90. Pandith, A.; Siddappa, R. G.; Seo, Y. J. Recent developments in novel blue/green/red/NIR small fluorescent probes for in cellulo tracking of RNA/DNA G-quadruplexes. *J. Photochem. Photobiol. C: Photochem. Rev.* **2019**, *40*, 81-116.
91. Murat, P.; Singh, Y.; Defrancq, E. Methods for investigating G-quadruplex DNA/ligand interactions. *Chem. Soc. Rev.* **2011**, *40* (11), 5293-5307.
92. Jin, J.; Hou, J.; Long, W.; Zhang, X.; Lu, Y.-J.; Li, D.; Zhang, K.; Wong, W.-L. Synthesis of fluorescent G-quadruplex DNA binding ligands for the comparison of terminal group effects in molecular interaction: Phenol versus methoxybenzene. *Bioorg. Chem.* **2020**, *99*, 103821.
93. Sun, R.; Guo, X.; Yang, D.; Tang, Y.; Lu, J.; Sun, H. c-Myc G-quadruplex is sensitively and specifically recognized by a fluorescent probe. *Talanta* **2021**, *226*, 122125.
94. Yan, C.; Zhang, Q.; Gao, H.; Zheng, X.; Yang, T.; Zheng, G.; Zhou, X.; Shao, Y. Concurrent formation of H- and J-aggregates of dyes with chiralities individually determined by G-quadruplex handedness. *Spectrochim. Acta - A: Mol. Biomol.*

Spectrosc. **2021**, *248*, 119270.

95. Czerwinska, I.; Juskowiak, B. Photoisomerizable arylstilbazolium ligands recognize parallel and antiparallel structures of G-quadruplexes. *Int. J. Biol. Macromol.* **2012**, *51* (4), 576-582.

96. Dhamodharan, V.; Harikrishna, S.; Jagadeeswaran, C.; Halder, K.; Pradeepkumar, P. I. Selective G-quadruplex DNA Stabilizing Agents Based on Bisquinolinium and Bispyridinium Derivatives of 1,8-Naphthyridine. *J. Org. Chem.* **2012**, *77* (1), 229-242.

97. Qin, H.; Ren, J.; Wang, J.; Luedtke, N. W.; Wang, E. G-quadruplex-modulated fluorescence detection of potassium in the presence of a 3500-fold excess of sodium ions. *Anal. Chem.* **2010**, *82* (19), 8356-8360.

98. He, H.-Z.; Chan, D. S.-H.; Leung, C.-H.; Ma, D.-L. G-quadruplexes for luminescent sensing and logic gates. *Nucleic Acids Res.* **2013**, *41* (8), 4345-4359.

99. Lim, K. W.; Amrane, S.; Bouaziz, S.; Xu, W.; Mu, Y.; Patel, D. J.; Luu, K. N.; Phan, A. T. Structure of the human telomere in K⁺ solution: a stable basket-type G-quadruplex with only two G-tetrad layers. *J. Am. Chem. Soc.* **2009**, *131* (12), 4301-4309.

100. Mohanty, J.; Barooah, N.; Dhamodharan, V.; Harikrishna, S.; Pradeepkumar, P. I.; Bhasikuttan, A. C. Thioflavin T as an efficient inducer and selective fluorescent sensor for the human telomeric G-quadruplex DNA. *J. Am. Chem. Soc.* **2013**, *135* (1), 367-376.

101. O'Hagan, M. P.; Morales, J. C.; Galan, M. C. Binding and Beyond: What Else Can G-Quadruplex Ligands Do? *Eur. J. Org. Chem.* **2019**, *2019* (31-32), 4995-5017.

102. Tishchenko, S.; Nikulin, A.; Fomenkova, N.; Nevskaya, N.; Nikonov, O.; Dumas, P.; Moine, H.; Ehresmann, B.; Ehresmann, C.; Piendl, W.; et al. Detailed analysis of RNA-protein interactions within the ribosomal protein S8-rRNA complex from the archaeon *Methanococcus jannaschii*. *J. Mol. Biol.* **2001**, *311* (2), 311-324.

103. Froeyen, M.; Herdewijn, P. RNA as a Target for Drug Design, the Example of Tat-TAR Interaction. *Curr. Top. Med. Chem.* **2002**, *2* (10), 1123-1145.

104. Kumar, A.; Parkesh, R.; Sznajder, L. J.; Childs-Disney, J. L.; Sobczak, K.; Disney, M. D. Chemical Correction of Pre-mRNA Splicing Defects Associated with Sequestration of Muscleblind-like 1 Protein by Expanded r(CAG)-Containing Transcripts. *ACS Chem. Biol.* **2012**, *7* (3), 496-505.

105. Disney, M. D. Targeting RNA with Small Molecules To Capture Opportunities at the Intersection of Chemistry, Biology, and Medicine. *J. Am. Chem. Soc.* **2019**, *141* (17), 6776-6790.
106. Dirks, R. W.; Tanke, H. J. Styryl Molecules Light-Up RNAs. *Chem. Biol.* **2006**, *13* (6), 559-560.
107. Zhang, Y.; Wang, L.; Rao, Q.; Bu, Y.; Xu, T.; Zhu, X.; Zhang, J.; Tian, Y.; Zhou, H. Tuning the hydrophobicity of pyridinium-based probes to realize the mitochondria-targeted photodynamic therapy and mitophagy tracking. *Sens. Actuators B Chem.* **2020**, *321*, 128460.
108. Dubinin, M. V.; Semenova, A. A.; Ilzorkina, A. I.; Markelova, N. Y.; Penkov, N. V.; Shakurova, E. R.; Belosludtsev, K. N.; Parfenova, L. V. New quaternized pyridinium derivatives of betulin: Synthesis and evaluation of membranotropic properties on liposomes, pro- and eukaryotic cells, and isolated mitochondria. *Chem. Biol. Interact.* **2021**, *349*, 109678.
109. Madaan, P.; Tyagi, V. K. Quaternary pyridinium salts: a review. *J. Oleo. Sci.* **2008**, *57* (4), 197-215.
110. Kurutos, A.; Orehovec, I.; Tomašić Paić, A.; Crnolatac, I.; Horvat, L.; Gadjev, N.; Piantanida, I.; Deligeorgiev, T. New series of non-toxic DNA intercalators, mitochondria targeting fluorescent dyes. *Dyes Pigm.* **2018**, *148*, 452-459.
111. Lu, Y.-J.; Deng, Q.; Hu, D.-P.; Wang, Z.-Y.; Huang, B.-H.; Du, Z.-Y.; Fang, Y.-X.; Wong, W.-L.; Zhang, K.; Chow, C.-F. A molecular fluorescent dye for specific staining and imaging of RNA in live cells: a novel ligand integration from classical thiazole orange and styryl compounds. *Chem. Commun.* **2015**, *51* (83), 15241-15244.
112. Vasilev, A. A.; Miteva, M.; Ishkitiev, N.; Dragneva, M.; Topalova, L.; Kandinska, M. I. Styryl Hemicyanine Dye (E)-3-Methyl-2-(4-thiomorpholinostyryl)benzo[d]thiazol-3-ium iodide for Nucleic Acids and Cell Nucleoli Visualization. *Molbank* **2022**, *2022* (2), M1392.



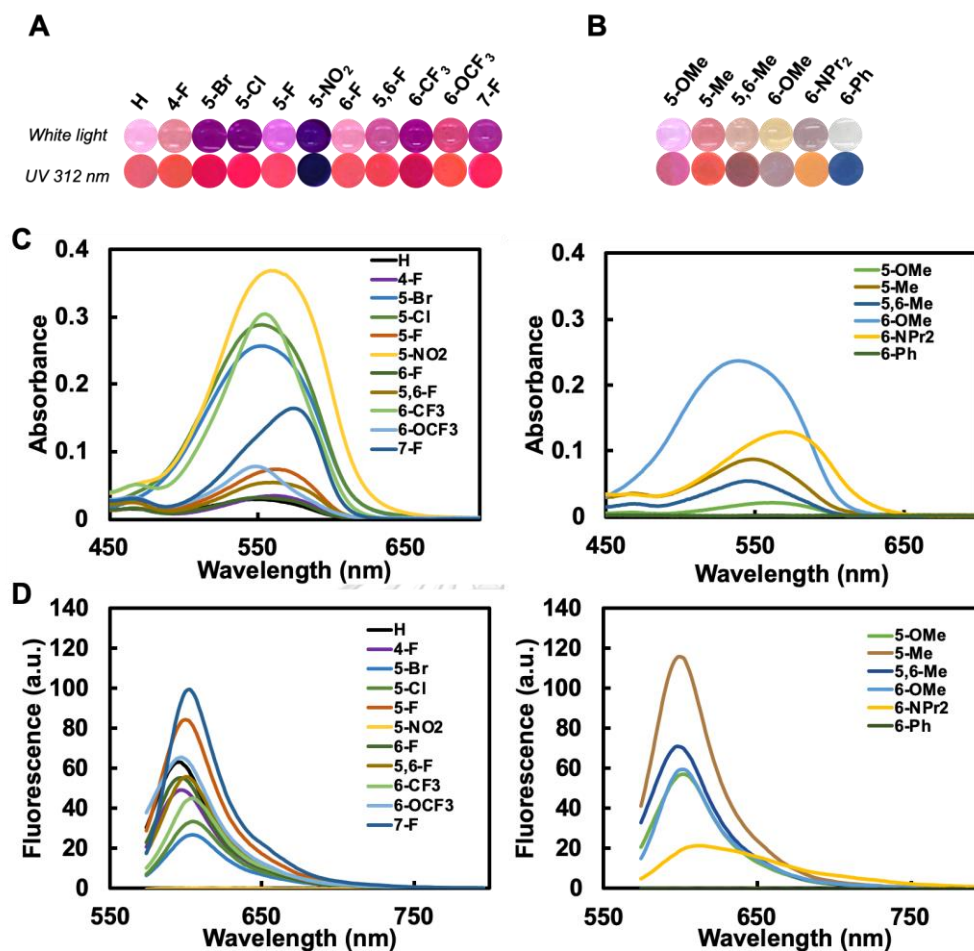
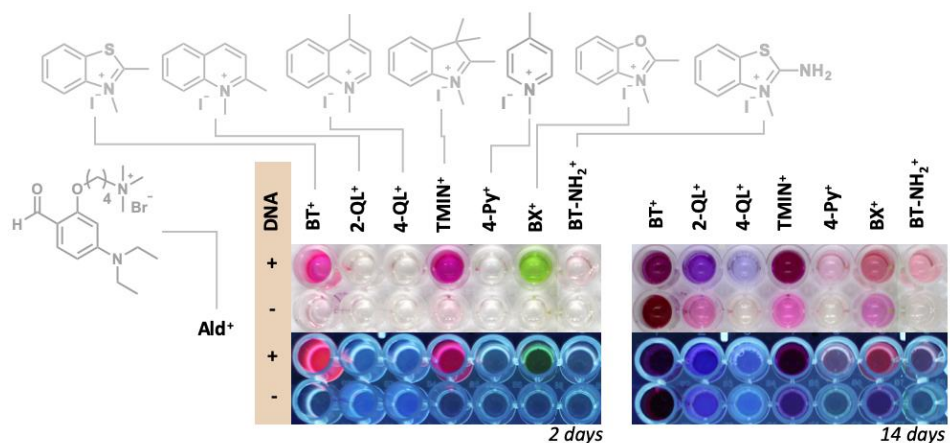
Substituent effect on BT⁺ substrates for DNA-templated synthesis

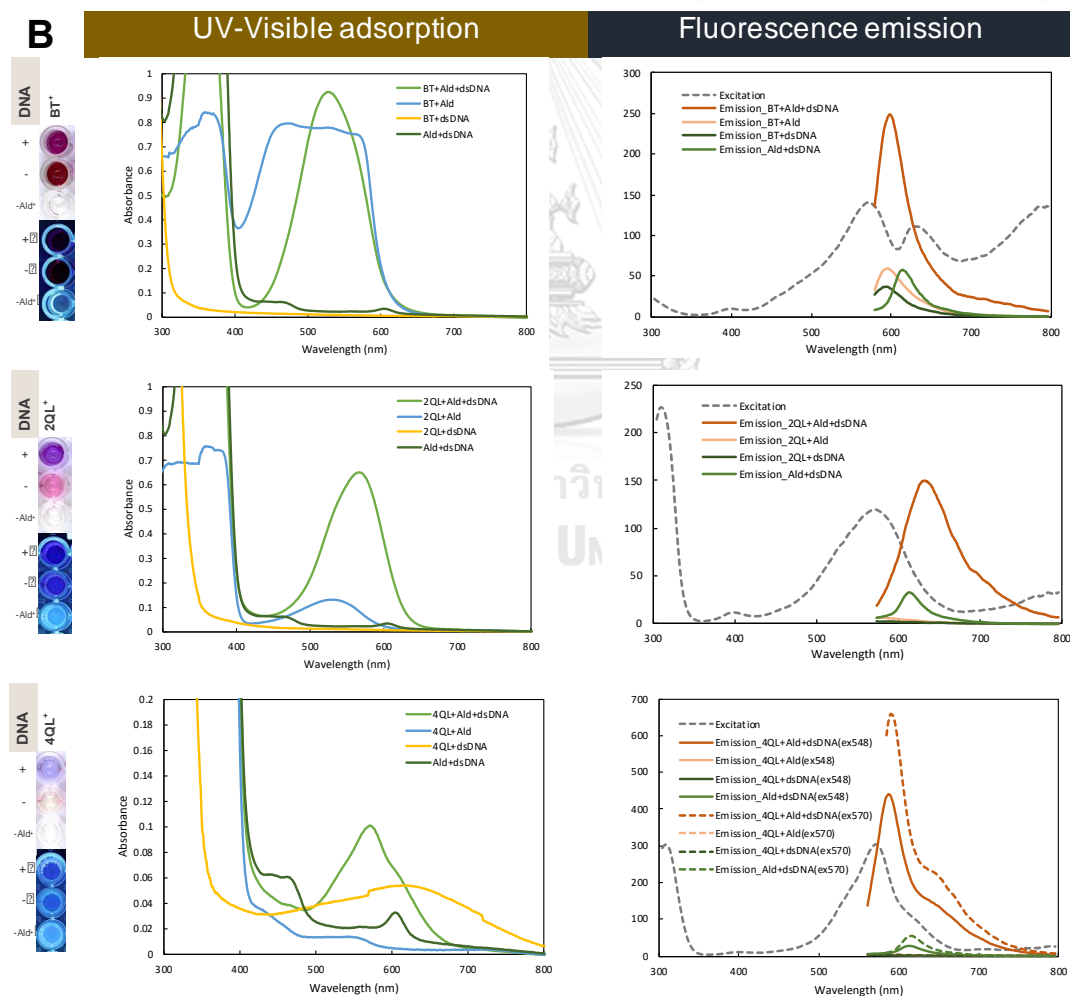
Figure A.1 Study of substituent effect on BT heteroaromatic substrate using diverse sets of (A) electron-withdrawing and (B) electron-donating substituents. Spectroscopic profiles; (C) Absorption spectra and (D) Emission spectra ($\lambda_{\text{ex}} = 565 \text{ nm}$) of dye-DNA bound form from combinatorial screening.

Combinatorial synthesis of styryl dyes from various cationic heteroaromatic substrates

A



B



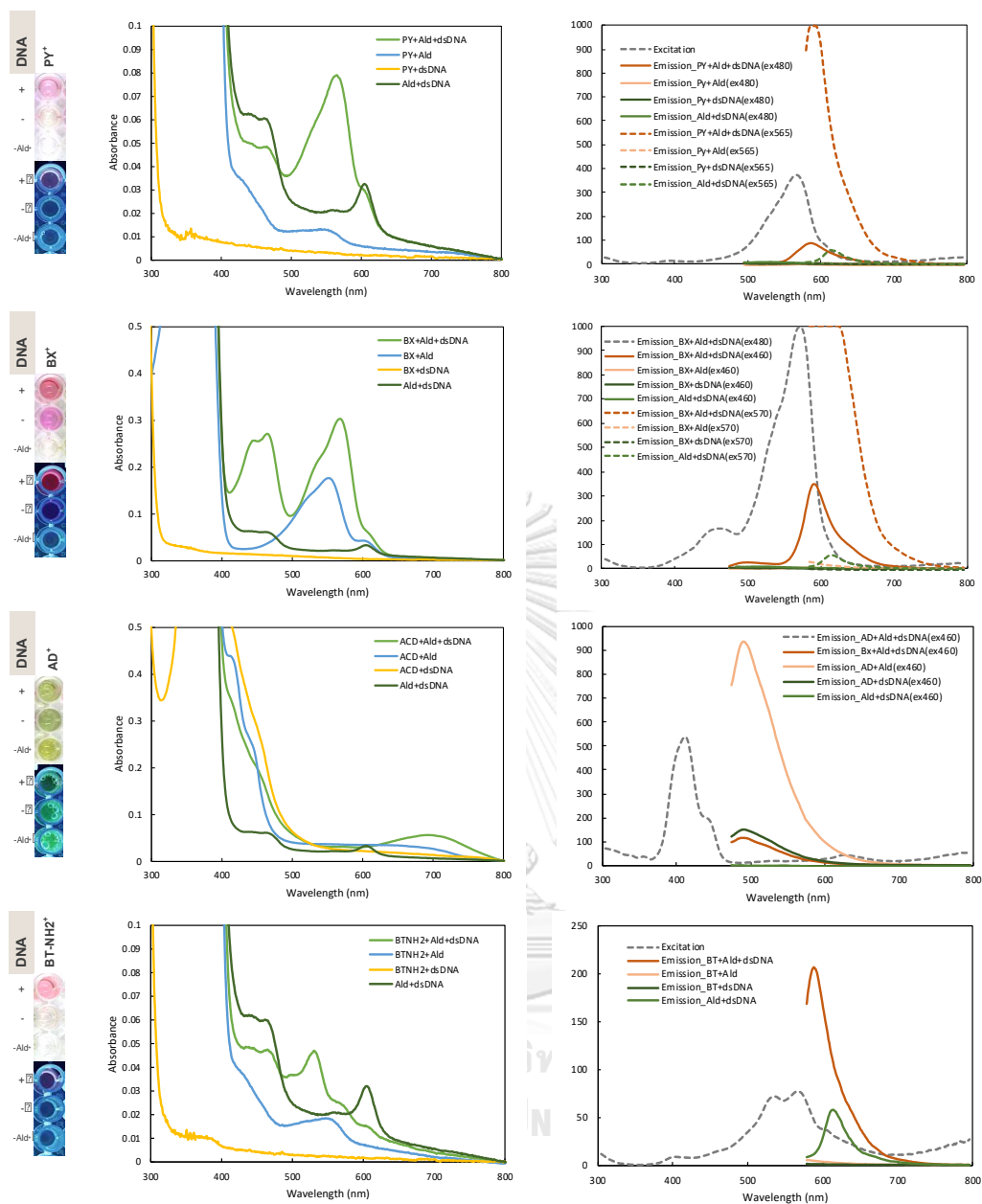


Figure A.2 Study of heteroaromatic effect on DNA-templated synthesis using various heterocycle substrates (A) templated reaction (B) UV-visible and fluorescence spectra.

Table A.1 Optical properties of the individually synthesized dyes from various heteroaromatic and *N,N*-diethylamino aromatic aldehyde. Conditions: [Dye] = 2 μ M, [DNA] = 1 μ M; [DNA (in bp)] : [Dye] = 15 : 1; all measurements were performed in 10 mM sodium phosphate buffer (pH 7.0).

dsDNA = 5'-CGCGGCGTACAGTGATCTACCATGCCCTGG-3' +
3'-GCGCCGCATGTCAGTAGATGGTACGGGACC-5'.

| Dye | λ_{Abs} (nm) | I_{Abs} | λ_{Em} (nm) | I_{Em} | $I_{\text{Em}}/I_{\text{Abs}}$ ($\times 10^5$) | Φ_F | |
|--|--------------------------------|------------------|-------------------------------|-----------------|---|----------|-------|
| | | | | | | Dye | +DNA |
| BT ⁺ -Ald(NEt ₂) ⁺ | 565 | 0.127 | 600 | 467946 | 37 | 0.004 | 0.371 |
| BX ⁺ -Ald(NEt ₂) ⁺ | 570 | 0.009 | 595 | 12106 | 13 | 0.006 | 0.426 |
| TMIN ⁺ -Ald(NEt ₂) ⁺ | 565 | 0.284 | 620 | 389408 | 14 | 0.004 | 0.124 |
| 4-PY ⁺ -Ald(NEt ₂) ⁺ | 565 | 0.053 | 590 | 117126 | 22 | 0.002 | 0.127 |
| 2-QL ⁺ -Ald(NEt ₂) ⁺ | 570 | 0.647 | 630 | 6481 | 0.11 | 0.001 | 0.025 |
| 4-QL ⁺ -Ald(NEt ₂) ⁺ | 570 | 0.057 | 590 | 898 | 0.16 | 0.001 | 0.057 |

^a Excitation wavelength (λ_{Ex}), 565 nm

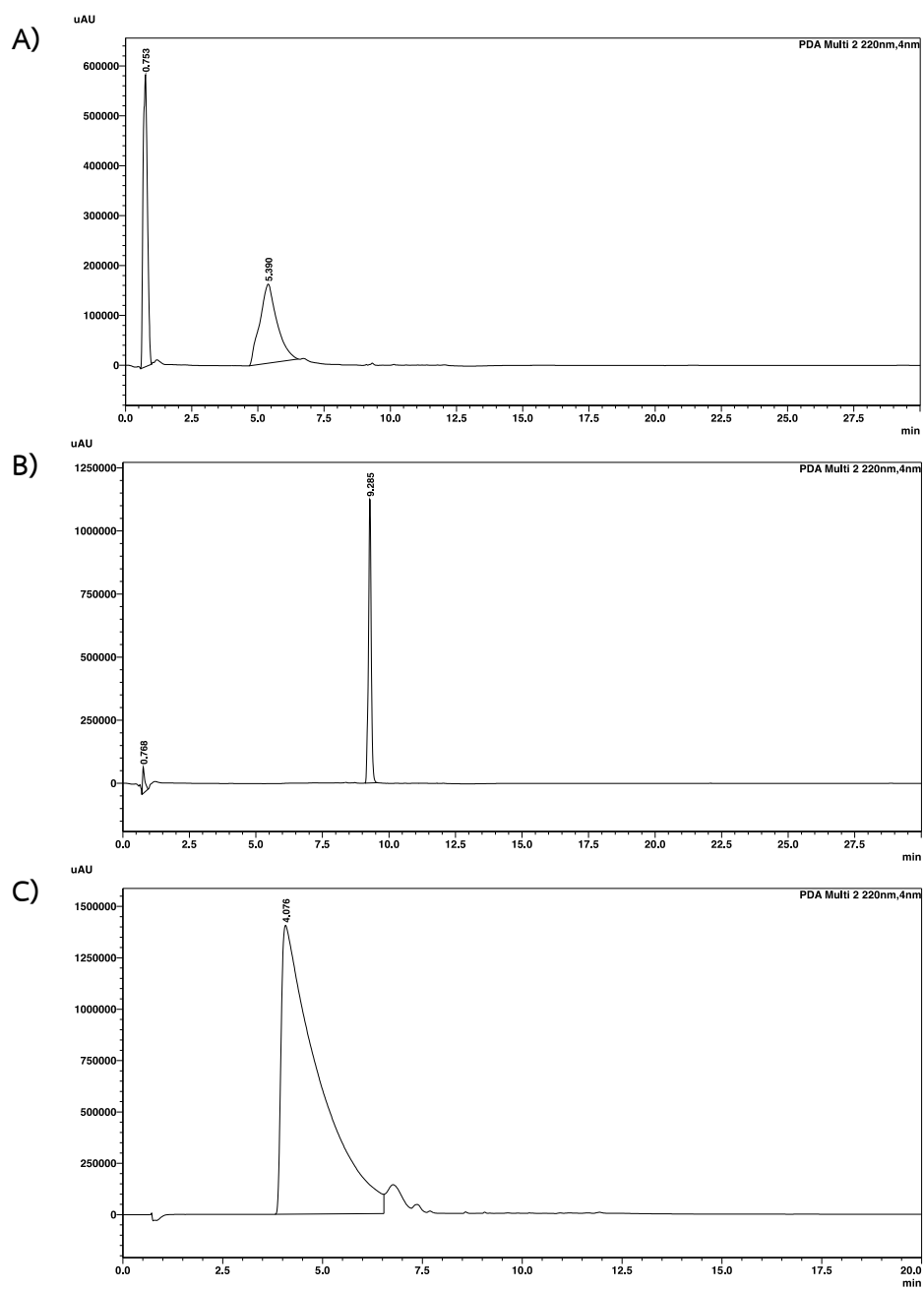


Figure A.3 HPLC chromatogram of (A) BT⁺ (B) Ald⁺ and (C) [BMIM]PF₆ observed at 220 nm.

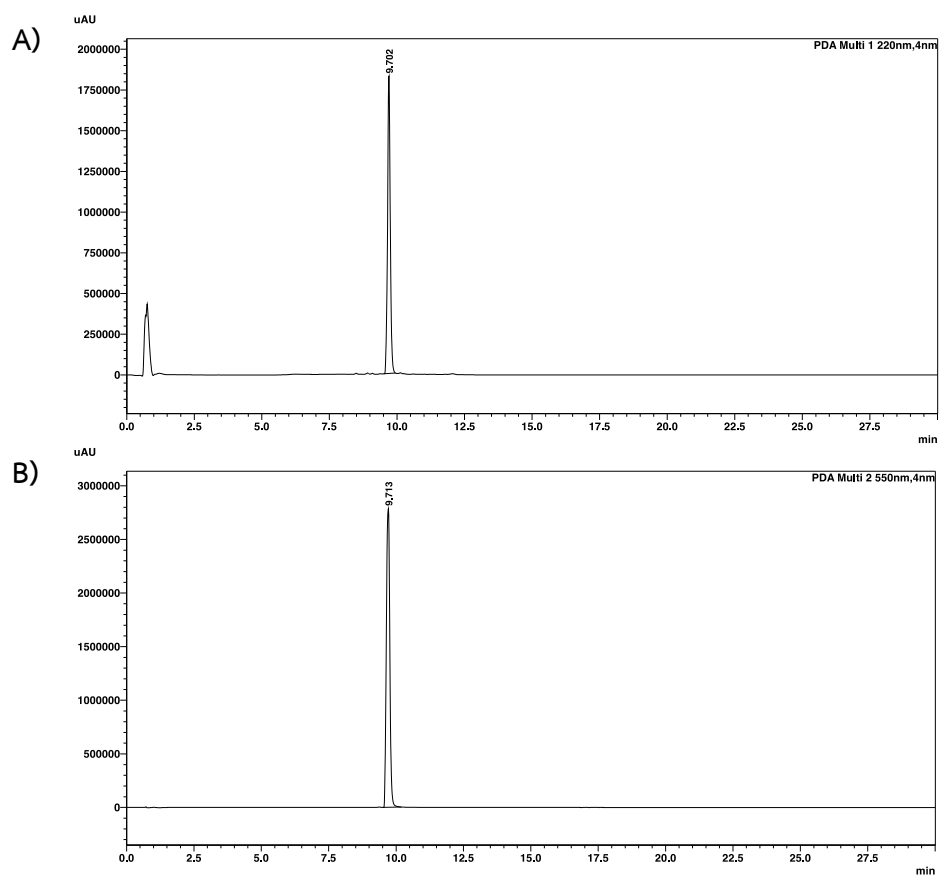


Figure A.4 HPLC chromatogram of BT⁺-Ald⁺ dye observed at (A) 220 nm and (B) 550 nm.

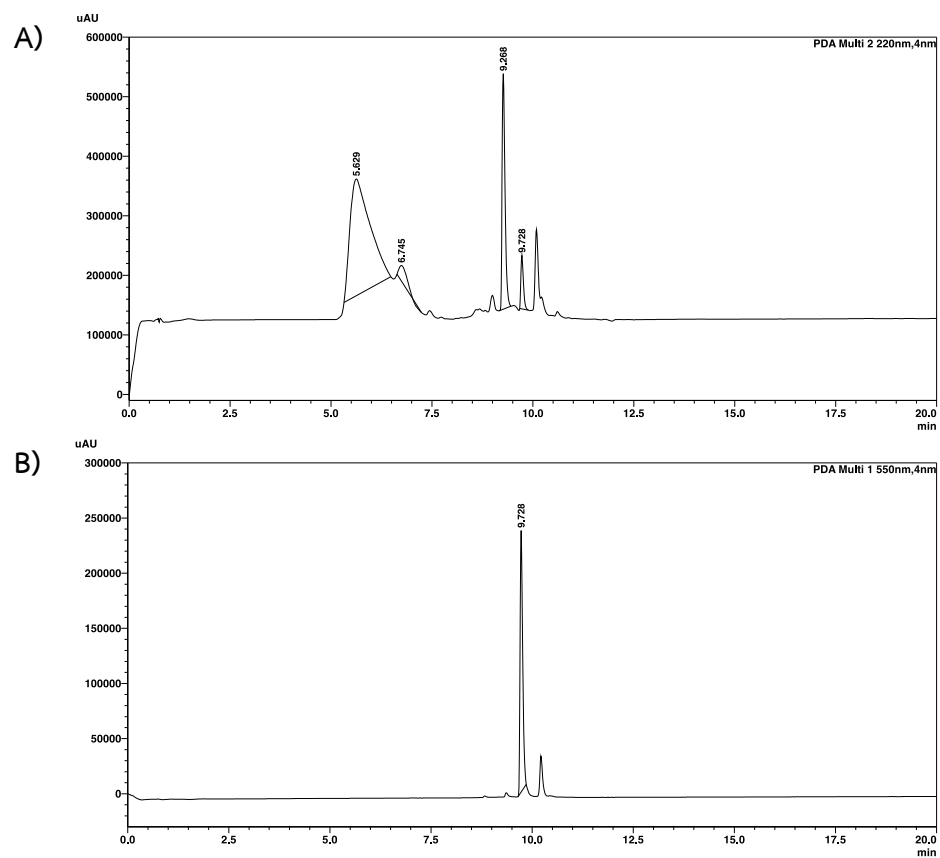


Figure A.5 HPLC chromatogram of crude from DNA-templated synthesis for BT⁺-Ald⁺ after incubating for 14 days observed at **(A)** 220 nm and **(B)** 550 nm.

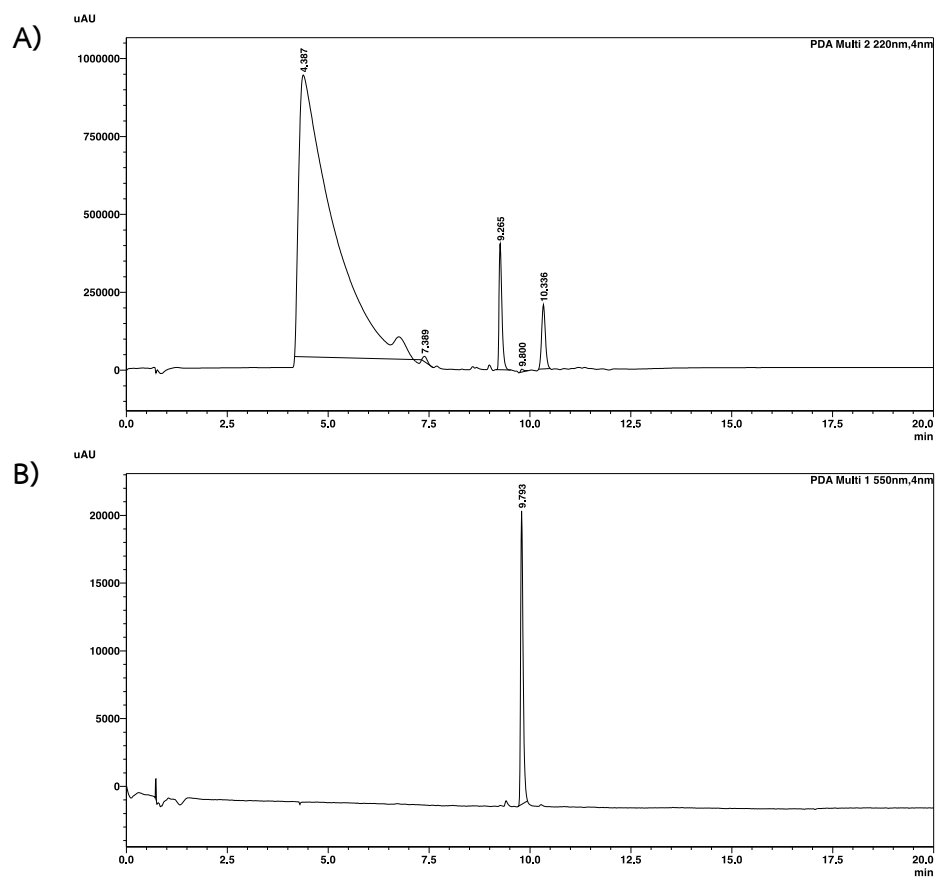


Figure A.6 HPLC chromatogram of crude from DNA-templated synthesis for 4-F-BT⁺-Ald⁺ after incubating for 2 days observed at (A) 220 nm and (B) 550 nm.

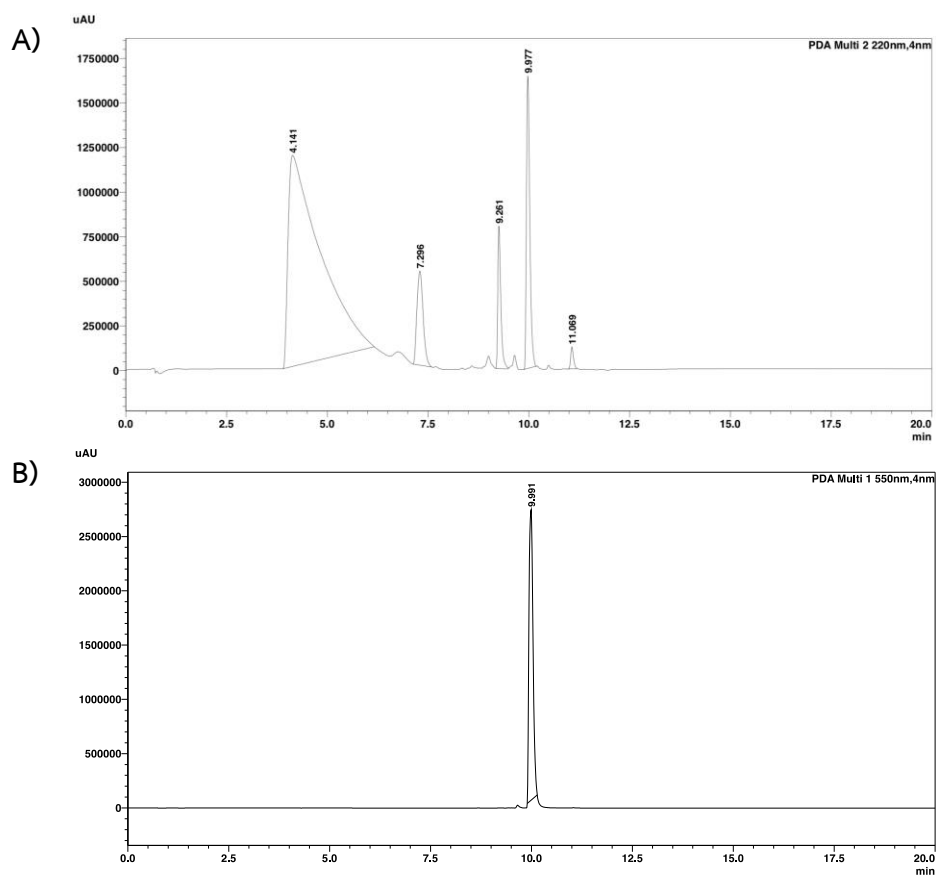


Figure A.7 HPLC chromatogram of crude from DNA-templated synthesis for 5-Br-BT⁺-Ald⁺ after incubating for 2 days observed at **(A)** 220 nm and **(B)** 550 nm.

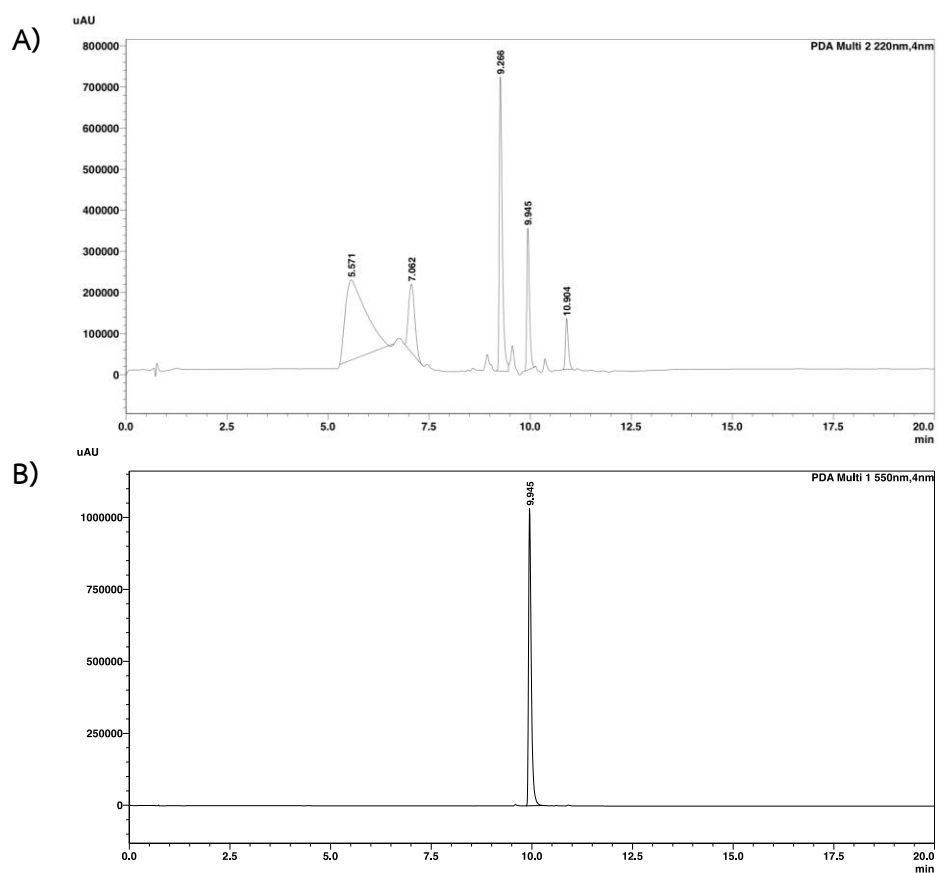


Figure A.8 HPLC chromatogram of crude from DNA-templated synthesis for 5-Cl-BT⁺-Ald⁺ after incubating for 2 days observed at (A) 220 nm and (B) 550 nm.

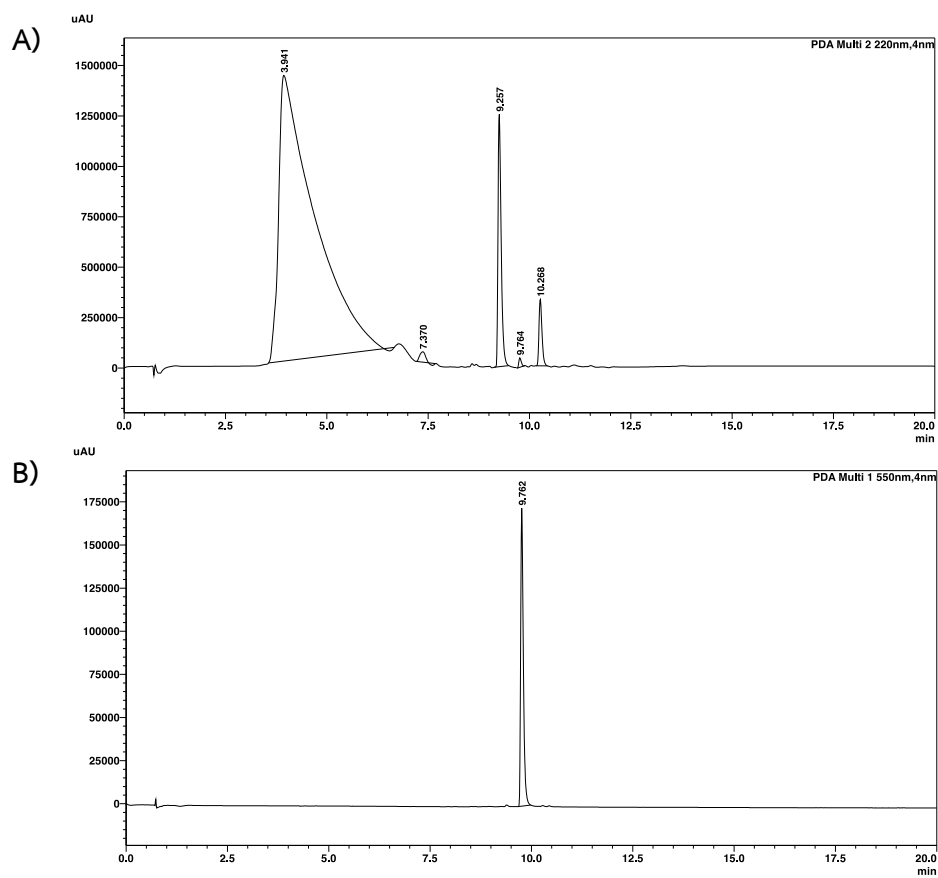


Figure A.9 HPLC chromatogram of crude from DNA-templated synthesis for 5-F-BT⁺-Ald⁺ after incubating for 2 days observed at **(A)** 220 nm and **(B)** 550 nm.

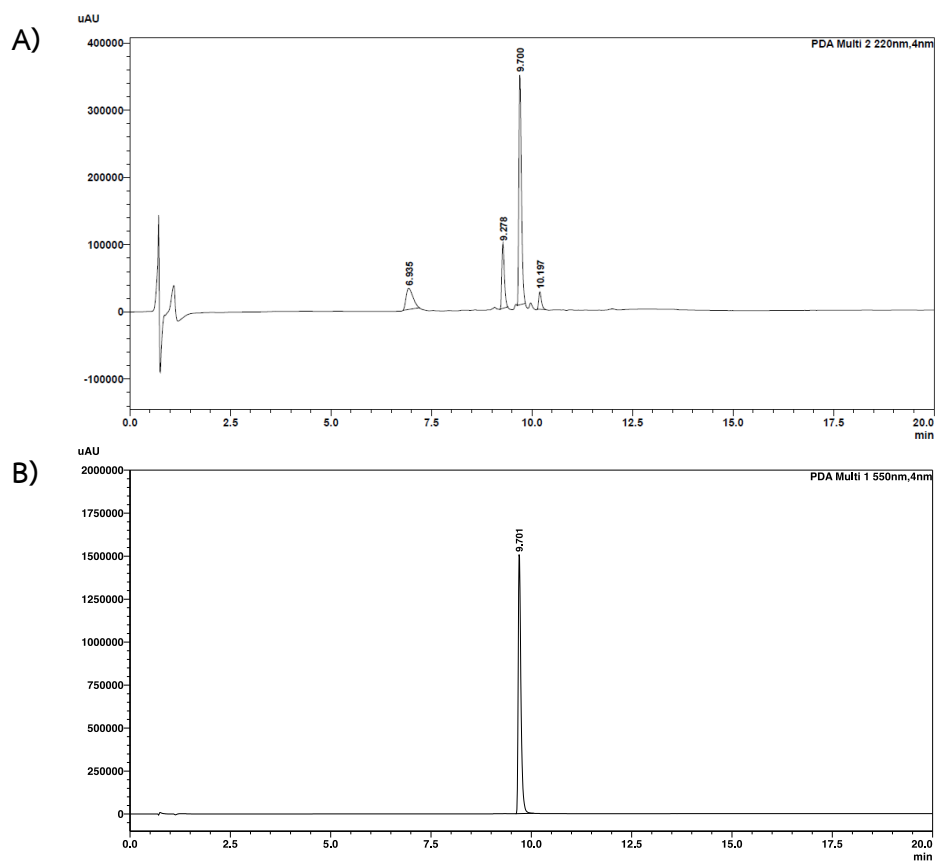


Figure A.10 HPLC chromatogram of crude from DNA-templated synthesis for 5-NO₂-BT⁺-Ald⁺ after incubating for 2 days observed at (A) 220 nm and (B) 550 nm.

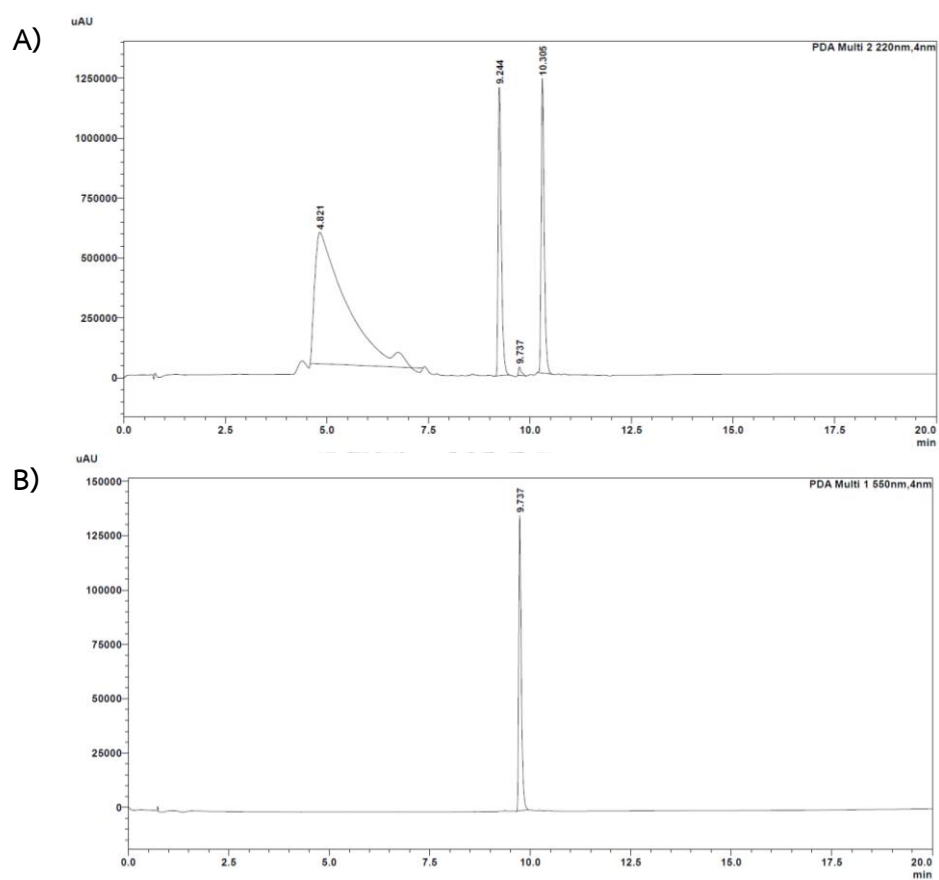


Figure A.11 HPLC chromatogram of crude from DNA-templated synthesis for 6-F-BT⁺-Ald⁺ after incubating for 2 days observed at (A) 220 nm and (B) 550 nm.

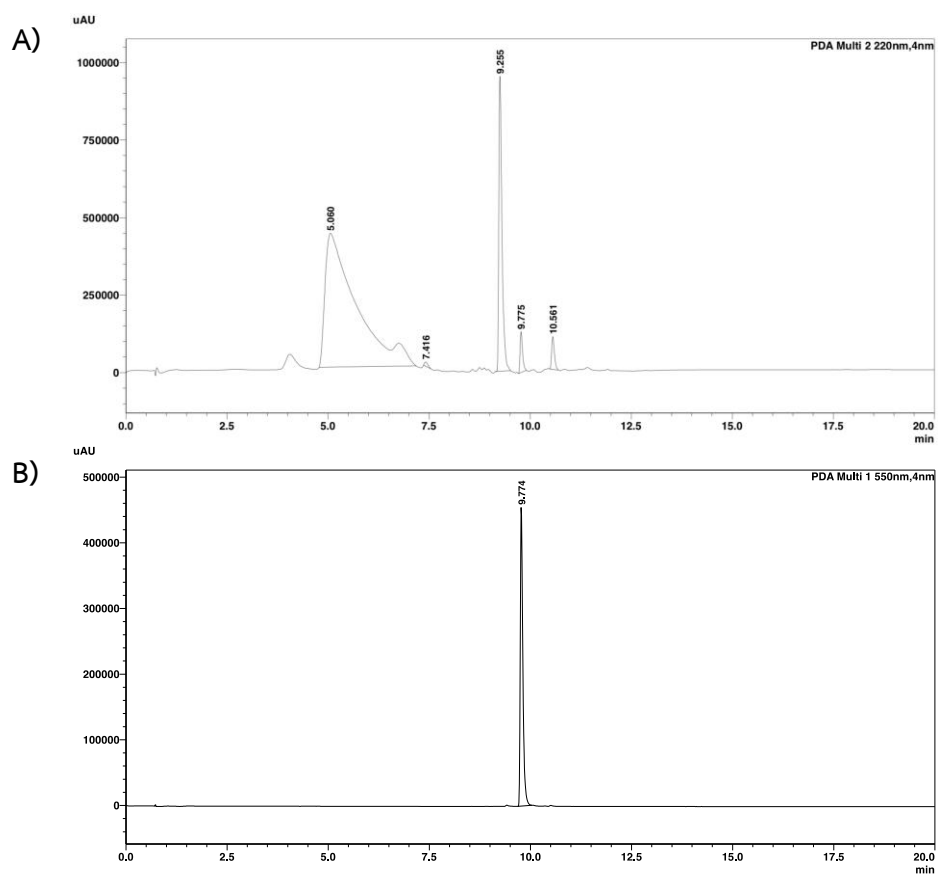


Figure A.12 HPLC chromatogram of crude from DNA-templated synthesis for 5,6-F-BT⁺·Ald⁺ after incubating for 2 days observed at (A) 220 nm and (B) 550 nm.

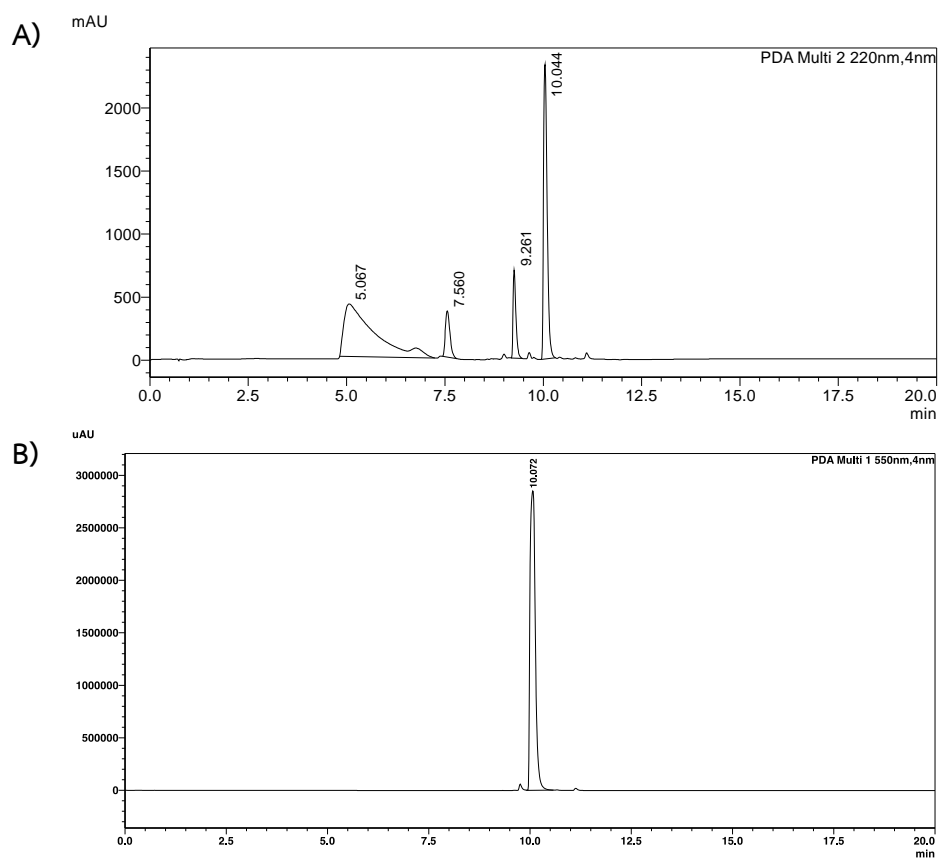


Figure A.13 HPLC chromatogram of crude from DNA-templated synthesis for 6-CF₃-BT⁺-Ald⁺ after incubating for 2 days observed at (A) 220 nm and (B) 550 nm.

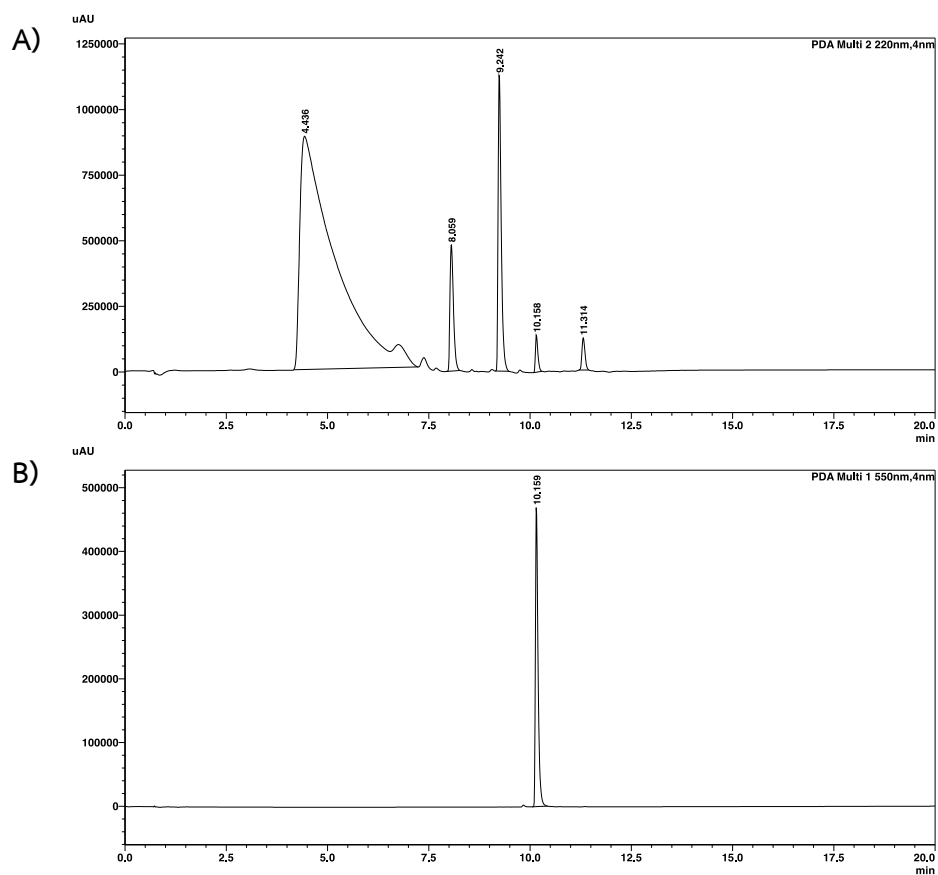


Figure A.14 HPLC chromatogram of crude from DNA-templated synthesis for 6-OCF₃-BT⁺-Ald⁺ after incubating for 2 days observed at (A) 220 nm and (B) 550 nm.

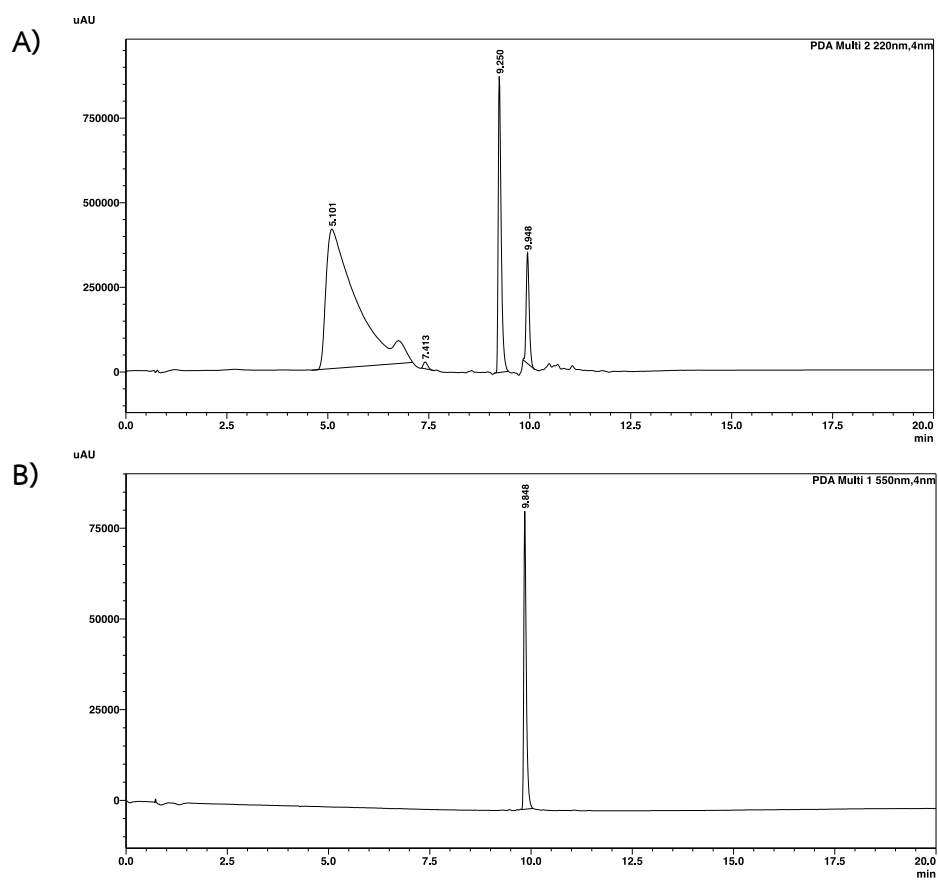


Figure A.15 HPLC chromatogram of crude from DNA-templated synthesis for 7-F-BT⁺-Ald⁺ after incubating for 2 days observed at **(A)** 220 nm and **(B)** 550 nm.

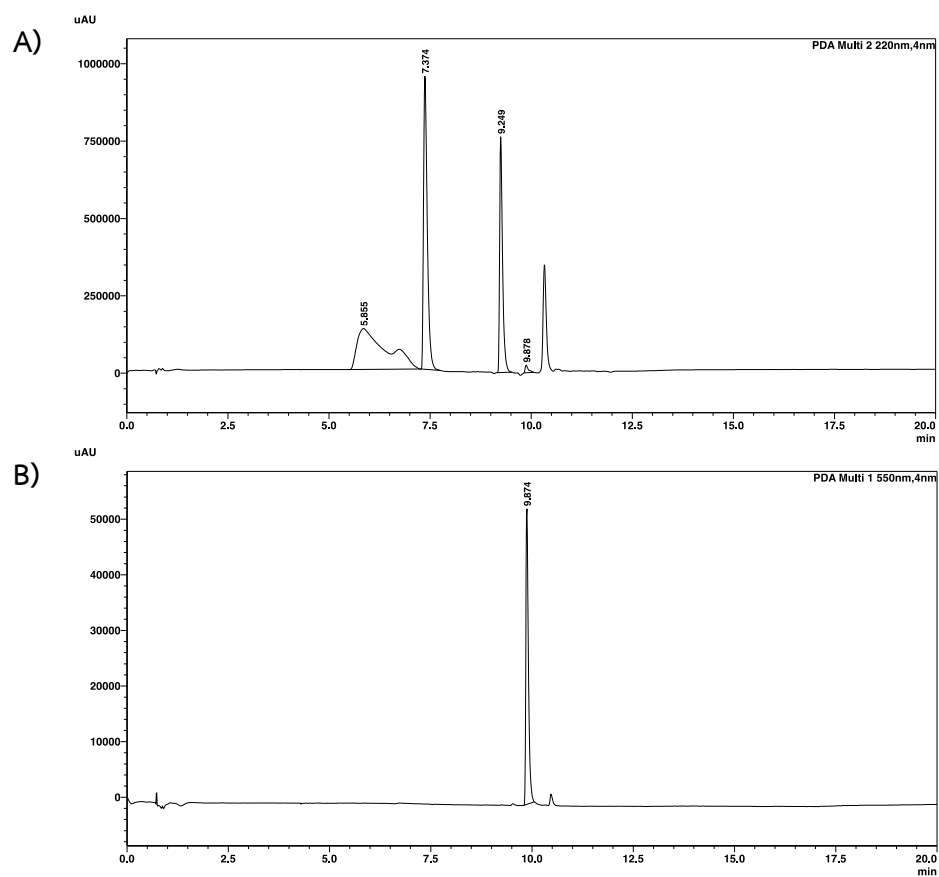


Figure A.16 HPLC chromatogram of crude from DNA-templated synthesis for 5-OMe-BT⁺·Ald⁺ after incubating for 2 days observed at (A) 220 nm and (B) 550 nm.

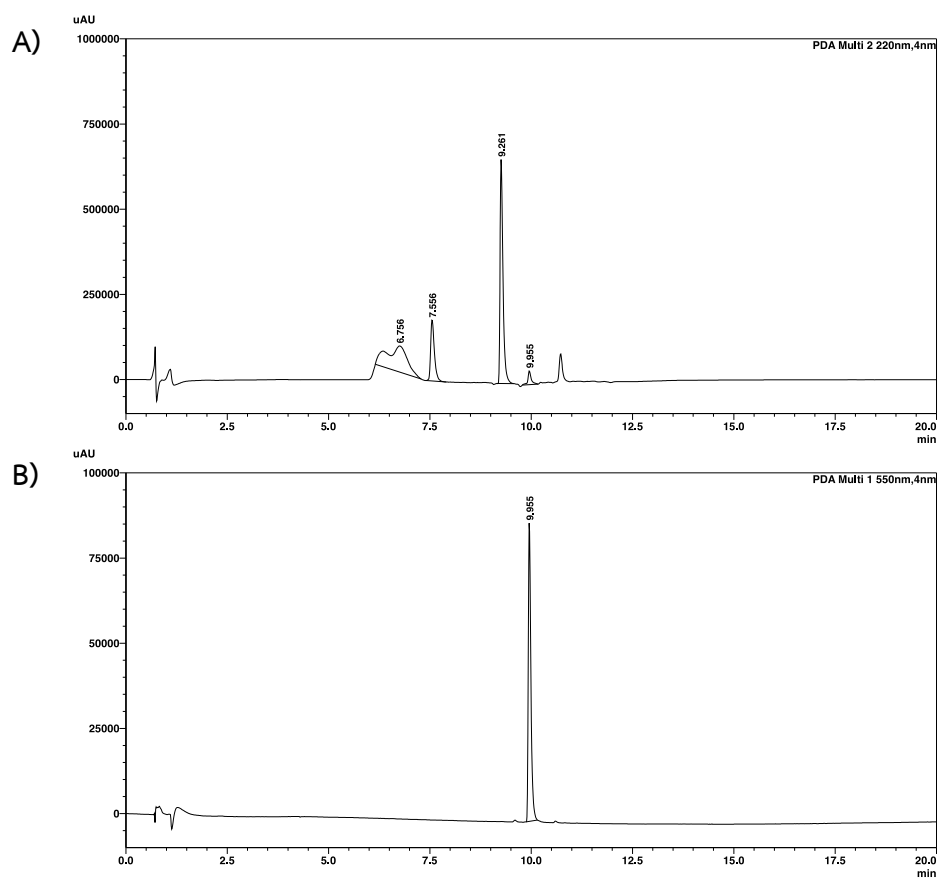


Figure A.17 HPLC chromatogram of crude from DNA-templated synthesis for 5-Me-BT⁺·Ald⁺ after incubating for 2 days observed at (A) 220 nm and (B) 550 nm.

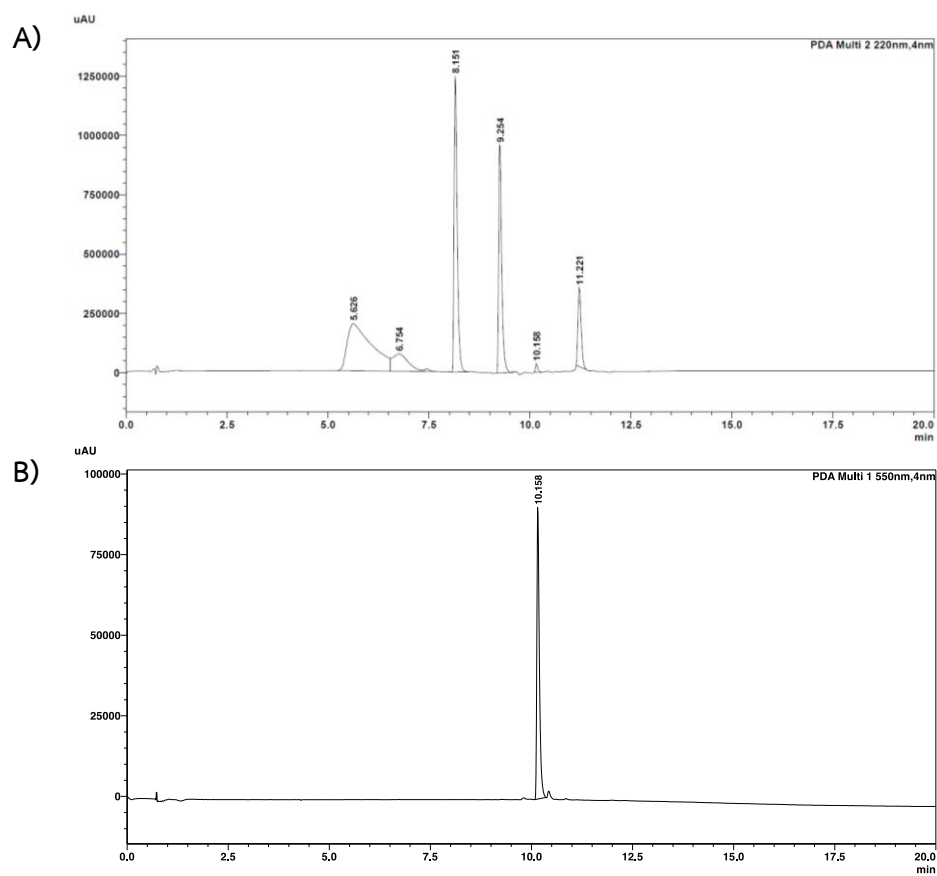


Figure A.18 HPLC chromatogram of crude from DNA-templated synthesis for 5,6-Me-BT⁺-Ald⁺ after incubating for 2 days observed at (A) 220 nm and (B) 550 nm.

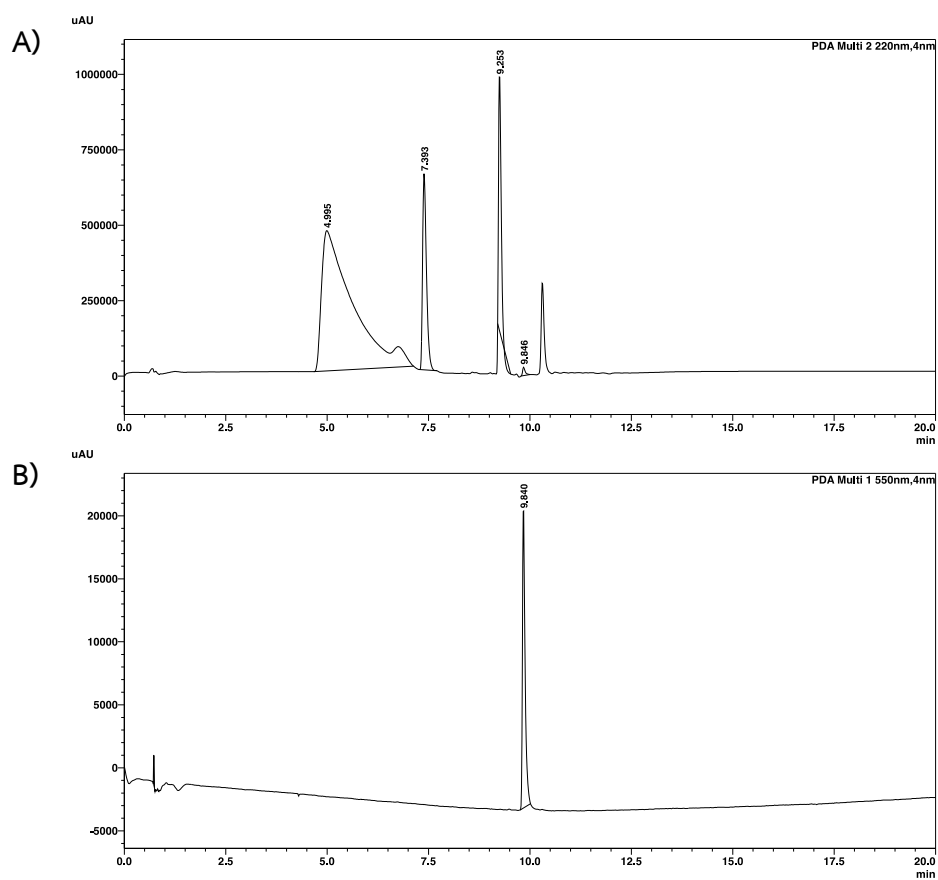


Figure A.19 HPLC chromatogram of crude from DNA-templated synthesis for 6-OMe-BT⁺·Ald⁺ after incubating for 2 days observed at (A) 220 nm and (B) 550 nm.

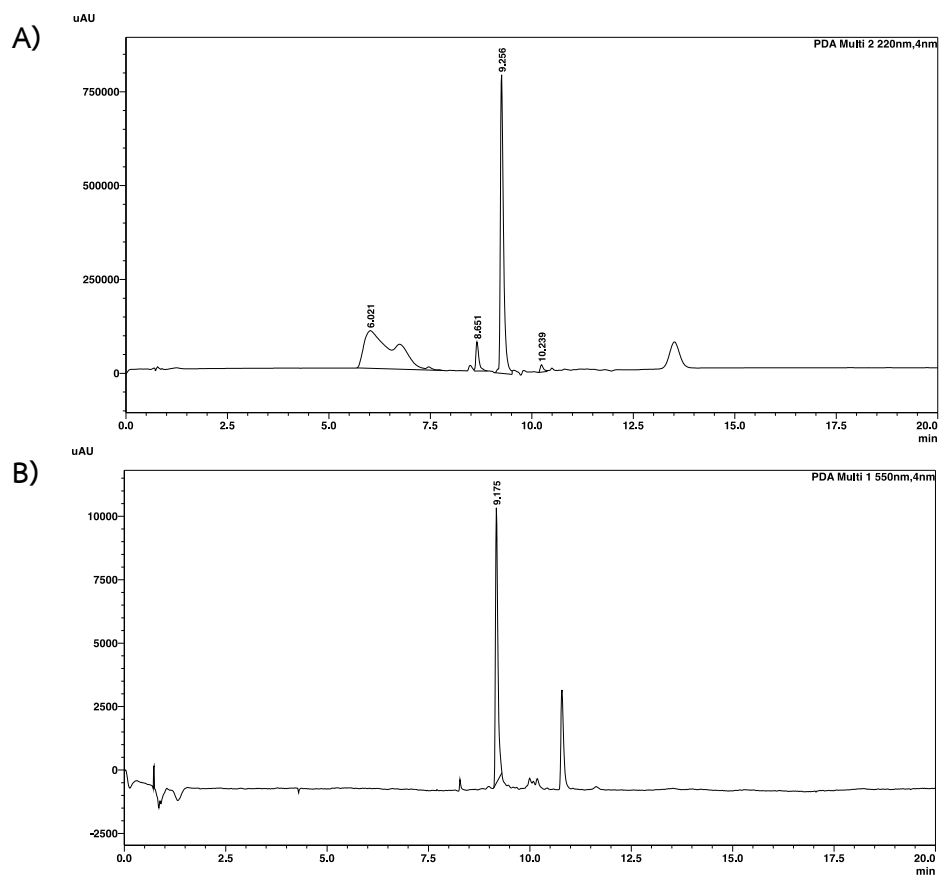


Figure A.20 HPLC chromatogram of crude from DNA-templated synthesis for 6-NPr₃-BT⁺-Ald⁺ after incubating for 2 days observed at (A) 220 nm and (B) 550 nm.

Characterization

Dye product from DNA-templated reaction

m/z calc. 452.273, found 452.286

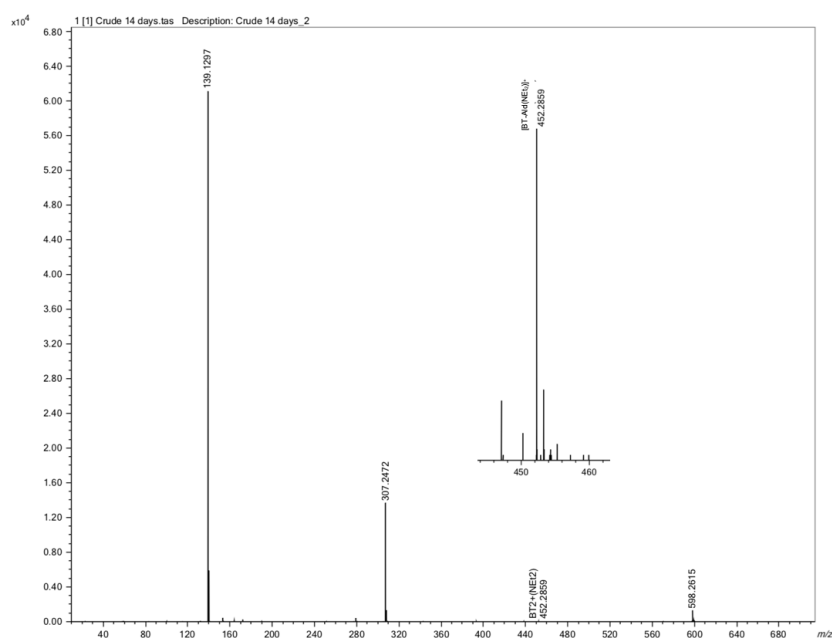


Figure A.21 Mass spectrum (MALDI-TOF) of crude from DNA-templated synthesis for $\text{BT}^+\text{-Ald}^+$.

m/z calc. 470.264, found 470.248

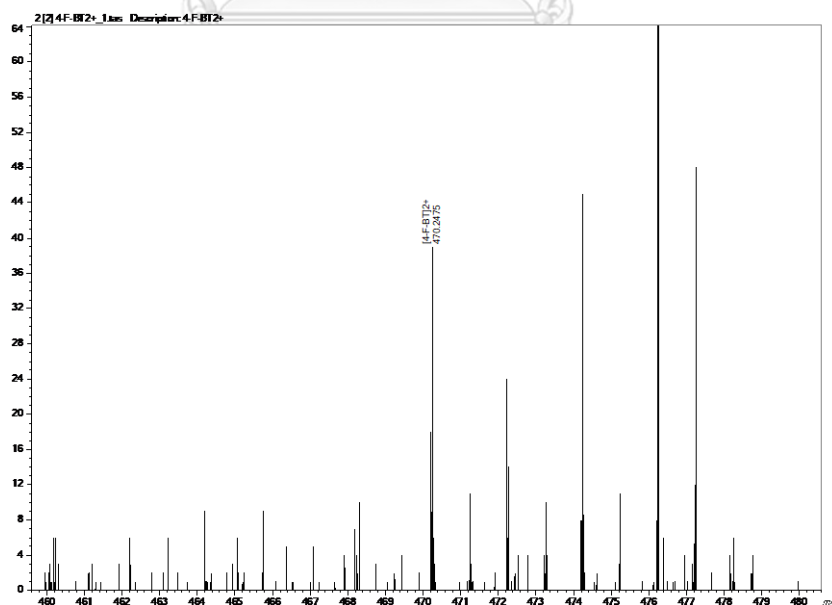


Figure A.22 Mass spectrum (MALDI-TOF) of crude from DNA-templated synthesis for $4\text{-F-BT}^+\text{-Ald}^+$.

m/z calc. 530.184 , found 530.205

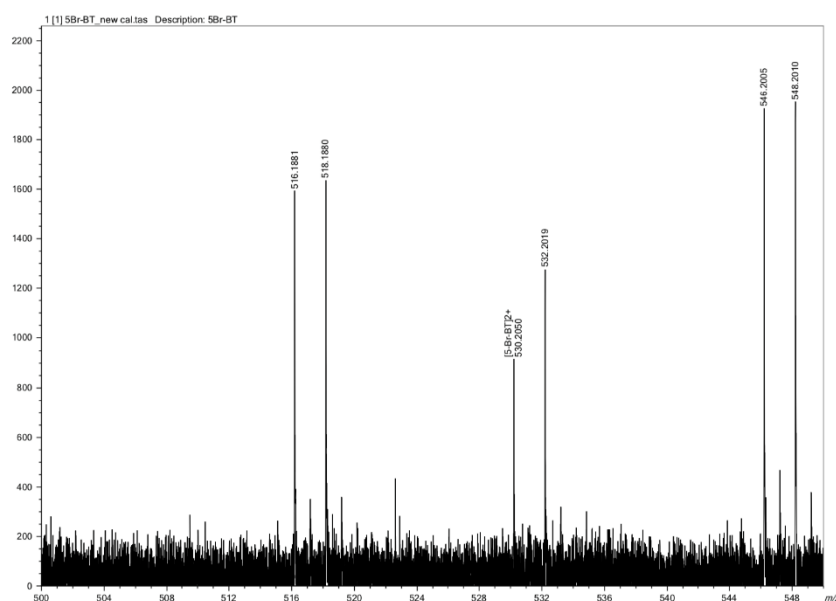


Figure A.23 Mass spectrum (MALDI-TOF) of crude from DNA-templated synthesis for 5-Br-BT⁺-Ald⁺.

m/z calc. 486.234 , found 486.251

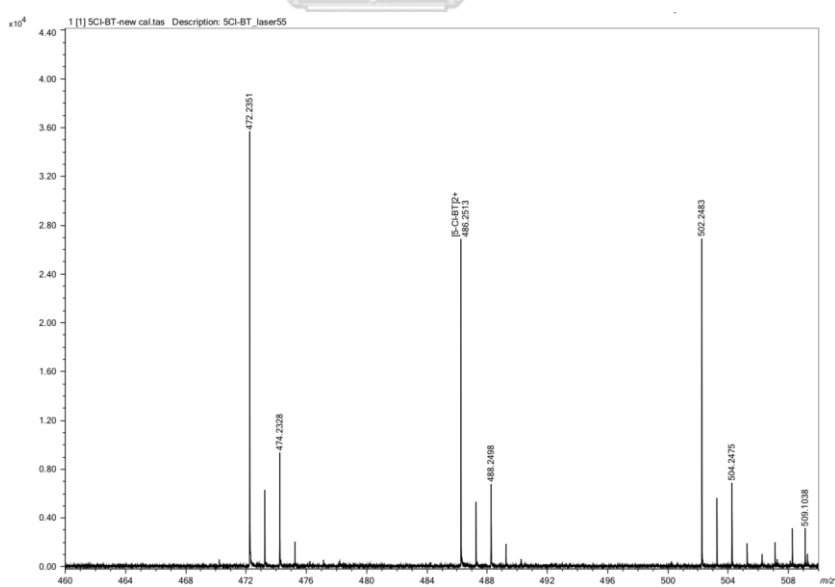


Figure A.24 Mass spectrum (MALDI-TOF) of crude from DNA-templated synthesis for 5-Cl-BT⁺-Ald⁺.

m/z calc. 470.264 , found 470.279

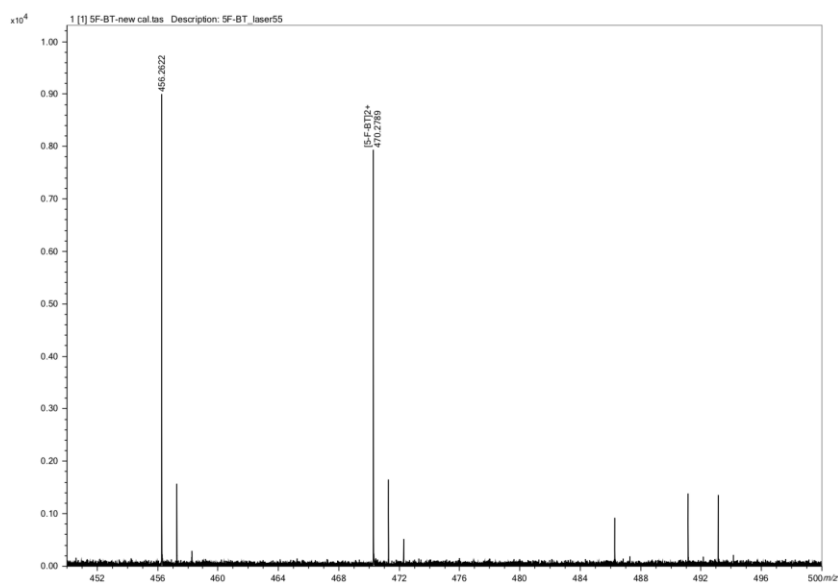


Figure A.25 Mass spectrum (MALDI-TOF) of crude from DNA-templated synthesis for 5-F-BT⁺-Ald⁺.

m/z calc. 497.258 , found 497.285

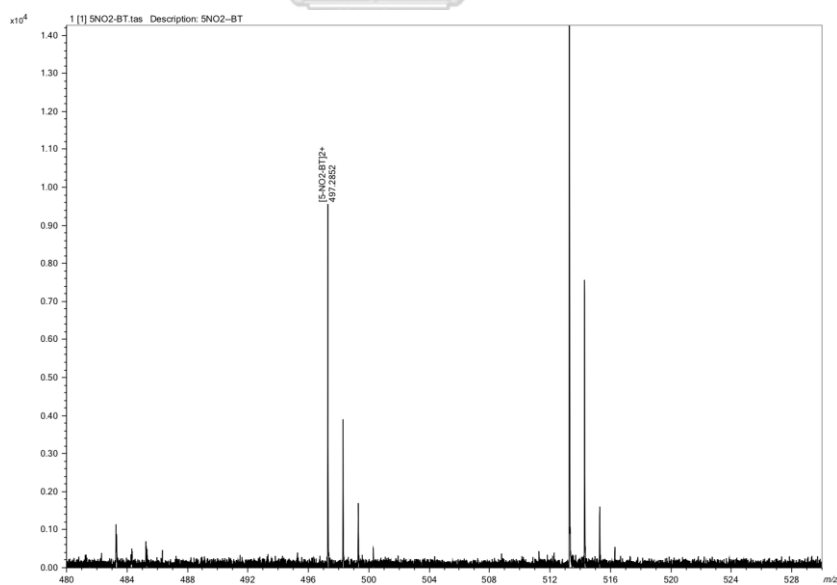


Figure A.26 Mass spectrum (MALDI-TOF) of crude from DNA-templated synthesis for 5-NO₂-BT⁺-Ald⁺.

m/z calc. 470.264, found 470.282

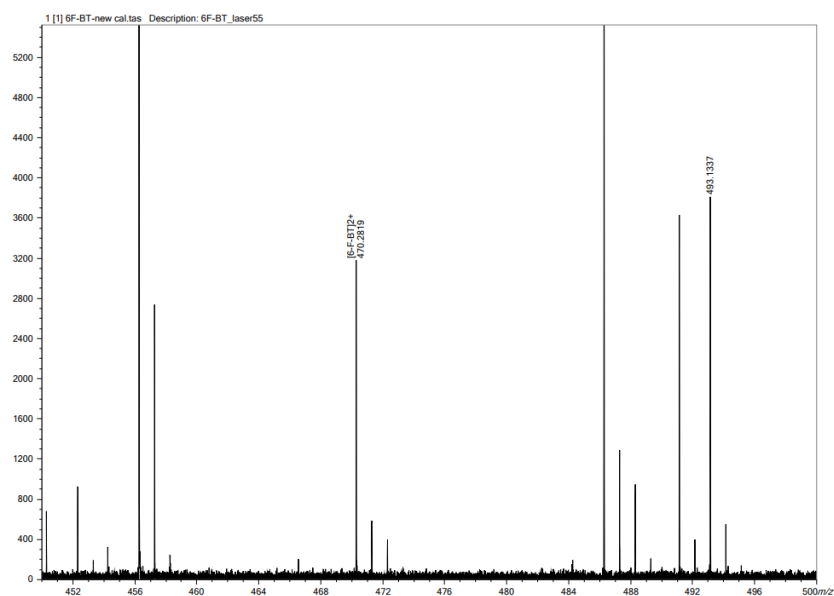


Figure A.27 Mass spectrum (MALDI-TOF) of crude from DNA-templated synthesis for 6-F-BT⁺-Ald⁺.

m/z calc. 488.254, found 488.276

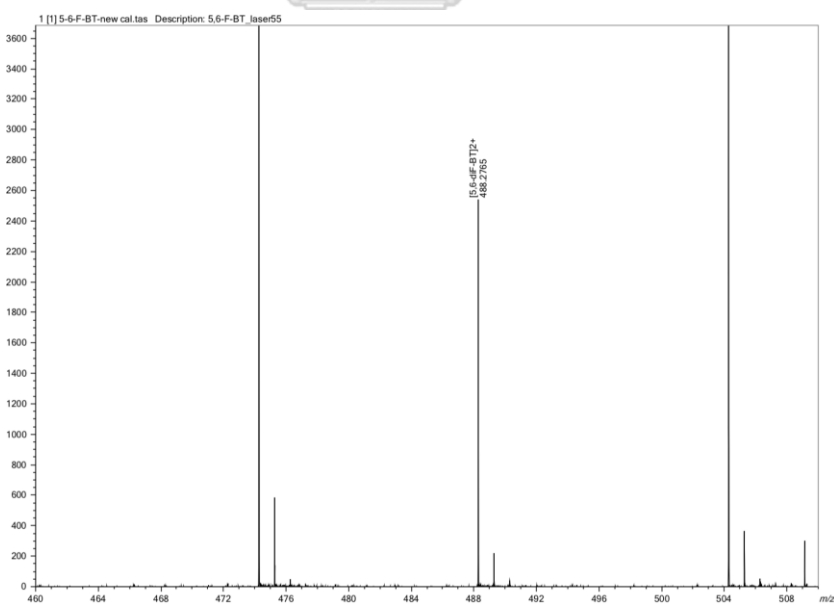


Figure A.28 Mass spectrum (MALDI-TOF) of crude from DNA-templated synthesis for 5,6-F-BT⁺-Ald⁺.

m/z calc. 520.260 , found 520.269

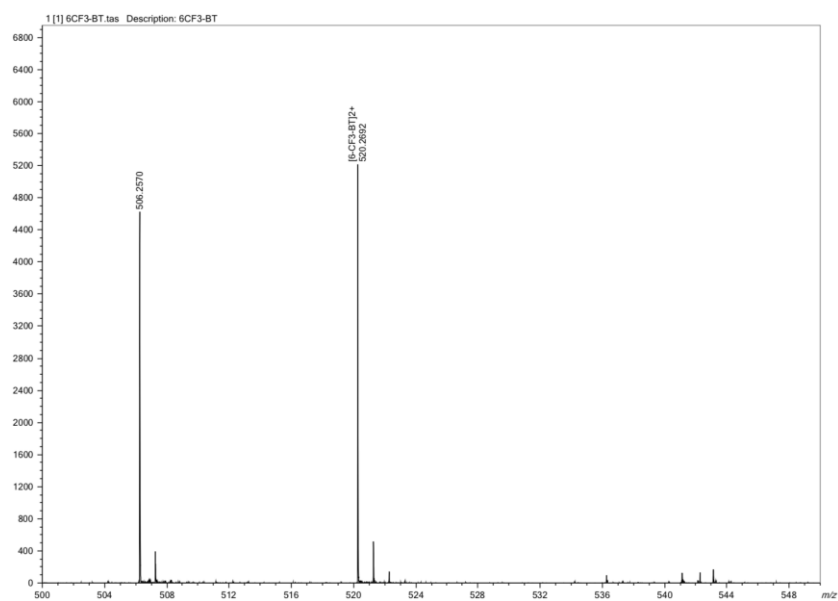


Figure A.29 Mass spectrum (MALDI-TOF) of crude from DNA-templated synthesis for $6-CF_3-BT^+-Ald^+$.

m/z calc. 536.255 , found 536.278

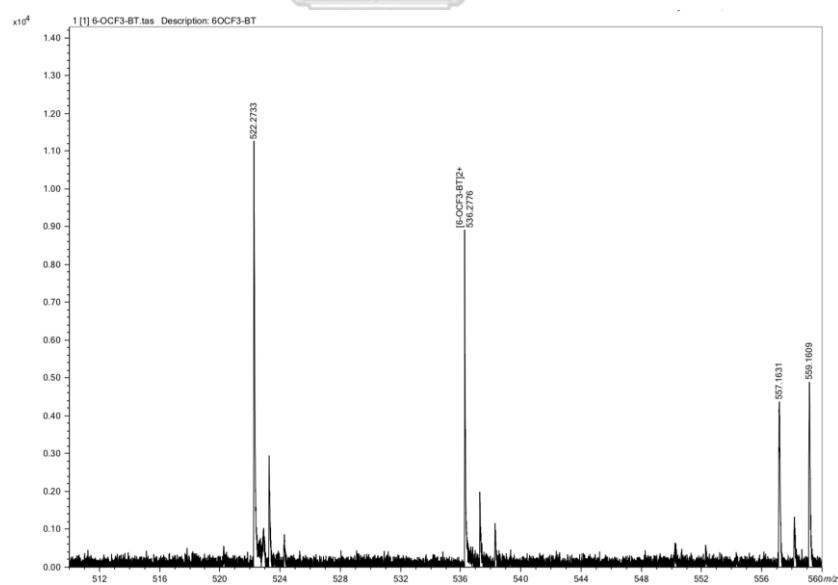


Figure A.30 Mass spectrum (MALDI-TOF) of crude from DNA-templated synthesis for $6-OCF_3-BT^+-Ald^+$.

m/z calc. 470.264 , found 470.284

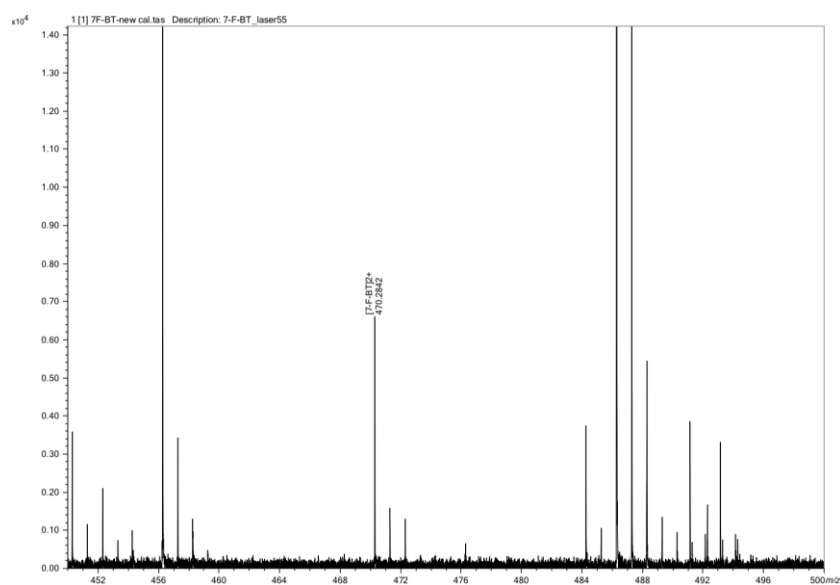


Figure A.31 Mass spectrum (MALDI-TOF) of crude from DNA-templated synthesis for 7-F-BT⁺-Ald⁺.

m/z calc. 482.284 , found 482.313

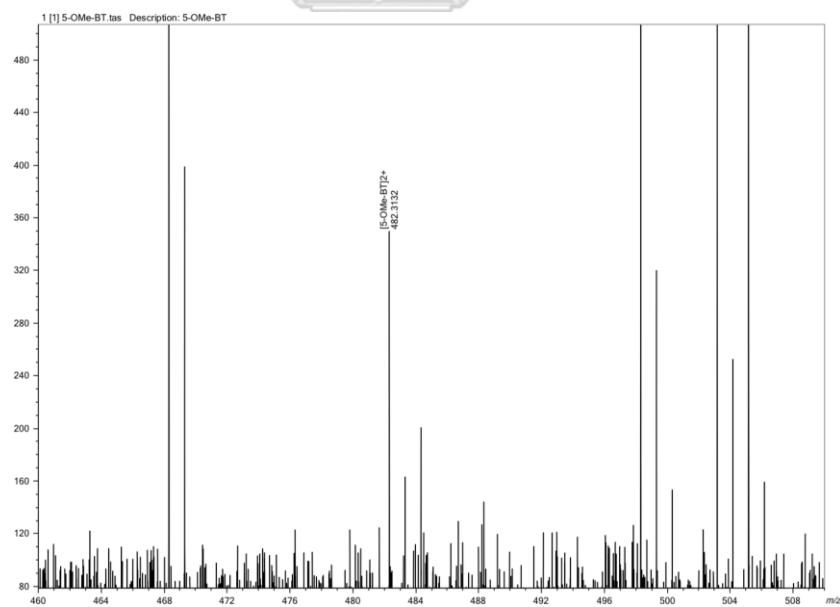


Figure A.32 Mass spectrum (MALDI-TOF) of crude from DNA-templated synthesis for 5-OMe-BT⁺-Ald⁺.

m/z calc. 466.289 , found 466.308

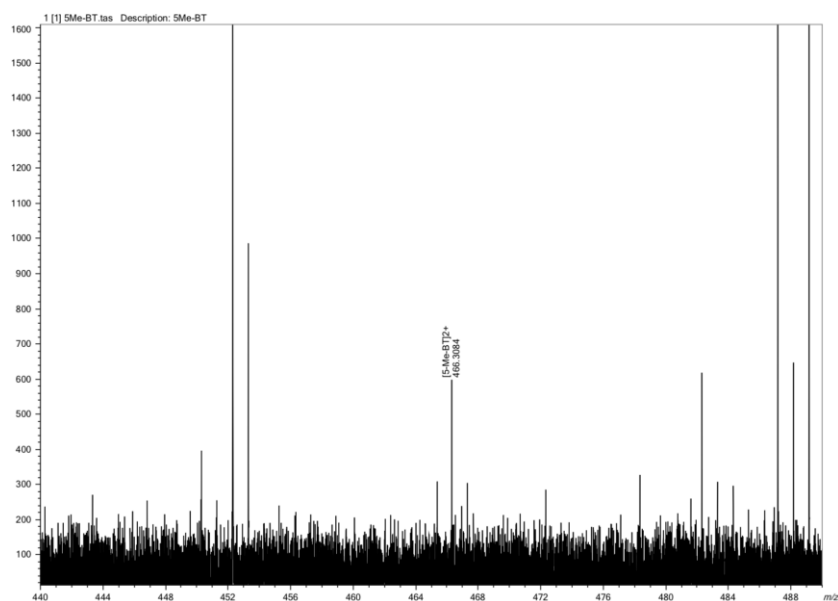


Figure A.33 Mass spectrum (MALDI-TOF) of crude from DNA-templated synthesis for 5-Me-BT⁺-Ald⁺.

m/z calc. 480.304 , found 480.328

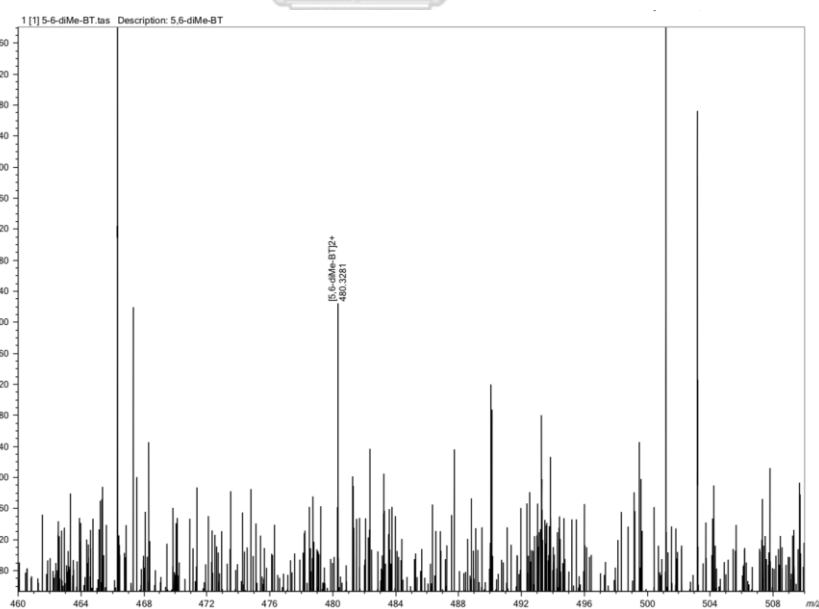


Figure A.34 Mass spectrum (MALDI-TOF) of crude from DNA-templated synthesis for 5,6-Me-BT⁺-Ald⁺.

m/z calc. 482.284 , found 482.314

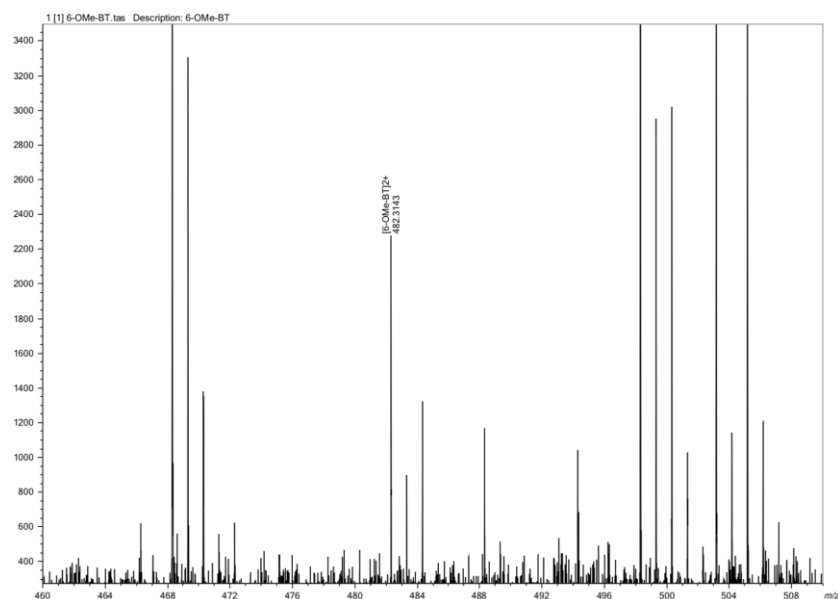


Figure A.35 Mass spectrum (MALDI-TOF) of crude from DNA-templated synthesis for 6-OMe-BT⁺-Ald⁺.

m/z calc. 551.378 , found 551.353

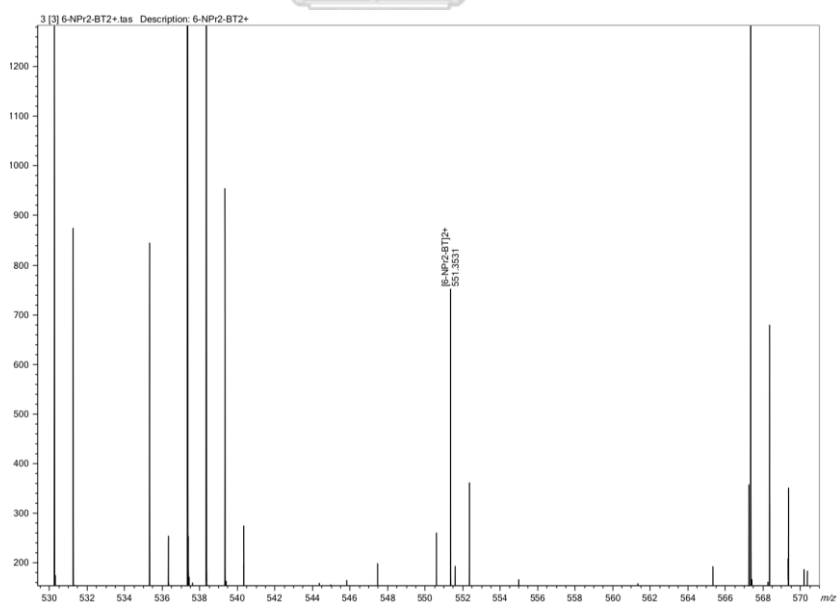


Figure A.36 Mass spectrum (MALDI-TOF) of crude from DNA-templated synthesis for 6-NPr₂-BT⁺-Ald⁺.

m/z calc. 436.296, found 436.289

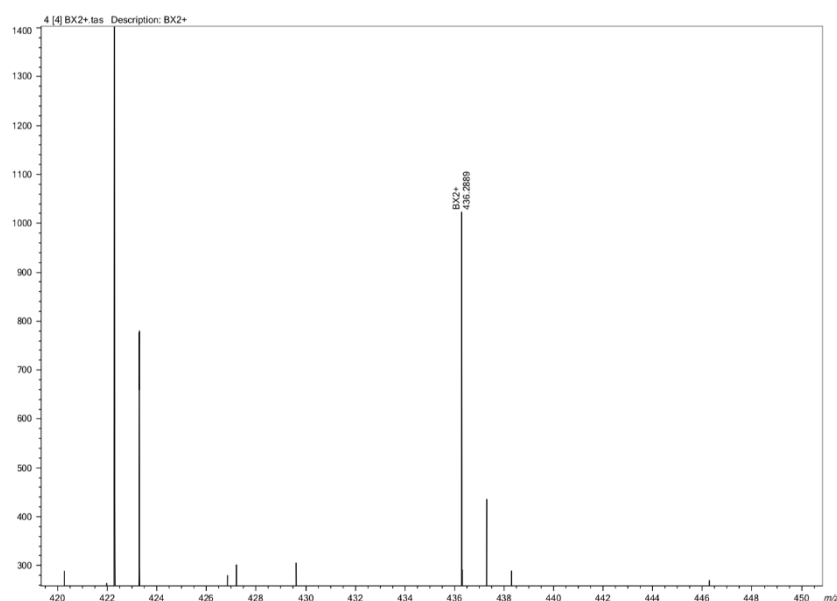


Figure A.37 Mass spectrum (MALDI-TOF) of crude from DNA-templated synthesis for BX⁺-Ald⁺.

m/z calc. 462.348, found 462.341

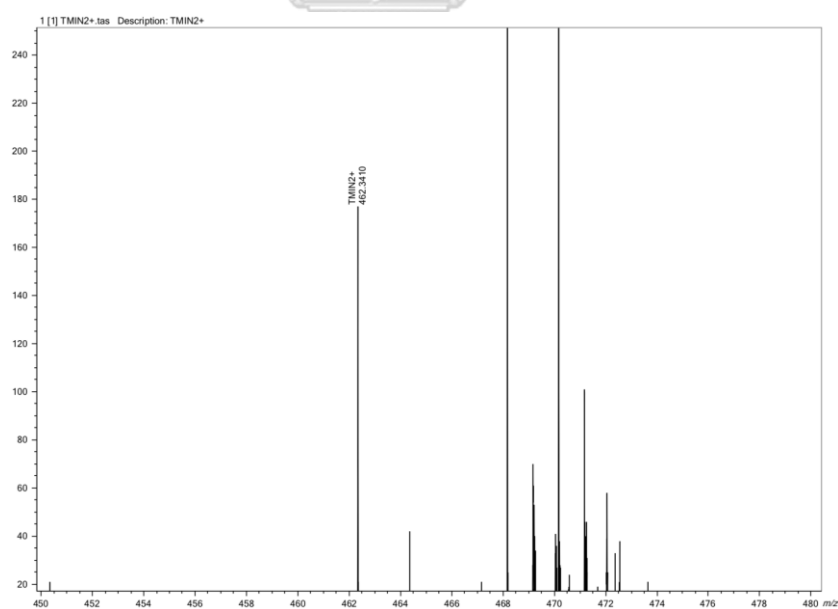


Figure A.38 Mass spectrum (MALDI-TOF) of crude from DNA-templated synthesis for TMIN⁺-Ald⁺.

m/z calc. 446.317, found 446.281

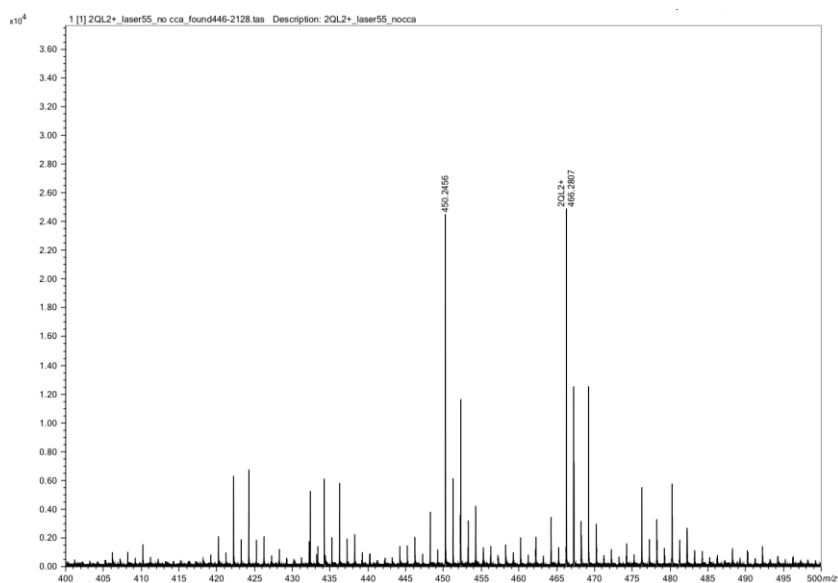


Figure A.39 Mass spectrum (MALDI-TOF) of crude from DNA-templated synthesis for 2-QL⁺-Ald⁺.

m/z calc. 446.317, found 446.238

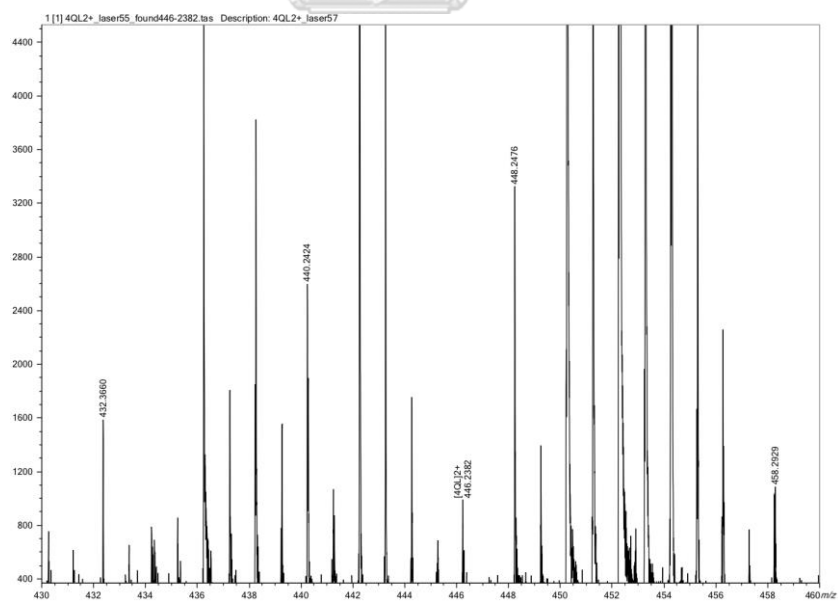


Figure A. 40 Mass spectrum (MALDI-TOF) of crude from DNA-templated synthesis for 4-QL⁺-Ald⁺.

m/z calc. 396.301, found 396.308

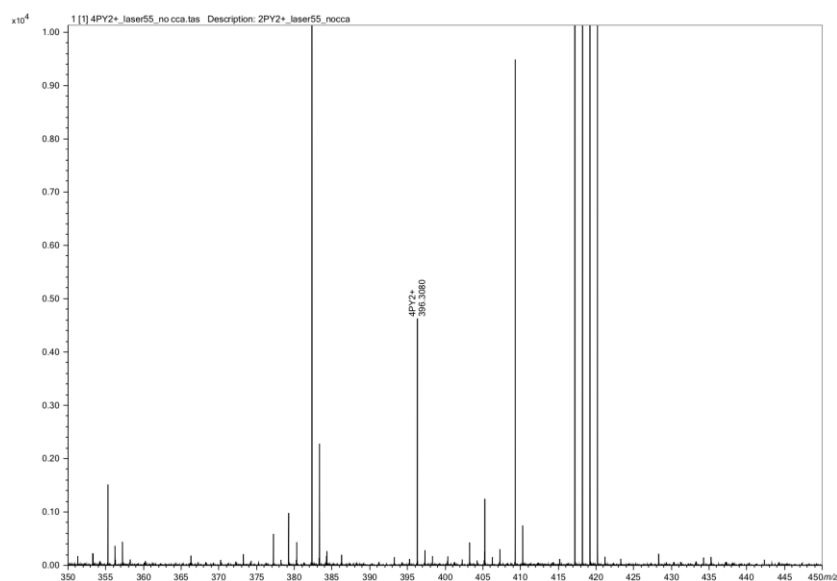


Figure A.41 Mass spectrum (MALDI-TOF) of crude from DNA-templated synthesis for $4\text{-PY}^+\text{-Ald}^+$.

m/z calc. 453.268, found 453.268

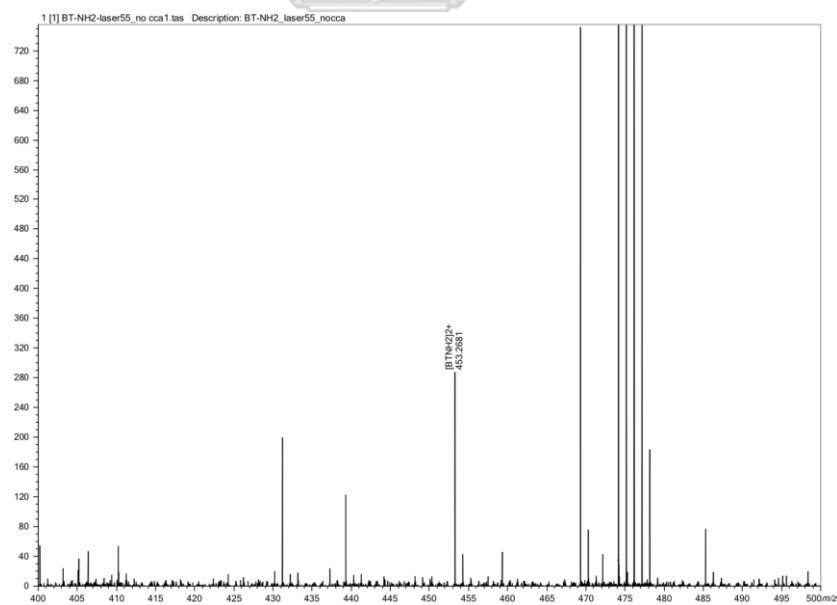


Figure A.42 Mass spectrum (MALDI-TOF) of crude from DNA-templated synthesis for $\text{BT-NH}_2^+\text{-Ald}^+$.

m/z calc. 460.296, found 460.284

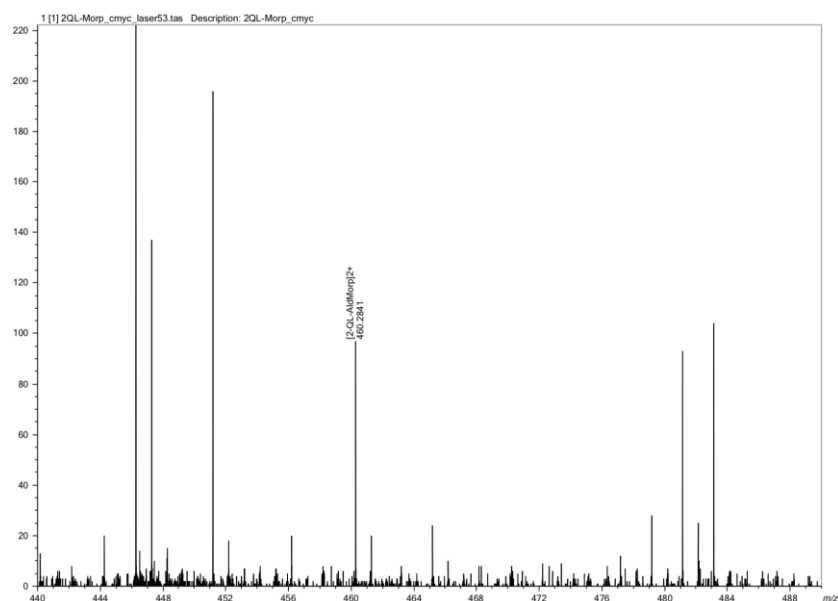


Figure A.43 Mass spectrum (MALDI-TOF) of crude from DNA-templated synthesis for 2-QL⁺-MorpAld⁺ catalysed by c-MYC.

m/z calc. 460.296, found 460.285

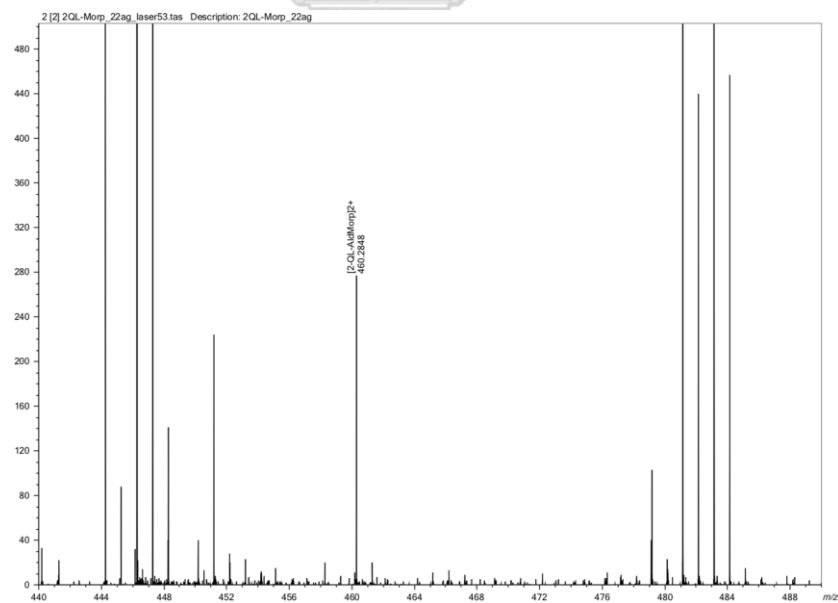


Figure A.44 Mass spectrum (MALDI-TOF) of crude from DNA-templated synthesis for 2-QL⁺-MorpAld⁺ catalysed by c-MYC.

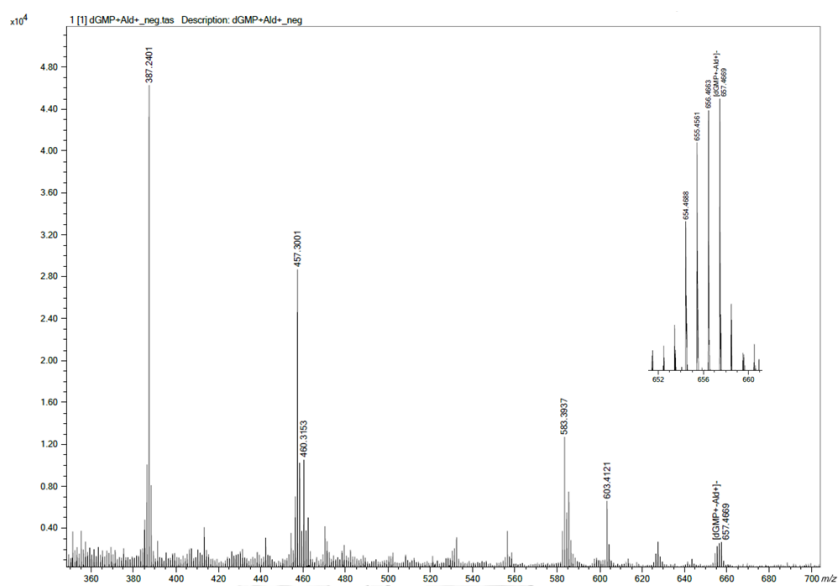


Figure A.45 Mass spectrum (MALDI-TOF) of crude from dGMP-Ald⁺.



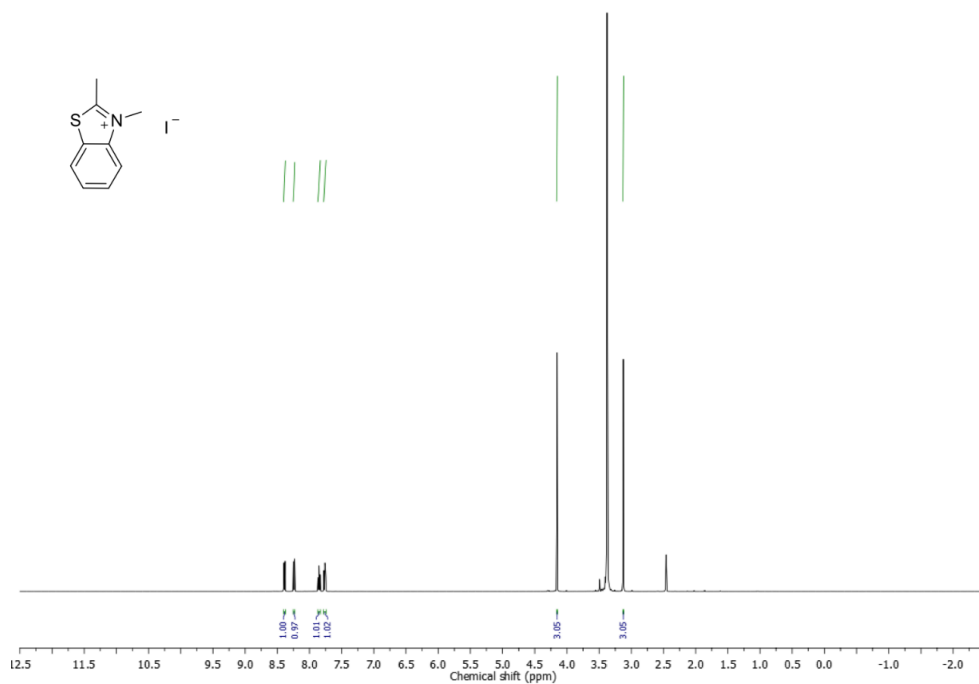


Figure A. 46 ¹H NMR spectrum of 2,3-dimethylbenzo[d]thiazol-3-ium iodide (BT⁺).

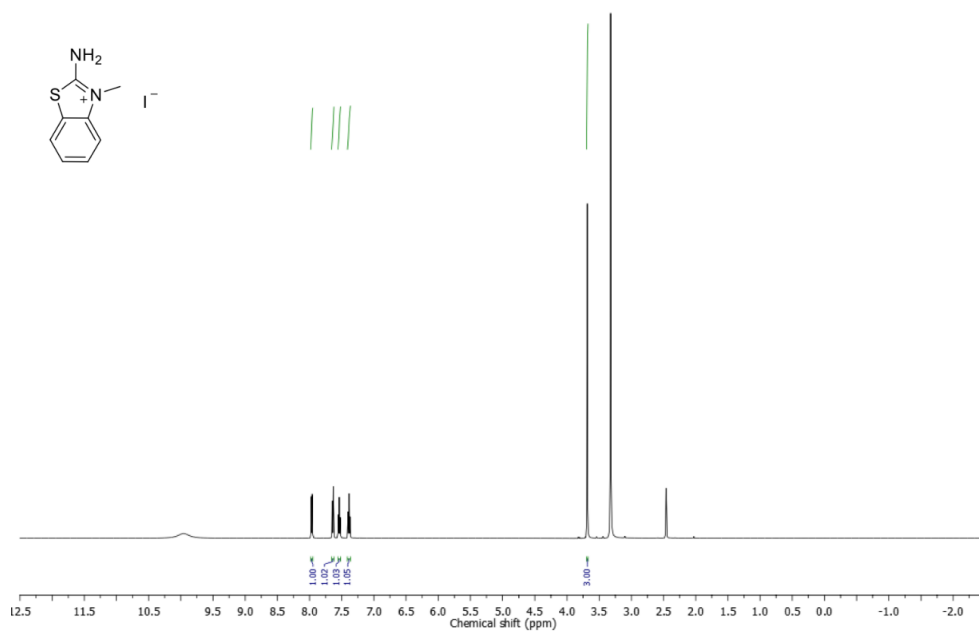


Figure A. 47 ¹H NMR spectrum of 2-amino-3-methylbenzo[d]thiazol-3-ium iodide (BT-NH₂⁺).

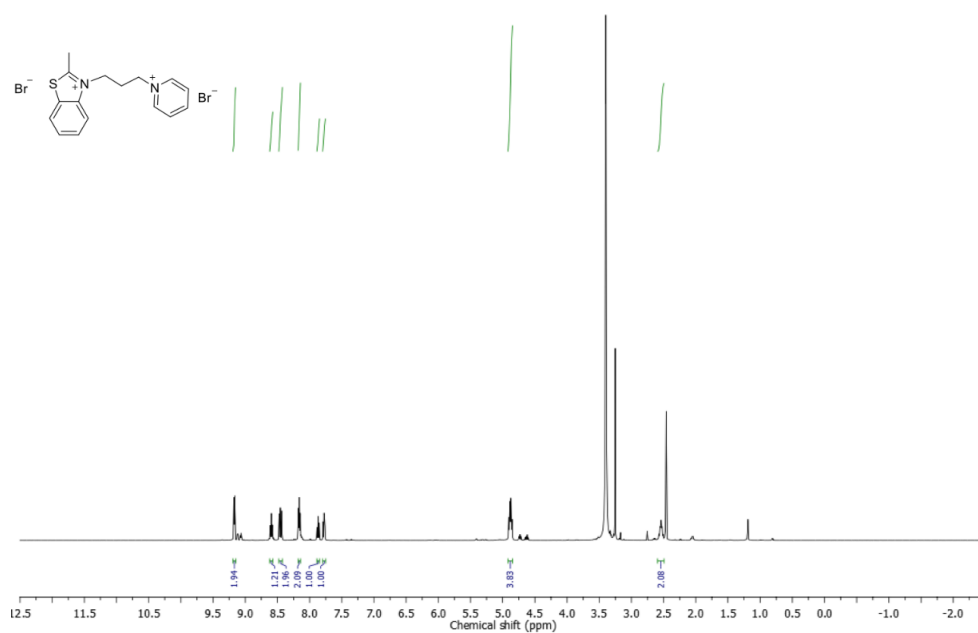


Figure A.48 ¹H NMR spectrum of 2-methyl-3-(3-(pyridin-1-ium-1-yl)propyl)benzo[d]thiazol-3-ium bromide (BTC3Py²⁺).

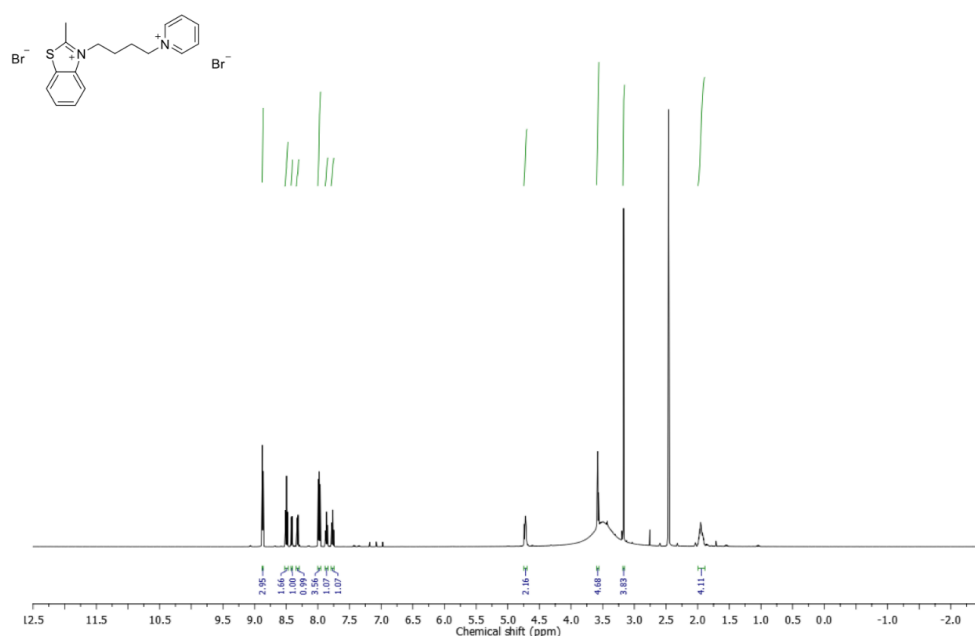


Figure A.49 ¹H NMR spectrum of 2-methyl-3-(4-(pyridin-1-ium-1-yl)butyl)benzo[d]thiazol-3-ium bromide (BTC4Py²⁺).

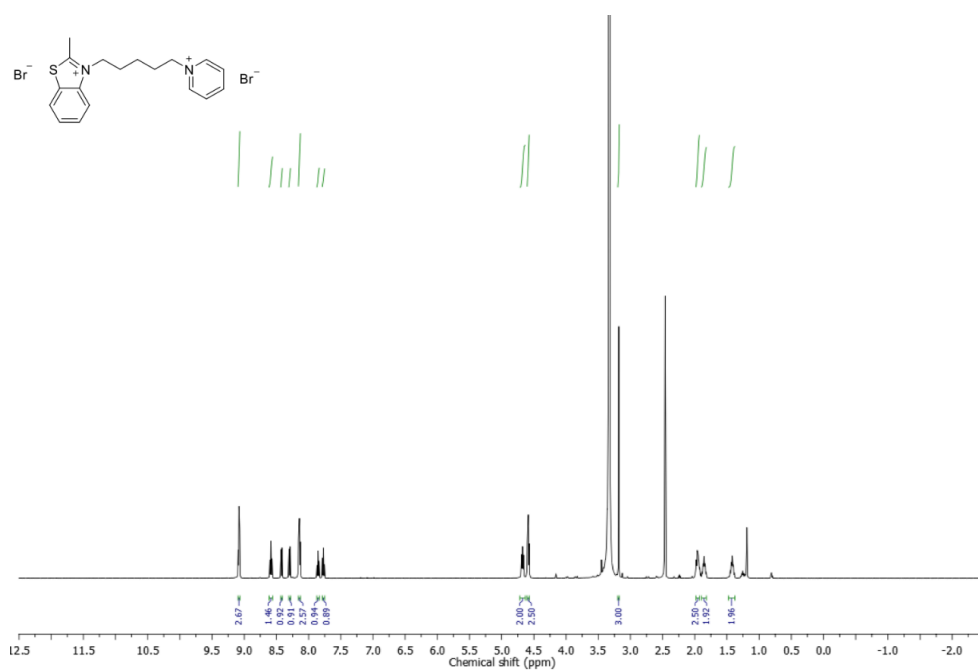


Figure A.50 ¹H NMR spectrum of 2-methyl-3-(5-(pyridin-1-ium-1-yl)pentyl)benzo[d]thiazol-3-ium bromide (BTC5Py²⁺)

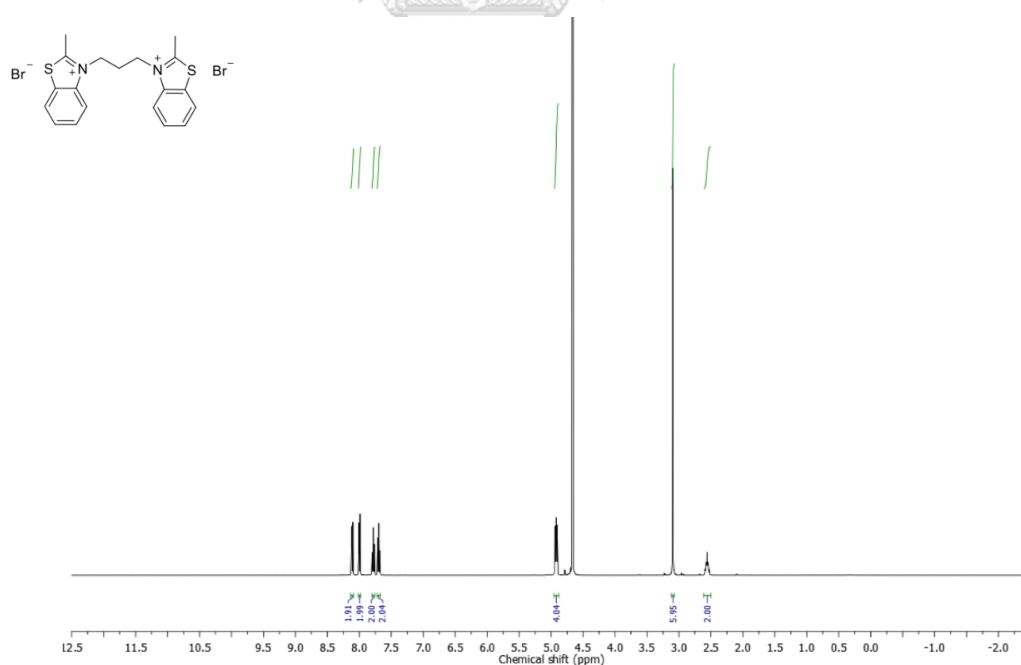


Figure A.51 ¹H NMR spectrum of 3,3'-(propane-1,3-diyl)bis(2-methylbenzo[d]thiazol-3-ium) bromide (BisBT²⁺).

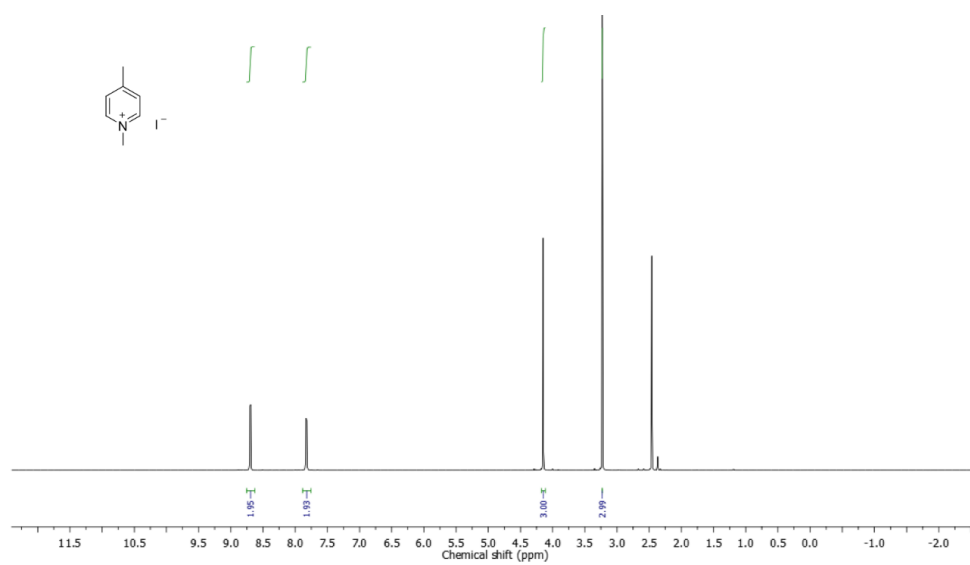


Figure A.52 ^1H NMR spectrum of 1,4-dimethylpyridin-1-ium iodide (4-Py $^+$).

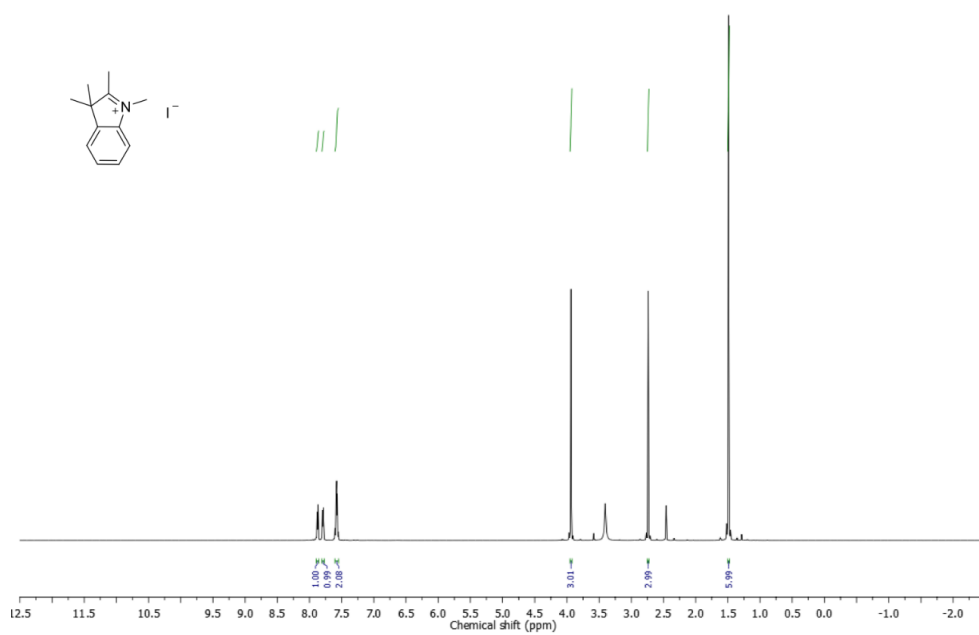


Figure A.53 ^1H NMR spectrum of 1,2,3,3-tetramethyl-3H-indol-1-ium iodide (TMIN $^+$).

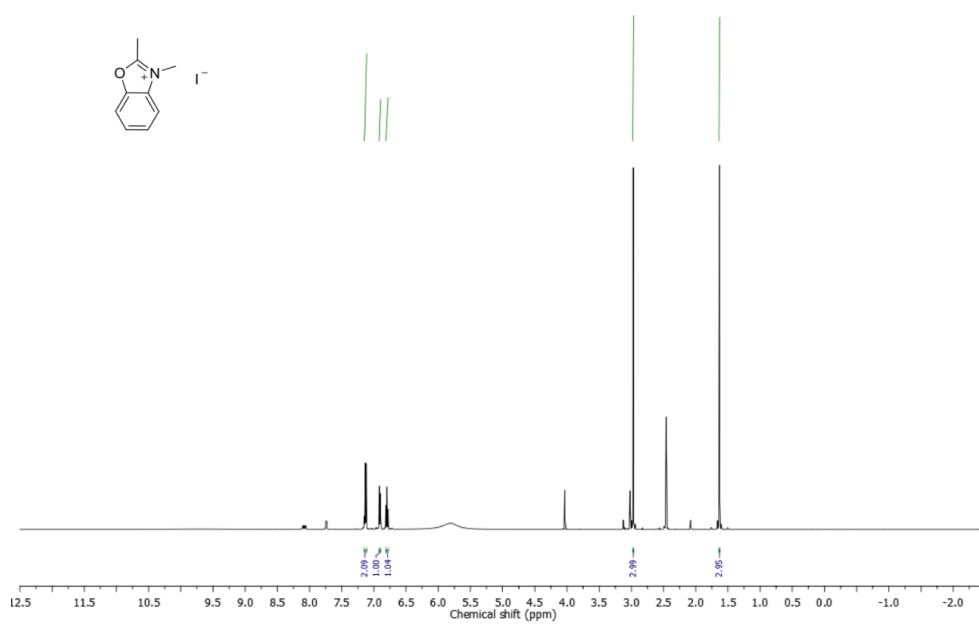


Figure A.54 ¹H NMR spectrum of 2,3-dimethylbenzo[d]oxazol-3-ium iodide (BX⁺).

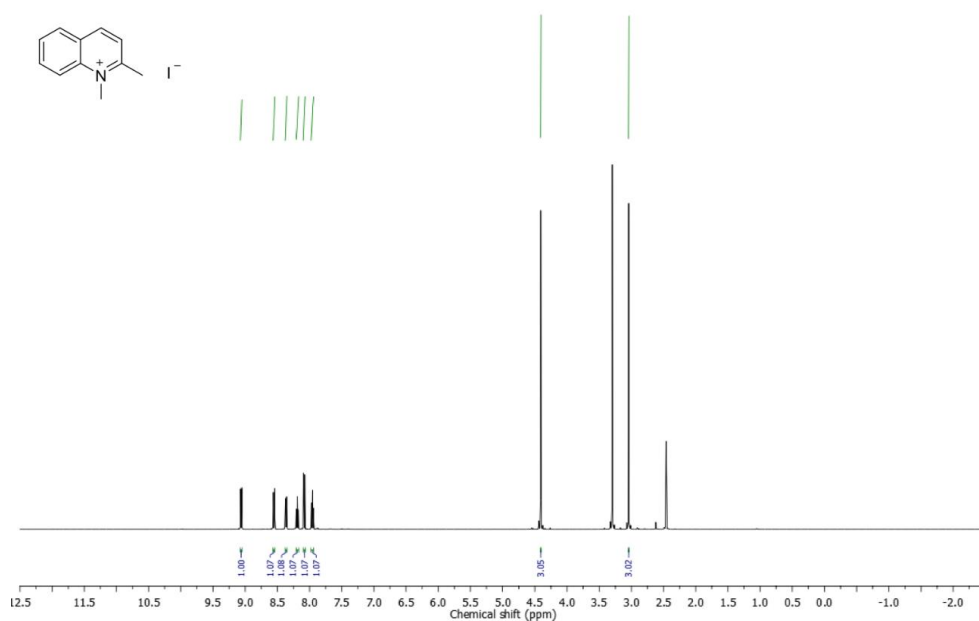


Figure A.55 ¹H NMR spectrum of 1,2-dimethylquinolin-1-ium iodide (2-QL⁺).

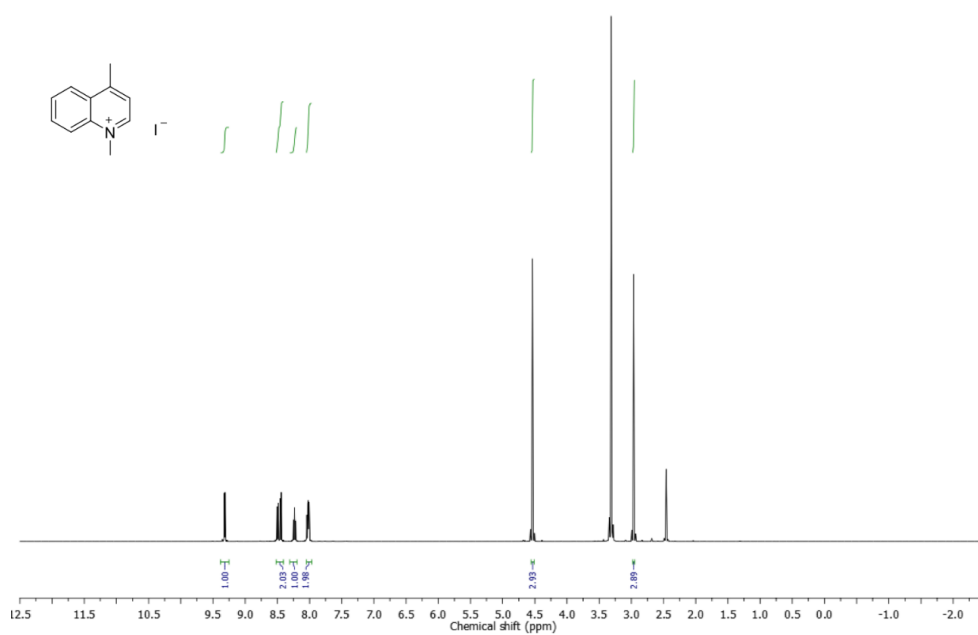


Figure A.56 ^1H NMR spectrum of 1,4-dimethylquinolin-1-ium iodide (4-QL $^+$).

Characterization of aromatic aldehydes with positively charged side chains

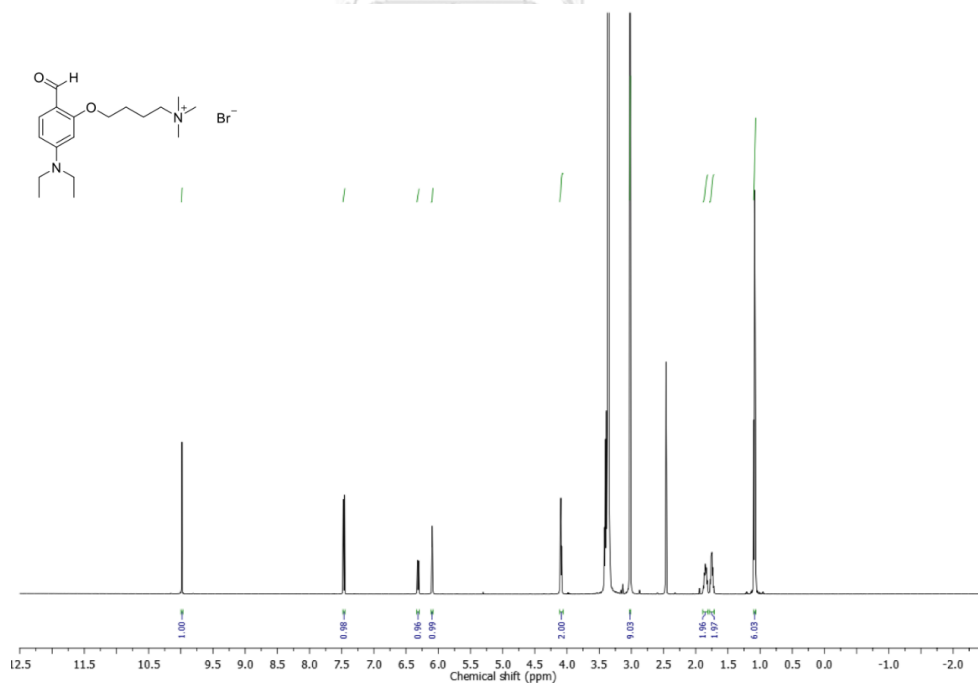


Figure A.57 ^1H NMR spectrum of 4-(5-(diethylamino)-2-formylphenoxy)-*N,N,N*-trimethylbutan-1-aminium bromide (Ald(NEt $_2$) $^+$).

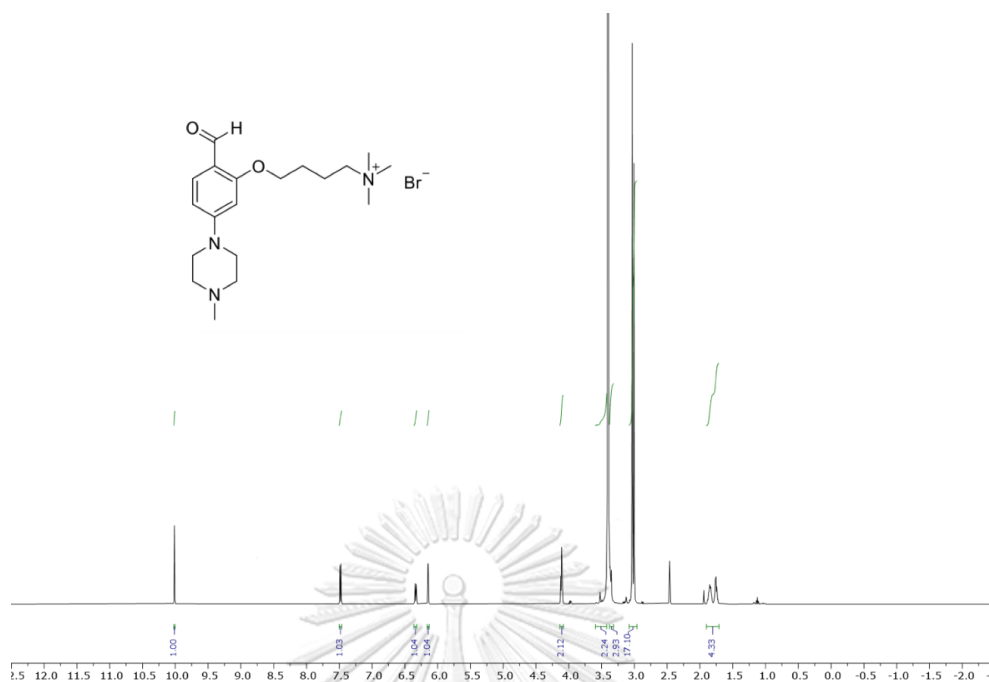


Figure A.58 ¹H NMR spectrum of 4-(2-formyl-5-(4-methylpiperazin-1-yl)phenoxy)-*N,N,N*-trimethylbutan-1-aminium bromide (Ald(Piz)⁺).

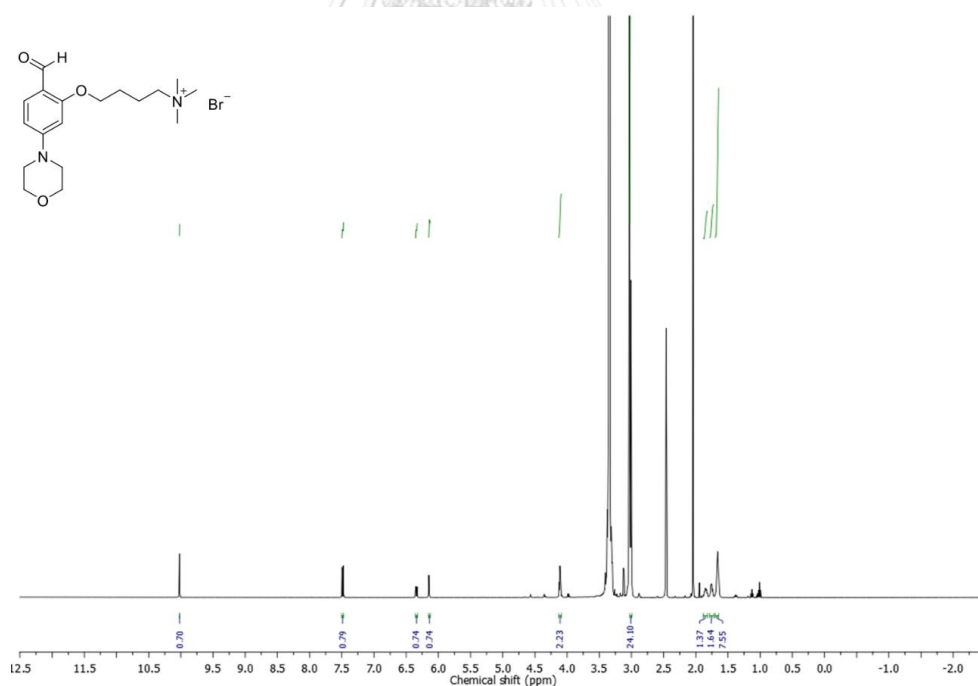


Figure A.59 ¹H NMR spectrum of 4-(2-formyl-5-morpholinophenoxy)-*N,N,N*-trimethylbutan-1-aminium bromide (Ald(Morp)⁺).

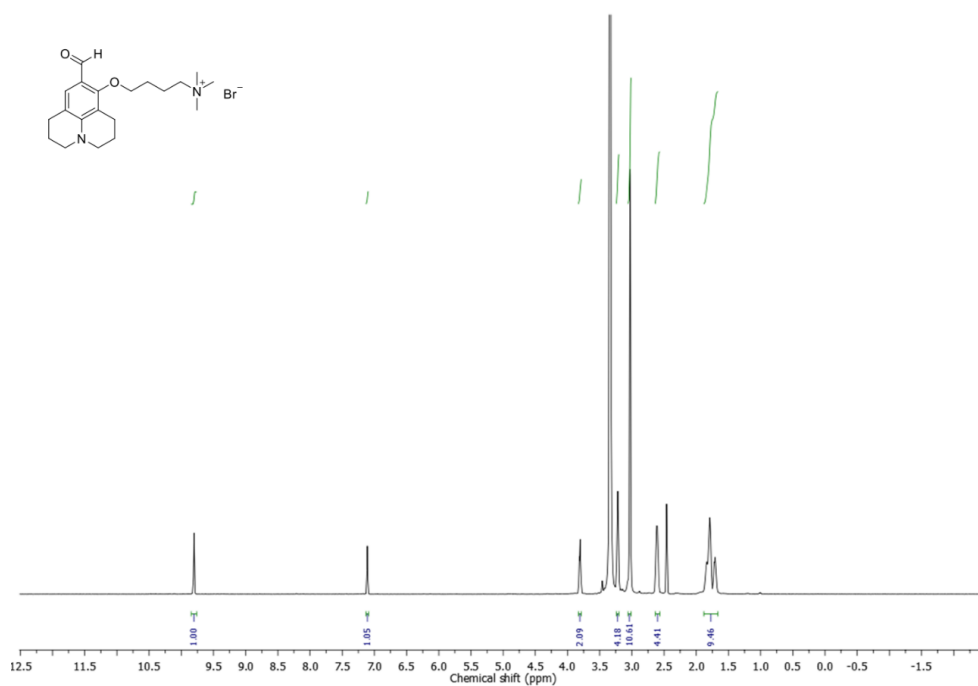


Figure A.60 ¹H NMR spectrum of 4-((9-formyl-2,3,6,7-tetrahydro-1H,5H-pyrido[3,2,1-ij]quinolin-8-yl)oxy)-N,N,N-trimethylbutan-1-aminium bromide (Ald(Ju)⁺).

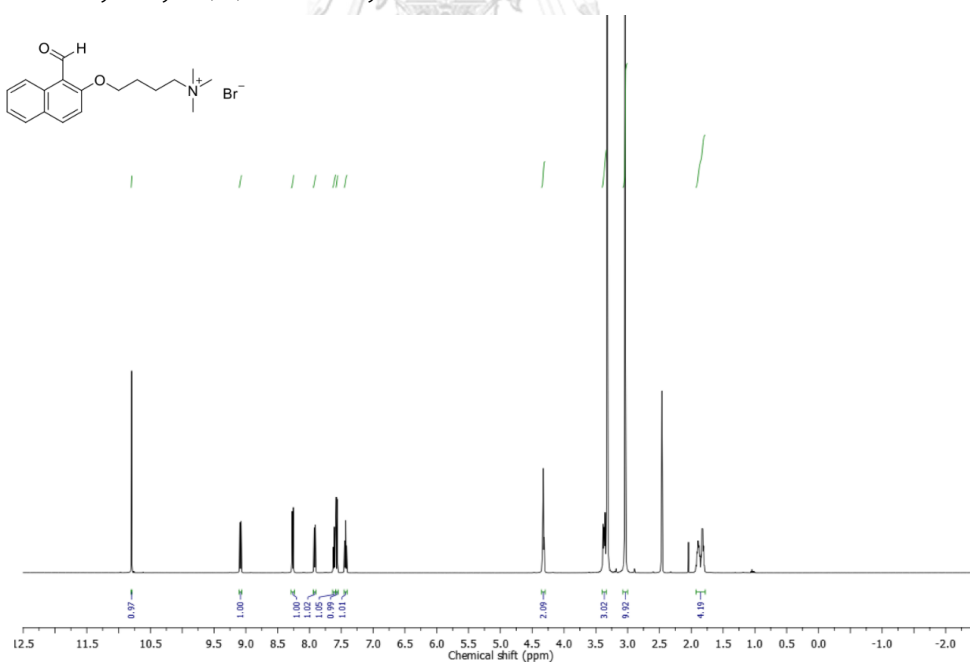


Figure A.61 ¹H NMR spectrum of 4-((1-formylnaphthalen-2-yl)oxy)-N,N,N-trimethylbutan-1-aminium bromide (NaphAld⁺).

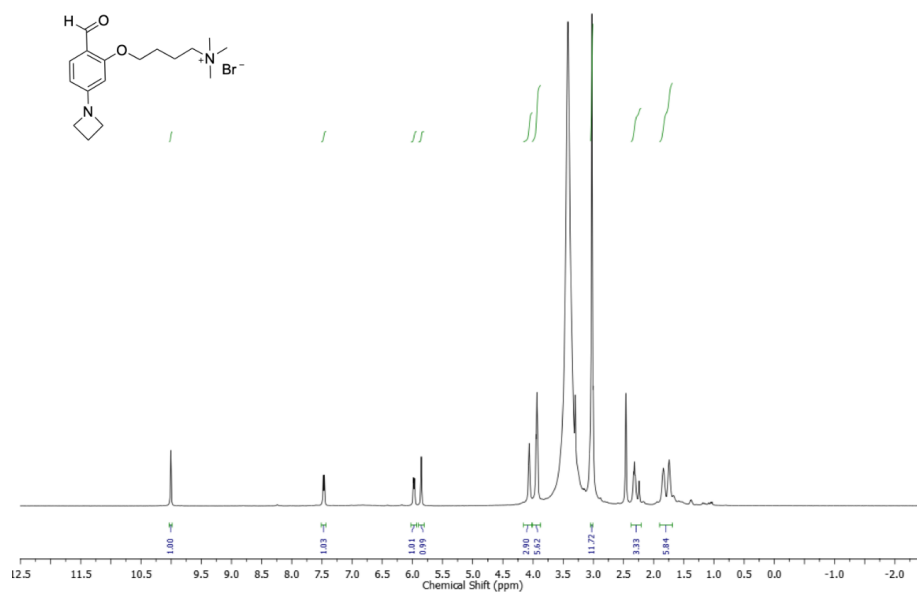


Figure A.62 ¹H NMR spectrum of 4-(5-(azetidin-1-yl)-2-formylphenoxy)-N,N,N-trimethylbutan-1-aminium bromide (Ald(Aze)⁺).

Characterization of isolated cationic styryl dyes

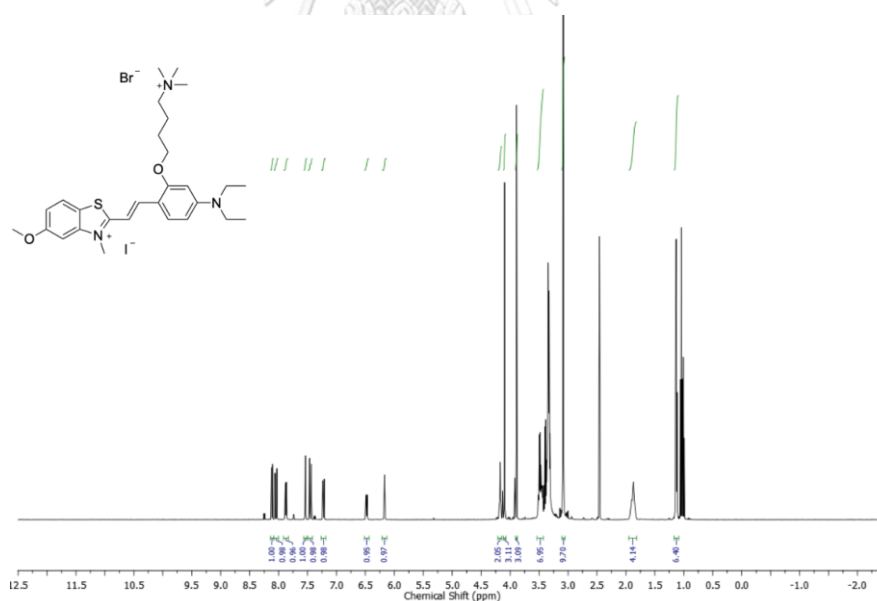


Figure A.63 ¹H NMR spectrum of (E)-2-(4-(diethylamino)-2-(4-(trimethylammonio)butoxy)styryl)-5-methoxy-3-methylbenzo[d]thiazol-3-ium bromide iodide (5-OMe-BT⁺-Ald(NEt₂)⁺).

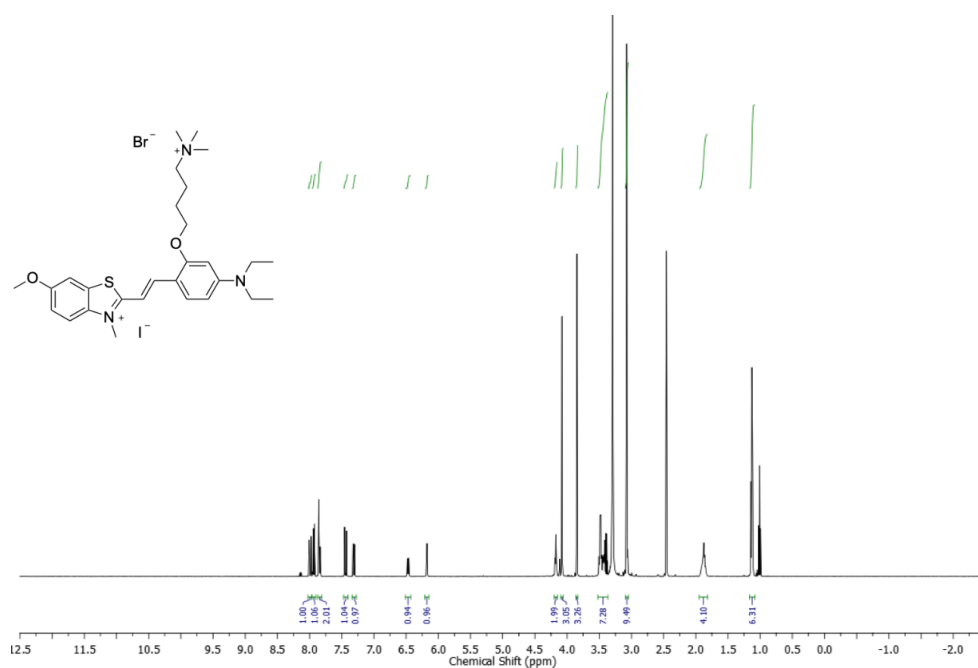


Figure A.64 ^1H NMR spectrum of (*E*)-2-(4-(diethylamino)-2-(4-(trimethylammonio)butoxy)styryl)-6-methoxy-3-methylbenzo[d]thiazol-3-ium bromide iodide ((6-OMe-BT⁺-Ald(NEt₂)⁺)).

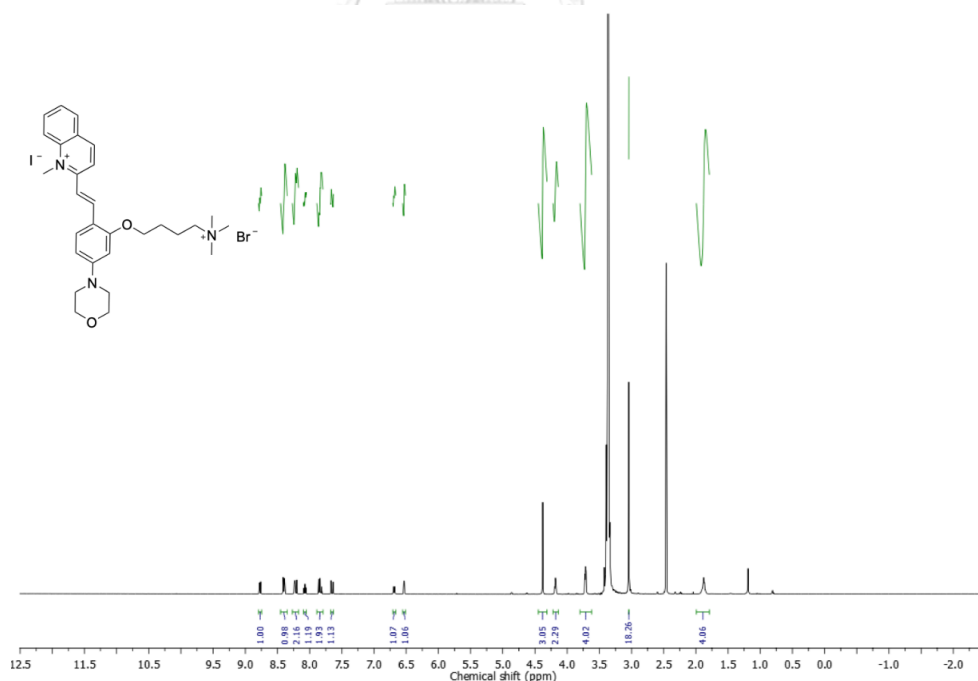


Figure A.65 ^1H NMR spectrum (*E*)-1-methyl-2-(4-morpholino-2-(4-(trimethylammonio)butoxy)styryl)quinolin-1-ium bromide iodide (2-QL⁺-MorpAld⁺).

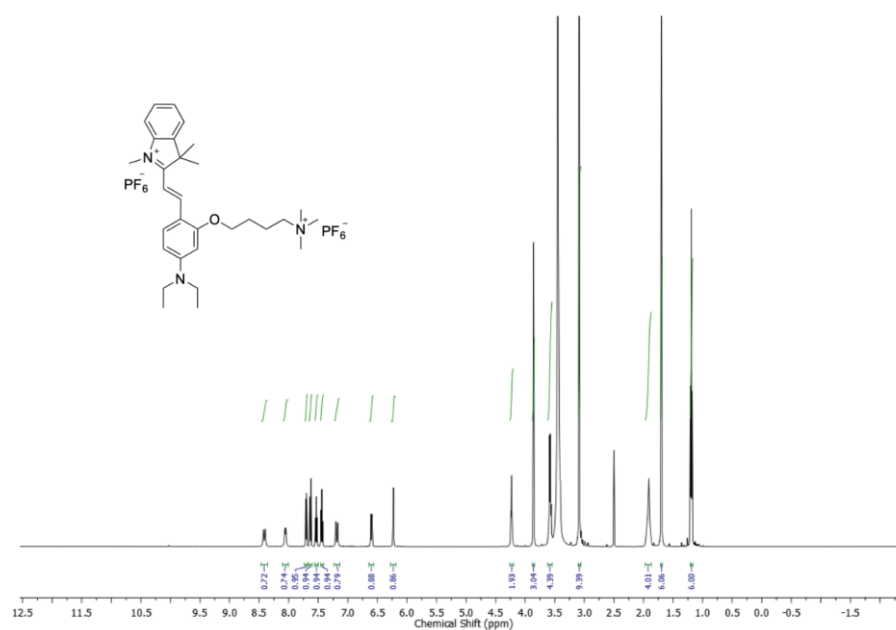


Figure A.66 ¹H NMR spectrum (E)-2-(4-(diethylamino)-2-(4-(trimethylammonio)butoxy)styryl)-1,3,3-trimethyl-3H-indol-1-ium hexafluorophosphate (TMIN⁺-Ald⁺).

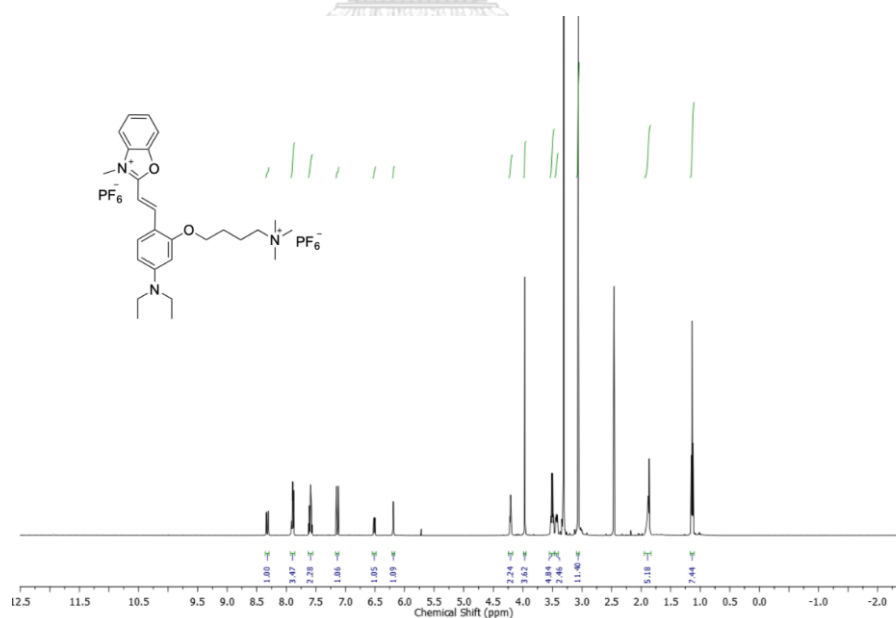


Figure A.67 ¹H NMR spectrum (E)-2-(4-(diethylamino)-2-(4-(trimethylammonio)butoxy)styryl)-3-methylbenzo[d]oxazol-3-ium hexafluorophosphate (BX⁺-Ald⁺).

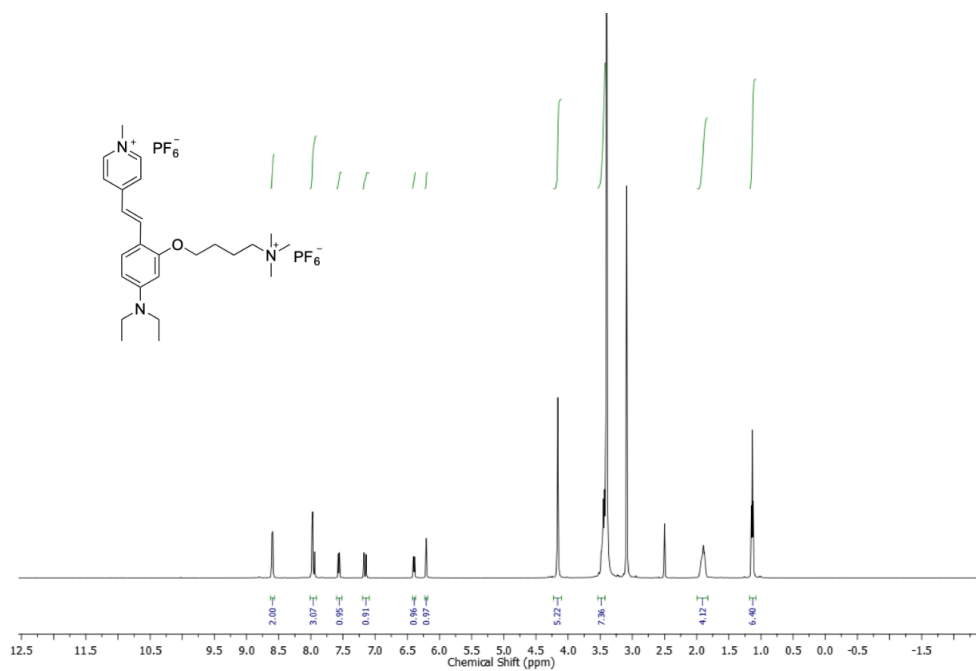


Figure A. 70 ^1H NMR spectrum (E) -4-(4-(diethylamino)-2-(4-(trimethylammonio)butoxy)styryl)-1-methylpyridin-1-ium hexafluorophosphate (2-PY⁺-Ald(NEt₂)⁺).

VITA

NAME Kriangsak Faikhruea

DATE OF BIRTH 27 November 1992

HOME ADDRESS 358/68 The tree bang po station, Bang sue, Bang sue,
Bangkok, THAILAND, 10330

